Loading of microcontainers for oral drug delivery

Marizza, Paolo; Boisen, Anja; Keller, Stephan Sylvest; Müllertz, Anette

Publication date:
2014

Document Version
Peer reviewed version

Ph.D. Thesis

Loading of microcontainers for oral drug delivery

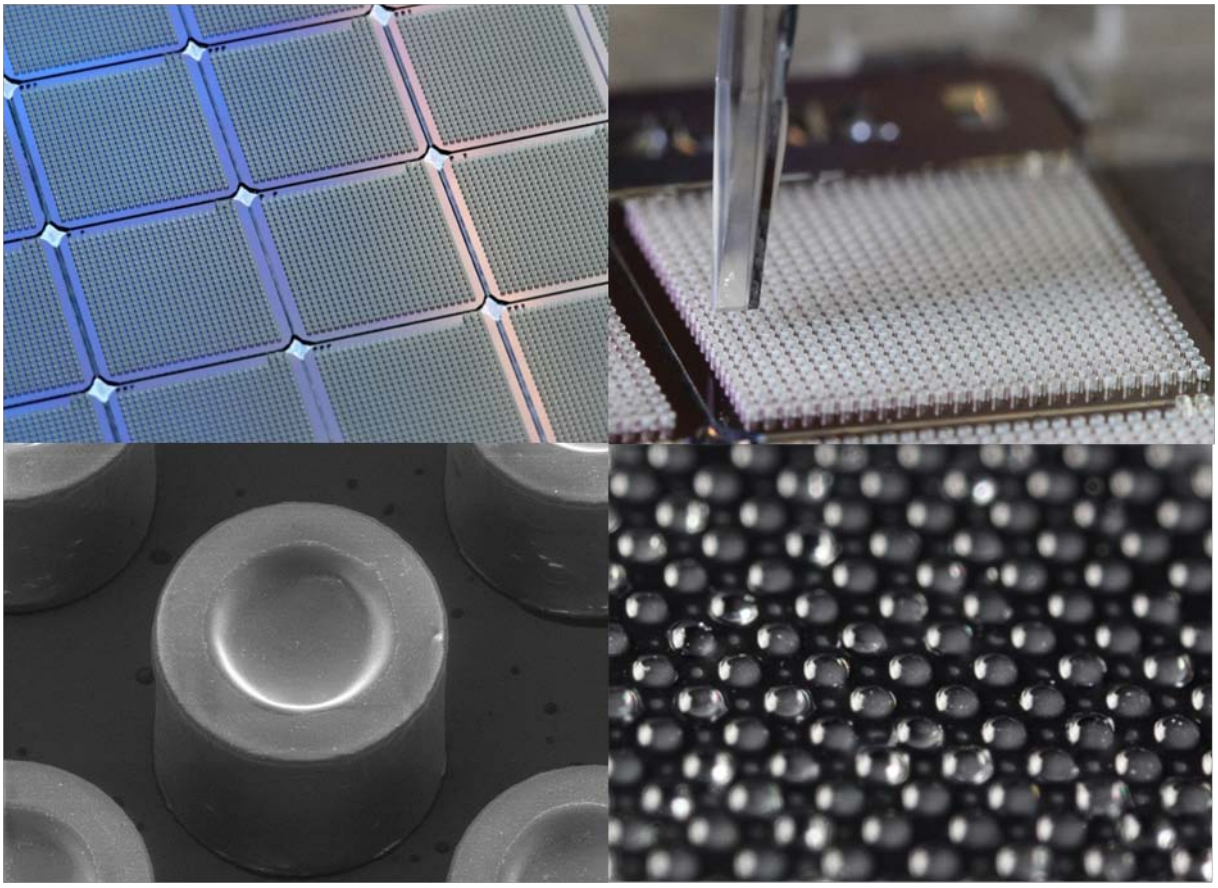

Paolo Marizza

February 2014

Department of Micro- and Nanotechnology
Technical University of Denmark

Abstract

The pharmaceutical research is facing several obstacles in the development of drug products for the oral delivery. The main problem deals with the intrinsic chemical nature of the new drug candidates, which are often poorly soluble and barely absorbed in the gastro-intestinal tract. Furthermore, they are usually degraded before they are absorbed. These combined factors considerably reduce the bioavailability of many active ingredients. Several strategies have been developed to overcome these challenges. One of them are microfabricated drug delivery devices. Microreservoir based-systems are characterized by small dimensions (100-500 µm), mucoadhesive properties, asymmetric geometry and unidirectional drug release. In the fabrication of these microcontainers, an important task is the drug loading. The state of the art in this field is based on traditional methods used in microtechnology, which for this application in most cases are cost ineffective and unsuitable for large scale production.

The goal of this project was to develop novel techniques for loading of poorly soluble drugs and macromolecules in microcontainers. The research focused on simple and cost effective methods, suitable for a large group of drugs and with the perspective of mass production.

In a first instance, the suitability of inkjet printing as filling method was elucidated. Solutions containing furosemide and lipid based formulations of insulin were dispensed into microcontainers. Secondly, this technique was successfully utilized for the deposition of polymer matrices in microcontainers, which afterwards were loaded with the drug. For this purpose, inkjet printing of solutions of poly(vinylpyrrolidone) was developed. The polymer deposition was homogeneous and reproducible, which demonstrated that inkjet printing is a valuable technology to dispense controlled amounts of polymer into microcontainers. Subsequently, polymer filled-containers were loaded with drug. To achieve this, supercritical impregnation technology was successfully employed. Furthermore, *in vitro* drug dissolution studies showed that the loading yields and the release properties of the microdevices can be tuned. The effect of different impregnation process parameters on the loading yields was studied, and the drug-polymer interactions were characterized with various spectroscopic techniques. This technique allowed loading of large arrays of the microcontainers in one single operation with high accuracy and repeatability. Furthermore, the combination of inkjet printing and supercritical impregnation allows to minimize the waste of possibly expensive active ingredients.

A successful process for the definition of micropatterns of poly(vinylpyrrolidone) hydrogel by means of UV photolithography was developed. The fabrication of polymer patterns was optimized and loading with both small hydrophobic drugs and proteins was demonstrated. Finally, structural properties of hydrogels were elucidated by rheology and NMR with the perspective of controlling the drug release.

The loading techniques developed in this thesis represent a novelty in the field of microfabricated drug delivery devices. The methods utilized in this research work are potentially integrated in the fabrication process of biopolymer microcontainers.

Danske Resumé

Den farmaceutiske industri står overfor adskillige forhindringer i forbindelse med udvikling af lægemidler til oral indtagelse. Det største problem handler om selve den kemiske beskaffenhed af de nye lægemidler, som ofte er vanskeligt opløselige og som absorberes dårligt i mave-tarmsystemet. Desuden bliver de som regel nedbrudt, før de absorberes. Disse faktorer reducerer i vid udstrækning biotilgængeligheden af mange af de aktive ingredienser. Mange strategier er blevet udviklet for at overkomme disse udfordringer. Et eksempel herpå er de såkaldte micro-fabrikerede doserings-devices.

Systemer baseret på micro-reservoirs er karakteriseret ved: Små dimensioner (100-500 µm), evnen til at klæbe på slimhinder, usymmetrisk geometri og frigivelse kun i én retning. Under fremstillingen af disse micro-beholdere består en vigtig udfordring i, hvordan de skal fyldes med lægemidlet. Den mest anvendte metode baserer sig på traditionelle micro-teknologiske teknikker, som ofte er dyre og uegnede til produktion i stor skala.

Formålet med dette projekt har været at undersøge nye teknikker til påfyldning af svært opløselige og ustabile lægemidler i disse micro-beholdere. Dette forskningsforsøg har fokuseret på simple og kost-effektive metoder, som er velegnede til masseproduktion for en stor gruppe af lægemidler.

I den første del er egnetheden af inkjet-printning som påfyldningsmetode blevet undersøgt. Opløsninger med furosemid- og lipidbaserede formuleringer af insulin blev fyldt i micro-beholderne. Herefter er denne teknik med succes blevet anvendt til fremstilling af polymer-matricer inde i micro-beholdere, hvori lægemidlet blev påfyldt efterfølgende. Inkjet-printning blev testet med opløsninger af poly(vinylpyrrolidon). Mængden af deponeret polymer viste sig at være homogen og reproducérbar, hvilket demonstrerede at inkjet-printning er en teknologi, der egner sig til påfyldning af nøjagtige mængder af polymer i micro-beholdere med næsten intet spild.

Dernæst blev micro-beholderne påfyldt lægemiddel. Hertil blev superkritisk imprægneringsteknologi anvendt med succes. Desuden viste *in vitro* forsøg med opløsning af lægemidler, at det er muligt at tilpasse dels mængden af påfyldt lægemiddel og dels micro-beholdernes frigivelse af lægemidlet. Indflydelsen af forskellige operationsparametre (tryk, temperatur og tid) på den påfyldte mængde blev undersøgt, og interaktionerne imellem lægemiddel og polymer blev karakteriseret vha. forskellige spektroskopiske teknikker. Den nævnte teknik muliggjorde samtidig påfyldning af mange micro-beholdere på én gang, og med stor nøjagtighed samt repetérbarhed.

En velegnet proces til at definere micro-mønstrene i en poly(vinylpyrrolidon) hydrogel blev udviklet vha. UV fotolitografi. Fremstillingen af polymermønstre blev optimeret, og der blev foretaget effektive påfyldninger med både små, hydrofobiske lægemidler og med proteiner. Til sidst blev hydrogelernes strukturelle egenskaber belyst med det formål at kontrollere frigivelsen af lægemidlet.

Preface

The research work described in this thesis was carried out at DTU Nanotech, Department of Micro- and Nanotechnolgy, DTU. The thesis was written under the supervision of Professor Anja Boisen, Assistant Professor Stephan Sylvest Keller and Professor Anette Müllertz. The project started on the 1st of February 2011 and was finished on the 31st of January 2014.

Kongens Lyngby, January 31st 2014.

Paolo Marizza

DTU Nanotech - Department of Micro- and Nanotechnolgy, DTU
Technical University of Denmark
DTU – Building 345 east
DK-2800 Kongens Lyngby
Denmark

Acknowledgements

I would like to thank my supervisors Professor Anja Boisen, Associate Professor Stephan Sylvest Keller and Associate Professor Anette Müllertz for work guidance, support and feedback. Their help has been very precious to me. In particular, I wish to express my appreciations to Stephan, who has been my guiding "Polar Star" during these three years. I really appreciate his help, and I am very happy to work with him.

I also would like to acknowledge Professor Mario Grassi for his valuable ideas and great contributions to my project. Professor Thomas Rades has also been very important to this project. His inputs have been very precious to my work.

Thanks to the laboratory technicians at Danchip for the help in the cleanroom activities. I would like to remember the entire NAMEC team, for the interesting discussions and feedbacks during our meetings. Also, I acknowledge Line Nielsen and Ping Li for introducing me to the world of pharmacy, and for their help in the analyses.

Special thanks go to my parents Patrizia and Franco and my sister Sarah, for my education and for the support during my studies.

I wish to express my gratitude to my office mates Alberto Cagliani and Sanjukta Bose for the help and for the good times at work. Finally I would like to say thanks to the whole Nanoprobes group, for the great work environment, the good and fruitful discussions at group meetings, and for a lot of good times.

In the following table are listed in chronological order all the collaborators and people involved in the project together with the related research activities and their affiliation.

People	Institution	Activity
Hagner Nielsen L., Li P., Yun Y. H.	KU Pharma (Denmark)	Experiments and analyses in KU Farma
Hegner M., Lukacs G.	CRANN, Dublin (Ireland)	Research activity in Dublin
Moneghini M., De Zordi N., Kikic I., Cortesi A., Solinas D., Pontoni L.	University of Trieste (Italy)	Supercritical impregnation experiments, master project co-supervision
Grassi M., Fiorentino S., Abrami M., Posocco P.	University of Trieste (Italy)	Rheology and NMR experiments, data modelling, molecular simulation
Lessèl R., Schmidt R.	ChemPilots A/R (Farum, Denmark)	Supecritical facilities
Faralli A, Larsen N.	DTU Nanotech	Confocal microscopy
Goswami K., Ladegaard A.	DTU Chemical Eng.	Rheology and DSC analyses
Mateiu R. V.	DTU CEN	Environmental SEM

The Villum Kann Rasmussen Foundation and DTU Nanotech are acknowledged for their financial support of this project.

Watch your thoughts; they become words.
Watch your words; they become actions.
Watch your actions; they become habits.
Watch your habits, they become character.
Watch your character; it becomes your destiny.

by Laozi

Degrees of ability vary, but the basic principle remains the same: the degree of a man's independence, initiative and personal love for his work determines his talent as a worker and his worth as a man. Independence is the only gauge of human virtue and value. [...] There is no substitute for personal dignity. There is no standard of personal dignity except independence.

from"Fountainhead"

by Ayn Rand

Contents

1. Introduction 1
1.1 Current challenges in oral drug delivery 1
1.2 Poorly soluble drugs: trends, challenges and perspectives 2
1.2.1 Drug crystallinity and stability 2
1.2.2 Particle size reduction 3
1.2.3. Particle asymmetry and mucoadhesive properties 4
1.3 Microdevices for oral drug delivery 4
1.4 Overview of the NAMEC Drug Delivery project 5
1.5 State of the art of the existing research 7
1.6 Aim of the PhD and thesis outline 10
Bibliography 11
2. Theory and methods 15
2.1. Fabrication of microcontainers 15
2.1.1 Microcontainers in SU-8 15
2.1.2 Microcontainers in PCL and PLLA 17
2.1.3 Fabrication of glass masks 18
2.2 Inkjet printing technology 19
2.2.1 Introduction 19
2.2.2 Equipment description and operation 19
2.3 Supercritical technology 20
2.3.1 Principles of supercritical processing 20
2.3.2. Solubility of active ingredients in supercritical carbon dioxide 21
2.3.3 Supercritical impregnation 23
2.4 Drug dissolution measurements 23
2.4.1 Dissolution 23
2.4.2 Dissolution equipment: µDISS profiler 24
2.5 Solid state characterization 24
2.5.1 X-ray Powder Diffraction 24
2.5.2 Raman spectroscopy 25
2.5.3 Attenuated Total Reflection Infrared Spectroscopy (ATR-IR) 25
2.6. Hydrogel characterization and imaging 26
2.6.1 Rheological characterization of hydrogels 26

2.6.2. Nuclear magnetic resonance (NMR) spectroscopy 33
2.6.3 Enviromental SEM on gels 43
Bibliography 44
3. Inkjet printing as a drug loading method 51
3.1 Inkjet printing in life sciences and drug delivery 51
3.1.1 Application in high throughput screening (HTS) 51
3.1.2 Application in drug delivery 52
3.2 Equipment description and operation 52
3.2.1 Equipment description 52
3.2.2 Spotting operation 53
3.2.3 Sample alignment 54
3.2.4 Spotting of liquid 55
3.3 Materials 55
3.3.1 Furosemide 55
3.3.2 Poly(vinylpyrrolidone) 55
3.3.3 Sodium alginate and calcium chloride 56
3.3.4 Lipid solutions for SNEDDS-based formulations 56
3.4 Inkjet printing of furosemide solutions 57
3.4.1 Preparation of solutions 57
3.4.2 Results of spotting 57
3.5 Confined crosslinking of alginate matrices 59
3.5.1. Experimental procedure 59
3.5.2 Results 61
3.6 Inkjet printing of PVP solutions 63
3.6.1 Printability of PVP solutions 63
3.6.2 Inkjet printing of PVP solutions 63
3.6.3 Microcontainer filling 63
3.6.4 Level of microcontainer filling 65
3.6.5 Effect of surface tension on deposition 66
3.7 Inkjet printing of lipid based formulations for insulin delivery 67
3.8 Conclusion on inkjet printing 68
Bibliography 69
4. Supercritical impregnation 71

4.1 Concepts of drug loading by polymer swelling 71
4.2 Materials and methods 73
4.2.1 Solubility of ketoprofen in supercritical CO2 73
4.2.2 Swellability of PVP by supercritical CO2 74
4.2.3 Deposition of PVP solution in the microcontainers and preparation of PVP films 75
4.2.4. High pressure equipment and experimental procedure 75
4.2.5 Preparation of micro-tablets 76
4.2.6 Spectroscopic characterization and X-ray diffraction 76
4.2.7 In vitro drug dissolution studies 77
4.3 Result and discussion 77
4.3.1 Inkjet printing of PVP solutions into microcontainer 77
4.3.2 Loading of ketoprofen into polymer-filled microreservoirs 77
4.3.3 Controlled in vitro drug release from impregnated microdevices and Raman characterization 79
4.3.4 Comparison with physical mixtures and XRPD characterization 81
4.3.5 Spectroscopic characterization of impregnated PVP films 83
4.3.6 Effect of temperature on impregnation yield 84
4.4 Conclusions 86
Bibliography 87
5. Photocrosslinking of PVP hydrogels 89
5.1 Hydrogels in drug delivery 89
5.1.1 Introduction 89
5.1.2 UV Photocrosslinking of PVP hydrogels 90
5.1.3 Hydrogel matrices in microcontainers 91
5.1.4 Microgels 91
5.2 Fabrication of PVP microgels 92
5.2.1 Overview of the process 92
5.2.2 Materials and methods 94
5.2.3 Spin coating 94
5.2.4 UV exposure of PVP films 95
5.3 Loading of microgels 97
5.3.1 Confocal microscopy 97
5.3.2 Loading of small molecules 97
5.3.3 Loading of macromolecules 99

5.4 Structural properties of PVP hydrogels 100
5.4.1 Gel preparation 100
5.4.2 Rheological Characterization of gels 101
5.4.3 Average mesh size estimations 103
5.4.4 NMR spectroscopy of gels 107
5.5 Integration in microcontainers 109
5.6 Conclusions 110
Bibliography 111
6. Conclusions and perspectives 115
6.1 Conclusions 115
6.2 Outlook 117
Bibliography 119
APPENDIX 1 121
APPENDIX 2 129

List of scientific contributions

This section lists the scientific contributions presented during the PhD study.

Oral presentations

The 6th Symposium of The Pharmaceutical Solid State Research Cluster (PSSRC), "Inkjet printing as a novel drug loading technique of micro-containers", Lisbon 26-28 August 2012.

The 7th Symposium of The Pharmaceutical Solid State Research Cluster (PSSRC),"Loading of micro-containers for oral delivery with supercritical CO_2 aided impregnation", Lille, July 3-6, 2013.

The 40th Annual Meeting and Exhibition of Controlled Release Society (CRS) "Drug-polymer filled micro-containers for oral delivery loaded using supercritical CO_2 aided-impregnation", Honolulu, July 21-24, 2013.

Poster presentations

The 38th International Conference on Micro and Nano Engineering "Inkjet printing as a technique for filling of micro-wells with bio-compatible polymers", Toulouse 16-20September 2012.

Publications

"Inkjet printing as a technique for filling of microwells with biocompatible polymers ", P. Marizza, S. S. Keller, A. Boisen, Journal of Microelectronic Engineering, 111 (2013) 391-395.

"Polymer-filled microcontainers for oral delivery loaded using supercritical impregnation" P. Marizza, S. S. Keller, A. Müllertz, A. Boisen, Journal of Controlled Release 173 (2014) 1-9.

1. Introduction

1.1 Current challenges in oral drug delivery

One of the most demanding challenges in the pharmaceutical research is finding safe, less invasive and effective solutions for the administration of active pharmaceutical ingredients (APIs). The oral route is still the preferred administration form, avoiding pain, offering good patient compliance and usually requiring no assistance by trained health care staff. However, the pharmaceutical industry is presently facing several severe obstacles when developing oral drug delivery systems, primarily because of the intrinsic physico chemical nature of the new drug candidates.

Traditionally, oral dosage forms have been produced by powder technology and the most popular oral delivery systems are tablets and pills. Tablets are manufactured by compression of powders. Their manufacturing process is performed with granulation (in a dry or wet regime) and subsequent compression [1]. The main advantage of dry granulation is that the powders are not exposed to moisture, but on the other hand the applied mechanical stresses may cause phase transitions [2]. Furthermore, when materials to be compacted exhibit low bulk density or poor flow properties their compression is tricky [3].

In a wet granulator a blend of API and excipients undergoes wet massing followed by sieving and drying steps [4]. In this case, a typical drawback is the occurrence of crystalline polymorphism in the API [5]. Costs of the tabletting process can be reduced when the granulation process is avoided and the tablet manufacturing is performed with a direct compression of powders [6]. However, in this case lower manufacturing costs are compromised by the need of filler materials, whose physical properties are highly critical for the final compression result: particle size, compactability, flowability and bulk density are crucial parameters [3, 7]. Nowadays, the most used fillers are microcrystalline cellulose sucrose and lactose. Direct compression of powders requires a very accurate selection of fillers, and its main limitation is that it does not allow a drug loading higher than 30% [7].

Besides the complexity of the fabrication process, tablets usually have large sizes, because of the presence of different components, like for instance tablet disintegrants, wetting agents, absorption enhancers, and enteric and bioadhesive coatings. Thus, the tablets can be hard to swallow especially for elderly and early age patients [8].

Between the oral ingestion and the final effect of the API, there is a sequence of barriers which the active compound must overcome in order to execute its action [9]. Starting from the mouth, any ingested material is exposed to the action of biological metabolism [10]: Typically an API encounters enzymatic degradation, hydrolysis and chemical deactivation in the acidic gastric environment. Once in the small intestine, many active compounds exhibit a poor solubility in the intestinal fluid, and slow dissolution compared to a relatively rapid peristaltic flow in the upper intestine. Finally, drug molecules often exhibit a limited permeation through the mucosa. In all these passages, an increasing fraction of the API is lost and the bioavailability of the therapeutic agent is considerably reduced. A direct consequence of this fact is that often frequent administrations are needed in order to maintain an efficient therapeutic action. Also, high drug doses are used, increasing the probability of serious adverse effects which for certain substances are unavoidable [11].

1.2 Poorly soluble drugs: trends, challenges and perspectives

One of the most important factors influencing the bioavailability of orally delivered drug is solubility in the physiological fluids. In the Biopharmaceutical Classification System (BCS) standard, drugs are divided into four main groups (see figure 1.1), based on their solubility and permeability in the gastro-intestinal tract (GIT) [12]. A drug is classified as having high solubility, if the correspondent therapeutic dose (for humans) can be dissolved in 250 mL of water in a pH interval between 1 and 7.5. A drug is highly permeable if the absorbed fraction is more than 90% of the assumed dose. More than 90% of active compounds discovered and approved since 1995 belong either to class II or IV [13]. Moreover, the general trend in pharmaceutical research is towards APIs with high molecular weight which often means low solubility and permeability.
Another very important parameter besides the solubility is the dissolution rate of a drug. According to Hsia and coworkers [14], the dissolution process can be considered as the sum of four main consecutive steps: surface wetting, crystal lattice destruction, solute molecule solvation and diffusion in the bulk liquid phase. The most energy-demanding process is the breakdown of the crystal structure, which can be considered as a transition from a solid to a liquid phase in a heterogeneous environment. Therefore, it is clear that the solubility of the drug in the receptor phase plays an important role.
In the field of pharmaceutical technology, several strategies have been developed in order to enhance both solubility and dissolution rate of APIs. These approaches include the modification of both physical and chemical properties of the API [15]. The physical modification focuses mostly on the reduction of particle size [16] and on the crystallinity of the solid phase of the drug. Other strategies act instead on the chemical solvation mechanism, e.g. by means of surfactants or complexation with cyclodextrins [17].

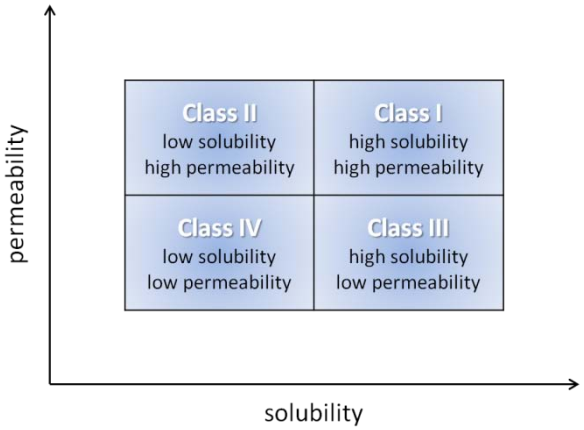

Figure 1.1: Schematic illustration of the BCS dividing drugs into four groups according to their aqueous solubility and permeability through the intestinal membrane.

1.2.1 Drug crystallinity and stability

Drug crystallinity has a strong influence on both its solubility and dissolution rate. The preparation of amorphous drug is an important achievement for poorly soluble drugs, since amorphous forms have enhanced solubility and dissolution rate compared to more stable crystalline solid forms. However, long term stability is frequently a challenge for amorphous drugs and usually represents a big concern for the pharmaceutical industry. For instance, Abbott launched the drug 'Ritonavir' in 1996. The active ingredient was in a crystalline form now called form I, but after two years a more stable (and less soluble) polymorph of the drug (form II) was discovered. Since the transition from polymorph I to polymorph II was very fast and entailed a substantial decrease of therapeutic effect, the company decided the withdrawal of the medicine from the market [18].

The main factors influencing drug stability are: Humidity, heat, oxidation agents and light.
Humidity can have a relevant effect on the stability of pharmaceutical products. Shibata and coworkers [19] have studied the effect of moisture uptake on the recrystallization of drugs in solid dispersions with crospovidone [19], discovering that high humidity may cause a faster crystal growth.
Oxidation of solid dosage forms is usually due to the effect of atmospheric oxygen. To avoid this, particular chemicals with anti-oxidizing properties are included in the formulation product [20]. A reduced interfacial area with the surrounding environment or an impermeable and inert coating may also have a beneficial effect. The effect of heat on drug stability is in general related to the kinetics of the recrystallization process: it is generally believed that at temperatures above the glass transition temperature (T_g), amorphous drugs tend to crystallize at a higher rate than below T_g because of the higher mobility of molecules in the crystal growth process. This mobility can also be enhanced by means of a isothermal heat transfer as shown by Yoshioka *et al*. [20]. It is well known that the exposure to light affects the stability of pharmaceuticals, especially in the UV wavelength range [21].The main effects are chemical degradation of the active ingredient [22], the formation of potentially harmful sub products [23, 24], and changes of physico chemical properties [25].
In light of the abovementioned limitations, one possible way to reduce and delay drug recrystallization would be to protect the API with a coating or shell with inert and impermeable properties.

1.2.2 Particle size reduction

The alternative physical method to enhance dissolution is micronization, where the API and binders are encapsulated into particles with dimensions in the micro and nano scale. Reduction of particle size can be performed with two principal approaches: association of molecularly dispersed drug or comminution of previously formed larger particles e.g. by mechanical grinding [26]. In several years of research in particle engineering a large variety of methods has been developed with the aim of preparing solid dispersions [27]. Challenges in this field include: control of flow properties within the pipeline, online monitoring of materials in upscaled unit operations [28] and avoidance of particle agglomeration due to charging [29] to which the stability of the solid form of API is tightly connected. In many cases, particles generated by micronization techniques still show a wide size distribution [26]. In figure 1.2, as an example of polydispersity, the size distributions of cilostazol particles are plotted, as a result of different milling operations [30].

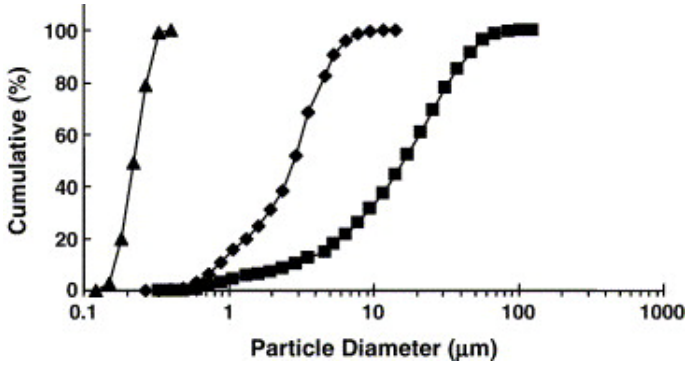

Figure 1.2: The median particle diameters of cilostazol in the hammer-milled (squares), the jet-milled (diamonds) and the commercial spray dried (triangles) (adapted from [30]).

1.2.3. Particle asymmetry and mucoadhesive properties

Independent of the crystallinity or the particle size, there is a further aspect limiting the bioavailability of any drug, but particularly those with poor solubility: a spherical microparticle floating in the luminal fluid releases the drug in any directions with a consequent inevitable loss of substance. An asymmetric drug carrier, in some way, would reduce drug waste in the luminal flow. Furthermore, one additional solution to improve drug release location and increase retention time in the intestine was found by applying mucoadhesive properties to formulations of micro- and nanoparticles [31, 32] or tablets [33, 34].

1.3 Microdevices for oral drug delivery

Due to the challenges discussed in the previous sections, improvements are still needed and possible. Recently, the interest in microfabricated drug delivery devices is increasing [35, 36]. In light of the biological barriers of the human gut and the open questions regarding design and manufacturing of traditional oral dosage forms, a new concept for an oral drug delivery device of a poorly soluble drugs would aim to address the following needs:

- be easy to swallow
- provide protection of the API against gastrointestinal barriers with a resistant shell
- deliver the API at a specific absorptive region in the GIT (preferably the small intestine)
- have small dimensions falling in the range of microns with a narrow size distribution
- limit drug dispersion and loss in the intestine by means of a combination of unidirectional release and adhesion to the intestinal walls
- enhance retention time
- preserve the stability of the formulation

Such a device can be conceived as a microreservoir containing a drug formulation. The microreservoir supplies an inert shell protecting the API from destabilizing and degrading agents. It has an opening on one side, from which the drug is released. A schematic of the microcontainer concept is illustrated in Figure 1.3.

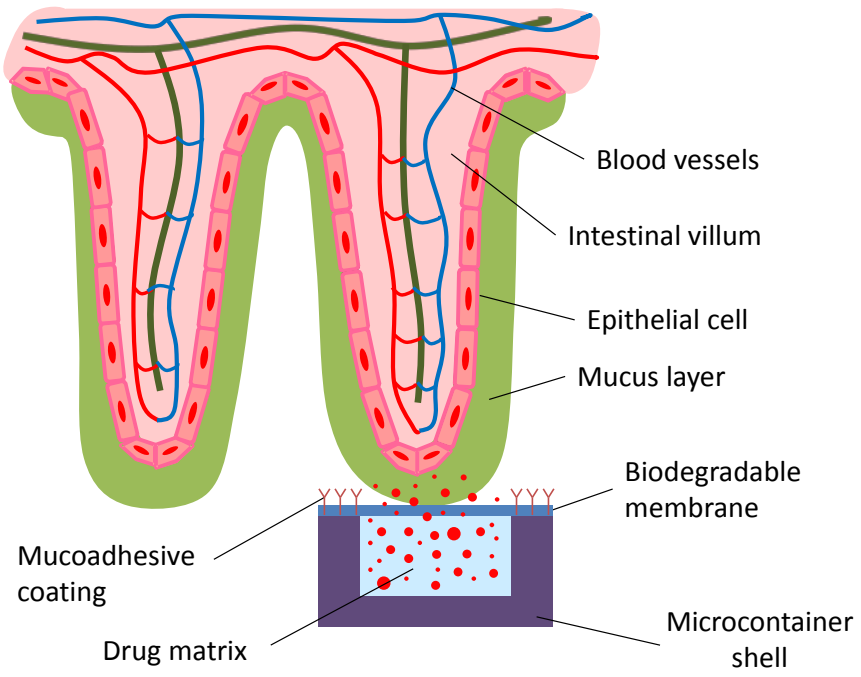

Figure 1.3: Schematic representation of a microcontainer in the intestinal environment.

As a formal requirement, materials and procedures for fabrication of the microdevice should be approved for oral administration by the Food and Drug Administration (FDA). Assuming that only the API should be absorbed in the body, all the other materials of the device should be biocompatible and not accumulated in the body. Preferably, they should be biodegradable so that the products of their degradation are expelled. Among FDA approved polymers, poly(L-lactic acid) (PLLA) and polycaprolactone (PCL) are used for oral products. To determine the optimal size of the microdevice, it is worth to make the following considerations. The fluid regime in the intestine is far from being steadily laminar [37] because the efflux from the stomach is discontinuous. Peristalsis contractions further reduce the lumen section and therefore the flux out of the stomach is accelerated An usual problem for tablets is an incomplete drug release combined to a relatively short retention time in the upper intestine as a result of the drag force applied by the fluid to the large tablet. This is one more justification for reducing the size of drug delivery devices. On the other hand, microcontainers size should not be below 500 nm, in order to avoid cellular endocytosis by the intestinal epithelium [38]. The microcontainer size should also be defined taking into account other important issues like fabrication limitations with proposed materials and processes and the loading capacity. These topics will be discussed in the following section.

1.4 Overview of the NAMEC Drug Delivery project

The present PhD project is carried out as part of a larger research consortium called NAMEC – NanoMEChanical sensor and actuators, fundamentals and new directions – a VKR Centre of Excellence financed by the Villum Kann Rasmussen Foundation, working on drug delivery microdevices and pharmaceutical applications of micro- and nanosensors. The partners of the drug delivery project belong to the Department of Micro- and Nanotechnology, the Department of Electrical Engineering and Department of Applied Mathematics and Computer Science (all from Technical University of Denmark, DTU) and the Department of Pharmacy (University of Copenhagen, KU).

According to the requirements discussed in section 1.3, it was decided that the microdevice for oral drug delivery should include the following elements (figure 1.3):

- an asymmetric shell providing protection of the drug
- a drug matrix with a given formulation
- a permeable or degradable membrane to be opened at the absorption site
- a conformal mucoadhesive coating to ensure attachment and unidirectional release through the intestinal epithelium

According to these features, the drug delivery device has been developed in separate but coordinated tasks: (1) microcontainer fabrication, (2) drug formulation and loading, (3) deposition of lid and mucoadhesive coating. These are the main tasks that the multidisciplinary team in NAMEC has addressed. The research activities were initiated in the fall 2009, and the main results regarding the development of the microcontainer concept are presented below.
The fabrication of cylindrical microcontainers was developed by Nagstrup *et al*. [39]: thousands of containers with defined dimensions can be fabricated in the biodegradable polymers poly(L-lactic acid) (PLLA) and polycaprolactone (PCL) by means of hot embossing. Typically the containers have an outer diameter of 300 µm and a cavity depth of 65 µm (see figure 1.4). More recently, a “hot punching” technique was developed as a technical solution to remove the microdevices from the residual material after the hot embossing process.

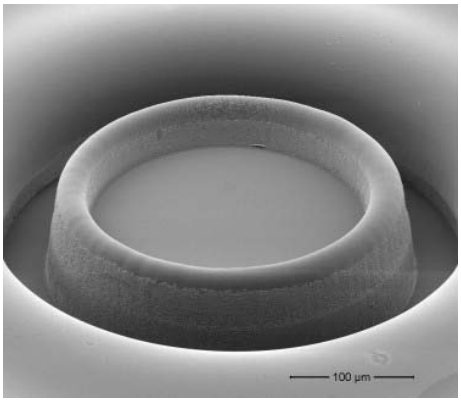

Figure 1.4: SEM image of en embossed PLLA microcontainer. The well diameter is 300 µm and cavity depth is 65 µm [39].

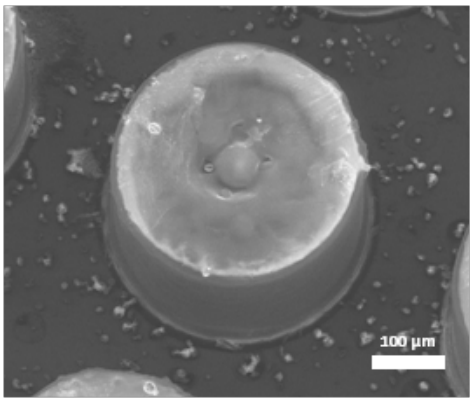

Figure 1.5: Microcontainer with a lid of Eudragit L 100.

The effect of spatial confinement on formulation stability has been studied. Nielsen *et al*. [40] have shown that the crystallization of amorphous indomethacin can be slowed down when the API is confined inside microcontainers compared to bulk formulation. Furthermore, the smaller the microwells are, the higher is the drug stability. In another study the effect of the drug amorphization procedure on stability inside microcontainers was elucidated [41]. The application of an enteric polymer coating based on Eudragit L 100 (see figure 1.5) on the open face of drug filled microcontainers has shown that the drug can be protected from degradation in the gastric environment and that the release can be triggered at a specific region of the GIT according to the pH of the surrounding fluid.

Furthermore, several oral drug formulations have been designed with the purpose of delivering therapeutics using microcontainers as a carrier: amorphous furosemide salts [42] and insulin laden SNEDDS (Self Emulsifying Drug Delivery Systems) [43]. However, the development of a feasible, robust and effective loading procedure for microcontainers has been proven to be a non trivial task. Several trials were accomplished with the use of hot embossing: a thin layer of drug-polymer matrix was embossed into microcontainers and residual portions between the containers were subsequently removed by Reactive Ion Etching (RIE). This technique has the advantage of being quite simple, but entails a large loss of material. Also, if the containers have initially been fabricated with a similar embossing process (e.g. using biopolymers), there is a narrow temperature window where the embossing can be performed without deforming the containers. Finally, the used drug might be damaged or degraded due to elevated temperatures during embossing as well as RIE.

An alternative technique for filling containers using screen printing [44] has shown interesting results: a stencil mask with holes matching the inner diameter of containers is aligned on top of a wafer with microcontainers. Next the drug powder is pressed through the stencil and afterwards the stencil is removed with any excess powder. The main drawback of this method lies in the need of alignment of the stencil on top of the substrate and its stabilization during the powder compression. This point might be improved by designing a specific system for alignment and stencil clamping. However, the procedure is difficult to standardize (quantity and homogeneity of filling) and to automate with the available instrumentation.

Another procedure for container filling developed in our research group, deals with solvent casting. A liquid solution containing the drug and excipient is poured on top of the containers and the liquid is distributed on the entire surface by manual tilting. The drug solution fills container cavities driven by the surface tension, while the excess solution runs off the substrate. Again an advantage of this approach is the simplicity, but it also implies substantial limitations. Firstly, the material deposited outside the containers represents a waste of material. Secondly, once casted, the solvent in the liquid formulation needs to evaporate, which often causes drug recrystallization. Finally, there is a problem related to the use of organic solvent, which for hydrophobic drugs is often a choice difficult to avoid. Given the difficulties encountered in the abovementioned loading methods, before the achievements described in this thesis,

the “state of the art” in NAMEC project, respect to microcontainers filling, consisted in manual pressing the drug powder into the devices (without stencil), and blowing away the residual powder in between the devices with an air gun. This method entailed a large waste of materials and therefore needed to be replaced with a more efficient technique.

1.5 State of the art of the existing research

In section 1.3 the main concepts of a device for oral delivery for poorly bioavailable therapeutics have been explained. It is deductable that it is very unlikely that methods traditionally used in the field of pharmaceutical technology can address all these tasks in one or a couple of steps. This is especially evident, when we think about having an asymmetric drug release and a conformal bioadhesive coating. In order to bestow such complex features to a single device, multiple steps are required. They have to be performed in a logic sequence in order to be compatible with each other, not compromising the final result. The common *bottom up* design itself, with tuning of accurate mixing and transformation of chemical compounds seems quite difficult to apply for our purpose. Fabrication methods with a *top-down* approach seem more appropriate.

A device with the features listed in section 1.3 has been originally conceived in a patent filed 07.01.2000 and later presented as research work. [45]. The first microdevices developed with these features were realized using porous silicon microparticles loaded with protein-based therapeutics as a proof of concept [46, 47]. At a later stage, several groups around the world have contributed substantially to this research field with innovative microfabricated systems for oral drug delivery. Particular interest was aroused by reservoir-based microdevices for water unsoluble compounds and protein-based therapeutics. In the following paragraphsan overview of the current state of the art of reservoir-based microfabricated devices for oral drug delivery is given, with particular focus on the drug loading.

The group of Tejal Desai at the University of California (San Francisco) has developed many prototypes of microfabricated devices for oral drug delivery. Their achievements can be considered the state of the art in this field. The first devices were manufactured in silicon [48]. In this feasibility study, a bioadhesive coating, based on surface functionalization with lectins, was tested on microwells for the first time. In later works *in vitro* experiments were performed on CaCo-2 cell monolayers to measure bioadhesion [49]. Also, further surface chemistry protocols were developed, becoming one of their most advanced competences. Several more advanced prototypes were developed over a period of 13 years using various materials: poly(methyl methacrylate) (PMMA) [50], poly(lactic-co-glycolic acid) (PLGA) and gelatin [51]. Typical dimensions of these devices are 50-200 µm in width and 3-15 µm in height. The volume available for the drug loading is 9.6-19 pL [50, 52]. In 2002, a first prototype was developed in silicon (see figure 1.6a and b) [53]. More recently, a multilayered microdevice for controlled release of different therapeutics was fabricated in SU-8 shown in figure 1.7a [54]. The latest prototype developed is a bioadhesive microcontainer in PMMA with multiple drug reservoirs (see figure 1.7b) [52]. This design allows the loading of different therapeutics (see picture 1.7a and b) which can be delivered either sequentially, simultaneously, or independently and with tunable release kinetics. All these devices have in common a flat geometry, which has a relevant advantage both from operation and fabrication perspectives. Indeed, a thin and flat microdevice was demonstrated to have a stronger adhesion to a cell monolayer simulating the intestinal epithelium as compared to spherical microparticles [50]. The low thickness is also an advantage for the definition of the cavity depth, when using relatively slow technologies like wet chemical etching [53] or dry ion etching [52]. A wide and flat compartment also allows a relatively easy drug loading step, which can be carried out by dispensing a drug solution on large arrays of devices or by spin-coating and subsequent selective UV-crosslinking [52]. On the other hand a small cavity volume entails a low loading capacity and therefore a larger amount of microdevices is needed for a certain drug dose. The influence of particle size and shape on the shear stress in the intestine is still a point of discussion, and a compromise between dimension and loading volume must be found. The main issue regarding the abovementioned loading techniques is that they are strictly

dependent on the solvent properties: figure 1.6 shows that the filling with water solution (figure 1.6a) works fine, but with the oil (figure 1.6b) it is much less controllable. The combination of spin-coating and UV-crosslinking allows a more precise filling: A mixture of protein and polymer is casted on the microdevices. Spinning is applied to the microdevices and a thin layer is leveled. Thereafter, the portions of the layer inside the microdevices cavities are exposed to UV light and crosslinked.The uncrosslinked portions are lost. In figure 1.7a a multi-layered squared microcontainer, loaded with different labeled proteins is shown [54]. Different proteins are loaded in the same container cavity at different depths. Figure 1.7b shows a container with multiple reservoirs, each loaded with a different fluorophore tagged-protein. In this case each cavity can be crosslinked independently, which allows control of the release kinetics of the drug. Spin coating deposition can be controlled by modulating parameters like spin rate, acceleration, time, and viscosity and surface tension of the liquid. Nevertheless, the drawback lies in the large amount of material which is typically required to obtain a uniform coating. By experience, more than 50% of the dispensed solution is lost during spinning. The exposure to UV light is also critical for photosensitive APIs, causing degradation and potentially generating unsafe byproducts [55, 56].

The group of Derek Hansford Ohio State University has carried out remarkable research within the field of self folding microcapsules for oral drug delivery [57-59]. Material used in this case are PLGA, poly(ethylene glycol methacrylate) (PEGMA), and chitosan [57]. Typical sizes for the microstructures fall in the range of 45-90 µm wide containers containing reservoirs of 3-7 µm in depth. The volume available for drug loading is in the picoliter scale (2-7 pL). To fill the microreservoirs, the authors have used discontinous dewetting, which exploits the different wetting properties of the drug solutions on the hydrophilic microstructures compared to the hydrophobic surrounding surface. In figure 1.8 an optical micrograph of PEGMA microwells loaded with NaCl crystals is shown [57]. This technique is rapid and uniform, although it is generally dependent on the solvent surface tension. Moreover, if the solution to be loaded is more viscous, for example when the drug is mixed with a stabilizing polymer, the discontinuous dewetting will most likely be complicated and less accurate.

The group of David H. Gracias at John Hopkins University has developed different self-folding microcarriers for drug delivery [60-62]. These devices are generally prepared by deposition of one or more layers of polymer solution on a flat substrate, micropatterning with the desired geometry and release by dissolution of an underlaying sacrificial layer. Figure 1.9 shows an SU-8 microcube with PCL hinges. The folding from 2D to a 3D arrangement is driven by surface tension: the microstructures are heated above the melting point of the hinge material and the faces close like shown in figure 1.9b. Azam and coworkers [60] have succeeded in encapsulating living biological components like bacteria and mammalian cells (see figure 1.9a). The loading is carried out by immersion of the microdevices in the culture media and the encapsulation is obtained by energetic tumbling. In this case the loading mechanism is based on self assembly and thus it appears less controllable. In addition, the use of SU-8 entails always a cytotoxicity issue, which for the therapeutic delivery of cells is rather relevant.

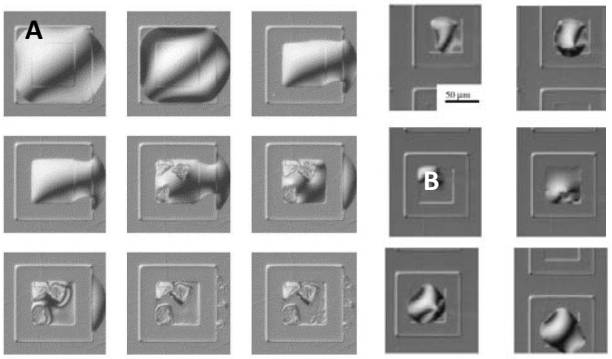

Figure 1.6: (a) Time series of water-based loading of squared silicon microdevices with micro-injection. (b) Microcontainers filled with oil-based solution (modified from [53])

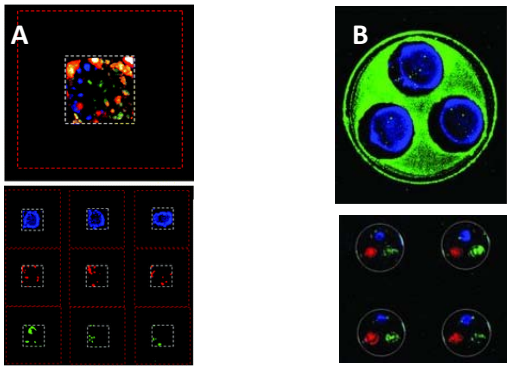

Figure 1.7: (a) Fluorescent micrograph of a squared SU-8 microcontainer filled with layered hydrogel loaded with three different labeled BSA (top) and with single labeled BSA (bottom) (from [54]). (b) Fluorescent micrograph of a multi-reservoir container, showing the presence of one single model drug (top) and three different model drugs in separate reservoirs (bottom) (from [52])

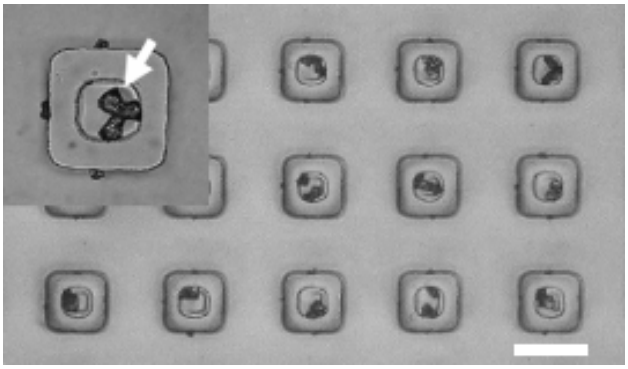

Figure 1.8: Optical micrograph of microdevices made in resins of PEGMA and PEGDMA, loaded by discontinuous dewetting with water solution of NaCl. The inset shows an enlarged microdevice containing NaCl crystals (from [57]).

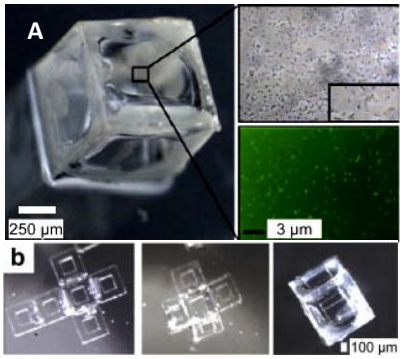

Figure 1.9: Cubic self-folding microcapsule in SU-8 and PCL filled with E. coli 24 h after staining (modified from [60])

1.6 Aim of the PhD and thesis outline

The goal of my PhD project was the development of methods and techniques for the loading of poorly soluble and fragile biological macromolecules into microcontainers. The research in drug loading was applied to a device fabricated with the epoxy resin SU-8, a material not approved by FDA for oral ingestion. The reason for this choice was the fact that the development of biodegradable devices (carried out in another PhD project running in parallel) was not yet concluded. The SU-8 container has instead an optimized and relatively fast fabrication and was therefore chosen as a prototype in this project to test different loading techniques.
In this work the attention was focused on small model molecules belonging to BCS type IV (low solubility and permeability) and type II (low solubility and high permeability). In the final part of the project the loading of biomacromolecules was investigated. The research work aimed to address the following issues:

1. to investigate the suitability of inkjet printing as a technique for microcontainer filling and loading
2. to develop loading methods that can be up scaled to a production level
3. to characterize materials and technologies in light of developing a controlled release device
4. to combine loading methods with existing optimized formulations for oral delivery of poorly soluble and fragile APIs

The present thesis is structured as follows:

- Chapter 2: In this chapter the fabrication process of SU-8 microcontainers is illustrated. The utilized experimental techniques are described each with a concise theoretical background needed for a complete understanding of the results.
- Chapter 3: This chapter is dedicated to a feasibility study of inkjet printing as a technology for the filling of microcontainers with different drug formulations.
- Chapter 4: Here the application of supercritical impregnation of PVP with ketoprofen is described as a drug loading technique for microcontainers. A section is dedicated to the in depth characterization of this technology with respect to drug loading yield and influence of the process parameters. The drug-excipient molecular interactions are investigated with different experimental techniques.
- Chapter 5: In this chapter a new fabrication approach is developed, based on the patterning of micro-hydrogels by means of UV photocrosslinking. The microgels are meant to be the polymer matrix hosting the drug after loading. Gel matrix features are elucidated in terms of drug loading capacity and release properties.
- Chapter 6: The final chapter comments on the overall PhD project, the unsolved issues and the future perspectives for the combination of the achievements in the drug loading with the fabrication steps of biodegradable microdevices.

Bibliography

[1] R. Agrawal, Y. Naveen, Pharmaceutical processing–A review on wet granulation technology, International journal of pharmaceutical frontier research, 1 (2011) 65-83.
[2] G.G. Zhang, D. Law, E.A. Schmitt, Y. Qiu, Phase transformation considerations during process development and manufacture of solid oral dosage forms, Advanced Drug Delivery Reviews, 56 (2004) 371-390.
[3] M. Jivraj, L.G. Martini, C.M. Thomson, An overview of the different excipients useful for the direct compression of tablets, Pharmaceutical science & technology today, 3 (2000) 58-63.
[4] J. Parmar, M. Rane, Tablet formulation design and manufacture: Oral immediate release application, Pharma times, 41 (2009) 21-29.
[5] W. Li, G.D. Worosila, W. Wang, T. Mascaro, Determination of polymorph conversion of an active pharmaceutical ingredient in wet granulation using NIR calibration models generated from the premix blends, Journal of Pharmaceutical Sciences, 94 (2005) 2800-2806.
[6] A. G Mirani, S. P Patankar, V. S Borole, A. S Pawar, V. J Kadam, Direct compression high functionality excipient using coprocessing technique: A brief review, Current Drug Delivery, 8 (2011) 426-435.
[7] P. Wright, M. Gibson, Pharmaceutical Preformulation and Formulation: A Practical Guide from Candidate Drug Selection to Commercial Dosage Form, in, Taylor & Francis Group, CRC Press Boca Raton, FL, 2004.
[8] O. Andersen, O. Zweidorff, T. Hjelde, E. Rødland, Problems when swallowing tablets. A questionnaire study from general practice], Tidsskrift for den Norske lægeforening: tidsskrift for praktisk medicin, ny række, 115 (1995) 947.
[9] B. Steffansen, C.U. Nielsen, B. Brodin, A.H. Eriksson, R. Andersen, S. Frokjaer, Intestinal solute carriers: an overview of trends and strategies for improving oral drug absorption, European Journal of Pharmaceutical Sciences, 21 (2004) 3-16.
[10] O. Ipatova, T. Torkhovskaya, N. Medvedeva, V. Prozorovsky, N. Ivanova, A. Shironin, V. Baranova, A. Archakov, Bioavailability of oral drugs and the methods for its improvement, Biochemistry (Moscow) Supplement Series B: Biomedical Chemistry, 4 (2010) 82-94.
[11] K.D. Rainsford, An analysis of the gastro-intestinal side-effects of non-steroidal anti-inflammatory drugs, with particular reference to comparative studies in man and laboratory species, Rheumatol Int, 2 (1982) 1-10.
[12] H. Chavda, C. Patel, I. Anand, Biopharmaceutics classification system, Systematic Reviews in Pharmacy, 1 (2010) 62.
[13] A. Dahan, J.M. Miller, G.L. Amidon, Prediction of solubility and permeability class membership: provisional BCS classification of the world's top oral drugs, AAPS J, 11 (2009) 740-746.
[14] D.C. Hsia, C.-K. Kim, D.O. Kildsig, Determination of energy change associated with dissolution of a solid, Journal of Pharmaceutical Sciences, 66 (1977) 961-965.
[15] C. Leuner, J. Dressman, Improving drug solubility for oral delivery using solid dispersions, European Journal of Pharmaceutics and Biopharmaceutics, 50 (2000) 47-60.
[16] M. Grau, O. Kayser, R. Müller, Nanosuspensions of poorly soluble drugs—reproducibility of small scale production, International Journal of Pharmaceutics, 196 (2000) 155-159.
[17] D. Hörter, J. Dressman, Influence of physicochemical properties on dissolution of drugs in the gastrointestinal tract, Advanced Drug Delivery Reviews, 46 (2001) 75-87.
[18] J. Bauer, S. Spanton, R. Henry, J. Quick, W. Dziki, W. Porter, J. Morris, Ritonavir: an extraordinary example of conformational polymorphism, Pharmaceutical research, 18 (2001) 859-866.
[19] Y. Shibata, M. Fujii, A. Suzuki, N. Koizumi, K. Kanada, M. Yamada, Y. Watanabe, Effect of storage conditions on the recrystallization of drugs in solid dispersions with crospovidone, Pharmaceutical development and technology, (2013) 1-7.
[20] S. Yoshioka, V.J. Stella, Stability of drugs and dosage forms, Springer, 2000.

[21] T.E. Doll, F.H. Frimmel, Fate of pharmaceuticals—photodegradation by simulated solar UV-light, Chemosphere, 52 (2003) 1757-1769.
[22] B.A. Kerwin, R.L. Remmele, Protect from light: Photodegradation and protein biologics, Journal of Pharmaceutical Sciences, 96 (2007) 1468-1479.
[23] D. Vogna, R. Marotta, R. Andreozzi, A. Napolitano, M. d'Ischia, Kinetic and chemical assessment of the UV/H2O2 treatment of antiepileptic drug carbamazepine, Chemosphere, 54 (2004) 497-505.
[24] L. Costanzo, G.D. Guidi, G. Condorelli, A. Cambria, M. Fama, Molecular mechanism of drug photosensitization–II. Photohemolysis sensitized by ketoprofen, Photochemistry and photobiology, 50 (1989) 359-365.
[25] H.H. Tønnesen, Formulation and stability testing of photolabile drugs, International Journal of Pharmaceutics, 225 (2001) 1-14.
[26] N. Rasenack, B.W. Müller, Micron-size drug particles: common and novel micronization techniques, Pharmaceutical development and technology, 9 (2004) 1-13.
[27] D. Sharma, S. Joshi, Solubility enhancement strategies for poorly water-soluble drugs in solid dispersions: A Review, Asian J. Pharm, 1 (2007) 9-19.
[28] K.R. Morris, J.G. Stowell, S.R. Byrn, A.W. Placette, T.D. Davis, G.E. Peck, Accelerated Fluid Bed Drying Using NIR Monitoring and Phenomenological Modeling, Drug Development and Industrial Pharmacy, 26 (2000) 985-988.
[29] M.M. de Villiers, Influence of cohesive properties of micronized drug powders on particle size analysis, Journal of pharmaceutical and biomedical analysis, 13 (1995) 191-198.
[30] J.-i. Jinno, N. Kamada, M. Miyake, K. Yamada, T. Mukai, M. Odomi, H. Toguchi, G.G. Liversidge, K. Higaki, T. Kimura, Effect of particle size reduction on dissolution and oral absorption of a poorly water-soluble drug, cilostazol, in beagle dogs, Journal of Controlled Release, 111 (2006) 56-64.
[31] E. Déat-Lainé, V. Hoffart, G. Garrait, J.-F. Jarrige, J.-M. Cardot, M. Subirade, E. Beyssac, Efficacy of mucoadhesive hydrogel microparticles of whey protein and alginate for oral insulin delivery, Pharmaceutical research, (2012) 1-14.
[32] S. Sajeesh, C.P. Sharma, C. Vauthier, Mucoadhesive Nanoparticles for Oral Delivery of Insulin, Nanotechnology and Nanomedicine in Diabetes, (2012) 165.
[33] I.A. Sogias, A.C. Williams, V.V. Khutoryanskiy, Chitosan-based mucoadhesive tablets for oral delivery of ibuprofen, International Journal of Pharmaceutics, (2012).
[34] N.A. Peppas, J.J. Sahlin, Hydrogels as mucoadhesive and bioadhesive materials: a review, Biomaterials, 17 (1996) 1553-1561.
[35] P. Colombo, F. Sonvico, G. Colombo, R. Bettini, Novel platforms for oral drug delivery, Pharmaceutical research, 26 (2009) 601-611.
[36] M. Caldorera-Moore, N.A. Peppas, Micro- and nanotechnologies for intelligent and responsive biomaterial-based medical systems, Advanced Drug Delivery Reviews, 61 (2009) 1391-1401.
[37] K. Sugano, Aqueous boundary layers related to oral absorption of a drug: from dissolution of a drug to carrier mediated transport and intestinal wall metabolism, Molecular pharmaceutics, 7 (2010) 1362-1373.
[38] K. Yin Win, S.-S. Feng, Effects of particle size and surface coating on cellular uptake of polymeric nanoparticles for oral delivery of anticancer drugs, Biomaterials, 26 (2005) 2713-2722.
[39] J. Nagstrup, S. Keller, K. Almdal, A. Boisen, 3D microstructuring of biodegradable polymers, Microelectronic Engineering, 88 (2011) 2342-2344.
[40] L.H. Nielsen, S.S. Keller, K.C. Gordon, A. Boisen, T. Rades, A. Müllertz, Spatial confinement can lead to increased stability of amorphous indomethacin, European Journal of Pharmaceutics and Biopharmaceutics, (2012).
[41] L.H. Nielsen, S.S. Keller, A. Boisen, A. Müllertz, T. Rades, A slow cooling rate of indomethacin melt spatially confined in microcontainers increases the physical stability of the amorphous drug without influencing its biorelevant dissolution behaviour, Drug Delivery and Translational Research, (2013) 1-7.

[42] L.H. Nielsen, S. Gordon, R. Holm, A. Selen, T. Rades, A. Müllertz, Preparation of an amorphous sodium furosemide salt improves solubility and dissolution rate and leads to a faster< i> T</i>< sub> max</sub> after oral dosing to rats, European Journal of Pharmaceutics and Biopharmaceutics, (2013).
[43] P. Li, H.M. Nielsen, A. Müllertz, Oral delivery of peptides and proteins using lipid-based drug delivery systems, Expert Opinion on Drug Delivery, 9 (2012) 1289-1304.
[44] J. Nagstrup, A. Boisen, S.S. Keller, Micro fabrication of biodegradable polymer drug delivery devices, in, Technical University of DenmarkDanmarks Tekniske Universitet, Department of Micro-and NanotechnologyInstitut for Mikro-og Nanoteknologi, NanoprobesNanoprobes, 2013.
[45] F.J. Martin, C. Grove, Microfabricated drug delivery systems: concepts to improve clinical benefit, Biomedical Microdevices, 3 (2001) 97-108.
[46] M.H. Cohen, K. Melnik, A.A. Boiarski, M. Ferrari, F.J. Martin, Microfabrication of silicon-based nanoporous particulates for medical applications, Biomedical Microdevices, 5 (2003) 253-259.
[47] A.B. Foraker, R.J. Walczak, M.H. Cohen, T.A. Boiarski, C.F. Grove, P.W. Swaan, Microfabricated porous silicon particles enhance paracellular delivery of insulin across intestinal Caco-2 cell monolayers, Pharmaceutical research, 20 (2003) 110-116.
[48] A. Ahmed, C. Bonner, T.A. Desai, Bioadhesive microdevices for drug delivery: a feasibility study, Biomedical Microdevices, 3 (2001) 89-96.
[49] K.M. Ainslie, R.D. Lowe, T.T. Beaudette, L. Petty, E.M. Bachelder, T.A. Desai, Microfabricated Devices for Enhanced Bioadhesive Drug Delivery: Attachment to and Small-Molecule Release Through a Cell Monolayer Under Flow, Small, 5 (2009) 2857-2863.
[50] S.L. Tao, M.W. Lubeley, T.A. Desai, Bioadhesive poly (methyl methacrylate) microdevices for controlled drug delivery, Journal of Controlled Release, 88 (2003) 215-228.
[51] S.L. Tao, T.A. Desai, Microfabrication of multilayer, asymmetric, polymeric devices for drug delivery, Advanced Materials, 17 (2005) 1625-1630.
[52] H.D. Chirra, T.A. Desai, Multi-Reservoir Bioadhesive Microdevices for Independent Rate-Controlled Delivery of Multiple Drugs, Small, (2012).
[53] A. Ahmed, C. Bonner, T.A. Desai, Bioadhesive microdevices with multiple reservoirs: a new platform for oral drug delivery, Journal of Controlled Release, 81 (2002) 291-306.
[54] K.M. Ainslie, C.M. Kraning, T.A. Desai, Microfabrication of an asymmetric, multi-layered microdevice for controlled release of orally delivered therapeutics, Lab Chip, 8 (2008) 1042-1047.
[55] A. Zanocco, Kinetics and Mechanism of the Photosensitized Oxidation of Furosemide*, Photochemistry and photobiology, 68 (1998) 487-493.
[56] V.J. Pereira, H.S. Weinberg, K.G. Linden, P.C. Singer, UV degradation kinetics and modeling of pharmaceutical compounds in laboratory grade and surface water via direct and indirect photolysis at 254 nm, Environmental science & technology, 41 (2007) 1682-1688.
[57] J. Guan, H. He, L.J. Lee, D.J. Hansford, Fabrication of Particulate Reservoir-Containing, Capsulelike, and Self-Folding Polymer Microstructures for Drug Delivery, Small, 3 (2007) 412-418.
[58] J. Guan, N. Ferrell, L. James Lee, D.J. Hansford, Fabrication of polymeric microparticles for drug delivery by soft lithography, Biomaterials, 27 (2006) 4034-4041.
[59] J. Guan, H. He, D.J. Hansford, L.J. Lee, Self-folding of three-dimensional hydrogel microstructures, The Journal of Physical Chemistry B, 109 (2005) 23134-23137.
[60] A. Azam, K.E. Laflin, M. Jamal, R. Fernandes, D.H. Gracias, Self-folding micropatterned polymeric containers, Biomedical Microdevices, 13 (2011) 51-58.
[61] T.G. Leong, C.L. Randall, B.R. Benson, A.M. Zarafshar, D.H. Gracias, Self-loading lithographically structured microcontainers: 3D patterned, mobile microwells, Lab on a Chip, 8 (2008) 1621-1624.
[62] C.L. Randall, T.G. Leong, N. Bassik, D.H. Gracias, 3D lithographically fabricated nanoliter containers for drug delivery, Advanced Drug Delivery Reviews, 59 (2007) 1547-1561.

2. Theory and methods

This chapter covers all the microfabrication processes and the main characterization methods used in this PhD project. A first section describes the technologies involved in the fabrication of arrays of microcontainers made in SU-8 on custom-made silicon substrates to facilitate the following loading steps. The process regarding the fabrication of silicon slides and arrays of SU-8 microcontainers was published in the full paper ´"Inkjet printing as a technique for filling of micro-wells with biocompatible polymers", where also the use of inkjet printing as a filling method is presented (see Appendix 1).
A second section is dedicated to the fabrication of PCL and PLA microdevices, for which few tests were performed mainly to investigate the applicability of the developed loading methods.
The third section deals with the fabrication of glass masks utilized for the definition of micro hydrogels by means of UV photocrosslinking. The microfabrication processes of SU-8 microcontainers and glass masks were performed at the DTU Danchip clean room facilities.
The supercritical experiments were performed in the laboratories of ChemiPilots A/S (Farum, Denmark) and in collaboration with the Department of Industrial Engineering and Information Technology, University of Trieste (Italy). The X-ray spectroscopy activities and the dissolution experiments were performed in the laboratories situated of the Department of Pharmacy at the University of Copenhagen.
The rheological measurements and the NMR experiments were carried out at the University of Trieste (Italy). Additional rheological tests were performed at the Department of Chemical Engineering at DTU.

2.1 Fabrication of microcontainers

2.1.1 Microcontainers in SU-8

SU-8 is a negative photoresist (SU-8 2075, Microchem, USA) based on an epoxy resin which is commonly used in micro and nanotechnology for fabrication of high aspect-ratio microstructures [1, 2]. This material was originally patented by IBM in 1989 [3] and since then its use has been widely investigated and nowadays SU-8 processing is established in the field.
SU-8 was chosen as material for microcontainer because of the simplicity of the fabrication process: The chosen microdevice dimensions are far from the resolution limits for patterning of this material, which allows the use of standard fabrication equipment.
SU-8 was utilized is several drug delivery microdevices [4-6] and its currently most diffused application in drug delivery is in the fabrication of molds for polymer microneedles in transdermal delivery [7-9].
Several studies showed that SU-8 does not inhibit cell growth [10], and allows cell cultures persisting for more than 3 months [11]. Subcutaneous in vivo implantations of SU-8-coated drug eluting devices induced a limited leukocyte adhesion in rats after 21 days [12]. On the other hand it has been known that SU-8 hydrophobicity limits cell attachments [13, 14] and therefore the depositions of white cells on the photoresist might not be a reliable parameter for tracing immune response. As a consequence, the biocompatibility and safety of SU-8 is not proven, and thus, as mentioned in chapter 1, SU-8 is not yet approved by FDA for drug delivery.

In this work the fabrication of microcontainers has been performed on silicon wafers. As a first step, trenches were etched (see figure 2.1a and b) to facilitate the partition into fragments for further esperiments. In particular, the etching trenches were designed to allow to cleave the wafer manually into rectangular slides, fitting the tray of an inkjet printer as shown in figure 2.1c. Each slide can further be cleaved into squared chips, containing 625 microwells, aligned into a 25×25 matrix, as depicted in the SEM micrograph in figure 2.1d.

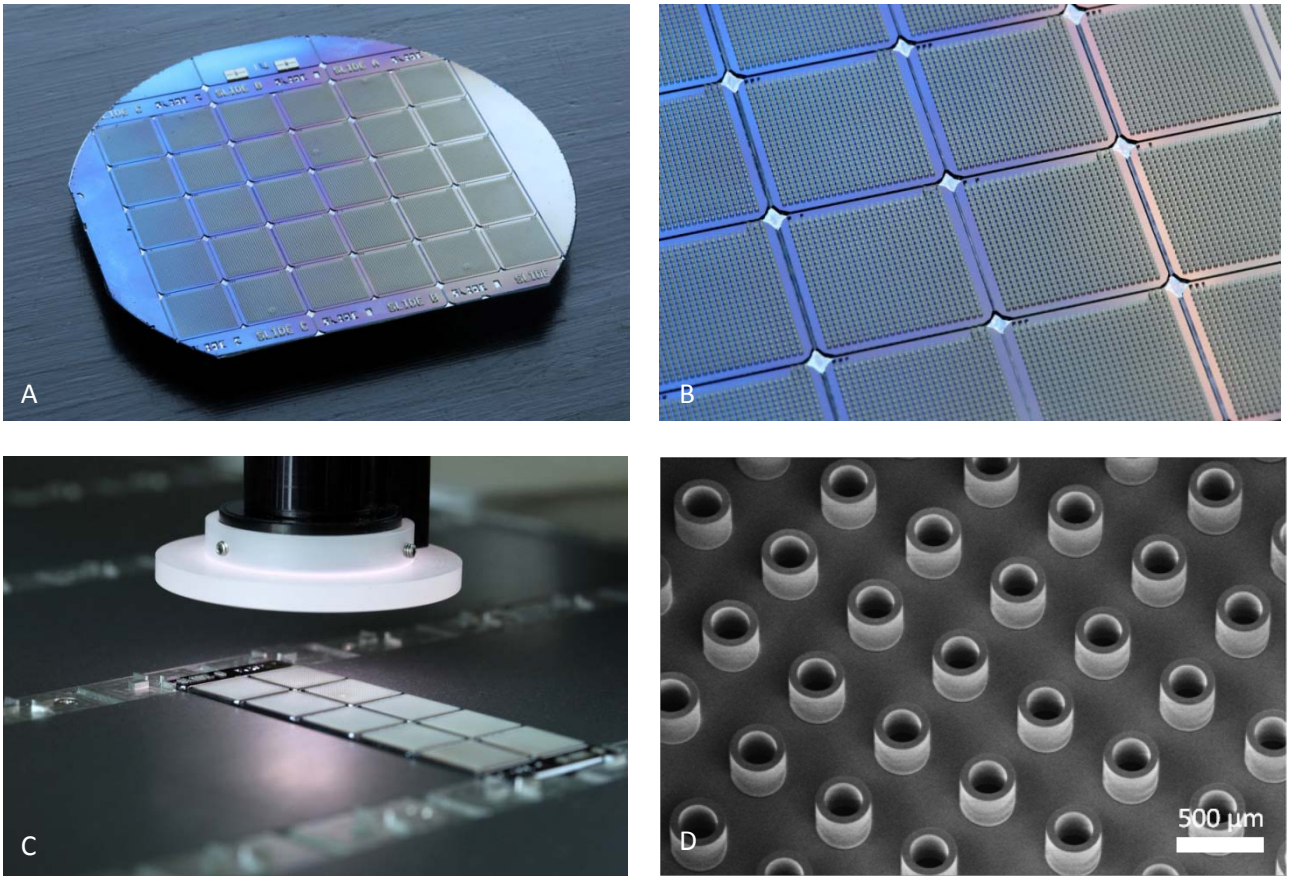

Fig. 2.1: (a) Silicon wafer etched with trenches, (b) zoom of trenches and squared chips with 625 containers, (c) silicon slide fitting the slots of an inkjet printer tray, (d) SEM micrograph of microcontainer arrays.

The fabrication process of SU-8 microwells is composed by two main steps. (I) Anisotropic etching is used to define trenches in a silicon substrate in order to obtain easy-breakable rectangular substrates fitting into the slots of the inkjet printer tray, (II) negative photolithography is used for the definition of the micro-wells. In figure 2.2 the overall fabrication process is schematically illustrated step by step.
On a silicon wafer an oxide layer (2 µm) was deposited by LPCVD (figure 2.2a). A positive photoresist (AZ 5214e) was spin coated on the front side and patterned by photolithography (figure 2.2b). Afterwards, the same resist was spin coated on the back side. The resist pattern on the front side and the back side layer acted as protective mask for the etching of the silicon oxide layer (BHF for 30 min) (figure 2.2c). The resist was then stripped and an anisotropic etching in KOH (4 h, 80 °C) defined the trenches for the aligned cleavage of the wafer after microwell fabrication (figure 2.2d). The remaining oxide layer was then removed in BHF (4 min) to improve SU-8 adhesion in the next fabrication step. For the container fabrication, a first layer of SU-8 2075 (thickness 35 µm) was spin coated (figure 2.2e) and selectively exposed to define the bottom of the microwells (figure 2.2f). A second layer (255 µm) of the same resist was spin coated and patterned (g). Finally, the uncrosslinked resist was developed in propylene glycol methyl ether acetate (PGMEA). The silicon wafer was cleaved along the trenches into rectangular slides (figure 2.2h). Slides sizes

are designed to fit into the slots of the inkjet printer tray, as depicted in the optical picture in figure 2.1c. Each slide contains ten squares, each having 625 containers (see figure 2.1a). The containers are aligned into a 25 × 25 matrix. Microwells are fabricated with cavity diameters of 50 µm, 100 µm, 200 µm, 300 µm corresponding to a cylindrical cavity volumes of approximately 0.5, 2, 8, 18 nL respectively. The width of the well walls is 50 µm and the center-to-center spacing is 450 µm for all wells.

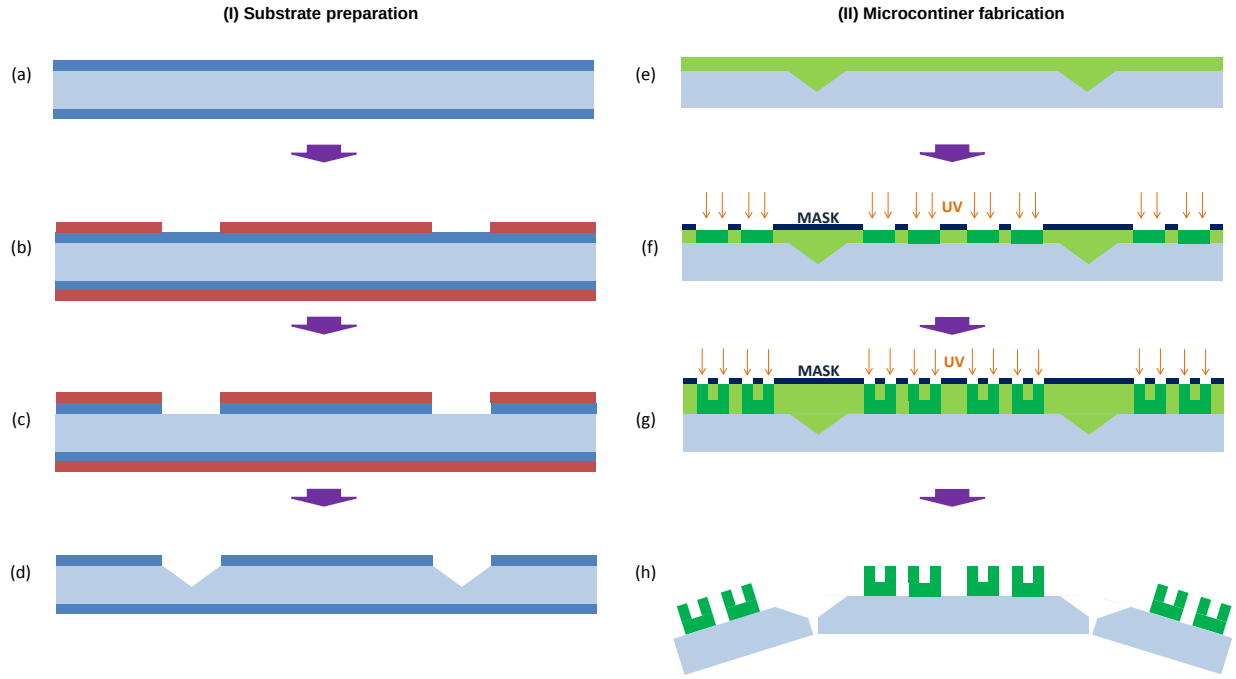

Fig. 2.2: Process flow for the fabrication of microcontainers on Si microscope slides: (a) LPCVD (2 µm) on silicon wafer; (b) photolithography with positive resist on the front side (2.2 µm), spin coating of the resist (2.2 µm) on the back side; (c) wet etching of oxide in BHF; (d) resist stripping and wet etching of Si in KOH; (e) SU-8 spin coating (35 µm), (f) selective UV exposure, (g) spin coating of second layer of SU-8 (255 µm) and masked exposure; (h) SU-8 development; chips are cleaved in microscope slides.

2.1.2 Microcontainers in PCL and PLLA

Poly(lactic acid) (PLLA) and poly(caprolactone) (PCL) are biodegradable polymers approved by FDA for oral dosage forms. Thus, these materials are eligible for microcontainer fabrication. This project has not dealt with the fabrication process described in this paragraph, but since feasibility tests on the drug loading of these devices were performed, it is worth to briefly discuss the technology used for their preparation, which was developed in the Nanoprobes group.

Many different techniques for polymer microstructuring exist, such as injection molding, micromilling, three dimensional printing, etching, laser cutting, laser writing, and embossing. The main criteria driving the choice for manufacturing of microcontainers were the simplicity and the potential for large production. Hot embossing has been considered one the most suitable methods for this purpose [15, 16].

The principle of hot embossing relies on thermoplasticity that is the ability of polymers of turning from stiff to pliable and moldable when a certain temperature, called glass transition temperature (T_g), is crossed. Above this temperature and up to the melting point, the polymer is in a rubbery state, and can be deformed and shaped with a mold if pressure is applied. The transition is often reversible, therefore when the polymer is cooled below T_g, it recovers the initial stiffness maintaining the shaped during the molding.

A polymer film is heated up to a defined temperature and a stamp is pressed onto the film, for a period of time. Finally, the polymer is cooled down and afterwards the pressure of the stamp is released. Important parameters for a good pattern transfer are the temperature, the pressure and the time of embossing. For

PLLA microstructuring, the embossing temperature was found to have a relevant influence on the shape of the microdevice. The T_g of PLLA is around 60°C and a good molding was obtained at 120°C. The glass transition of PCL occurs around -60°C and at room temperature the polymer is in rubbery state. The technical limitation of the available embossing tool did not allow to work at room temperature, therefore the embossing was performed close to the melting temperature (T_m=60°C). In this case the heating rate was very important because of the proximity to the melting point: the polymer melting must be avoided in order to have a complete release of the stamp from the polymer film. An optimal setting of 60°C at 5°C/min was found.
For any other steps subsequent to container fabrication, like for instance the drug loading, microcontainers should not be processed at temperatures higher than the polymer glass transition in order not to compromise the shape transferred by hot embossing.

2.1.3 Fabrication of glass masks

Glass masks were used to study the reaction of photocrosslinking of PVP solutions, which is discussed in chapter 5. The masks were fabricated by means of reverse photolithography, metal deposition and lift-off. Several designs of masks were produced, with circular pattern with different sizes and center-to center distance. The basic steps of the process flow are schematically shown in figure 2.3.
A pyrex glass 4 inch wafers was dipped in buffered hydrofluoric acid (BHF) bath for 60 sec to improve the adhesion of resist on glass in the next fabrication step. A positive resist (AZ 5214e) was spin coated (2.2 µm) on the front side (figure 2.3a), baked in oven at 90°C for 60 sec, and patterned by photolithography (49 mJ/cm^2) with a similar mask used for the fabrication of microcontainers (figure 2.3b). The wafer was then put on a hotplate at 120°C for 120 sec to activate the crosslinking of the exposed areas (figure 2.3c). Afterwards the resist was exposed to UV light without mask (figure 2.3d) and the resist previously not exposed is made soluble in developer in the following development step.
A thin cromium layer (100 nm) is then deposited by E-beam metal evaporation onto the wafer front side. Finally, the pattern with the metal coating on top was lifted off in acetone with ultrasound for 30 min (f) and the wafer was rinsed in a water bath for 3 min and then dried. In alternative to the initial pretreatment in BHF, the wafers can be put in an oven for 20 min at 250°C. The obtained mask is then diced into square chips for further utilization (figure 2.4).

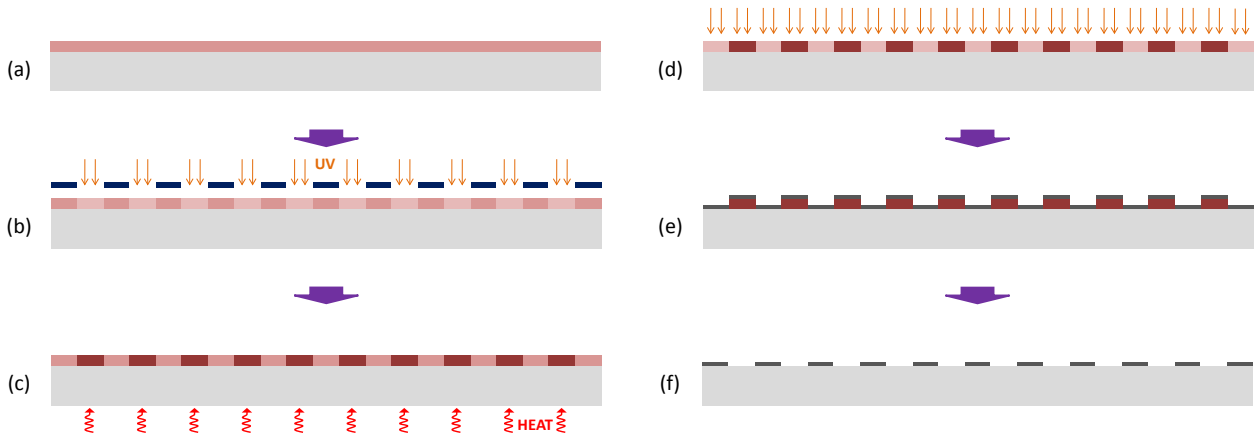

Figure 2.3: Fabrication process flow of glass masks. (a) Spin coating of positive resist (2.2 µm), (b) selective UV exposure, (c) inversal bake, (d) flood UV exposure, (e) development and E-beam metal deposition, (f) lift off in acetone.

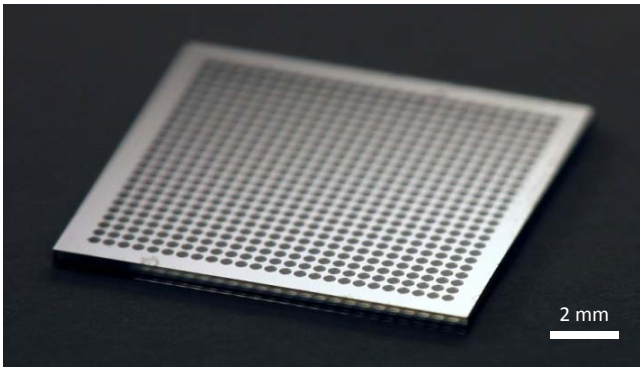

Figure 2.4: Image of diced square of glass mask chip (12.8×12.8 mm).

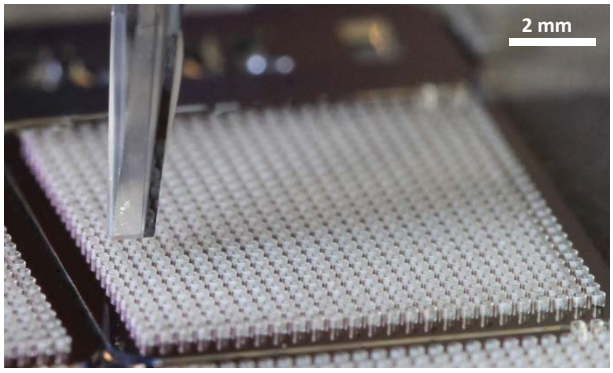

Figure 2.5: Image of a dispensing tip placed on top of an array of microcontainers.

2.2 Inkjet printing technology

2.2.1 Introduction

Inkjet printing is a familiar technology which originally was designed to transfer electronic data onto flexible substrates and overhead transparencies. Recently, more and more applications were investigated for this technology and versatile tools were developed to dispense accurate minute amounts of a broad range of materials for various manufacturing processes. Inkjet has become one of the most promising technologies in several fields. It has been employed for high precision deposition of polymers onto MEMS switches [17], metallic solders in micro-electronic soldering [18], and UV curable epoxy resins for micro-optical applications [19], representing a valuable mold-free manufacturing technique to fabricate large arrays of 3D micro-objects [20]. In these last years the use of inkjet printing has been extended to the fields of biotechnology and pharmacy, finding application in large screening of genomic material [21] for cell culturing [22, 23], for functionalization of Bio MEMS [24] and drug delivery [25-27]. The main advantage of this technique lies in the accuracy and throughput of fluids. Nano and picoliter droplets of liquid can be dispensed onto very precisely localized positions with high uniformity which makes this equipment capable of producing precise micro features [28, 29].

Inkjet operation can be fundamentally divided into two operations modes: continuous jet mode, and drop-on-demand mode (DOD). In continuous mode, a liquid is subjected to pressure and ejected through a nozzle; the main application of this mode is in graphics. In DOD mode the fluid jet is subjected to a pulsed perturbation which deforms the jet creating droplets. Martin and coworkers have described the physics of this operation in a very valuable publication [30]. The perturbation of the fluid jet is induced by stimuli of different physical natures: thermal, piezoelectric, electrostatic and acoustic.

In the following section the basics of the operating system used in this work are discussed with respect to its use as a loading method for microcontainers.

2.2.2 Equipment description and operations

In this work an inkjet printer (Nanoplotter NP 2.1, GeSiM, Germany) equipped with piezo-driven pipettes was utilized for the loading of microcontainers; a dispensing tip on top of microcontainers arrays is shown in figure 2.5. In the equipment in use the pipette aspires the liquid from a titer plate and dispenses the liquid by ejection. In the piezo driven-dispenser the fluid ejection is actuated by the deformation of the piezoelectric material in response to a voltage pulse: the change in volume of the piezo causes pressure waves in the fluid contained in the pipette, which results in a droplets being ejected from the orifice [31].

In piezo-driven injection, crucial properties for the liquid to be dispensed are viscosity, surface tension and density [32]. These fluid properties determine the formation mechanism, the shape and the size of the

liquid droplets formed by a voltage pulse. From a physical perspective fluid characteristics can be described by the dimensionless numbers: the *Weber number* (We), comparing inertial and capillary forces, and the *Reynolds number* (Re), comparing inertial and viscous forces. The *Ohnesorge number* (Oh) is another dimensionless number, which is defined as the ratio of the square root of the Weber number and the Reynolds number.

$$\mathrm{We} = \frac{\rho D \upsilon^2}{\gamma} \quad ; \quad \mathrm{Re} = \frac{\rho D \upsilon}{\eta} \quad ; \quad \mathrm{Oh} = \frac{\eta}{\sqrt{D \rho \gamma}} \tag{2.1}$$

Where υ is the average travel velocity of the sprayed droplet, ρ is the density, γ is the surface tension, η is the viscosity of the fluid in the nozzle and D is the characteristic dimension of the geometry (here the orifice diameter) respectively. Jang et al. [32] have studied the printability of fluids relating the *in situ* droplet formation dynamics to the dimensionless number Z, defined as the inverse of the Ohnesorge number. In that investigation, a good quality of printing was defined by the formation of a single droplet, positional accuracy, minimum stand-off distance and maximum allowable jetting frequency. A printable range fulfilling these requirements, was found to be $2<Z<14$. For the chosen test solutions (water and ethylene glycol), the most decisive parameter, influencing the Z value within the printable range, is viscosity. The viscosity limit for the printer used in this work is 5 mPa·s. In order to dispense more viscous liquids, it is possible to use heatable pipettes, in which the aspired sample can be heated up to 120°C. Further considerations on the importance of viscosity on inkjet printing of lipid based and polymer solutions will be discussed in chapter 3.
The most important operating parameters in the piezo-triggered inkjetting are voltage amplitude, width and frequency of the impulse generating the droplets. Typically droplet ejection speed and volume are linear functions of the applied voltage, while the dependency from pulse duration and frequency is more complex [33]. In this project, inkjet printing was used to dispense various solutions of the water insoluble drug furosemide, lipid based formulations, and solutions of PVP.

2.3 Supercritical technology

2.3.1 Principles of supercritical processing

A supercritical process is a technology which utilizes one or more chemical compounds above the critical point. In thermodynamics a critical point is defined as conditions in which the boundaries between phases in equilibrium disappear. Typically the vapor-liquid critical point is referred to, as it is the most broadly studied. When a substance crosses the critical point, gas and liquid merge together in a homogeneous phase characterized by a density close to the liquid, and viscosity, thermal conductivity, interfacial tension and diffusivity similar to a gas. In figure 2.6 the phase diagram with the supercritical state is illustrated (from [34]). A fluid above its critical pressure and temperature is called supercritical (sc). By virtue of these properties, the use of sc fluids has been widely explored in the field of pharmaceutical technology. The liquid-like solvent properties are beneficial in drug solubilization, polymer plasticization, and extraction of solvent and impurities, while the gas-like behavior enhances mass transfer, promoting extraction or reaction selectivity. A further advantage of sc state is the high compressibility of fluid near the critical region, which enables to tune the solvent power of the fluid within microseconds by a simple change of pressure or temperature. For most of polar chemicals, the transition to supercritical state occurs at high temperatures, which makes it prohibitive for pharmaceutical manufacturing. In this work supercritical carbon dioxide was used as a solvent to impregnate a model hydrophobic drug in a polymer matrix previously fixed inside microcontainers by inkjet printing. In this process the drug is first solubilized in the sc fluid and then impregnated into the polymer. The dissolution in supercritical CO_2 is a crucial step for this

application, and therefore it is worth to mention the conditions required to accomplish $scCO_2$ assisted impregnation.

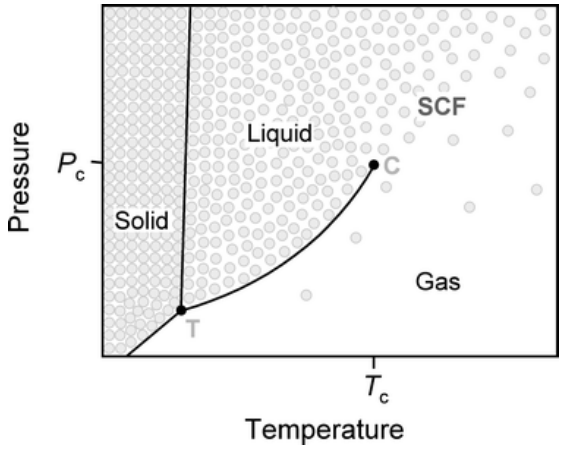

Figure 2.6: Schematic pressure–temperature phase diagram for a pure component showing the supercritical fluid (SCF) region (from [34]).

2.3.2. Solubility of active ingredients in supercritical carbon dioxide

Carbon dioxide is probably the most widespread chemical used at supercritical conditions in the pharmaceutical field. There are indeed many properties that make it a particularly attractive solvent, including non flammability, low toxicity, limited cost and environmental compatibility. The critical point of carbon dioxide is 73.8 bar at 31.1 °C. These are favorable conditions for the treatment of many thermolabile drugs. However, many drug substances and excipients exhibit low solubility in supercritical CO_2. Despite its non polar properties, it is often the case that supercritical carbon dioxide is a poor solvent for many lipophilic molecules at pressures lower than 500 bar. There are though a large group of class II and IV drugs which have a discrete solubility in CO_2 at moderate pressures. In a very interesting publication about sc fluids in drug product development [35], Panza and Beckman have identified the necessary properties for a compound to be soluble and miscible with CO_2 at moderate pressures. The characteristics for $scCO_2$-philic compounds are summarized in Table 2.1.

Table 2.1: Important characteristics for CO_2-soluble compounds (adapted from [35])

Characteristic	Importance	Reference
Electron-donating functional groups	Specific solute-solvent interaction (Lewis acid/base interactions, CO_2 electron acceptor)	[36-38]
Electron-accepting functional groups	Specific solute-solvent interaction (Lewis acid/base interactions, CO_2 electron donor)	[39]
Polarity/partial dipoles	Interact with the quadrupole moment of CO_2	[40-42]
Molecular architecture	Free volume and flexibility as indicated by low glass transition temperatures	[40, 42-45]
Low surface tension	Weak intramolecular interactions more significant than compound-CO_2 interaction	[38]
Balance between entropy and enthalpy of mixing	A point of diminishing return will be reached (too many favorable interactions leads to unfavorable entropy)	[38, 44, 45]

The first important property is the presence of functional groups which can interact with the CO_2 molecule by electron-donor groups (like carbonyl groups) or electron-acceptor groups (like Lewis bases).
Although carbon dioxide is a non-polar molecule, its reciprocally neutralizing dipoles can interact with other compounds. Therefore, a substance eligible for dissolution in CO_2 should contain some polar character [36, 38, 39]. Regarding the molecular structure, large molecules, especially polymers, must exhibit large free volume with a high degree of flexibility which means a low glass transition temperature [40, 42].
Another feature for solubility in CO_2 deals with having a low surface tension i.e. a low cohesive energy density close to the one of CO_2. This means that the solute should not have strong interactions with itself due to hydrogen bonds, or Lewis acid/base or polar molecular bonds.
Finally, interactions with CO_2 are favoured in presence of a balance between enthalpy and entropy in the mixing. The presence of many interaction sites in the molecule reduces the enthalpy of mixing. However, too many hinders the increase of solution entropy, "freezing" the mixing inward CO_2 [44, 45].
The solubility of solid solutes in supercritical fluids depends on temperature, pressure and eventual cosolvent concentration. In the regions below the critical point, the solubility initially decreases with increasing pressure, reaching a minimum, and then rises rapidly in the region of the critical pressure [46]. In supercritical conditions, the solubility, at constant temperature, is an increasing monotonic function of pressure. At isobaric conditions the dependence of solubility on temperature follows a more complex behavior. For pressures below a certain pressure P_L^*, called *lower crossover pressure*, and above P_U^*, *upper crossover pressure*, the solubility increases with temperature. On the contrary, between $P_L^*$and P_U^*, the solubility decreases with temperature. This is explained by the rapid decrease of the fluid density [47]. The overall phenomenon is due to competing effects of temperature. On one hand, a rise in temperature causes a density decrease and a consequent reduction in the fluid solvent power. On the other hand, a temperature rise produces an increase of the sublimation pressure of the solute, i.e. a higher volatility, which results in a higher solute molar pressure in the fluid. When the fluid pressure is equal to P_L^*or P_U^*, these competing effects balance each other, and the solubility isotherms intersect. The influence of temperature on solubility will be also deepened in chapter 4, with respect to the loading efficiency.
As previously stated, $scCO_2$ is far from being a super-solvent for hydrophobic APIs. Nevertheless, several solutions have been investigated to overcome this major limitation. Three methods have been developed: use of surfactants, use of cosolvents, and covalent modification of the insoluble compounds this so called CO_2-philic "pony tails"[35].
The use of surfactants as solubilization enhancers is widely spread in pharmaceutical research. In the case of CO_2, the surfactant is composed by a CO_2-philic segment interacting with the CO_2 and by a CO_2-phobic segment that can be chosen among the compounds most akin to the solute to be dissolved. Several CO_2-surfactants have been created based on fluorinated polymers, silicon-based chemicals and CO_2-philic hydrocarbons [48-51]. Also, CO_2-surfactants have been synthesized for emulsification of large biomolecules like proteins and enzymes in $scCO_2$. Johnston and colleagues [52] successfully included bovine serum albumin (BSA) in water-in-CO_2 microemulsions. Ghenciu *et al.* extracted a protein from a cell culture media, preserving most of its biological activity [53]. Holmes and coworkers showed enzyme reactivity in water-in-CO_2 microemulsions [54].
The addition of cosolvents to CO_2 is another strategy which potentially extends the use of this technology to a larger number of substances which dissolve in organic solvents but not in $scCO_2$. The enhancement of solubility of many APIs by means of this method has been widely studied [55-58] and in some cases it has brought relevant advantages. While the presence of a second solvent (generally an organic solvent) facilitates the dissolution into CO_2, it also modifies the physico-chemical properties of the supercritical fluid, in particular the density and diffusivity, which could entirely counterbalance the benefits accrued with the use of supercritical conditions. The use of certain cosolvents could also compromise the intrinsic advantages of non flammability, ecological sustainability and cost-effectiveness of the process.
A less explored solution to dissolve essentially insoluble substances into CO_2 is the modification of the compound by covalent attachment of CO_2-philic functional groups. Ghenciu and Beckman [59] have synthesized a high affinity CO_2-surfactant, chemically bonded to biotin, for the extraction of avidin. In that

work an emulsion encapsulating the protein was created in the CO_2 phase, and then the protein was recovered by stripping liquid CO_2, with a continuous removal of the biotin-avidin complex. Similarly, Panza *et al.* [60] covalently attached a CO_2 amphiphilic molecule to a coenzyme, proving that after extraction of an enzyme in the supercritical phase, the biocatalytic action of the compound was still functional.

2.3.3. Supercritical impregnation

Polymers frequently require impractically high pressure to dissolve in CO_2. Therefore, the absorption of CO_2 in polymers is often much more feasable. Supercritical CO_2 is a well known impregnating agent for many materials of pharmaceutical and biomedical interest: poly(methyl methacrylate) (PMMA) [61, 62], poly(dimethylsiloxane) (PDMS) [63, 64], poly(lactic-co-glycolic) acid (PLGA) [65], hydroxypropyl methylcellulose (HPMC) [66], poly(ethylenglycole) (PEG) [67] polyvinylpyrrolidone (PVP) [68, 69], polycaprolactone (PCL) [70, 71], polylactide acide (PLA) [72], chitosan [73, 74], cyclodextrins [75], just to cite the most known.

The mechanism of supercritical impregnation of polymers consists of three physicochemical steps, as suggested by Kazarian *et al* [35]: i) the solubilization of the solute in the supercritical CO_2, ii) the swelling of the polymer matrix by supercritical solution and the introduction of the solute in the polymer, and iii) the polymer deswelling by CO_2 depressurization fixing the solute in the matrix. The good success of the operation depends on the mutual molecular interaction between solute, polymer and supercritical fluid. In particular, the solute must form a stable solution with CO_2 but at the same time have a strong affinity to the polymer, in order to be incorporated in the matrix and not being extracted when the fluid is removed. In this sense, the limited solubility of certain compounds in CO_2 can reveal itself an advantage. Moreover, the polymer must be swelled by $scCO_2$ but should not be dissolved, in order to avoid its removal during the fluid depressurization. All these constraints determine the suitability of the abovementioned materials, and limit the operation ranges of pressure and temperature for the impregnation.

The effects of CO_2 absorption in polymers are various: volumetric expansion [76], decrease of density and increase of porosity [77, 78], change of intrinsic diffusion coefficient [79, 80] and depression of T_g and T_m, with possible transitions to rubbery state and liquid state respectively [80]. This fact entails often significant changes in viscosity and surface tension of the polymer. Gerhardt and coworkers [81] have measured, by means of an extrusion rheometer modified for high pressure operations, the shear viscosity of CO_2-swollen PDMS melts. They discovered that the absorption of CO_2 resulted in a dramatic decrease of viscosity of nearly one order of magnitude. In the case of liquid polystyrene (PS), it was observed that CO_2 uptake induced a decrease in surface tension on pendant droplets [82]. All these results clearly reveal that dense CO_2 acts as effective plasticizers for polymers, increasing the free volume of chains and enhancing their mobility. Besides the pressure and temperature of CO_2, the swelling of a polymer (or likewise the solubility of CO_2 in a polymer) depends on intrinsic properties of the material, where polymer molecular weight [68] degree of crystallinity [76], degree of crosslinking [83] are the most important ones.

2.4. Drug dissolution measurements

2.4.1. Dissolution

The dissolution speed of the active ingredient in the physiological fluid is an extremely important feature of a pharmaceutical product because it affects the time at which the therapeutical agent reaches the target.

Dissolution is a kinetic property and the dissolution rate is the speed with which the drug is released from the delivery device to the solvent. Dissolution rate depends both on the physicochemical properties of the formulation and solvent compositions, and on the hydrodynamic regime in the dissolution medium, besides the physico-chemical properties of the drug delivery systems, as discussed in section 1.2. *In vitro* dissolution tests are used as a preliminary study, which should mimic what happens *in vivo*, where the drug is supposed to be released in the gastrointestinal tract. Several apparatuses are available for dissolution studies; the United States Pharmacopeia (USP) suggests different experimental methods and setting

according to the dosage form (tablets or capsules) and the hydrodynamic conditions [84, 85]. The dissolution apparatuses have different designs, and consequently different hydrodynamics. An important role is also attributed to agitation speed, solvent viscosity as well as volume and geometry of the vessel where the dissolution takes place [84, 86]. Within the intestine, there are various flow velocities, depending on the distance from the mucosa and this is a phenomenon difficult to simulate *in vitro* [87]. Nevertheless, dissolution results are still important to give indicative information about the drug dissolution behaviour for the *in vivo* performance. The dissolution tests presented in this thesis were performed with commercial dissolution equipment, which did not aim to provide information relevant for *in vivo* simulation, but to study the drug dissolution compared to other formulations.

2.4.2 Dissolution equipment: µDISS profiler

A µDISS Profiler™ (Pion, USA) is a dissolution apparatus for the detection of concentration of drugs, down to µg/mL. A photograph of the equipment is shown in figure 2.7a. The dissolution vessels, schematized in figure 2.7b can contain up to 20 mL. The instrument can measure up to six simultaneous dissolutions of occuring in respective vials. It has been shown that a µDISS profiler can be used for testing the dissolution behaviour and obtaining the dissolution rate of drugs [88]. A µDISS profiler has previously been used to evaluate apparent solubility and dissolution rate of poorly soluble drugs. The only requirement for the drug is a strong chromophore, detectable also in small concentration [88, 89]. The solute concentration is measured by means of in situ fiber optics UV probes as shown in figure 2.7b. The light beam is directed in the liquid through a slit of different width (0.5 mm in this study) and reflected from a mirror at the edge of the probe. Thus, the radiation passes through a layer with liquid gap equal to the double of the slit (i.e. 1 mm). The absorption spectrum of the solute is shown in real time with an acquisition time ranging within 50-100 ms. A wavelength between 200 and 780 nm can be selected, and the corresponding intensity in the absorption spectrum is translated to a concentration value. A rotation speed of 100 rpm and a temperature of 37°C were set during the dissolution experiments. Before each measurement, a calibration curve is carried out for each probe, with 20 concentration points.

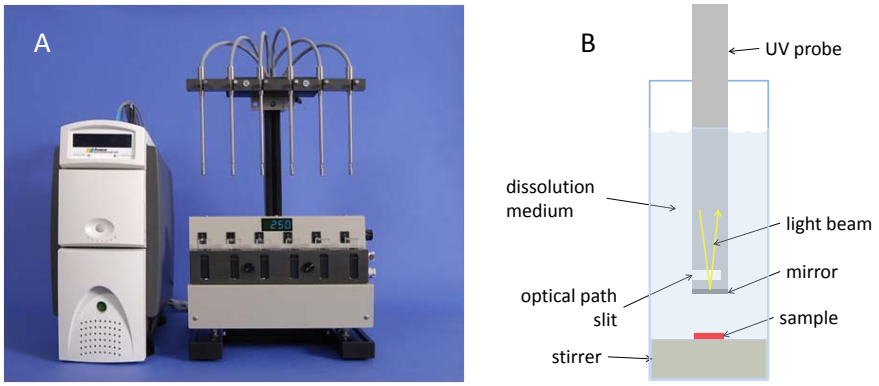

Figure 2.7: (a) Picture of the dissolution apparatus µDISS™ Profiler; (b) schematic of a dissolution vessel with a measuring probe immersed.

2.5. Solid state characterization

As discussed in section 1.2.1, the solid state of a formulation is an essential feature with regards to drug solubility and dissolution rate. When employing the amorphous form of a drug, it is necessary to monitor the stability of the drug over time, as it tends to recrystallize. It is often necessary to combine several methods of solid state analysis in order to have a complete characterization of the sample.

2.5.1 X-ray Powder Diffraction

The diffraction of X-ray (XRPD) provides important understanding of the crystalline structure of the formulation, and characterization of crystal lattice properties. However, this technique does not give information about the chemical composition of the sample [90, 91]. XRPD is a non-destructive method, where a small quantity of sample is required (few milligrams), and can be used both for qualitative and quantitative purposes [92, 93]. The beam penetration is estimated to be in the range of hundreds of microns [94, 95] and the presence of minimum 5% of non-crystalline material in the sample can be quantified. In this study, X-ray diffraction was used to investigate the solid state of the drug inside microcontainers after loading. The analyses were performed using an X'Pert PRO X-ray diffractometer (PANalytical, Almelo, The Netherlands), equipped with a Cu KR anode (λ = 1.541 Å;45 kV; 40 mA).

2.5.2 Raman spectroscopy

In Raman spectroscopy monochromatic radiation is projected on the sample, and an inelastic scattering is produced. The difference in energy between the incident and the scattered light results in a characteristic Raman shift [90, 96]. The nature of the scattering depends on the chemical structure of the sample, and two cases can occur: the irradiated light is scattered back with the same wavenumber (Rayleigh scattering), or with a different wavenumber (Raman scattering). In the Raman scattering the wavenumber of scattered radiation can be higher than the incident one (anti-Stokes scattering), or more often lower (Stokes scattering). The difference in wavenumber corresponds to a transition in the vibrational energy of the molecule and this occurs if there is a change in the electron polarisability of the analyte [97, 98]. For drug solid state analysis Raman scattering represent a powerful tool, since typical functional groups of drug molecules are good Raman scatterers.

Raman spectroscopy is a non destructive method, and offers the advantage of analyzing samples of small dimensions. The sample volume submitted to radiation exposure is few cubic microns. The transparency of glass and water allows to avoid the distortion of the signal, and to perform experiments in aqueous environments, e.g. to perform measurements of crystal precipitation during dissolutions [90]. The exposure of small sampling areas to radiation entails nonetheless unwanted effects like local heating, photo bleaching and fluorescent emissions, which may considerably affect the results. To amend this inconvenience, it is possible to choose among several excitation wavelengths and filters [91].

In this study, Raman spectroscopy was used to elucidate the presence of interaction of the drug with excipients after the loading. For the analyses descrbed in this thesis, were performed with DXR Raman microscope (Thermo Scientific, Germany) equipped with a frequency-stabilized single mode diode laser (780 nm).

2.5.3 Attenuated Total Reflection Infrared Spectroscopy (ATR-IR)

In IR spectroscopy, the radiation is absorbed in the sample, generating intramolecular vibrations. A transition from a ground state to a fundamental mode occurs at fundamental frequencies, which are characteristic for each bonds and functional goups, allowing the identification of the chemical structure of the sample, and eventual molecular interactions between components.

The advantages of IR spectroscopy in an enhanced spatial resolution, which allows the detection of smaller particle sizes, often occurring in pharmaceutical formulations. The potential of applications of ATR-IR imaging for polymeric materials of industrial interest was illustrated recently [99, 100].

The ATR-IR is a non destructive method requiring a small amount of sample, which can be in form of powder, paste, or liquid. The sample is placed in contact to a refractive crystal, and pressed onto it by means of a torque wrench. A good contact between the sample and the crystal is very important in order to obtain a reliable FT-IR image. Reflection IR imaging requires a very flat and smooth surface of the sample in order to produce a good signal-to-noise ratio (SNR) within a reasonable acquisition time. In ATR mode, infrared light is directed through a high refractive index material (the ATR crystal) and is totally internally reflected at the interface between a sample and the crystal. At this interface, the electric field of the IR light penetrates into the sample as an evanescent wave, which causes an attenuation effect on the incident wave. The attenuated radiation is detected in form of an IR spectrum (usually called the ATR-IR spectrum).

The typical penetration dephts of the evanescent wave travel in the analysis of a pharmaceutical or polymeric sample range from 0.2 μm to a few micrometers [101]. In this work, IR spectroscopy was used to study the chemical interactions of the drug after the loading. For the analyses a Spectrum100 spectrometer was used (Perkin Elmer, Germany) equipped with an MIR source and a TGS detector.

2.6. Hydrogel characterization and imaging

Hydrogels obtained by photocrosslinking are used in oral drug delivery as carriers for poorly soluble drugs and fragile biomacromolecules. An important feature of polymeric hydrogels is that they absorb large volumes of water, modifying their nanoscopic structure. They can be designed for drug delivery purposes, as they can release the APIs in a controlled manner. This is particularly interesting for drugs requiring a prolonged release, like for instance insulin. The correlation between drug release kinetics and mesh size of hydrogel network has been extensively elucidated [102-105]. Hence it is important to control the crosslinking density in a polymer network for a controlled release device. In this section, different methods for hydrogels characterization are discussed which will be used in chapter 5 to investigate their mechanical and the structural properties. The first group of methods investigates the nanometric structure of the material addressing the estimation of mesh size of the polymer network. To this group belong rotational rheometry and nuclear magnetic resonance. A second group of techniques were utilized for imaging and size measurement of gel micropatterns obtained by selective photocrosslinking of polymer films. For this purpose optical and contact profilometry, confocal microscopies as well as environmental scanning electron microscopy (e-SEM) were used. For rheometry and NMR spectroscopy, a deeper theoretical background was included in the respective introductive sections due to the complexity of the measured physical variables and for a more complete understanding of physical and numerical models used in the data treatment.

2.6.1 Rheological characterization of hydrogels

Rheology is the science that studies mechanical behaviour of fluids and correlates it with its structural properties. In detail the topic of the study is the *deformation* γ of a material, liquid or solid, under the action of an applied stress τ in flow conditions [106]. Rheometry refers to the experimental techniques used to determine the rheological properties of materials. From the mechanical response of the material, the structural properties of complex systems, like for instance dispersions, emulsion and gels, can be elucidated by means of elaborated theories and models. In particular for gels, the combination of measurements and modeling can reveal the *mean mesh size* of the polymer network.

In this work, the rheological characterization was performed by a rotational rheometer HAAKE Rheostress RS-150™ (at the University of Trieste) equipped with a set of sensors with different geometries designed to stress the samples with different shear strains. Additional tests were performed at the Department of Chemical Engineering (DTU) with the PhD student Kaustav Goswami. A stress controlled rheometer was used (AR2000, TA Instruments), equipped with 25 mm parallel plate geometry.

In a rheometer, a magnetic field applies a torque T to a rotating probe (rotor) put in contact with the sample (see figure 2.8). The sample is placed in between the rotating probe and a steady plate. The available geometries are parallel plates for high viscous samples, and cone-plate for low viscous samples. As the rotor is put in motion, the resistance of the material to the flow produces a displacement of the rotor in respect to the applied torque, which is recorded by the instrument.

Given the softness of the gels under investigations, a parallel plate geometry was used in this work, with a rotor 20 mm in diameter and milled surface in order to minimize the slippage phenomena. The parallel plate geometry is designed to measure rheological properties of *non-Newtonian fluids* and for the characterization of *viscoelastic* materials. However, when using a rotational measuring system, special attention must be paid in order to limit systematic errors during the operative phase [107]. The commonest sources of errors are listed below.

- *Inertial effects*: at high shear rate, secondary fluxes occur within the sample lead to an overestimation of the viscous properties and, as consequence, the resulting torque moment is higher than real. This is an artifact not related to the rheological properties.
- *Geometrical effects*: when an excessive amount of sample is placed, asymmetric edge effects are generated; others error can be generated by misalignment resulting in acentric rotation, and vertical oscillations of the rotor.
- *Instability effects*: the applied torque is too high and produces a fracture in the material, resulting in loss of adherence, slippage, and loss of the sample by centrifugal forces.
- *Shear heating*: due to energy dissipation, a non uniform temperature field can be present inside the gap.

In order to ensure more consistent environmental conditions and to limit the evaporation, a glass bell (solvent trap) was used to cover the measuring device in all the experiments (see figure 2.9).

Figure 2.8: Parallel plates system. The rotor and the plate surface have a milled surface to improve the contact with soft materials.

Figure 2.9: The rotational rheometer HAAKE Rheostress RS-150™ equipped with a solvent trap.

2.6.1.1 Stress sweep tests

In the stress sweep test (SS) the *storage modulus* G' (also known as elastic modulus) and the *loss modulus* G" (also called viscous modulus) are measured as a function of the applied stress. The first is related to the elastic energy stored in the material upon deformation, the second to the energy dissipation due to internal viscosity of the fluid. In the SS test the stress is applied with a sinusoidal pulse, with a constant frequency *f* (1Hz) and increasing amplitude. The strain γ, shear rate $\dot{\gamma}$ and stress τ are related to the following equations:

$$\gamma = \gamma^0 \sin(\omega t) \quad (2.2)$$

$$\dot{\gamma} = \gamma^0 \omega \cos(\omega t) = \dot{\gamma}^0 \cos(\omega t) \quad (2.3)$$

$$\tau = \tau^0 \sin(\omega t + \delta) = \tau^0 \cos\delta \cdot \sin(\omega t) + \tau^0 \sin\delta \cdot \cos(\omega t) \quad (2.4)$$

where ω is the angular frequency or pulsation ($\omega=2\pi f$), δ is the phase shift between stress and deformation while γ^0 , τ^0 and $\dot{\gamma}^0$ are the maximum strain, stress and shear rate during oscillation motion, respectively. The first term of equation (2.4), $\tau^0 \cos\delta \cdot \sin(\omega t)$, is in phase with the strain to the elastic component, while the second $\tau^0 \sin\delta \cdot \cos(\omega t)$, is in phase the shear rate. In the limiting cases $\delta=0$ and $\delta=\pi/2$, we get the purely elastic or purely viscous behaviours, respectively.

$$\tau = \tau^0 \sin(\omega t) = G\gamma^0 \cdot \sin(\omega t) \quad \text{(for } \delta=0\text{)} \quad (2.5)$$

$$\tau = \tau^0 \cos(\omega t) = \eta\dot{\gamma}^0 \cos(\omega t) \quad \text{(for } \delta=\pi/2\text{)} \quad (2.6)$$

where G is the shear modulus and η the viscosity. Equation 2.4 can be rewritten by introducing the viscoelastic quantities G' and G":

$$\tau = G'\gamma^0 \cdot \sin(\omega t) + G''\gamma^0 \cdot \cos(\omega t) \quad (2.7)$$

From equation (2.7) the stress τ can be expressed with a contribution in phase with the deformation and one in square phase with it, and with the storage modulus G' and the dissipation modulus G" as the respective weights of these contributions.

2.6.1.2 Plate-stage gap determination: short stress sweep (sSS) tests

In rheometry, the placement of the sample on the plate is a very important step. Accordingly, in the case of systems that cannot be spread on the lower plate of the rheometer (this usually happens for gels), the system is first cut in a disc matching the rotor geometry, and the rotor is moved down until it gets in visible contact with the sample. A bad contact often results in a false value for the moduli (typically lower than real), and a rotor too close to the stage can squeeze the sample causing internal fractures, which compromise the measurement and the integrity of the material. The determination of optimal plate-stage distance is carried out by short stress sweep tests, gradually reducing the gap, and performed within the linear viscoelastic region, generally at τ=1 Pa and *f*=1 Hz, in order to avoid irreversible modification of the sample. The sequence of sSS starts with a large gap, and proceeds until a maximal value for G' is reached and further changes produce a change lower than 10% of the maximal value. Then the gap obtained with this procedure is kept constant for all the further tests. A plot of elastic moduli measured at different gaps is shown in figure 2.10, for a gel 20% PVP in water.

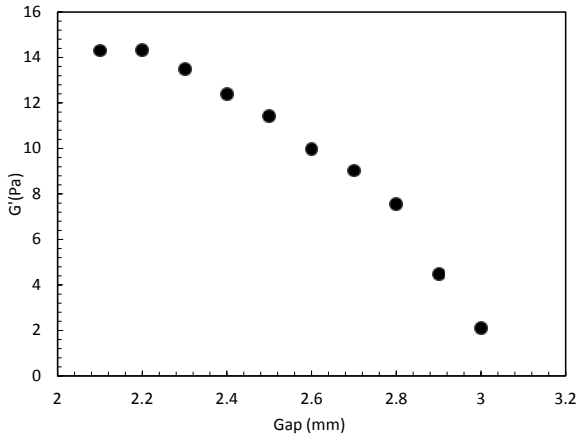

Figure. 2.10: Values of elastic modulus G' measured at different plate-stage gaps (sSS test on a gel PVP 20%).

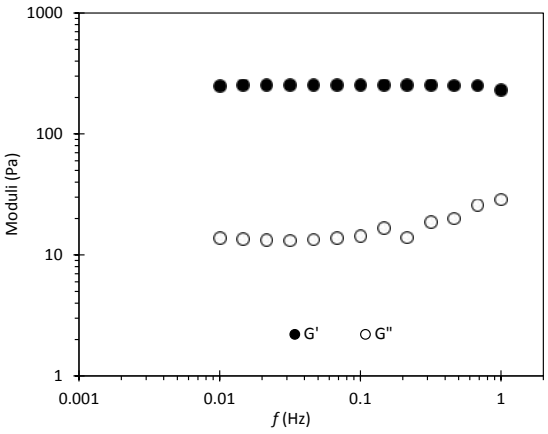

Fig. 2.11: Typical mechanical spectrum of a strong gel (PVP 20% in water).

2.6.1.3 Frequency sweep tests

The frequency sweep tests (FS) consists in the application of a sine wave stress, with constant amplitude and variable frequency usually in the range 0.01-100 Hz. The stress amplitude value is chosen within the linear viscoelastic region. The plot of G' and G" versus frequency are typically called *mechanical spectra*. In figure 2.11 a typical mechanical spectrum of a gel is shown. In a gel mechanical behaviour is characterized by having a G' not depending on the frequency, and a G" showing a bending. A strong gel, in general, exhibits a G' higher than G" of more than a decade being both G' and G'' frequency independent [106]. In a FS test, when the applied deformation lasts longer than the time necessary to the structure to relax (relaxation time λ), the time frame is long enough for the material to respond as a viscous-like system to

the applied stress. On the opposite side, with a deformation time shorter than the relaxation time, the elastic reaction is more pronounced.

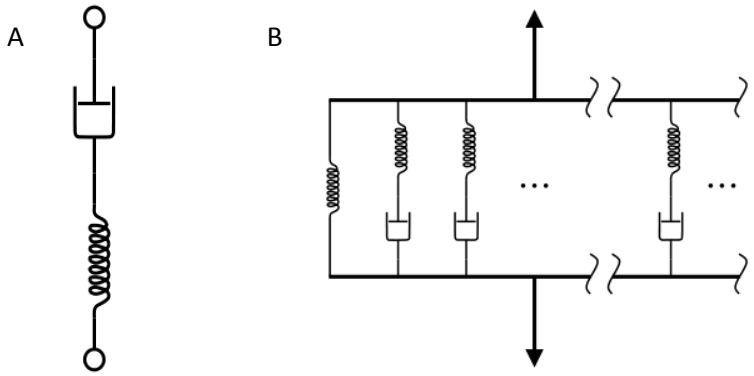

Fig. 2.12: (a) Maxwell element; (b) several Maxwell elements put in parallel with a pure elastic element.

2.6.1.4 Correlation models

Several models are used in theoretical rheology to describe the viscoelastic behaviour of fluids. Regarding interpretations of mechanical spectra, the most popular theory is the Maxwell´s model. According to this theory, a reaction of viscoelastic materials to stress, can be schematized by a dashpots and a spring in series (see figure 2.12a). This physical approximation, is described by the following equation (2.8):

$$\tau + \frac{\eta}{g}\frac{\partial \tau}{\partial t} = -\eta\dot{\gamma} \tag{2.8}$$

where τ is the stress, γ is the deformation, t is the time, η is the dashpot viscosity, g is the spring constant and $\lambda=\eta/g$ is the relaxation time. The solution to the equation (2.8), in case of sin wave deformation, $\gamma = \gamma^0 \sin(\omega t)$, leads to a stress defined as equation (2.7) $\tau = G'\gamma^0 \cdot \sin(\omega t) + G''\gamma^0 \cdot \cos(\omega t)$, where:

$$G'(\omega) = \frac{g(\lambda\omega)^2}{1+(\lambda\omega)^2} \tag{2.9}$$

$$G''(\omega) = \frac{g\lambda\omega}{1+(\lambda\omega)^2} \tag{2.10}$$

Equations (2.9) and (2.10) can be plotted as a function of ω in a bilogarithmic scale, and the point where the plots intersect each other is given by $\omega=1/\lambda$, corresponding to the maximal value of G". Generally the mechanical response of a viscoleastic material needs a more complex model. For this purpose, *n* Maxell elements can be combined in series (see figure 2.13b) building the so called *generalized Maxwell model*. Each element is characterized by a relaxation time λ_k, and a viscosity η_k (or, alternatively, the storage moduli $g_k = \eta_k/\lambda_k$). The moduli expressions result in:

$$G'(\omega) = \sum_{k=1}^{n} \frac{g_k(\lambda_k\omega)^2}{1+(\lambda_k\omega)^2} \tag{2.11}$$

$$G''(\omega) = \sum_{k=1}^{n} \frac{g_k\lambda_k\omega}{1+(\lambda_k\omega)^2} \tag{2.12}$$

In this model, a pure elastic element (a spring), G_E, can be added besides the Maxwell elements. This element represents the asymptotic limit reached at low frequency, and is an element with infinite

relaxation time. The function $g_k(\lambda_k)$ is called *relaxation spectrum.* This model will be used to fit the mechanical spectra of gels. The parameters obtained from this fitting, will be used to estimate the average mesh size of the polymer network in the gel.

2.6.1.5 Estimation of average mesh size from rheological studies

As mentioned in the beginning of section 2.6, an important feature of a polymeric gel network, is the density of crosslinks, ρ_x, defined as the number of polymeric inter-chain junctions per gel unit volume expressed in moles. The crosslink density determines the diffusive properties of the gel and therefore the capability of releasing a loaded drug ina a controlled manner. In this sense, the rheological characterization is an important tool, as it allows to have a precise estimation of the average mesh size of the gel network from the values of the mechanical moduli as a function of the applied stress. From the Flory´s theory [108], a non compressible crosslinked gel subjected to swelling and deformation in the linear viscoelastic region, the shear modulus G is equal to one third of the Young modulus E [109], can be estimated from the sum of the Maxwell elastic element constant g_k +G_E:

$$G = G_E + \sum_{k=1}^{N} g_k \tag{2.13}$$

In turn, always relaying on the Flory´s theory, the gel crosslink density ρ_x can be estimated [108]:

$$\rho_x = \frac{G}{RT}\left(\frac{\nu_p}{\nu_{p0}}\right)^{\frac{2}{3}} \tag{2.14}$$

where R is the of ideal gas constant, T is the absolute temperature, while ν_{p0} and ν_p are, respectively, the volumetric polymer fraction in the reference conditions (after crosslinking) and in the rheological measurement conditions (after swelling in water). ν_{p0} can be evaluated on the basis of the polymer mass fraction, c_{p0}, in the crosslinking solution. Indeed, we have:

$$c_{p0} = \frac{m_p}{m_p + m_{H2O}} = \frac{\rho_p V_p}{\rho_p V_p + \rho_{H2O} V_{H2O}} \tag{2.15}$$

where m_p and m_{H2O} are, respectively, polymer and solvent mass while and ρ_p and ρ_{H2O} are, respectively, polymer and solvent density. At the same time, the following relation holds:

$$\nu_{p0} = \frac{V_p}{V_p + V_{H2O}} = \frac{m_p/\rho_p}{m_p/\rho_p + m_{H2O}/\rho_{H2O}} \tag{2.16}$$

From equation (2.15) we can find a relationship for V_p (polymer volume) as a function of c_0:

$$V_p = \frac{\rho_{H2O}}{\rho_p} \cdot \frac{c_{p0}}{1 - c_{p0}} V_{H2O} \tag{2.17}$$

Putting (2.17) into (2.16) we obtain an equation for ν_{p0}:

$$\nu_{p0} = \frac{1}{1 + \frac{1 - c_{p0}}{c_{p0}} \frac{\rho_p}{\rho_{H2O}}} \tag{2.18}$$

Upon gel swelling due to water absorption, the polymer volume fraction ν_p will decrease from its initial value ν_{p0}. This difference can be evaluated measuring the gel relative weight change due to swelling as it can be assumed that the weight change is prominently due to the absorption of water (as was experimentally observed, see chapter 5):

$$\Delta W = \frac{\Delta M_{H2O}}{M_0} = \frac{M - M_0}{M_0} \tag{2.19}$$

where M_0 is the gel mass in the reference state and M gel mass after swelling/de-swelling. Thus, the correspondent volume change is given by:

$$\Delta V_{H2O} = \frac{\Delta M_{H2O}}{\rho_{H2O}} \overset{eq.(2.19)}{\cong} \frac{\Delta W}{\rho_{H2O}} M_0 = \frac{\Delta W}{\rho_{H2O}} \left(m_p + m_{H2O}\right) = \Delta W \left(\frac{\rho_p}{\rho_{H2O}} V_p + V_{H2O}\right) \tag{2.20}$$

ν_p is by definition:

$$\nu_p = \frac{V_p}{V_p + V_{H2O} + \Delta V_{H2O}} \tag{2.21}$$

Substituting (2.20) and (2.17) in equation (2.21), we obtain an expression for ν_p which depends only on density values (known) and ν_{p0}, (i.e. from c_{p0} which is known as well):

$$\nu_p = \frac{\nu_{p0} \cdot \rho_{H2O} \cdot c_{p0}}{\rho_{H2O} \cdot c_{p0} + \Delta W \cdot \rho_p \cdot \nu_{p0}} \tag{2.22}$$

Coming back to the density of crosslinks, in equation (2.14), according to the *equivalent network theory,* we can estimate the *mean mesh size* of the polymeric network, ξ_a [110] from the value of ρ_x. The product of crosslink density and the Avogadro's number, ($\rho_x N_A$), gives the number of crosslinks per unit volume, and therefore the inverse is the mean, spherical, volume assigned to each crosslink.

$$\frac{1}{\rho_x N_A} = \frac{4}{3}\pi\left(\frac{\xi_a}{2}\right)^3 \qquad \text{that gives:} \qquad \xi_a = \sqrt[3]{\frac{6}{\pi \rho_x N_A}} \tag{2.23}$$

It is important to point out that ξ_a is the average value of the mesh size in the network. The network might be not homogeneous and a mesh size distribution would be more representative. For this purpose, NMR spectroscopy is used.

2.6.1.6 Alternative estimation method of average mesh size: The theory of Scherer

As alternative term of comparison to rheology, another method for the estimation of the average mesh size ξ_a was considered. In an interesting work about polymeric networks like gels [111], Scherer proposed an equation to correlate the hydraulic radius of network mesh (R_h) with polymeric chains radius R_f (the index f stays for fiber, as polymer chains are often called) and the polymeric network average mesh size ξ_a on the basis of mesh shape (schematized as a cubic, octahedric or tetrahedric cell unit). This model turned out to be especially appropriate for NMR data interpretation as this technique is affected by R_h [112]. The model is represented by the following key equation:

$$\frac{R_h}{R_f} = \frac{2C_0(1-\nu_p)}{2C_1\left(\frac{R_f}{\xi_a}\right)^2 - 3C_2\left(\frac{R_f}{\xi_a}\right)^3} \tag{2.24}$$

where C_o, C_1, C_2 are constants relative to the cell geometry (here assumed as cubic, where the constant values are 1, 3π,$8\sqrt{2}$ respectively [111]). The model is valid for $\nu_p < 0.942$ corresponding to a ratio R_f/ξ_a <0.5, that means for not too small mesh size. The author suggested also an approximation for R_h:

$$\frac{R_h}{R_f} \approx \frac{(1-0.58\,\nu_p)}{\nu_p} \tag{2.25}$$

Rearranging (2.24), it follows:

$$\frac{R_h}{R_f} = \left(\frac{\xi_a}{R_f}\right)^2 \frac{C_0(1-\nu_p)}{\left(C_1 - \frac{3}{2}C_2\frac{R_f}{\xi_a}\right)} \quad \text{and we have that} \quad R_h = \frac{\xi_a^2}{R_f}\frac{C_0(1-\nu_p)}{\left(C_1 - \frac{3}{2}C_2\frac{R_f}{\xi_a}\right)} \tag{2.26}$$

For large meshes, $R_f/\xi_a \approx 0$ (this is the usual condition met in polymeric gels) and (2.26) can be approximated by the following expression:

$$R_h = \frac{\xi_a^2}{R_f}\frac{C_0(1-\nu_p)}{C_1} \tag{2.27}$$

By combining the two approximations (2.25) and (2.27) together, we obtain the mesh size ξ_a:

$$\frac{(1-0.58\,\nu_p)}{\nu_p}R_f = \frac{\xi_a^2}{R_f}\frac{C_0(1-\nu_p)}{C_1} \quad \text{, solving with respect to } \xi_a: \quad \xi_a = R_f\sqrt{\frac{(1-0.58\,\nu_p)}{\nu_p(1-\nu_p)}\frac{C_1}{C_0}} \tag{2.28}$$

Being ν_p known from equation (2.22), ξ_a can be calculated once and R_f is known.
The molecular radius of PVP, R_f , was predicted using the techniques of mechanical/molecular dynamics, as follows. Ten different polymer chains were modelled using the method of rotational isomeric states [113], and thereafter, each of these has been optimized geometrically balanced by applying a molecular mechanics / heating cycles coupled to molecular dynamics. The polymer is assumed linear and atactic. The molecular size has been averaged over 10 configurations. The value obtained for R_f is 0.91 nm. All simulations were conducted using the software Materials Studio™.
It is worth noting that the value of ξ_a from Scherer´s theory is purely theoretical, as it is derived by the assumption that the network is a lattice composed of regular cells (in our case cubic cells). Nonetheless, this theory was successfully used for the interpretation of NMR data by many works in this field [112]. For a more “real” picture of the gel structure, it is necessary to use the NMR technique to determine a distribution of mesh sizes in the network.

2.6.2. Nuclear magnetic resonance (NMR) spectroscopy

NMR spectroscopy allows to quantify the interaction between water and the polymer network. More specifically, it provides an estimation of the response of water protons spin to a magnetic excitation, which is strictly connected to their degree of interaction with the polymer chains. This information, combined with the estimation of the average mesh size of the network ξ_a obtained from theoretical (Scherer) or semi-empirical (Flory) models, allows to determine a mesh size distribution.

In the following sections, the physical principles of NMR are described to allow for a complete understanding of gel characterization and results interpretation. Sections 2.6.2.1-2.6.2.4 provide the basic theoretical background behind NMR. In section 2.6.2.5 the NMR experiment and the models used in the data treatment are described. Finally section 2.6.2.6 explains how rheology and NMR are combined to estimate the nanoscopic structure of hydrogels.

2.6.2.1 Quantum mechanics model for isolated nucleus

The physical principles of Nuclear Magnetic Resonance (NMR) spectroscopy, are based on the magnetic behaviour of atomic nuclei [114]. According to quantum mechanics, the excitation of an atomic nucleus by an external magnetic field, produces a transition of the nucleus energy in quantized energetic levels. The nuclear magnetic energy is restricted to discrete values, called *autovalues*. The autovalues are associated to the *autostates*, also called steady states that are the only possible existing states of an elementary particle. The exposure of the nucleus to an electromagnetic radiation of appropriate frequency, induces a transition within steady states. The energetic absorption can be detected by the instrument and registered as a signal on a spectrum. This technique allows to obtain the spectrum of a compound that contains atoms with nuclear magnetic moment different from zero. The most analyzed nuclei are the protons ^{1}H, fluorine ^{19}F, the isotopes ^{14}N and ^{15}N of nitrogen and the isotope ^{13}C of carbon [114]. Many atomic nuclei have an angular moment, P, that is responsible for the exhibition of a magnetic moment, μ [115]. The relation between P and μ is expressed by the following equation:

$$\mu = \gamma \cdot P \tag{2.29}$$

where γ is the *gyromagnetic ratio*, depending on the nucleus composition. According to quantum theory, the angular moment and the magnetic moment are quantized. The allowed autovalues of the angular moment maximum component in the z direction in an arbitrary Cartesian system, are defined by the equation:

$$P_z = \frac{h}{2\pi} m_I \tag{2.30}$$

where m_I is the quantum number of the correspondent nucleus steady states and h is the Plank constant. The magnetic quantum number m_I is related to the nuclear spin quantum number, I, and has the value of an integer number within +I and –I.

As a consequence, the number of possible autostates (or energy levels) is equal to 2I+1. For the proton (^{1}H), the nuclear spin quantum number is I = 1/2 and the z component of angular moment is given by:

$$P_z = \frac{h}{2\pi} I \tag{2.31}$$

The hydrogen nucleus can therefore exist only in two quantum states characterized by m_I = +1/2 and m_I = -1/2. The magnetic moment in the z direction is given by:

$$\mu_z = \gamma \frac{h}{2\pi} m_I \qquad \text{and the modules are:} \qquad \mu_z = \pm\gamma \frac{h}{4\pi} \tag{2.32}$$

In such a representation, the proton is represented as a magnetic dipole, where μ_z is parallel or antiparallel to the positive direction of the z axis as depicted in figure 2.13. Without an external magnetic field (figure 2.13a), the two states are *degenerated* that is they have the same energy. In presence of an external magnetic field B_0, (figure 2.13b), the interaction with μ causes an energetic splitting of the two states. If B_0 is parallel to the z axes, the magnetic dipole assumes an energy equal to $+\mu_z B_0$ when the dipole is oriented in the same direction of B_0 , while the energy is $-\mu_z B_0$, when it is oriented in opposite direction. The energy difference between the two spin states is proportional to the intensity of B_0, as follows:

$$\Delta E = 2\mu_z B_0 \tag{2.33}$$

The state at lower energy, m_I = +1/2 is more stable, and the transition to the higher energy state m_I = -1/2 requires an energy ΔE by a radiation with the frequency given by:

$$\nu_0 = \frac{\Delta E}{h} = \frac{\gamma B_0}{2\pi} \tag{2.34}$$

$$\omega_0 = \gamma \cdot B_0 \tag{2.35}$$

ν_0 is called *Larmor frequency* and ω_0 the angular frequency. The proton has a gyromagnetic ration of $\gamma_H = 2.675 \cdot 10^8\ T^{-1}s^{-1}$. For a magnetic field of 1.41 T, the Larmor frequency is 60 MHz corresponding to a radiation of wavelength λ=5 meters, in the field of radio waves. For nuclei with I=1 the available quantum numbers are m_I=-1, 0, +1 but the possible transitions are only from m_I=+1↔ 0 and m_I=0↔ -1, while transitions m_I=+1↔ -1 are not allowed.

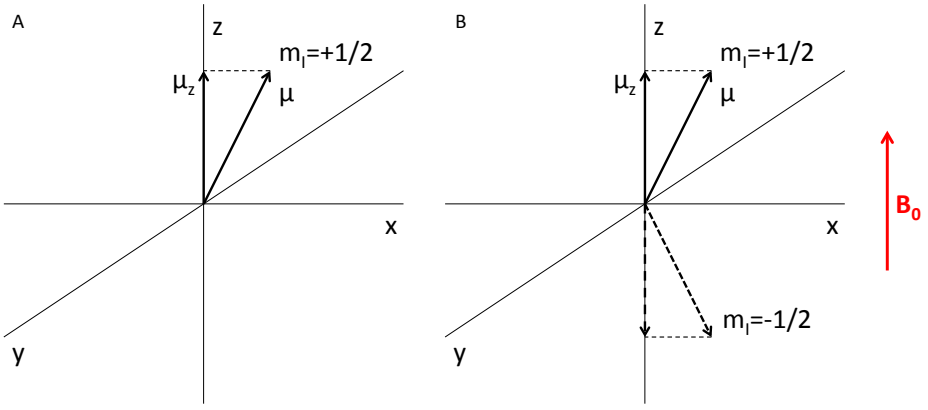

Figure 2.13: Vectorial representation of the magnetic moment μ (a) in absence or (b) in presence of an external magnetic field B_0.

2.6.2.2 Energy absorption mechanism: the resonance

The typical representation of nuclei with I=1/2, such as the protons ^{1}H, is a magnetic rod but. However, because of nuclei spin rotation, their behaviour is slightly different. Inside a static magnetic field B_0, the rotating nucleus does not align its magnetic moment to the direction of the field. On the contrary, similar to a spinning top in the gravitational field (figure 2.14a), their spin axis assumes a precession movement around the magnetic field direction (figure. 2.14a). The precession frequency corresponds to the Larmor frequency as seen in equation (2.34) [114, 115].

An increase in magnetic field intensity, produces a faster precession. However, the orientation of the magnetic moment μ can be modified by the presence of a rotating magnetic field (B_1) perpendicular to B_0. When the *rotation frequency* ν_{RF} of B_1 equals the precession frequency ν_0, a resonance condition is established and the nucleus absorbs energy resulting in a variation of the angle θ between vector μ and the static magnetic field B_0 (figure 2.15). This energy transfer does not change the precession frequency.

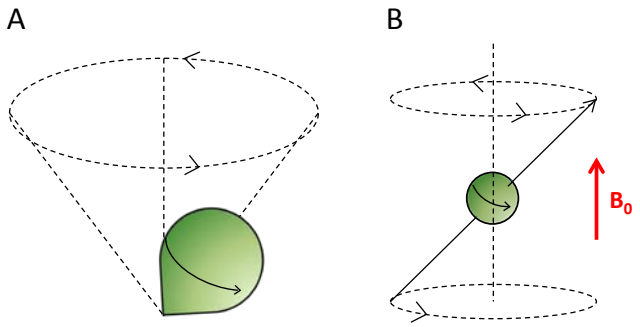

Figure 2.14: (a) A spinner follow a precession in the gravitational field of the earth, (b) the nuclear magnetic moment precesses in a magnetic field.

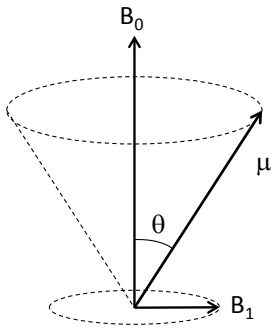

Figure 2.15: The application of a rotating magnetic field B_1 perpendicular to B_0, moves the nuclear magnetic moment μ by an angle θ.

2.6.2.3 Macroscopic magnetization

When a sample is analyzed by NMR, a huge number of nuclei are subjected to a magnetic field. The *nuclear magnetization* defined as magnetic moment per unit volume, M, is a vector divided into three components: M_z, is conventionally aligned to B_0 ; M_x and M_y, are perpendicular to B_0. For a nucleus with I=1/2, all the magnetic moments precess at the same frequency. Because magnetization vectors are randomly oriented on x and y axis, they cancel themselves and the overall M_{xy}=0 (condition of no phase coherence). On the contrary, there is a small excess of nuclei parallel to the B_0 direction (figure 2.16 a) in the z direction because the Boltzmann distribution favors the lower energy state. The difference between parallel and antiparallel magnetized nuclei populations (N_1 and N_2) (see figure 2.16b), generates a macroscopic magnetization M_z (figure 2.16).

$$M_z = \gamma h(N_1 - N_2) \qquad (2.36)$$

When an external rotating field B_1 is applied, the spin resonance modifies the casual orientation of nuclei, and a magnetization component $M_{xy}\neq 0$ appears in the xy plane (condition of phase coherence) (figure 2.16c).

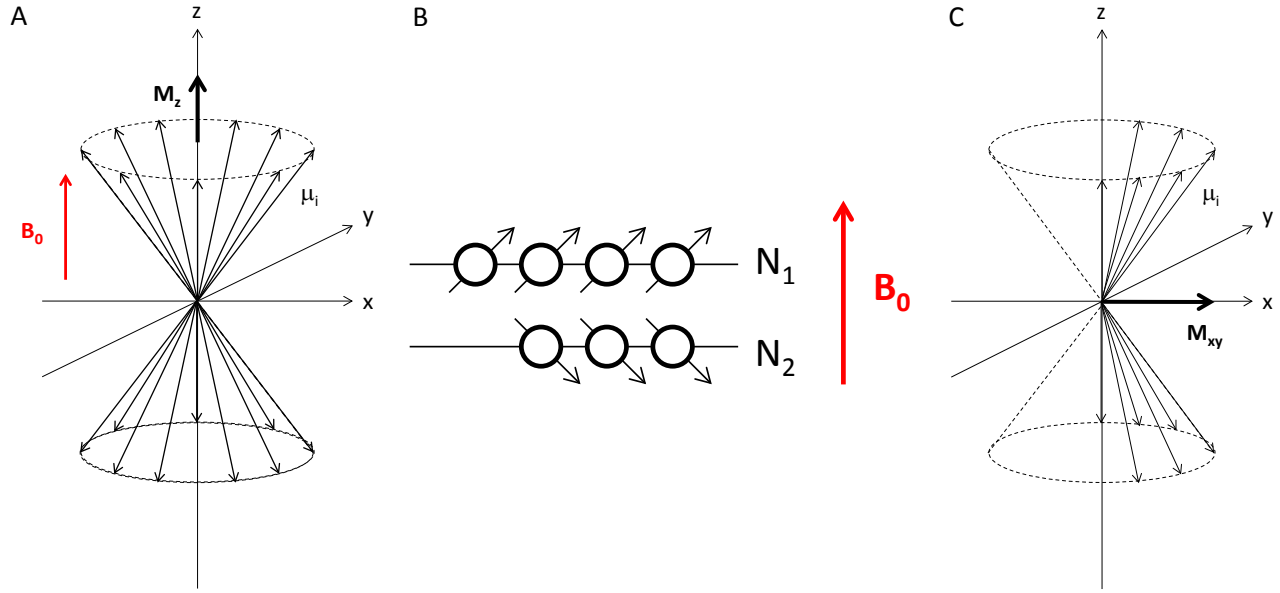

Figure 2.16: (a) Vectorial representation of magnetic moments of I=1/2 nuclei, following a precess around the z axis (conventionally all vectors have a common origin) with overall magnetization M_z, no magnetization on xy plane M_{xy}. (b) Excess of nuclei with magnetic moment aligned with B_0. (c) Spin system in phase coherence, $M_{xy}\neq 0$.

2.6.2.4 The NMR experiment

A schematic representation of NMR equipment is shown in figure 2.17. The sample is put in a cylindrical glass vial inside a slit in the middle of a coil which creates a highly homogeneous static magnetic field B_0. The phase coherence within spins is induced by a rotating magnetic field (B_1) perpendicular to B_0 and the generation of a M_{xy} magnetization component with a ω_0 precession (resonance frequency) (figure 2.18). When B_1 is removed, magnetization undergoes a relaxation process, which causes the loss of phase coherence ($M_{xy}\neq 0$) and a restoring of the initial equilibrium situation ($M_{xy}=0$). The relaxation implies an exponential decay of M_{xy} characterized by a time constant T_2 (*transversal relaxation time*). The result of the relaxation is a transient signal, captured by a sensor on the x axes, with ω_0 frequency and decay speed of $1/T_2$ called Free Induction Decay (FID) (figure 2.18) [116]. The NMR spectral signals are produced by the small displacement of resonance frequency ω_0 in the nuclei population under analysis caused by the physico-chemical environment. When different ω_0 and as a consequence different $1/T_2$ are present the resulting FID is a superimposition of all signals. The complex FID originating by multiple signals is solved using a Fourier Transformation (FT) that changes the transient signal in a normal spectrum (figure 2.18). The NMR spectrum is a diagram where intensity is a function of frequency, whereas in FID, the intensity is a function of time. The time domain and frequency domain are connected by the Fourier Transformation [116].

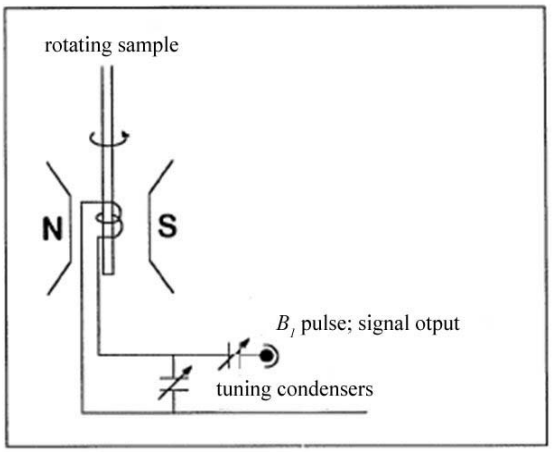

Figure 2.17: Schematic representation of the NMR spectroscope. The sample is positioned within the magnetic field B_0 generated by a magnet (N-S) and surrounded by a spire, tuned on the resonance frequency, that produces the B_1 pulse (from [107]).

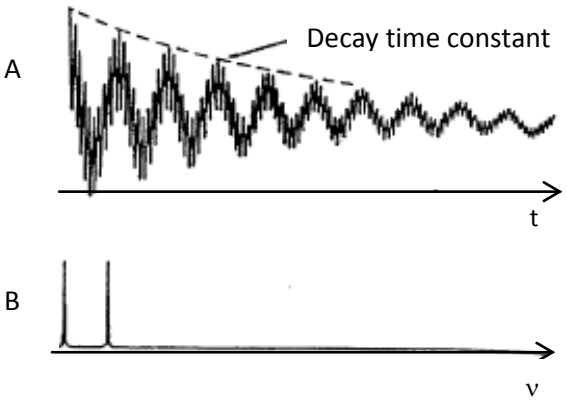

Figure 2.18: (a) FID of two NMR signal. (b) The spectrum obtained applying the Fourier transform to the FID (adapted from [107]).

Similarly to the precession in the B_0 field, the precession concept can be extended to B_1 using a conceptual artifact of a rotating reference system. With respect to this new rotating axis system, B_1 becomes a static field. When B_1 is applied (B_1 is aligned to the rotating axes x', the equilibrium magnetization M_0, aligned to z, follows a precession around B_1. The precession frequency of M_0 is:

$$\omega_1 = \gamma B_1 \tag{2.37}$$

ω_1 is and angular frequency (radiant s^{-1}). M_0 rotates with an angle given by:

$$\theta = \gamma B_1 t_p \tag{2.38}$$

where t_p is the pulsation time for B_1, and (γB_1) is the pulse amplitude or power. After a pulse of 90° ($\pi/2$), $M_{xy}=M_0$ (figure 2.19b). After a 180° pulse (π), $M_z=-M_0$ (figure 2.19c).

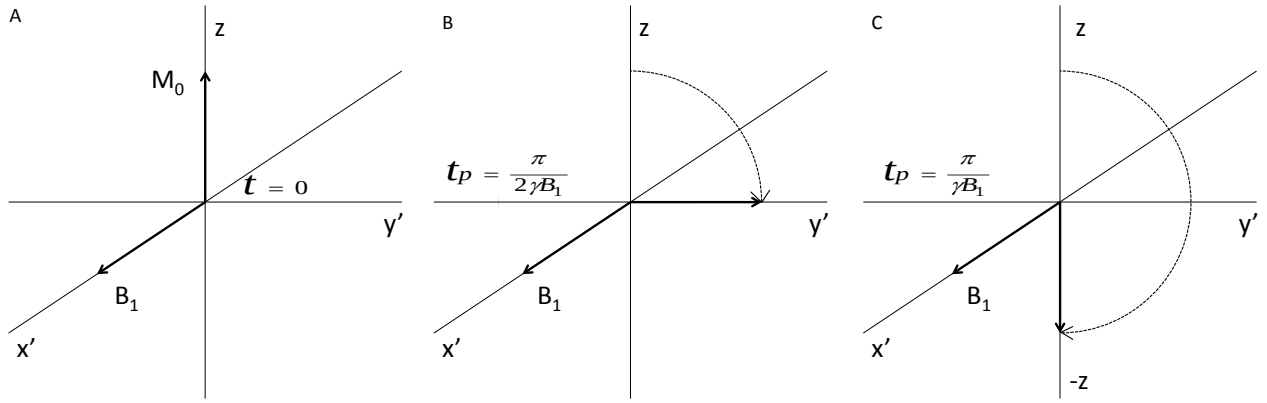

Figure 2.19: Effect of the rotating magnetic field B_1 application on the magnetization M_0 (x' and y' belong to a reference system rotating with the same frequency of B_1. (a) Time zero; (b) after a 90° pulse; (c) after 180° pulse.

To evaluate the effect of a B_1 pulse on the nuclear levels populations, a system of two state levels α (parallel to B_0) and β (antiparallel to B_0) is considered, overall containing N nuclei that could be in one state

or in the other. For degenerate levels, there should be N/2 nuclei in each state. However, because the α magnetic has a lower energy compared to state β, there is a small excess of nuclei in the α state. Calling δ the excess of nuclei, the number of nuclei in each population can be written as (N+δ)/2 or (N-δ)/2 for α and for β respectively.
With respect to a magnetization a macroscopic level, the nuclei situation it is better described by the M_z component. On the contrary, considering the α and β nuclei population, it is better to consider the deviation from N/2 defined as P_α=+δ/2 and P_β=-δ/2. In every moment, M_z is proportional to the difference within levels:

$$M_z \propto P_\alpha - P_\beta \tag{2.39}$$

or in other words $M_z \propto \delta$. Moreover,

$$P_\alpha + P_\beta = 0. \tag{2.40}$$

After the application of B_1, M_z becomes:

$$M_z = M_0 \cos\theta \tag{2.41}$$

and, consequently:

$$P_\alpha - P_\beta = \delta \cos\theta \tag{2.42}$$

that combined with equation (2.42) gives:

$$P_\alpha = \frac{\delta \cos\theta}{2} \tag{2.43}$$

$$P_\beta = -\frac{\delta \cos\theta}{2} \tag{2.44}$$

When a magnetization pulse changes from $\pi/2$ to π, a change of population is induced, as shown by equations (2.18) and (2.29). For $\theta = \pi/2$, $P_\alpha = 0$ and each state is equally populated. For $\theta = \pi$, $P_\alpha = \delta/2$ and the populations are inverted.
Equation (2.23) correlates the deflection angle caused by the pulse with the pulse amplitude (or intensity) γB_1 and the pulse time t_p. Both can be modified in order to obtain the desired deflection angle. When θ = 90°, magnetization is on the xy plane and the signal has the maximum intensity (Fig. 2.20b). At θ = 180° the magnetization is inverted and becomes antiparallel to the z axis.
Figure 2.20 illustrates in details the change of the magnetization during a pulsed NMR experiment in a rotating coordinate system. A rotating field deflects the vector M_z (same direction of B_0) with a certain angle, generating the M_{xy} magnetization component. M_{xy} exponentially decays with the time constant T_2 , emitting a signal which is detected on a receiving spire on the x axis. The signal collected is called free induction decay (FID). At the beginning the overall magnetization M_0 is aligned to the magnetic field B_0 (figure 2.20a) After application of rotating field, the magnetization deflects by $\pi/2$ (90°), and the magnetization vector moves (figure 2.20b). For a pulse of sufficient duration, it reaches the final position on the x'y' plane generating the M_{xy} magnetization component (figure 2.20c). At the end, when B_1 is removed, the relaxation process starts and the phase coherency is lost, causing the decay of M_{xy} component (figure 2.20d and e). This relaxation process is called *transversal relaxation* or *spin-spin* and it proceeds with a constant time T_2 by the energy transfer within high energy nuclei without loss of energy [116].

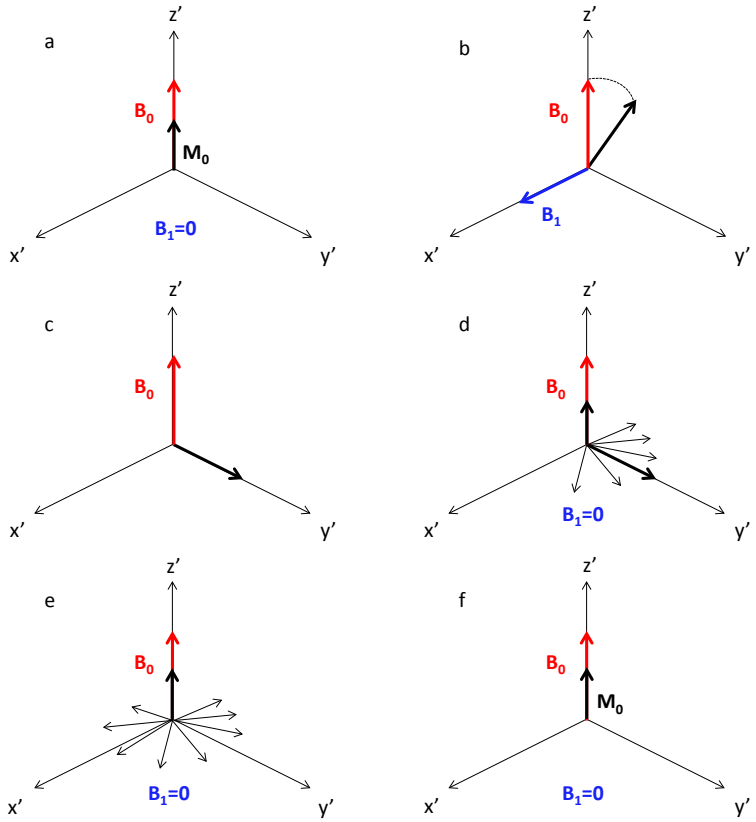

Figure 2.20: Diagrams in the rotating coordinate system x'y'z' showing the magnetization during an NMR experiment. (a) The overall magnetization M_0 is aligned to B_0. (b) and (c) A rotating field B_1 is applied perpendicular to B_0; the pulse length is sufficient to rotate the magnetization by 90°. (d) and (e) after B_1 ceasing, the spins start to relax by a spin-spin mechanism on the x'y' plane (time constant T_2) and by a spin-lattice mechanism on the z' direction (time constant T_1). (f) After sufficient time, the starting equilibrium magnetization M_0 is re-established.

The relaxation of M_{xy} decrease is given by

$$\frac{dM_{xy}}{dt} = -\frac{M_{xy}}{T_2} \tag{2.45}$$

giving the following solution

$$M_{xy} = M_0 \cdot e^{-\frac{t}{T_2}} \tag{2.46}$$

The value of T_2 can be estimated by the middle height of the spectral peak ($\Delta\nu_{0.5}$) by the equation

$$\Delta\nu_{0.5} = \frac{1}{\pi T_2} \tag{2.47}$$

Together with M_{xy}, also the longitudinal component of magnetization M_z returns during relaxation to the initial equilibrium magnetization M_0. This type of relaxation process is known as *longitudinal relaxation* or *spin-lattice* and proceeds with a time constant T_1.

$$\frac{dM_z}{dt} = -\frac{M_0 - M_z}{T_1} \tag{2.48}$$

$$M_z = M_0 \cdot \left(1 - e^{\frac{t}{T_1}}\right) \tag{2.49}$$

2.6.2.5. Low field NMR

Low field NMR provides informations on the structure of the material surrounding the interacting nuclei. NMR can be applied to both solid and liquid samples, suspension, gels and emulsions. It is non destructive method. The exciting field magnitude is between 0,23 and 1,53 T corresponding to 10 and 65 MHz respectively, and a temperature varying within -10 and +70°C. The shape and amplitude of the resonance signal are related to the physical environment surrounding the nuclei. The amplitude is a function of the nuclei degree of freedom of movement in the physical environment. This represents an useful information in polymer chemistry and solid state physics, as T_2 depends on nucleus mobility. In solids, T_2 is low (1-100 ms) because the nuclei have a reduced mobility. In gel systems, water is trapped in small domains, and T_2 ranges from 200 and 800 ms. Iin liquids nuclei have complete mobility, and T_2 is high (800-2500 ms).

For the structural analysis of hydrogels, the time domain NMR spectrum of the ^{1}H proton magnetization spectrum, allows to distinguish the different phases protons belong to, i.e. to polymer chain, water entrapped in the polymeric network, water in eventual microchannels and free water [117]. It is important to point out that in the samples under study, it was not possible to measure the relaxation of the protons belonging to the polymer backbone, since their relaxation resulted too fast to be detected by the equipment in use. That means that the first peak to the left in figure 2.21 was out of range for the tested systems.

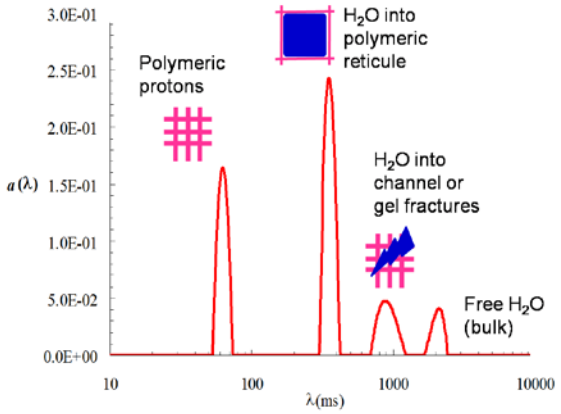

Figure 2.21: Typical example of ^{1}H relaxation spectrum of a non homogeneous hydrogel (adapted from [107]).

2.6.2.6. Data analysis of NMR spectroscopy and calculation of mesh size distribution

The NMR equipment used in this investigation is a Bruker Minispec mq20™, which operates at a frequency of 20 MHz (corresponding to ~0.47 T, for B_0 which is the commonly accepted value corresponding to the ^{1}H Larmor precession frequency) and at controlled temperature. The measurement consists of a sequence of magnetic excitations, followed by an acquisition interval: first a 90° pulse, a time interval τ, a series of 180° pulses applied at 2τ intervals are forwarded by the last 180° pulse after a τ interval. The sequence is repeated 8 times every 5 seconds. The T_2 relaxations curves collected in the scanning, are fitted by a multi-exponential function [118]:

$$\sum_{k=1}^{N} A_k e^{-\frac{t}{T_2^k}} \tag{2.50}$$

where t is time, A_k is the pre-exponential factor of the k component, and T_2^k is the relaxation time of the k component. The total number of exponential functions, N, is the one minimizing the product $(N \cdot \chi^2)$, where χ^2 is the sum of the squared difference between the fitting function (2.35) and the experimental data. The procedure which was followed for the data treatment described below was recently presented in the work of Pescosolido *et al.* [119] and here re-proposed for a better understanding.

Once N, A_1, .., A_N, T_2^1, .., T_2^N are estimated by the best fitting, a continuous distribution of T_2 can be calculated by fitting the time t decay of the experimental intensity signal I_s related to the extinction of the x-y magnetization component M_{xy} according to:

$$I(t) = \int_{T_2^{min}}^{T_2^{max}} a(T_2) e^{-\frac{t}{T_2}} dT_2 \tag{2.51}$$

where I(t) is the theoretical estimation of I_s, $a(T_2)$ is the unknown amplitude of the spectral component at relaxation time T_2, $e^{-\frac{t}{T_2}}$ is the decay term, while $T_2^{max} - T_2^{min}$ is the range of the T_2distribution. The determination of $a(T_2)$ requires eq.(2.51) fitting to the experimental I_s data. At this purpose, eq.(2.51) integral was discretisized with the criterion suggested by Whittal and MacKay [120]:

$$I(t) = \int_{T_2^{min}}^{T_2^{max}} a(T_2)e^{-\frac{t}{T_2}}dT_2 \approx \sum_{i=1}^{N} a_i\left(T_2^i\right)e^{-\frac{t}{T_2^i}}\left(T_2^{i+1} - T_2^i\right) = \sum_{i=1}^{N} A_i(T_2^i)e^{-\frac{t}{T_2^i}} \quad (2.52)$$

where the range of the T_2 distribution ($T_2^{min} - T_2^{max}$) was logarithmically subdivided into N=200 parts (higher N values were unnecessary). To reduce the noise in the signal, data fitting accounted for a smoothed version of χ^2 ($\chi_s{}^2$):

$$\chi_s^2 = \sum_{i=1}^{N}\left(\frac{I_s(t_i) - I(t_i)}{\sigma_i}\right)^2 + \mu\sum_{i=1}^{N-2}|A_{i+2} - 2A_{i+1} + A_i|^2 \quad (2.53)$$

where σ_i is the standard deviation of the i^{th} data point, while μ is the smoothening term proposed by Provencher [121]. The value of μ have a bearing on the value of χ as results shown in the plot shown in figure 2.22. Therefore, μ was chosen adopting the strategy suggested by Wang and Ni [122]: the value chosen for μ (in the example μ=261) was the one corresponding to the slope variation of the plot ln(χ) vs. ln(μ). Data fitting of (2.53) was carried out by a Visual Basic ''User Defined Function'' code embedded in Microsoft Excel worksheet and solved by ''Solver" function.

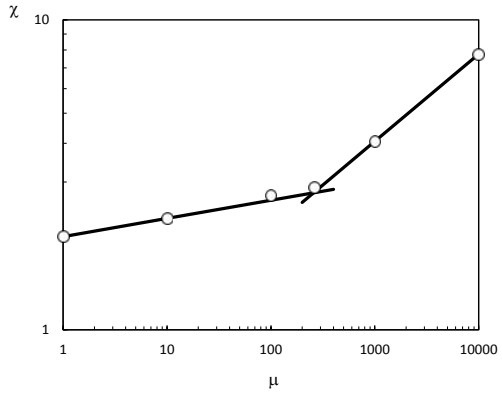

Figure 2.22: Bi-logarithmic plot of χ as a function of the smoothening term μ. According to the criterion of Wang and Ni [122], μ is chosen where the plot displays a change of slope.

Finally, the determination of the mesh size distribution is determined separately for the evaluations of average mesh sizes with rheology and Scherer´s theory.
For the "rheological" value, the distribution was performed as stated in a ''two fraction fast exchange model'' [123]. The quantitative relation between the relaxation time (T_{2i}) of the water confined inside a mesh of diameter ξ_i is:

$$\frac{1}{T_{2i}} = \frac{1}{T_{2,H_2O}} + \frac{1}{k\xi_i} \quad (2.54)$$

where $T_{2,H2O}$ is the free water relaxation time (3007 ± 20 ms at 25°C) and k is an unknown constant, depending on temperature, the nature of fluid filling the polymer mesh, the magnetic field strength and the chemical characteristics of the polymer. The most important hypothesis at the basis of equation (2.54) is that the fraction of bulk water molecules (i.e. those not in contact with the mesh wall) is much bigger than the fraction of surface water molecules (i.e. those in contact with the mesh wall). Equation (2.54) holds for ξ_i >8 nm.
Assuming that k does not depend on mesh size [124], relation (2.54) can be re-written for a system composed of meshes of different diameters:

$$\frac{1}{T_{2a}} = \frac{1}{T_{2,H_2O}} + \frac{1}{k\xi_a} \tag{2.55}$$

where T_{2a} is the average relaxation time and ξ_a is the average mesh size. Once T_{2a} (calculated from relaxation tests) and ξ_a (estimated according to rheological experiments) are known, k value is calculated from equation (2.55). Equation (2.55) allows to correlate each relaxation time (T_{2i}) with a corresponding mesh diameter (ξ_i), and as a consequence, the conversion of the T_2 distribution a(T_2) into the normalized mesh size distribution:

$$P = \frac{a(\xi)}{\int_{\xi_{min}}^{\xi_{max}} a(\xi)d(\xi)} \tag{2.56}$$

The result is a distribution of mesh sizes centered in the average value ξ_a.
The link connecting Scherer´s theory with the interpretation of NMR data, lays in the hydraulic radius of the polymer fiber R_h. Chui *et al.* [125] proposed the following relationship to calculate the average relaxation time:

$$\left\langle \frac{1}{T_2} \right\rangle = \frac{1}{T_{2,H_2O}} + \frac{2\mathcal{M}}{R_h} \tag{2.57}$$

W here T_2 is the relaxation time of water in the gel, $T_{2,H2O}$ is the relaxation time of bulk water (3007 ± 20 ms at 25°C), and $\mathcal{M}$ is an empirical sink parameter at the surface accounting for polymeric chains effect on water protons. R_h can be conveniently replaced by ξ according to a proper combination of equations (2.25) and (2.27):

$$\frac{R_h}{\xi} = \sqrt{\frac{(1-0.58\,\nu_p)(1-\nu_p)}{\nu_p}\frac{C_0}{C_1}} = f(\nu_p) \qquad \text{or likewise:} \qquad R_h = \xi \cdot f(\nu_p) \tag{2.58}$$

Therefore, equation (2.57) becomes:

$$\left\langle \frac{1}{T_2} \right\rangle = \frac{1}{T_{2,H_2O}} + \frac{2\mathcal{M}}{\xi \cdot f(\nu_p)} \tag{2.59}$$

Similarly to the case of rheology, $\mathcal{M}$ estimation allows finding a relation between the relaxation times T_{2i} and ξ_i. It is easy to see that eq.(2.59) gives a physical interpretation of parameter *k* appearing in eq.(2.55).
From the achievement of (2.59) it is clear that the main advantage of using the previously obtained approximated solution (2.27) over the analytical expression of Scherer (2.24) stays in the possibility of establishing a direct correlation between the hydraulic radius R_h (obtained by NMR spectroscopy, [123]) and the network mesh size.

2.6.3 Enviromental SEM on gels

Enviromental scanning electron microscopy (E-SEM) was used for the imaging of gel micropatterns obtained by selective crosslinking of polymer. The observation were aimed to visualize microstructure in the swollen conditions. All the images were collected by Ramona Valentina Mateiu, at the Centre of Electron Nanoscopy (DTU CEN).
The analysis was done in an FEI Quanta 200 ESEM FEG. The samples were attached to an aluminum stub with a double sided carbon tape and the electrical grown was made with copper tape. All samples were imaged with the gaseous secondary electron detector at room temperature and 2 mbar partial water vapor pressure. The acceleration voltage was set to 15 keV and the spot size to 4 in all cases. The sample was tilted to 40 degrees and the working distance was adjusted between 22 and 27 mm as needed.

Bibliography

[1] J. Liu, B. Cai, J. Zhu, G. Ding, X. Zhao, C. Yang, D. Chen, Process research of high aspect ratio microstructure using SU-8 resist, Microsystem Technologies, 10 (2004) 265-268.
[2] A. Del Campo, C. Greiner, SU-8: a photoresist for high-aspect-ratio and 3D submicron lithography, Journal of Micromechanics and Microengineering, 17 (2007) R81.
[3] J.D. Gelorme, R.J. Cox, S.A. Gutierrez, Photoresist composition and printed circuit boards and packages made therewith, in, Google Patents, 1989.
[4] J. Guan, H. He, D.J. Hansford, L.J. Lee, Self-folding of three-dimensional hydrogel microstructures, The Journal of Physical Chemistry B, 109 (2005) 23134-23137.
[5] K.M. Ainslie, C.M. Kraning, T.A. Desai, Microfabrication of an asymmetric, multi-layered microdevice for controlled release of orally delivered therapeutics, Lab Chip, 8 (2008) 1042-1047.
[6] A. Azam, K.E. Laflin, M. Jamal, R. Fernandes, D.H. Gracias, Self-folding micropatterned polymeric containers, Biomedical Microdevices, 13 (2011) 51-58.
[7] J.-H. Park, M.G. Allen, M.R. Prausnitz, Polymer microneedles for controlled-release drug delivery, Pharmaceutical research, 23 (2006) 1008-1019.
[8] D.V. McAllister, P.M. Wang, S.P. Davis, J.-H. Park, P.J. Canatella, M.G. Allen, M.R. Prausnitz, Microfabricated needles for transdermal delivery of macromolecules and nanoparticles: fabrication methods and transport studies, Proceedings of the National Academy of Sciences, 100 (2003) 13755-13760.
[9] F. Perennes, B. Marmiroli, M. Matteucci, M. Tormen, L. Vaccari, E. Di Fabrizio, Sharp beveled tip hollow microneedle arrays fabricated by LIGA and 3D soft lithography with polyvinyl alcohol, Journal of Micromechanics and Microengineering, 16 (2006) 473.
[10] M. Hennemeyer, F. Walther, S. Kerstan, K. Schürzinger, A.M. Gigler, R.W. Stark, Cell proliferation assays on plasma activated SU-8, Microelectronic Engineering, 85 (2008) 1298-1301.
[11] G. Kotzar, M. Freas, P. Abel, A. Fleischman, S. Roy, C. Zorman, J.M. Moran, J. Melzak, Evaluation of MEMS materials of construction for implantable medical devices, Biomaterials, 23 (2002) 2737-2750.
[12] G. Voskerician, M.S. Shive, R.S. Shawgo, H.v. Recum, J.M. Anderson, M.J. Cima, R. Langer, Biocompatibility and biofouling of MEMS drug delivery devices, Biomaterials, 24 (2003) 1959-1967.
[13] Y. Wang, J.-H. Pai, H.-H. Lai, C.E. Sims, M. Bachman, G. Li, N.L. Allbritton, Surface graft polymerization of SU-8 for bio-MEMS applications, Journal of Micromechanics and Microengineering, 17 (2007) 1371.
[14] S.L. Tao, K.C. Popat, J.J. Norman, T.A. Desai, Surface modification of SU-8 for enhanced biofunctionality and nonfouling properties, Langmuir, 24 (2008) 2631-2636.
[15] J. Nagstrup, A. Boisen, S.S. Keller, Micro fabrication of biodegradable polymer drug delivery devices, in, Technical University of DenmarkDanmarks Tekniske Universitet, Department of Micro-and NanotechnologyInstitut for Mikro-og Nanoteknologi, NanoprobesNanoprobes, 2013.
[16] J. Nagstrup, S. Keller, K. Almdal, A. Boisen, 3D microstructuring of biodegradable polymers, Microelectronic Engineering, 88 (2011) 2342-2344.
[17] S. Nakano, T. Sekitani, T. Yokota, T. Someya, Low operation voltage of inkjet-printed plastic sheet-type micromechanical switches, Applied Physics Letters, 92 (2008) 053302.
[18] Q. Liu, M. Orme, High precision solder droplet printing technology and the state-of-the-art, Journal of Materials Processing Technology, 115 (2001) 271-283.
[19] V.J. Cadarso, J. Perera-Núñez, L. Jacot-Descombes, K. Pfeiffer, U. Ostrzinski, A. Voigt, A. Llobera, G. Grützer, J. Brugger, Microlenses with defined contour shapes, Opt. Express, 19 (2011) 18665-18670.
[20] L. Jacot-Descombes, M. Gullo, V. Cadarso, J. Brugger, Fabrication of epoxy spherical microstructures by controlled drop-on-demand inkjet printing, Journal of Micromechanics and Microengineering, 22 (2012) 074012.
[21] T. Goldmann, J.S. Gonzalez, DNA-printing: utilization of a standard inkjet printer for the transfer of nucleic acids to solid supports, Journal of Biochemical and Biophysical Methods, 42 (2000) 105-110.
[22] T. Xu, J. Jin, C. Gregory, J.J. Hickman, T. Boland, Inkjet printing of viable mammalian cells, Biomaterials, 26 (2005) 93-99.

[23] E.A. Roth, T. Xu, M. Das, C. Gregory, J.J. Hickman, T. Boland, Inkjet printing for high-throughput cell patterning, Biomaterials, 25 (2004) 3707-3715.
[24] P. Cooley, D. Wallace, B. Antohe, Applicatons of Ink-Jet Printing Technology to BioMEMS and Microfluidic Systems, Journal of the Association for Laboratory Automation, 7 (2002) 33-39.
[25] P.J. Tarcha, D. Verlee, H.W. Hui, J. Setesak, B. Antohe, D. Radulescu, D. Wallace, The application of ink-jet technology for the coating and loading of drug-eluting stents, Annals of Biomedical Engineering, 35 (2007) 1791-1799.
[26] N. Scoutaris, M.R. Alexander, P.R. Gellert, C.J. Roberts, Inkjet printing as a novel medicine formulation technique, Journal of Controlled Release, 156 (2011) 179-185.
[27] N. Sandler, A. Määttänen, P. Ihalainen, L. Kronberg, A. Meierjohann, T. Viitala, J. Peltonen, Inkjet printing of drug substances and use of porous substrates–towards individualized dosing, Journal of Pharmaceutical Sciences, 100 (2011) 3386-3395.
[28] J.-U. Park, M. Hardy, S.J. Kang, K. Barton, K. Adair, D. kishore Mukhopadhyay, C.Y. Lee, M.S. Strano, A.G. Alleyne, J.G. Georgiadis, High-resolution electrohydrodynamic jet printing, Nature materials, 6 (2007) 782-789.
[29] C. Reese, M. Roberts, M.-m. Ling, Z. Bao, Organic thin film transistors, Materials today, 7 (2004) 20-27.
[30] G.D. Martin, S.D. Hoath, I.M. Hutchings, Inkjet printing-the physics of manipulating liquid jets and drops, in: Journal of Physics: Conference Series, IOP Publishing, 2008, pp. 012001.
[31] J. Brünahl, A.M. Grishin, Piezoelectric shear mode drop-on-demand inkjet actuator, Sensors And Actuators A: Physical, 101 (2002) 371-382.
[32] D. Jang, D. Kim, J. Moon, Influence of fluid physical properties on ink-jet printability, Langmuir, 25 (2009) 2629-2635.
[33] N. Reis, C. Ainsley, B. Derby, Ink-jet delivery of particle suspensions by piezoelectric droplet ejectors, Journal of Applied Physics, 97 (2005) 094903-094903-094906.
[34] A.I. Cooper, Polymer synthesis and processing using supercritical carbon dioxide, Journal of Materials Chemistry, 10 (2000) 207-234.
[35] P. York, U.B. Kompella, B.Y. Shekunov, Supercritical fluid technology for drug product development, CRC Press, 2004.
[36] T.V. Harris, C.A. Irani, W.R. Pretzer, Enhanced oil recovery using CO. sub. 2 flooding, in, Google Patents, 1990.
[37] R. Quinn, J. Appleby, G. Pez, Salt hydrates: new reversible absorbents for carbon dioxide, Journal of the American Chemical Society, 117 (1995) 329-335.
[38] M. O'neill, Q. Cao, M. Fang, K. Johnston, S. Wilkinson, C. Smith, J. Kerschner, S. Jureller, Solubility of homopolymers and copolymers in carbon dioxide, Industrial & engineering chemistry research, 37 (1998) 3067-3079.
[39] J.C. Meredith, K.P. Johnston, J.M. Seminario, S.G. Kazarian, C.A. Eckert, Quantitative equilibrium constants between CO2 and Lewis bases from FTIR spectroscopy, The Journal of Physical Chemistry, 100 (1996) 10837-10848.
[40] F. Rindfleisch, T.P. DiNoia, M.A. McHugh, Solubility of polymers and copolymers in supercritical CO2, The Journal of Physical Chemistry, 100 (1996) 15581-15587.
[41] C.A. Mertdogan, H.-S. Byun, M.A. McHugh, W.H. Tuminello, Solubility of poly (tetrafluoroethylene-co-19 mol% hexafluoropropylene) in supercritical CO2 and halogenated supercritical solvents, Macromolecules, 29 (1996) 6548-6555.
[42] C.A. Mertdogan, T.P. DiNoia, M.A. McHugh, Impact of Backbone Architecture on the Solubility of Fluorocopolymers in Supercritical CO2 and Halogenated Supercritical Solvents: Comparison of Poly (vinylidene fluoride-co-22 mol hexafluoropropylene) and Poly (tetrafluoroethylene-co-19 mol hexafluoropropylene), Macromolecules, 30 (1997) 7511-7515.
[43] R. Fink, D. Hancu, R. Valentine, E. Beckman, Toward the development of “CO2-philic” hydrocarbons. 1. Use of side-chain functionalization to lower the miscibility pressure of polydimethylsiloxanes in CO2, The Journal of Physical Chemistry B, 103 (1999) 6441-6444.

[44] T. Sarbu, T. Styranec, E.J. Beckman, Non-fluorous polymers with very high solubility in supercritical CO 2 down to low pressures, Nature, 405 (2000) 165-168.
[45] T. Sarbu, T.J. Styranec, E.J. Beckman, Design and synthesis of low cost, sustainable CO2-philes, Industrial & engineering chemistry research, 39 (2000) 4678-4683.
[46] P.G. Debenedetti, S.K. Kumar, The molecular basis of temperature effects in supercritical extraction, AIChE Journal, 34 (1988) 645-657.
[47] N.R. Foster, G.S. Gurdial, J.S. Yun, K.K. Liong, K.D. Tilly, S.S. Ting, H. Singh, J.H. Lee, Significance of the crossover pressure in solid-supercritical fluid phase equilibria, Industrial & engineering chemistry research, 30 (1991) 1955-1964.
[48] K.A. Consan, R.D. Smith, Observations on the solubility of surfactants and related molecules in carbon dioxide at 50 C, The journal of Supercritical fluids, 3 (1990) 51-65.
[49] T. Hoefling, D. Newman, R. Enick, E. Beckman, Effect of structure on the cloud-point curves of silicone-based amphiphiles in supercritical carbon dioxide, The journal of Supercritical fluids, 6 (1993) 165-171.
[50] T. Hoefling, D. Stofesky, M. Reid, E. Beckman, R.M. Enick, The incorporation of a fluorinated ether functionality into a polymer or surfactant to enhance C0< sub> 2</sub>-solubility, The journal of Supercritical fluids, 5 (1992) 237-241.
[51] D. Newman, T. Hoefling, R. Beitle, E. Beckman, R. Enick, Phase behavior of fluoroether-functional amphiphiles in supercritical carbon dioxide, The journal of Supercritical fluids, 6 (1993) 205-210.
[52] K. Johnston, K. Harrison, M. Clarke, S. Howdle, M. Heitz, F. Bright, C. Carlier, T. Randolph, Water-in-carbon dioxide microemulsions: an environment for hydrophiles including proteins, Science, 271 (1996) 624-626.
[53] E. Ghenciu, A. Russell, E. Beckman, L. Steele, N. Becker, Solubilization of subtilisin in CO2 using fluoroether-functional amphiphiles, Biotechnology and bioengineering, 58 (1998) 572-580.
[54] J. Holmes, D. Steytler, G. Rees, B. Robinson, Bioconversions in a water-in-CO2 microemulsion, Langmuir, 14 (1998) 6371-6376.
[55] J.M. Dobbs, J.M. Wong, K.P. Johnston, Nonpolar co-solvents for solubility enhancement in supercritical fluid carbon dioxide, Journal of Chemical and Engineering Data, 31 (1986) 303-308.
[56] S.S. Ting, D.L. Tomasko, N.R. Foster, S.J. Macnaughton, Solubility of naproxen in supercritical carbon dioxide with and without cosolvents, Industrial & engineering chemistry research, 32 (1993) 1471-1481.
[57] Q. Li, Z. Zhang, C. Zhong, Y. Liu, Q. Zhou, Solubility of solid solutes in supercritical carbon dioxide with and without cosolvents, Fluid Phase Equilibria, 207 (2003) 183-192.
[58] Z. Huang, S. Kawi, Y. Chiew, Solubility of cholesterol and its esters in supercritical carbon dioxide with and without cosolvents, The journal of Supercritical fluids, 30 (2004) 25-39.
[59] E. Ghenciu, E. Beckman, Affinity extraction into carbon dioxide. 1. Extraction of avidin using a biotin-functional fluoroether surfactant, Industrial & engineering chemistry research, 36 (1997) 5366-5370.
[60] J.L. Panza, A.J. Russell, E.J. Beckman, Synthesis of fluorinated NAD as a soluble coenzyme for enzymatic chemistry in fluorous solvents and carbon dioxide, Tetrahedron, 58 (2002) 4091-4104.
[61] S.G. Kazarian, M.F. Vincent, B.L. West, C.A. Eckert, Partitioning of solutes and cosolvents between supercritical CO< sub> 2</sub> and polymer phases, The journal of Supercritical fluids, 13 (1998) 107-112.
[62] A.R. Berens, G.S. Huvard, R.W. Korsmeyer, F. Kunig, Application of compressed carbon dioxide in the incorporation of additives into polymers, Journal of Applied Polymer Science, 46 (1992) 231-242.
[63] M. Vincent, S. Kazarian, B. West, J. Berkner, F. Bright, C. Liotta, C. Eckert, Cosolvent effects of modified supercritical carbon dioxide on cross-linked poly (dimethylsiloxane), The Journal of Physical Chemistry B, 102 (1998) 2176-2186.
[64] P.D. Condo, S.R. Sumpter, M.L. Lee, K.P. Johnston, Partition coefficients and polymer-solute interaction parameters by inverse supercritical fluid chromatography, Industrial & engineering chemistry research, 35 (1996) 1115-1123.
[65] O. Guney, A. Akgerman, Synthesis of controlled-release products in supercritical medium, AIChE Journal, 48 (2002) 856-866.

[66] K. Gong, I.U. Rehman, J.A. Darr, Characterization and drug release investigation of amorphous drug–hydroxypropyl methylcellulose composites made via supercritical carbon dioxide assisted impregnation, Journal of pharmaceutical and biomedical analysis, 48 (2008) 1112-1119.
[67] M. Daneshvar, S. Kim, E. Gulari, High-pressure phase equilibria of polyethylene glycol-carbon dioxide systems, The Journal of Physical Chemistry, 94 (1990) 2124-2128.
[68] M. Banchero, L. Manna, S. Ronchetti, P. Campanelli, A. Ferri, Supercritical solvent impregnation of piroxicam on PVP at various polymer molecular weights, The journal of Supercritical fluids, 49 (2009) 271-278.
[69] L. Manna, M. Banchero, D. Sola, A. Ferri, S. Ronchetti, S. Sicardi, Impregnation of PVP microparticles with ketoprofen in the presence of supercritical CO< sub> 2</sub>, The journal of Supercritical fluids, 42 (2007) 378-384.
[70] O. Ayodeji, E. Graham, D. Kniss, J. Lannutti, D. Tomasko, Carbon dioxide impregnation of electrospun polycaprolactone fibers, The journal of Supercritical fluids, 41 (2007) 173-178.
[71] G.A. Leeke, J. Cai, M. Jenkins, Solubility of supercritical carbon dioxide in polycaprolactone (CAPA 6800) at 313 and 333 K, Journal of Chemical & Engineering Data, 51 (2006) 1877-1879.
[72] S.H. Mahmood, M. Keshtkar, C.B. Park, Determination of carbon dioxide solubility in polylactide acid with accurate PVT properties, The Journal of Chemical Thermodynamics, 70 (2014) 13-23.
[73] M.E. Braga, M.T.V. Pato, H.S. Silva, E.I. Ferreira, M.H. Gil, C.M. Duarte, H.C. de Sousa, Supercritical solvent impregnation of ophthalmic drugs on chitosan derivatives, The journal of Supercritical fluids, 44 (2008) 245-257.
[74] K. Gong, J. Darr, I. Rehman, Supercritical fluid assisted impregnation of indomethacin into chitosan thermosets for controlled release applications, International Journal of Pharmaceutics, 315 (2006) 93-98.
[75] M. Moneghini, I. Kikic, B. Perissutti, E. Franceschinis, A. Cortesi, Characterisation of nimesulide–betacyclodextrins systems prepared by supercritical fluid impregnation, European Journal of Pharmaceutics and Biopharmaceutics, 58 (2004) 637-644.
[76] B. Bonavoglia, G. Storti, M. Morbidelli, A. Rajendran, M. Mazzotti, Sorption and swelling of semicrystalline polymers in supercritical CO2, Journal of Polymer Science Part B: Polymer Physics, 44 (2006) 1531-1546.
[77] I. Tsivintzelis, A.G. Angelopoulou, C. Panayiotou, Foaming of polymers with supercritical CO2: An experimental and theoretical study, Polymer, 48 (2007) 5928-5939.
[78] L.I. Cabezas, I. Gracia, M.T. García, A. de Lucas, J.F. Rodríguez, Production of biodegradable porous scaffolds impregnated with 5-fluorouracil in supercritical CO2, The journal of Supercritical fluids, 80 (2013) 1-8.
[79] S. Areerat, E. Funami, Y. Hayata, D. Nakagawa, M. Ohshima, Measurement and prediction of diffusion coefficients of supercritical CO2 in molten polymers, Polymer Engineering & Science, 44 (2004) 1915-1924.
[80] O. Muth, T. Hirth, H. Vogel, Investigation of sorption and diffusion of supercritical carbon dioxide into poly (vinyl chloride), The journal of Supercritical fluids, 19 (2001) 299-306.
[81] L.J. Gerhardt, C.W. Manke, E. Gulari, Rheology of polydimethylsiloxane swollen with supercritical carbon dioxide, Journal of Polymer Science Part B: Polymer Physics, 35 (1997) 523-534.
[82] H. Park, C. Park, C. Tzoganakis, K. Tan, P. Chen, Surface tension measurement of polystyrene melts in supercritical carbon dioxide, Industrial & engineering chemistry research, 45 (2006) 1650-1658.
[83] A.R.C. Duarte, C. Martins, P. Coimbra, M.H.M. Gil, H.C. de Sousa, C.M.M. Duarte, Sorption and diffusion of dense carbon dioxide in a biocompatible polymer, The journal of Supercritical fluids, 38 (2006) 392-398.
[84] N. Fotaki, M. Vertzoni, Biorelevant dissolution methods and their applications in in vitro-in vivo correlations for oral formulations, Open Drug Deliv J, 4 (2010) 2-13.
[85] S. Klein, The use of biorelevant dissolution media to forecast the in vivo performance of a drug, AAPS J, 12 (2010) 397-406.
[86] J.B. Dressman, G.L. Amidon, C. Reppas, V.P. Shah, Dissolution testing as a prognostic tool for oral drug absorption: immediate release dosage forms, Pharmaceutical research, 15 (1998) 11-22.

[87] K. Greco, T.L. Bergman, R. Bogner, Design and characterization of a laminar flow-through dissolution apparatus: Comparison of hydrodynamic conditions to those of common dissolution techniques, Pharmaceutical development and technology, 16 (2011) 75-87.
[88] A. Avdeef, Solubility of sparingly-soluble ionizable drugs, Advanced Drug Delivery Reviews, 59 (2007) 568-590.
[89] J.H. Fagerberg, O. Tsinman, N. Sun, K. Tsinman, A. Avdeef, C.A. Bergström, Dissolution rate and apparent solubility of poorly soluble drugs in biorelevant dissolution media, Molecular pharmaceutics, 7 (2010) 1419-1430.
[90] N. Chieng, T. Rades, J. Aaltonen, An overview of recent studies on the analysis of pharmaceutical polymorphs, Journal of pharmaceutical and biomedical analysis, 55 (2011) 618-644.
[91] R.A. Storey, I. Ymen, Solid state characterization of pharmaceuticals, Wiley Online Library, 2011.
[92] D. Black, E. Lovering, Estimation of the degree of crystallinity in digoxin by X-ray and infrared methods, Journal of Pharmacy and Pharmacology, 29 (1977) 684-687.
[93] X. Chen, S. Bates, K.R. Morris, Quantifying amorphous content of lactose using parallel beam X-ray powder diffraction and whole pattern fitting, Journal of pharmaceutical and biomedical analysis, 26 (2001) 63-72.
[94] B.C. Hancock, G. Zografi, Characteristics and significance of the amorphous state in pharmaceutical systems, Journal of Pharmaceutical Sciences, 86 (1997) 1-12.
[95] B. Sarsfield, M. Davidovich, S. Desikan, M. Fakes, S. Futernik, J. Hilden, J. Tan, S. Yin, G. Young, B. Vakkalagadda, Powder X-ray diffraction detection of crystalline phases in amorphous pharmaceuticals, Advances in X-ray Analysis, 49 (2006) 322-327.
[96] H. Günzler, H.-U. Gremlich, M.-J. Blümich, IR spectroscopy: an introduction, Wiley-vch Weinheim, 2002.
[97] N.B. Colthup, L.H. Daly, S.E. Wiberley, Introduction to infrared and Raman spectroscopy, Academic press, 1990.
[98] C.J. Strachan, T. Rades, K.C. Gordon, J. Rantanen, Raman spectroscopy for quantitative analysis of pharmaceutical solids, Journal of Pharmacy and Pharmacology, 59 (2007) 179-192.
[99] S. Kazarian, G. Martirosyan, Spectroscopy of polymer/drug formulations processed with supercritical fluids: in situ ATR–IR and Raman study of impregnation of ibuprofen into PVP, International Journal of Pharmaceutics, 232 (2002) 81-90.
[100] K.A. Chan, S.V. Hammond, S.G. Kazarian, Applications of attenuated total reflection infrared spectroscopic imaging to pharmaceutical formulations, Analytical Chemistry, 75 (2003) 2140-2146.
[101] N.S. Berchane, K.H. Carson, A.C. Rice-Ficht, M.J. Andrews, Effect of mean diameter and polydispersity of PLG microspheres on drug release: Experiment and theory, International Journal of Pharmaceutics, 337 (2007) 118-126.
[102] M.T. am Ende, N.A. Peppas, Transport of ionizable drugs and proteins in crosslinked poly (acrylic acid) and poly (acrylic acid-co-2-hydroxyethyl methacrylate) hydrogels. II. Diffusion and release studies, Journal of Controlled Release, 48 (1997) 47-56.
[103] C.S. Brazel, N.A. Peppas, Modeling of drug release from Swellable polymers, European Journal of Pharmaceutics and Biopharmaceutics, 49 (2000) 47-58.
[104] M. Grassi, R. Lapasin, T. Coviello, P. Matricardi, C. Di Meo, F. Alhaique, Scleroglucan/borax/drug hydrogels: Structure characterisation by means of rheological and diffusion experiments, Carbohydrate Polymers, 78 (2009) 377-383.
[105] G. Turco, I. Donati, M. Grassi, G. Marchioli, R. Lapasin, S. Paoletti, Mechanical spectroscopy and relaxometry on alginate hydrogels: a comparative analysis for structural characterization and network mesh size determination, Biomacromolecules, 12 (2011) 1272-1282.
[106] M. Grassi, G. Grassi, R. Lapasin, I. Colombo, Understanding drug release and absorption mechanisms: a physical and mathematical approach, CRC, 2006.
[107] D. Perin, Biomaterials for biotechnological applications: synthesis and activity evaluations, (2010).
[108] Flory, P. J., Principles of polymer chemistry, Cornell University Press, 1953.

[109] R. Lapasin, S. Pricl, Rheology of industrial polysaccharides: theory and applications, Blackie Academic & Professional London, 1995.
[110] J. Schurz, Rheology of polymer solutions of the network type, Progress in Polymer Science, 16 (1991) 1-53.
[111] G.W. Scherer, Hydraulic radius and mesh size of gels, Journal of Sol-Gel Science and Technology, 1 (1994) 285-291.
[112] M. Abrami, I. D'Agostino, G. Milcovich, S. Fiorentino, R. Farra, F. Asaro, R. Lapasin, G. Grassi, M. Grassi, Physical characterization of alginate–Pluronic F127 gel for endoluminal NABDs delivery, Soft Matter, 10 (2014) 729-737.
[113] D.N. Theodorou, U.W. Suter, Detailed molecular structure of a vinyl polymer glass, Macromolecules, 18 (1985) 1467-1478.
[114] H. Günther, NMR spectroscopy: basic principles, concepts, and applications in chemistry, Wiley, 1992.
[115] T. Atta-ur-Rahman, Nuclear magnetic resonance: basic principles, Springer-Verlag New York, 1986.
[116] M. Choudhary, Solving problems with NMR spectroscopy, Access Online via Elsevier, 1996.
[117] L. Vanhamme, T. Sundin, P.V. Hecke, S.V. Huffel, MR spectroscopy quantitation: a review of time-domain methods, NMR in Biomedicine, 14 (2001) 233-246.
[118] W.H. Press, Numerical recipes in Fortran 77: the art of scientific computing, Cambridge university press, 1992.
[119] L. Pescosolido, L. Feruglio, R. Farra, S. Fiorentino, I. Colombo, T. Coviello, P. Matricardi, W.E. Hennink, T. Vermonden, M. Grassi, Mesh size distribution determination of interpenetrating polymer network hydrogels, Soft Matter, 8 (2012) 7708-7715.
[120] K.P. Whittall, A.L. MacKay, Quantitative interpretation of NMR relaxation data, Journal of Magnetic Resonance (1969), 84 (1989) 134-152.
[121] S.W. Provencher, A constrained regularization method for inverting data represented by linear algebraic or integral equations, Computer Physics Communications, 27 (1982) 213-227.
[122] X. Wang, Q. Ni, Determination of cortical bone porosity and pore size distribution using a low field pulsed NMR approach, Journal of Orthopaedic Research, 21 (2003) 312-319.
[123] D.P. Gallegos, K. Munn, D.M. Smith, D.L. Stermer, A NMR technique for the analysis of pore structure: Application to materials with well-defined pore structure, Journal of Colloid and Interface Science, 119 (1987) 127-140.
[124] G. Sørland, K. Djurhuus, H. Widerøe, J. Lien, A. Skauge, Absolute Pore Size Distributions from NMR, Diffusion Fundamentals, 5 (2007) 4.1-4.15.
[125] M.M. Chui, R.J. Phillips, M.J. McCarthy, Measurement of the porous microstructure of hydrogels by nuclear magnetic resonance, Journal of Colloid and Interface Science, 174 (1995) 336-344.

3. Inkjet printing as a drug loading method

This chapter investigates the feasibility of inkjet printing as a drug loading method for microcontainers. Initially, the investigation focused on printing solutions containing furosemide and lipid based-mixtures, principal component of SNEDDS (Self Emulsifying Drug Delivery Systems).
Then, the drug loading approach was divided into two steps: i) filling microcontainers with a polymer matrix, ii) loading the matrix with the drug. Inkjet printing was used to immobilize polymers inside microcontainers. This approach was tested with sodium alginate and poly(vinyl pyrrolidone) (PVP).
Preliminary experiments with PVP were performed in the laboratories at the Naughton Institute (Trinity College Dublin, CRANN) and at the Danish Technological Institute (DTI, Taastrup, Denmark).
Results of furosemide printing were presented in an oral presentation at the 6th Symposium of The Pharmaceutical Solid State Research Cluster (PSSRC) (Lisbon 26-28 August 2012).
The section regarding printing of PVP is based on the paper "Inkjet printing as a technique for filling of microwells with biocompatible polymers"(see Appendix 1). Some topics of this work were presented in a poster presentation at the 38th International Conference on Micro and Nano Engineering (Toulouse 16-20 September 2012)

3.1 Inkjet printing in life sciences and drug delivery

3.1.1 Application in high throughput screening (HTS)

In the last decade inkjet printing has become a key technology in life sciences. In fields like genomics, molecular biology and drug screening, the typically reduced amounts of biological material available for each test, and the need of more rapid and cost effective procedures, have edged more and more on computerization and scaling down processes. In high throughput screening (HTS) thousands of small quantities of compound are transferred from a master plate to the assay plate. The implementation of microdispensing technology for HTS offered the capability of minimizing reagent costs and optimizing the quantity of information from each plate run [1]. At the same time all the usually required dilution steps were faster [2]. Microarrays become soon a valuable replacement of manual pipetting in microtiter plates, allowing simultaneous analysis of several thousands of nanoliter assay spots with high density printing.
One of the first successful applications of inkjet printing has been the large scale screening of diverse genes by immobilization of DNA or synthetic oligonucleotides onto substrates, for the detection of genomic material by selective base-pair binding. In 2000, MacBeath and Schreiber [3] developed miniaturized assays of nanoliter-volumes, with a spatial density of 1300 dots/cm^2, for the simultaneous processing of thousands of proteins. In the same year, Goldmann and Gonzalez [4] used a commercial printer to deposit high resolution DNA arrays with a high density (300 dpi).
Microarray spotting has also found a valuable application in the fields of tissue engineering and cellular colony patterning. Roth and coworkers [5] used dispensed collagen solution to fabricate cellular scaffolds. Barralet *et al.* [6] created 3D angiogenic implants by spraying calcium phosphates onto hydroxyapatite and brushite based-ceramics biomaterials.

3.1.2 Application in drug delivery

Thanks to the improvements obtained in the control of droplets volume and jet direction, as well as the accuracy of spot placement, inkjet printing has become an interesting tool also in the field of drug delivery. Indeed, one of most important added values, which this technology can offer to drug delivery, is the capability of manufacturing personalized medication. Thermal inkjet technology was employed to create aerosol inhaler for local and systemic delivery of therapeutic proteins [7]. Goodman and coworkers showed that aerosol of insulin and human growth hormone solutions generated particles with a narrow size distribution and that the model proteins were not damaged by the inkjet operation. Tarcha *et al*. [8] has employed this technique to deposit 100 µg of drug, on the surface of a small stent, with a very high deposition efficiency.

The implementation of inkjet printing for pharmaceutical oral dosage forms is quite recent, and the literature regarding this field is limited. Inkjet printing has been employed by Haushild and collaborators [9] as alternative solution for the preparation of unilamellar vesicles for drug delivery. Ethanol solutions, containing both polymeric and lipid amphiphiles were printed into water, forming vesicles with diameter 50-200 nm. In this case the advantages of inkjet printing compared to traditional emulsions, are the narrow size distributions of vesicles, and the consequent high control of drug loading.

Sandler and coworkers have extensively studied the use of inkjet printing for drug formulation purposes [10-12] and combined it with flexopraphy [13]. Their work represents the state of the art in the use of printing for the manufacture of flexible doses and tailored drug delivery systems. The feasability of drug printing has been investigated for several APIs and sprayed droplets were characterized with scanning electron microscopy, X-ray diffraction and differential scanning calorimetry. Printed solutions containing caffeine and loperamide exhibited limited and no recrystallization events after deposition [10]. The printing of piroxicam was optimized for inkjet and impression printing [12] giving accelerated release of the drug. The effect of three different substrates on printed riboflavin solution was elucidated [13], demonstrating that the substrate composition influences significantly the drug release.

A deep understanding of the drug distribution in printed droplets of felodipine-poly(vinylpyrrolidone) mixtures was provided by Scoutaris *et al.* [14]; spectroscopic analysis and atomic force spectroscopy scanning revealed that the printed formulations remained homogeneous dispersions after printing, and that the drug release can be modulated by the drug loading.

3.2 Equipment description and operation

3.2.1 Equipment description

An inkjet printer is schematically represented in figure 3.1. The equipment used in this investigation is composed by a XYZ movable inkjet head (Nanoplotter NP 2.1, GeSiM, Germany) equipped with a piezo-driven micropipette (GeSiM nanotip) with a 70 µm orifice, and a tray where substrates with typical dimensions of microscope slides can be mounted. The spotting area can be isolated from the surrounding with a moveble glass box. In this way the dispensing tip can spot the liquid in an environment saturated with the desired level of humidity by means of a connected vaporizer. The temperature of the slide tray can be cooled from room temperature down to 4° C by means of a refrigerant system. The humidity level and the stage temperature are important parameters which influence both the surface tension and the evaporation time of the dispensed material. The sample is aspired by the pipette through the orifice from a well in a titer plate where the sample is stored in microliter volumes at the desired temperature.

The aspiration of the sample is driven by a pressure unit, through a system liquid (micro filtered deionized water) which is generally in contact with the sample during aspiration and dispensing. Eventually, an air gap can be interjected between the sample and the system liquid in order to avoid direct contact between the two liquids. This is particularly important for samples containing water unsoluble compounds, which would precipitate inside the pipette by the contact with water, causing pipette blockage.

The system liquid is also used to rinse the pipette, both internally and externally: the head moves to a washing station, where the tip is immersed in a water reservoir and system water is flushed through the pipette for a desired time period. The outside of the tip is then wiped with filter paper. The washing is performed by default before sample aspiration, and at the end of the spotting session.
The inkjet head is monitored by a control unit connected to a computer. A top microscope camera is integrated into the pipette head and allows the alignment of the pipette and the imaging of the spotting result, when the printing session is completed. The system is also supplied with a stroboscope camera (side view camera) which allows to visualize the jet direction and stability, as well as shape and diameter of the generated droplets.

3.2.2 Spotting operation

The spotting is performed as a sequence of steps: i)washing, ii)sample aspiration, iii)stroboscopic check of the jet, iv)spotting, v)pipette emptying, vi)washing. During the stroboscopic check, the voltage and pulse length of the piezo actuators can be changed, and the effects on the jet can be monitored in real time by the operator. The general requirements for a good spotting are the following:

1. vertical jet direction
2. ejection of a single droplet (or eventually second smaller satellite droplet in vertical position)
3. spherical droplet shape
4. jet stability (i.e. position of droplets in the stroboscope frames)

The fulfillment of these requirements is double-checked by a software interface. The software checks the jet quality according to the set of parameters given by the operator and measures the droplet diameter fitting a circle on the visualized droplet shade (see figure 3.2). This is particularly useful for overnight spotting sessions. If one of the requirements is not satisfied, the software aborts the spotting session, the pipette is rinsed, wiped, and a new sample volume is aspired. The total aspired volume of the spotting session is calculated by the number of droplets set by the operator and the volume calculated by the software. The intensity, duration, and frequency of the voltage applied to the piezoelectric actuator of the dispenser were tuned for optimized microcontainer filling and kept constant during the spotting session.

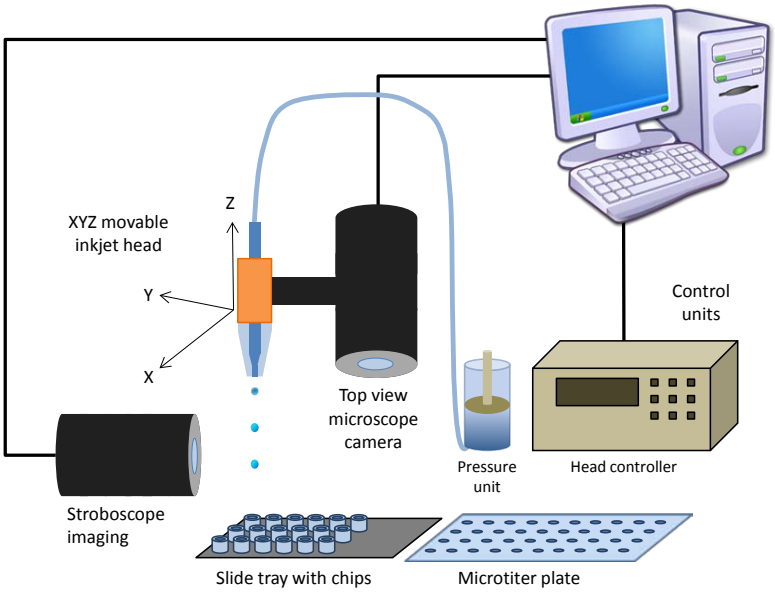

Figure 3.1: Schematic of the inkjet printer setup. The micropipette is mounted on a XYZ movable head. It aspires the liquid sample to be dispensed from a microtiter plate. The aspiration is driven by a dilutor pump. A functional pipette check takes place in the stroboscope. During spotting the pressure of the diluter pump is kept constant by system liquid (water).

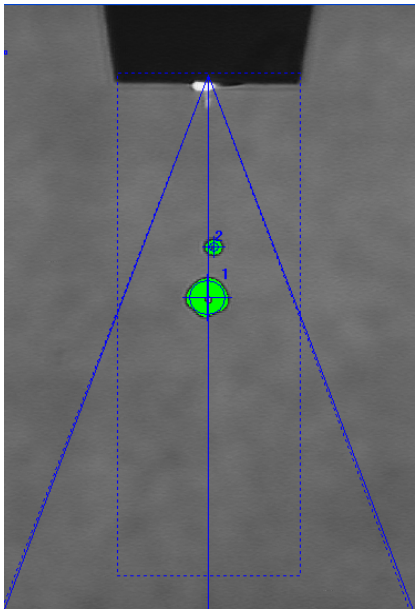

Figure 3.2: Stroboscope picture of in-fly droplets of buffer solution, ejected by a pipette (GeSiM nanotip). The software performs droplet recognition and allows the dispensing if the jet quality is good.

The intensity of the pulsatory voltage is a decisive parameter in the spotting experiment, as it strongly influences the droplet volume and shape. In table 3.1, droplet volume at different voltages and ejection frequencies are shown.

Table 3.1: Droplet volume (nL) at different voltages for a pulse width of 50 µs (averages on three GeSiM nanotips). Data adapted from manufacturer tests, performed on microfiltered water.

Ejection frequency [Hz]	Droplet volume (nL)		
	60 V	70 V	80 V
100	0.42 ±0.01	0.50 ±0.03	0.59 ±0.03
200	0.42 ±0.02	0.50 ±0.02	0.59 ±0.02
500	0.42 ±0.02	0.50 ±0.02	0.60 ±0.02
1000	0.45 ±0.01	0.52 ±0.06	0.56 ±0.11

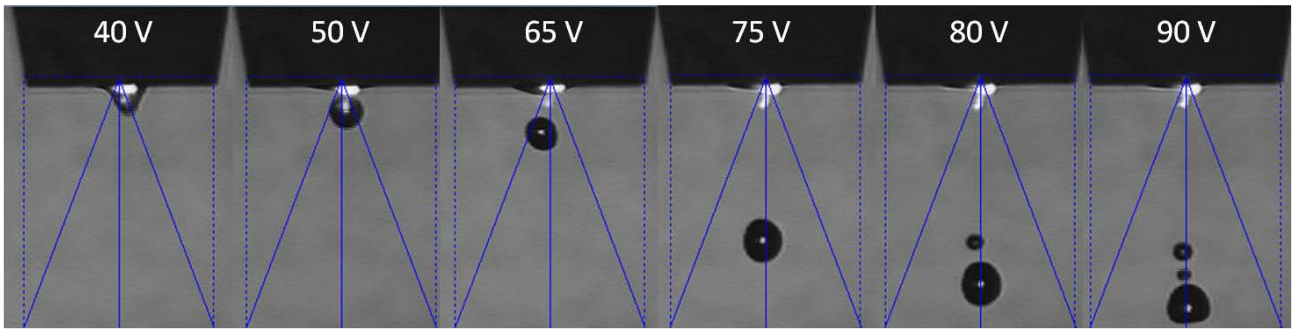

Figure 3.3: Consecutive stroboscope snapshots taken during ejection of water, at different voltage amplitudes. The increase of voltage reduces the delay of onset of droplet breakup.

In general, the pulse frequency does not have a significant effect on the ejected volume. Instead the voltage intensity modifies the droplet volume in a sensible way. From table 3.1 it can be observed that the ejected volume is proportional to the pulse amplitude. Another effect of voltage lies in the distance of the onset of droplet breakup for the tip, as shown in figure 3.3, where the droplet ejection of water at different voltage amplitudes is depicted.

3.2.3 Sample alignment

The alignment with the substrates on which the sample material is deposited on is another important feature of the equipment. The spotter in use offers the possibility of performing a manual alignment or implements an automatic recognition of pre-existing substrate patterns. The manual alignment is performed by assigning the offset between the pipette and microscope camera. The pipette and the camera are positioned upon the same recognizable object on the printing tray, and their (x,y) coordinates are annotated. The difference between the coordinates gives the offset. In alternative, the alignment step can be performed automatically by means of an object recognition program which finds the spotting target by their geometry. Once the alignment is done, the deposition pattern can be defined either manually (by positioning crosshairs in the microscope image), or alternatively drawn in a matrix scheme. Both are fast and efficient methods, and were preferred for the microcontainer filling, since the wells are arranged in squared matrices. Alternatively for complex deposition patterns a customized geometry can be drawn.

3.2.4 Spotting of liquid

As mentioned in section 2.2.2, a crucial requirement for inkjet printing of liquids, is that they exhibit a Newtonian behavior and a low viscosity. Indeed, the viscosity limit of the equipment used in this study is 5

mPa·s, which is five times larger than the viscosity of water. The droplet travel speed is up to 50 cm/sec. For this reason, dynamic viscosity of solutions were measured by means of a rotational rheometer prior to dispensing. One possibility to overcome the viscosity limitation, is offered by using heatable pipettes. These dispendser tips can be heated up to 120 °C allowing a substantial drop in viscosity for a large number of liquids.

3.3 Materials

3.3.1 Furosemide

Furosemide is a loop diuretic used for the treatment of hypertension and edema [15, 16]. It is a weak acid with pK_a values of 9.9 and 3.5. Its aqueous solubility ranges between 5 and 20 µg/mL at pH 7 combined with a low permeability. Furosemide is classified as a class IV drug and thereby as poorly soluble [17]. The oral bioavailability is highly variable (20-60%) and the absorption sites are stomach and upper small intestine [18]. Furosemide was the first candidate for direct inkjet printing of drug used in this project.

3.3.2 Poly(vinylpyrrolidone)

Poly(vinylpyrrolidone) (PVP) having molecular weights from 2500 to about 10^6 is mainly obtained by radical polymerization in solution [19]. The glass transition temperature of PVP is between 100°C (M_w=2500) and 175°C (M_w=10^6). In table 3.2 the main properties of PVP grades used in this study are summarized. K-values are often assigned to PVP commercial names. These values are derived from viscosity measurements by the manufacturer and are calculated according to Fikentscher´s formula [20]. PVP is a non-toxic polymer [21, 22], which is widely used as excipient for oral dosage forms e.g as binder and coating agent for tablets [19], as solubility enhancer for water insoluble pharmaceuticals [23], and as solubilizing agent for injections. PVP exhibits high solubility both in water and many organic solvents [24]. PVP forms complexes with various compounds, particularly with H-donors such as phenols and carboxylic acids. In the pharmaceutical field PVP is broadly used, as PVP K30 and K90 can be crosslinked by exposure to UV radiation [25, 26], giving a water insoluble compound that swells in water forming hydrogels. The crosslinked version of PVP is also used as tablet disintegrant due to its swelling property [27].

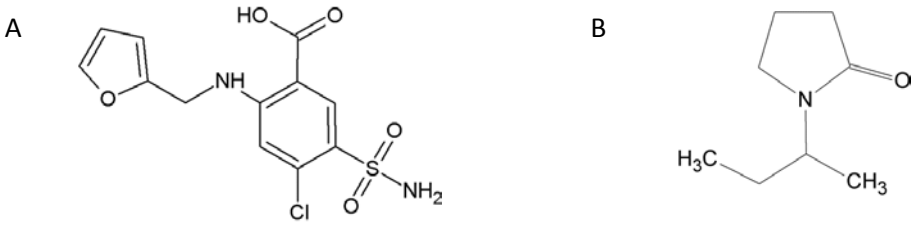

Figure 3.4: Molecular structure of (a) furosemide and (b) poly(vinylpyrrolidone) (PVP) monomer.

Table 3.2: Molecular weight and intrinsic viscosities of different grades of PVP [19].

K values	Molecular weight average (M_w)	Intrinsic viscosity (dL/g) [η]
K17	10^4	0.09
K30	$4{\cdot}10^4$	0.22
K90	10^6	1

3.3.3 Sodium alginate and calcium chloride

Sodium alginate is an anionic polysaccharide of natural origin. It derives from alginic acid, which is a linear copolymer with homopolymeric blocks of (1-4)-linked β-D-mannuronate (M) and its C-5 epimer α-L-guluronate (G) residues.

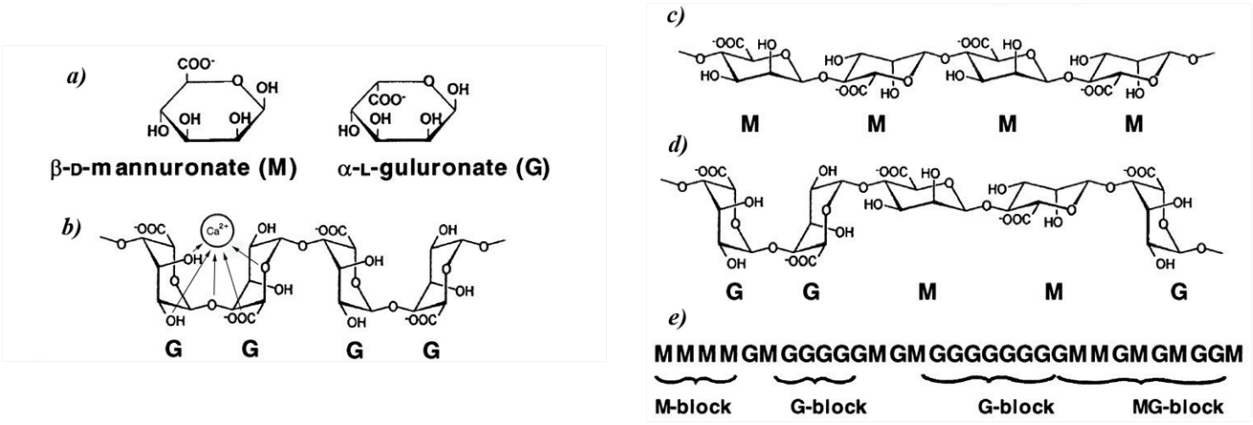

Figure 3.5: Alginate structure and monomers. (a) structure of β-D-mannuronic acid (M) and α-D-guluronic acid (G). (b) Polar coordination with a Ca^{2+} ion og G-blocks, (c) M-blocks region ,(d) MG-blocks region. (e) examples of blocks distributions inside polymer chain (adapted from [28])

A consequence of the spatial arrangement of G and M monomers is in the ability of the sodium alginates to form hydrogels in water solutions in presence of bivalent cations. The gelation is given by an ions exchange between the Na^+ of the G monomers with bivalent cations, like for instance Ca^{2+}. The bivalent of cation is interacts with G-blocks regions of adjacent polymer chains creating a three dimensional polymer network. This fact allows to convert alginate solution into hydrogels through reaction with solutions containing bivalent ions, like those of calcium chloride ($CaCl_2$) and several other compounds. The ion exchange reaction gives physically crosslinked hydrogel matrices, capable of swelling up to 100 times the dry polymer weight in water. Crosslinked alginates are broadly used in controlled release systems as well as for immobilization of biological agents such as live cells, proteins or active molecules in general.

3.3.4 Lipid solutions for SNEDDS-based formulations

SNEDDS (Self Nano-Emulsifying Drug Delivery System) are isotropic mixtures of oil, surfactant and co-surfactants designed to provide a protection to fragile biological therapeutics, against the harsh environment of the GIT.

When getting in contact with an aqueous environment (i.e.the physiological medium) SNEDDS formulations spontaneously form a nanoemulsion with nanomicelles encapsulating the protein therapeutics [29].

Such a formulation could be loaded inside microcontainers, which should release the therapeutic in the form of nanomicelles once they are in contact with the intestinal mucus.

One of the projects of our collaborators in NAMEC at KU Pharma, was dedicated to the development of a SNEDDS for the encapsulation of insulin. The aim of the study was to test the feasibility of inkjet printing for filling microcontainers with SNEDDS formulations. An optimized formulation for insulin developed by our collaborators [30], was composed by 50% Miglyol 812, 30% Medium-chain partial glycerides (Akoline MCMEP), 20% TW80 (a mixture of surfactants). The investigation presented in this thesis, consists of experiments which were carried out with samples not including insulin. For a preliminary study, it was believed that the contribution of insulin to parameters affecting the printability (e.g. viscosity) could be neglected.

3.4 Inkjet printing of furosemide solutions

3.4.1 Preparation of solutions

Furosemide dissolves in many organic solvents [31]. The equipment manufacturer discourages the use of methanol and dichloromethane, which cause the softening and dissolution of the glue used for the pipette assembly. Furthermore, the choice of solvent was directed to less toxic chemicals. Ethanol has a low boiling point, and preliminary printing tests revealed that ejected droplets evaporated before landing on the surface. Therefore, DMSO was added as cosolvent. Solubility of furosemide in ethanol ranges between 2 and 14 mg/mL [31, 32] and DMSO is over 50 mg/mL [31]. Solutions of furosemide were prepared by dissolving the drug (1, 5, 10 mg/mL) in mixtures of ethanol and DMSO at different volume ratio (10:90, 30:70, 50:50, 70:30, 90:10).

In a second stage of the investigation, solutions of furosemide in buffer solutions (pH 9.2) at a 5 mg/mL (reported solubility value is 10 mg/mL [33]) were printed on microcontainers. This was motivated by the intention of studying the effect of surface tension of the solvent on the deposition.

3.4.2 Results of spotting

3.4.2.1 Inkjet optimization

Due to the poor aqueous solubility of furosemide, the contact of the aspired solution with water had to be avoided to prevent solute precipitation inside the nozzle. As a consequence, a fixed volume of pure ethanol was sucked in the nozzle, prior the sample aspiration. With that, the ethanol flushed the internal volume of the tip prior to the washing step with system water at the end of the dispensing. Between the sample and ethanol, an air gap was used instead to avoid dilution of the solution.

Despite this procedure, in general the printing of furosemide solutions was barely reproducible, due to frequent clogging of the tips, occurring after few seconds, although the sample solution in the vials was stable for weeks after their preparation. This problem occured in any test performed, both with new and already used tips, and was getting worse at increasing drug concentration. This fact suggested that the tip obstruction was related to drug precipitation on the edge of the needle tip. From the stroboscopic imaging, it was observed that the progressive occlusion, deflected the jet direction for substantial angles (10-25°) with respect to the vertical direction. Printing of solutions containing 0.1-1 mg/mL was also tested, but clogging occurred even in this case. Clogged nozzles could in most cases be recovered, by manual flushing with pure ethanol, but in some cases tips were permanently damaged. Nevertheless, the stroboscopic imaging of the spray jet formation (droplet size and jet direction) allowed to identify a set of ejection parameters for a number of solutions (referred as type A, B and C). The optimal parameters for the solutions listed in table 3.3.

Table 3.3: Optimized printing setting for various furosemide solutions.

Sample type	Solution (v/v)	Drug conc. (mg/mL)	Pulse width (µs)	Voltage (V)	Frequency (Hz)	Humidity (%)
A	EtOH:DMSO (50:50)	1-5	112	64-70	370	42.9
B	EtOH:DMSO (10:90)	1-10	50	70-74	200	44.9
C	Buffer (ph 9.2)	1-5	90-100	63-90	370	32

3.4.2.2 Microcontainer filling

Directly after the printing, by means of the top view camera, it was possible to visualize the containers spotted without spillages, before the progressive obstruction of the orifice caused jet deflections. Microcontainers appeared visibly translucent. After the solvent evaporation, containers were inspected with an optical microscope. Top view micrographs of containers spotted with sample type A (see table 3.3), are shown in figure 3.6a. Optical pictures show one circular ring of particles outside the containers walls. It was believed that this outer ring was formed by the drug which crystallized. Apparently the solution flowed out of the microcontainer cavity. This flow was probably induced by a surface wetting effect. This conclusion was also supported by the translucence of SU-8 after the spotting. Thus, it was believed that, making microcontainer surface more hydrophilic would have helped to restrain the solution inside the cavity. For this purpose, the microwells were submitted to oxygen plasma (70mL/min O_2, 50 W, 0.5 mbar, 8 min) as suggested for a similar purpose in [34]. Oxygen ions react with the exposed surface generating more OH-groups, which renders SU-8 more hydrophilic [35]. Just after plasma activation, microcontainers were filled with sample type A. The result of the spotting is shown in the figure 3.6b. In this case, solution drying occurred both inside and outside of the wells. The solution spreading was improved, since furosemide deposited partially inside the cavities. However, the performance was not satisfactory yet.

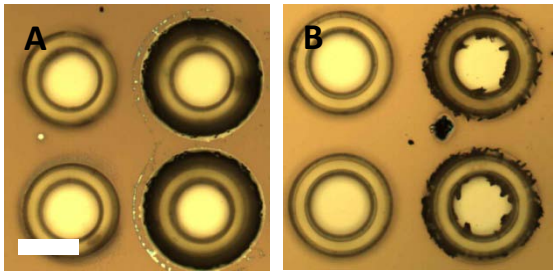

Figure 3.6: Top view micrograph of two containers (on the right) filled with sample type A before surface hydrophilization (a), and after surface hydrophilization (b). On the left, empty containers are shown as comparison (scale bar 200 µm)

A further attempt of inkjet deposition was accomplished with aqueous furosemide solutions (sample type C) with no plasma treatment. In figure 3.7 the result of printing is shown. From the stroboscopic check, the printing of buffer solutions gave a more stable jet formation, although nozzle clogging still occurred after few minutes. The result is a reproducible deposition of furosemide inside the containers. This fact confirmed that a water-based solution is more suitable for printing. Figure 3.8 shows the bottom of a container where crystalline material (buffer salts and furosemide) is visible at the edges. Nevertheless, the deposited drug amounts, even after multiple printing sessions, were still too small to quantify the loading or to detect a drug release.

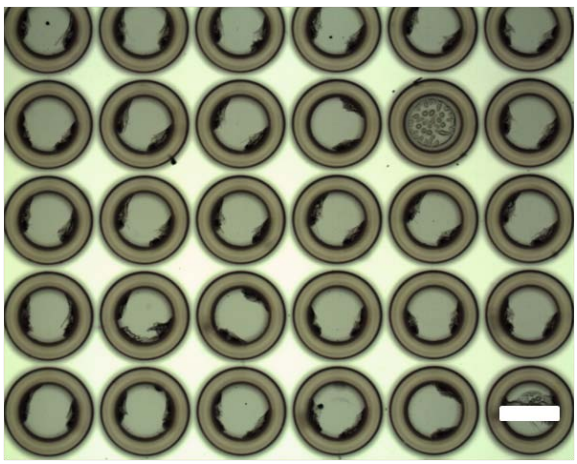

Figure 3.7: Optical microscope image of arrays of microwells filled with sample type C (scale bar 200 µm).

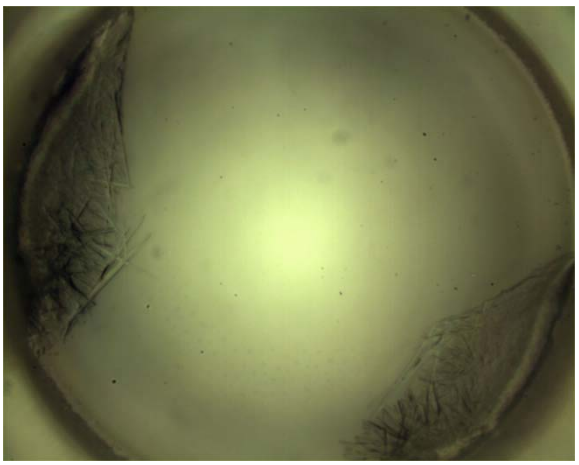

Figure 3.8 Optical microscope of a container bottom filled with sample type C.

3.5 Confined crosslinking of alginate matrices

The unsatisfactory printing of furosemide demonstrated the need to consider alternative approaches for drug loading of containers. Albeit the inkjet printing of water-unsoluble compounds revealed operational limitations, it was observed that water based-solution exhibited a more stable dispensation. Therefore, it was believed that this technique was a good choice for a precise deposition of minute amounts of materials fulfilling the requirements of low viscosity and compatibility with the system liquid of the printer.
A possible solution was dividing the drug loading into two steps: i) fixing a polymer matrix inside the microcontainers and ii) loading the drug by polymer swelling. In principle, the first step can be accomplished by inkjet printing as long as the dispensed solutions do not contain water insoluble compounds causing pipette clogging. The fixation can be performed by polymer deposition and a crosslinking reaction confined inside the microcontainer volume. Once the polymer matrix is fixed inside the container cavity, the second step can be carried out by the absorption of the drug solution. For this task it is important that the solvent used is both dissolving the API and swelling but not eroding or dissolving the matrix.

3.5.1. Experimental procedure

The printing of alginate solution could not be performed with the available equipment because of the high viscosity of the polymer solution even at low concentrations (3% w/v) [36]. An alternative approach for local crosslinking of alginate is schematized in figure 3.9. The procedure consists of printing aqueous solutions of the crosslinker ($CaCl_2$, calcium chloride) inside the containers (I), followed by a deposition of sodium alginate onto the whole chip. The gelation of the solution is activated inside the microwell. Finally, the uncrosslinked portions of the polymer are dissolved by immersion in water. The choice of putting the crosslinker injection step before the polymer deposition was motivated by the need to confine the gelation inside the cavity by diffusion of Ca^{2+} ions in the matrix, avoiding the risk of unspecific crosslinking.

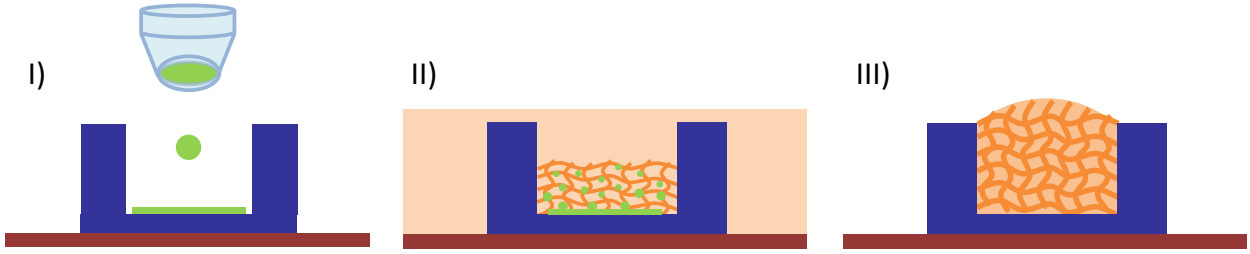

Figure 3.9: Schematic of confined crosslinking of sodium alginate: (I) inkjet printing of crosslinker ($CaCl_2$ in water), (II) deposition of alginate solution and activation of crosslinking reaction inside the microwell, (III) dissolution and removal of uncrosslinked polymer.

The crosslinker solution was prepared dissolving the chlorine salt $CaCl_2$ (anhydrous powder >97%, Sigma Aldrich) in microfiltered deionized water with the concentration of 0.45 M, under stirring for 1 hour at room temperature. The solution was filtered to remove particles which could block the inkjet nozzle. The printing resulted in a stable jet with an optimized setting (85 µs, 80 V, 100 Hz), giving droplets of 0.25 nL (volume estimated from stroboscopic check of droplet size). Figure 3.10 shows arrays of microcontainers filled with $CaCl_2$ crystals (dark halo). In each microwell were spotted 120 droplets, in 6 consecutive sessions of 20 droplets. The estimated $CaCl_2$ weight for each container was 1.5 µm. After printing, the chips were stored in vacuum at room temperature for 24 hours, to ensure a complete evaporation of the solvent. A SEM picture of salt crystals on the container bottom is shown in figure 3.11. Although during the stroboscopic check the liquid jet was stable, the amount of dispensed liquid in several cases did not appear uniform inside the wells, as also results from the top view image in figure 3.10.

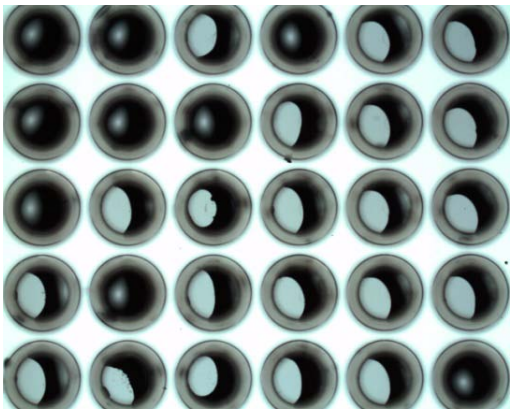

Figure 3.10: Microscope picture of arrays of 300 µm wide microcontainers filled with 120 droplets of crosslinker solution (black round halo), dispensed in six consecutive spotting sessions of 20 droplets each. The resulting total mass of $CaCl_2$ is 1.5 µg for container.

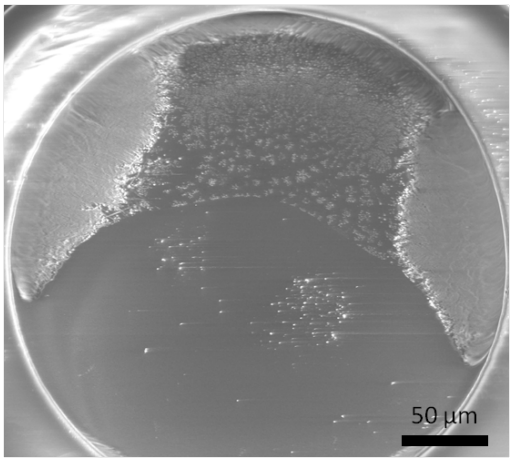

Figure 3.11: SEM picture of microcontainer bottom after spotting of 120 droplets of $CaCl_2$.

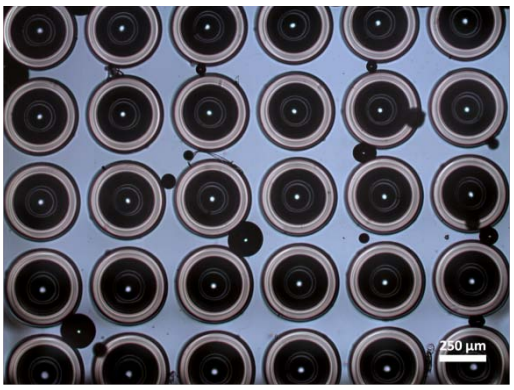

Figure 3.12: Optical microscope image of air bubbles inside containers, after pouring of 3% alginate solution. Air remains trapped because of the slow wetting by the solution; the high viscosity of the liquid hinders bubble release.

Sodium alginate was dispersed in deionized water, with the following concentrations: 0.5, 1, 2, 3% (w/v). The solution deposition onto microcontainers required a preliminary study to optimize the experimental procedure. In a first series of trials, pouring viscous water solutions of sodium alginate on hydrophobic SU-8 microcontainers resulted in a non homogeneous filling because of the entrapment of air bubbles, as shown in figure 3.12. To improve the wetting properties of SU-8, microcontainers were subjected to oxygen plasma treatment (70mL/min O_2, 50 W, 0.5 mbar, 8 min), as described in section 3.4.2. The subsequent immersion of plasma treated chips in alginate solution in an ultrasonic bath was also unsuccessful. As alternative to improve bubbles removal, the chip with containers was put inside a vacuum chamber and the solution was dosed on top of it by means of a syringe through rubber tubing placed on top of the chip. Most of the prepared solutions were too viscous for injection; as a result only 0.5% alginate (w/v) injection resulted suitable for the purpose. The standardized procedure, adopted in the experiments, is as follows:

1. A syringe is filled with 1 mL solution of 0.5% (w/v) alginate in water and approximately 5 mL of air;
2. the $CaCl_2$ laden-chip is placed in the vacuum chamber, which is then sealed;
3. the vacuum is applied for 5 minutes, during which the 5 mL of air in the syringe is sucked in;
4. 1 mL of alginate solution is injected onto the chip through the tubing;
5. the solution is aspired by the vacuum, and through the tubing, droplet starts to deposit onto the silicon surface with the microwells; later the first bubbles are released from the container volume.
6. After few minutes, when the last bubbles are released, the chamber is opened and the chip collected. The exceeding amount of polymer is removed with a spatula.

3.5.2 Results

The amounts of printed $CaCl_2$ had a relevant effect on the confinement of alginate gelation.

Experiments were performed on 18 nL volume containers (inner diameter 300 µm) filled with 30, 60 and 120 droplets (0.25 nL), of solution of 50 mg/mL ($CaCl_2$). This corresponds to approximately to 0.38, 0.75 and 1.5 µg of $CaCl_2$ per containers respectively. With a 0.5% (w/v) alginate solution (5 mg/mL), each cavity was filled approximately with 0.09 µg of polymer. Thus, in principle the alginate/$CaCl_2$ weight ratios within one container, filled with 30, 60 and 120 crosslinker droplets, were approximately equal to 1:4.5, 1:9 and 1:17 respectively.

Alginate dispensing, performed with a 1:18 ratio, resulted in the gelatinization of a continuous film of polymer, which could even be pealed off the chip surface. An example of continous gel film is shown in figure 3.13. In this optical picture the transparent film can be recognized by the halos of round edges of containers, imprinted on the film and shifted inrespect to the containers. This phenomenon was explained with the spreading of the gelling reaction to the volume outside the containers. Probably, the excess of $CaCl_2$ inside the well started to diffuse outward, reacting with external portions of polymer. This explanation was supported by a closer inspection of individual containers, as depicted in figure 3.14.

Deposition of alginate on containers filled with the smallest amounts of crosslinker (1:4.5 Alginate:$CaCl_2$ weight ratio), resulted in complete salt dissolution and in better confinement of gelation. An example is shown in picture 3.15. Thereafter, alginate filled containers were immersed in water to remove the uncrosslinked polymer from the surface in between the containers.

In figure 3.16 the same chip as the one shown in figure 3.15 can be seen after dissolution and removal of uncrosslinked alginate.

The level of alginate filling was measured by means of a visible light interferometer. The heights of well filling were very variable even on adjacent containers. This result was attributed to the difficult control of polymer deposition which had to occur inside a vacuum chamber, as well as to the issues with removal of air bubbles. The containers in the chip centre were covered first by sodium alginate which resulted in improved filling and with less residual bubbles than containers at the edges.

In general, the results of alginate deposition were unsatisfactory due to the complexity of the phenomena involved (surface wetting, bubble extraction).

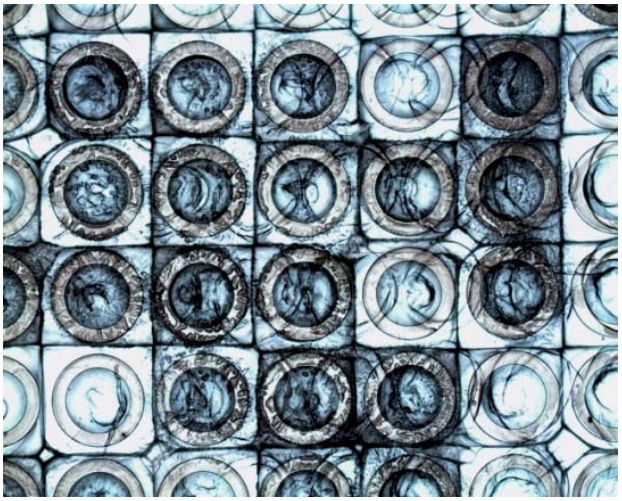

Figure 3.13: Optical microscope picture of local crosslinking of alginate. A transparent film with round halos is visible on top of microwells.

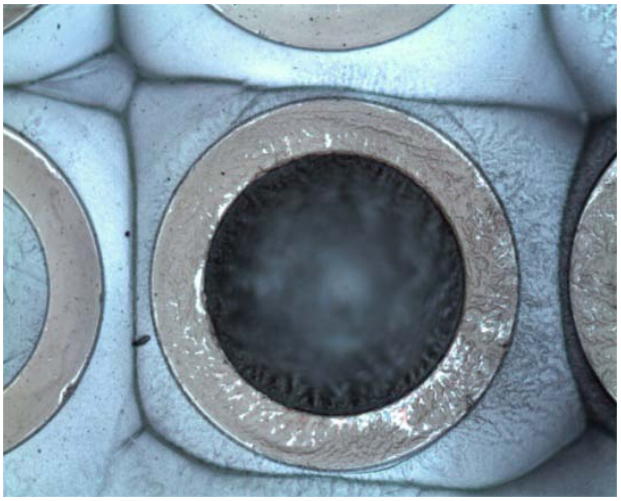

Figure 3.14: Optical microscope picture of particles migration occuring just after polymer deposition. The particles are probably $CaCl_2$ crystallites that are not fixed in the polymer and diffuse out the container cavity.

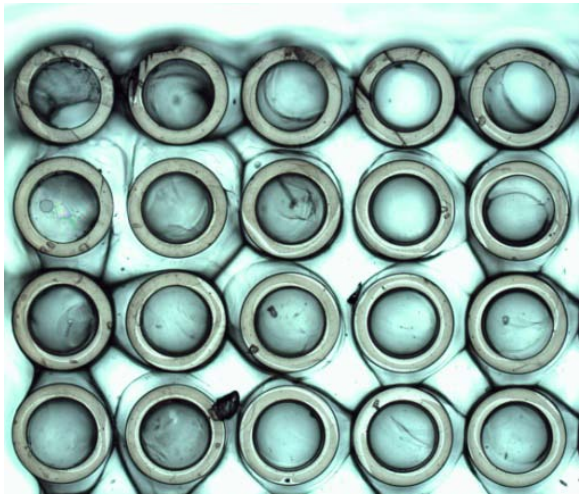

Figure 3.15: Optical microscope picture of arrays of containers after the crosslinking reaction (1:1 Alginate:$CaCl_2$). No residual crosslinker is visible.

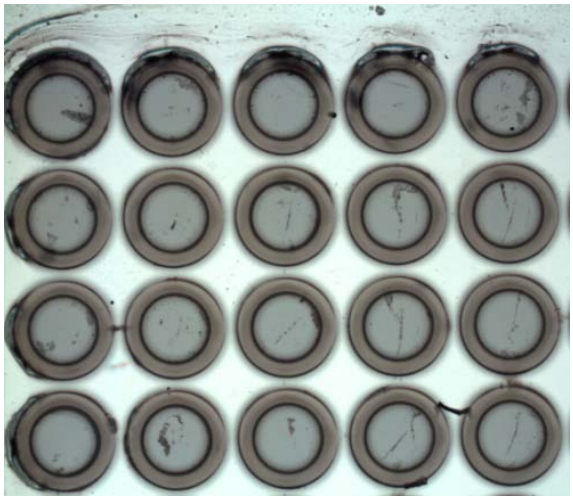

Figure 3.16: Optical microscope picture of the same group of containers shown in figure 3.15, taken after the removal of uncrosslinked alginate.

3.6 Inkjet printing of PVP solutions

This section contains results published in the paper: “Inkjet Printing as a technique for filling of microwells with biocompatible polymer”. Preliminary tests of printing of PVP solutions were performed at the Naughton Institute (Trinity College Dublin, CRANN) in the laboratories of Martin Hegner´s research group.

3.6.1 Printability of PVP solutions

Based on previous experiences printing of aqueous solutions was feasible with the equipment in use and resulted in a good reproducibility. As an alternative procedure for filling the containers in the dispensing a diluted aqueous solution of polymer into the microwells was identified. Poly(vinyl pyrrolidone) (PVP) was chosen because it is highly soluble in water and because the viscosity of solutions can be tuned to be compatible with the printer limitations. To reduce the risk of jet instability and shorten process time, an increase of polymer concentration would have limited the number of consecutive depositions. On the other hand, viscosity also increases with concentration. Furthermore higher concentration can induce the occurrence of non-Newtoninan behaviors, which is not suitable for printing. Therefore, a compromise between polymer concentration and printing feasibility was searched. Sadeghi et al. [37] reported the viscosity of aqueous solutions of PVP (M_w 10^4 Da) at different concentrations and temperatures. According to this work, PVP up to 17% (wt) has a viscosity below the operation limit of 5 mPa·s at room temperature. At T= 55°C, PVP solution with 25% wt can potentially be spotted. PVP was dissolved in different concentrations of 5, 10 and 20% wt and viscosity measurements were performed with a rotational rheometer to ensure that the solutions exhibit a Newtonian behavior and a viscosity value below 5 mPa·s. To investigate the effect of surface tension of spotted solutions on wetting of SU-8, solutions of PVP in isopropanol (2% wt) were also printed. These last tests were performed with another inkjet printer (Microdrop Dispenser Head, MD-K-130, Germany) at the Danish Technological Institute (DTI, Taastrup, Denmark).

3.6.2 Inkjet printing of PVP solutions

The intensity, duration, and frequency of the voltage applied to the piezoelectric actuator of the dispenser have been tuned for optimized microwell filling. The optimum set of parameters is a pulsing voltage of 90 V, a pulse width of 90 µs and a frequency of 175 Hz for all the solutions. The diameter of the droplets was measured with the stroboscope imaging to 47 µm for 20 % wt PVP and 53 µm for 5 and 10 % wt PVP.

3.6.3 Microcontainer filling

PVP solutions are dispensed by DOD inkjet printing into containers of different sizes. The number of droplets to dispense in each container is estimated dividing the cavity volume by the droplet volume. An overview of the spotting plan is shown in table 3.4. The typical time needed for spotting an array of 625 containers is around 12 minutes. To increase the polymer content inside the microcontainers, the spotting process is repeated up to three times on the same array in subsequent printing sessions, where during each session a solution volume equal to the cavity volume is dispensed into each microcontainer. Between the sessions, a waiting time for solvent evaporation is introduced in order to avoid spillover. The evaporation of the drops is observed with the top view camera and the time is measured. The typical drying times for isopropanol and water based-solutions were 1 and 2 minutes respectively. The polymer concentration did not sensitively affect the evaporation time of dispensed solutions. To measure the filling level of the microcontainers, the chips are coated with an Aluminum layer (15 nm, Alcatel SCM 600). The PVP thickness was then measured by means of an optical profiler (PLu Neox Optical Profiler, Sensofar), equipped with 50x (cavity diameter 300 and 200 µm) and 20x (100 and 50 µm) objective to measure. The profiler is set in confocal mode, with a monochromatic blue light (460 nm). Each microcontainer is scanned along a cross section passing through the container center within a scanning range of 400 µm with a resolution of 1 µm. Figure 3.17a shows a SEM image of a microcontainer, where the cross section is highlighted in red. In figure 3.17b the two dimensional profile of a polymer-filled container is plotted.

Table 3.4: Dispensed volumes of polymer solution for different well sizes for one inkjet session.

Cavity diameter (µm)	Cavity volume (nL)	Dispensed volume for one inkjet session			
		5%, 10% wt.	number of droplets	20% wt.	number of droplets
300	18	18	60	18	75
200	8	7.5	25	7.7	32
100	2	1.8	6	1.9	8
50	0.5	0.3	1	0.5	2

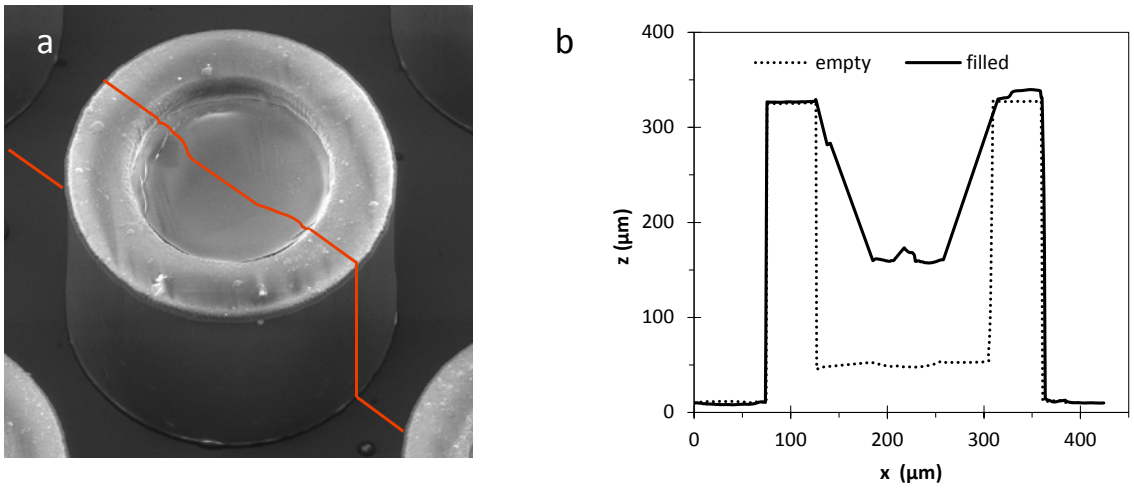

Figure 3.17: (a) SEM picture of a polymer filled microcontainer with outlined cross section, (b) 2D profiles of an empty (dotted line) and filled microcontainer (solid line) with 64 droplets of PVP 10% wt in water scanned with the optical profiler.

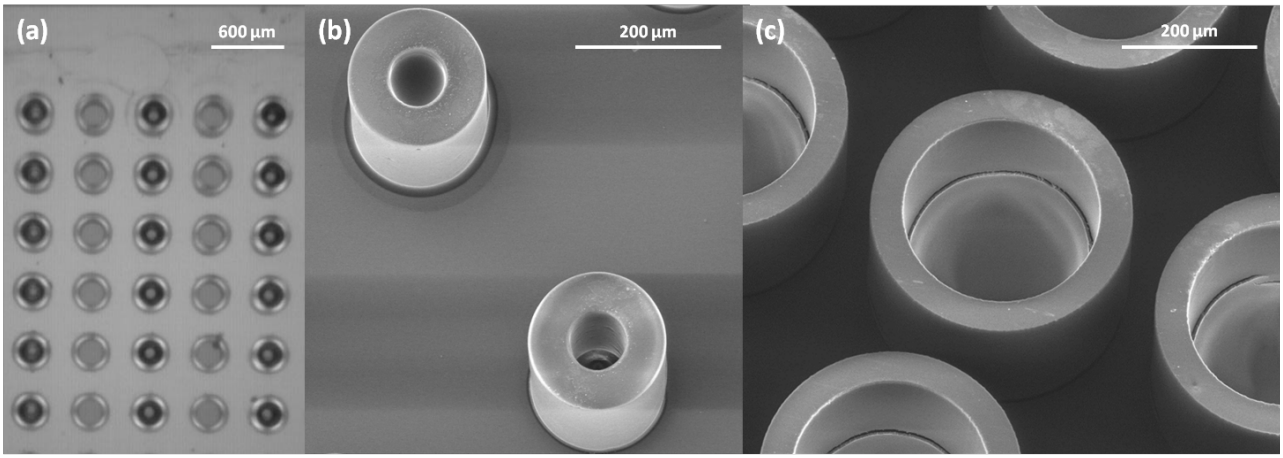

Figure 3.18: (a) Microscope image of three arrays of microcontainers filled with 10 wt % PVP. SEM images of (b) an empty (bottom right) and a filled well with diameter 50 µm (top left), (c) 300 µm inner diameter wells filled with 5 % wt PVP, 60 droplets.

3.6.4 Level of microcontainer filling

Arrays of containers with cavity diameter of 50, 100, 200 and 300 μm are filled with aqueous solutions of PVP at different concentrations. In figure 3.18a a microscope picture of three arrays of filled containers is shown. In figure 3.18b a SEM picture of an empty well (bottom right) and a filled one (top left) are shown. SEM pictures of microcontainers after filling revealed that large arrays of microwells can be filled with high precision. A quasi-no-waste deposition (see figure 3.18c) can be achieved when subsequent printing steps are performed on the same wells and a waiting time for solvent evaporation is included. According to the viscosity limit of the dispensing system, a concentration of polymer up to 20 % wt is successfully spotted. It is observed that water solutions can be spotted with a higher volume than the microcontainer cavity, because the high contact angle of water on SU-8 and the high surface tension of water confine the solution in a cap on the top of the microstructures (see figure 3.19). Upon drying of the liquid, the liquid cap shrinks, and the polymer is deposited in the cavity. After water evaporation the microcontainers were analyzed with scanning electron microscopy and the polymer deposition looked similar to figure 3.18c. The change of jet frequency was also investigated but it did not affect the coating performance. Thus the content of polymer in each microwell can be controlled by varying its original concentration in the solution and repeating several printing sessions. The level of polymer filling is measured with an optical profiler. An array of 25 microwells was scanned for each container dimension, for the three different level of filling (i.e. inkjet sessions), along their cross section passing through the centre. In table 3.5 the height of the polymer layer in the center of the microcontainers is shown. The reported values are the difference of the height of the polymer layer and the container bottom thickness (35 μm). By comparing the filling level with the corresponding number of droplets it can be noticed that the increase is non-linear. This is due to the fact that the polymer tends to be distributed also on the walls of the containers, and this coating layer gets gradually thicker with the level of filling. The roughness of the surface due to cracks induced by the polymer shrinking does not allow a more accurate computation of the polymer volume by numerical integration.

Table 3.5: Filling level of polymer for different container sizes after one, two and three inkjet sessions with solutions of PVP 20% wt. in water. Each value is the average of 25 microcontainers.

Cavity diameter (μm)	Polymer height after subsequent inkjet sessions					
	number of droplets	polymer height (μm)	number of droplets	polymer height (μm)	number of droplets	polymer height (μm)
300	75	8±2	150	20±1	225	24±1
200	32	88±7	64	132±9	96	155±2
100	8	102±3	16	223±7	24	246±5
50	2	125±5	4	182±4	6	282±8

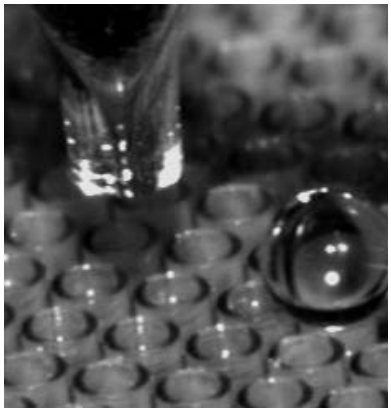

Figure 3.19: Microscope picture from the side of one microwell spotted with 4000 droplets of PVP in deionized water (2% wt) with a drop ejection frequency of 100 Hz.
Picture taken with a custom-made side view microscope, mounted on an inkjet spotter (Microdrop technologies, GmbH, Germany) at Martin Hegner´s laboratory (CRANN, Trinity College Dublin).

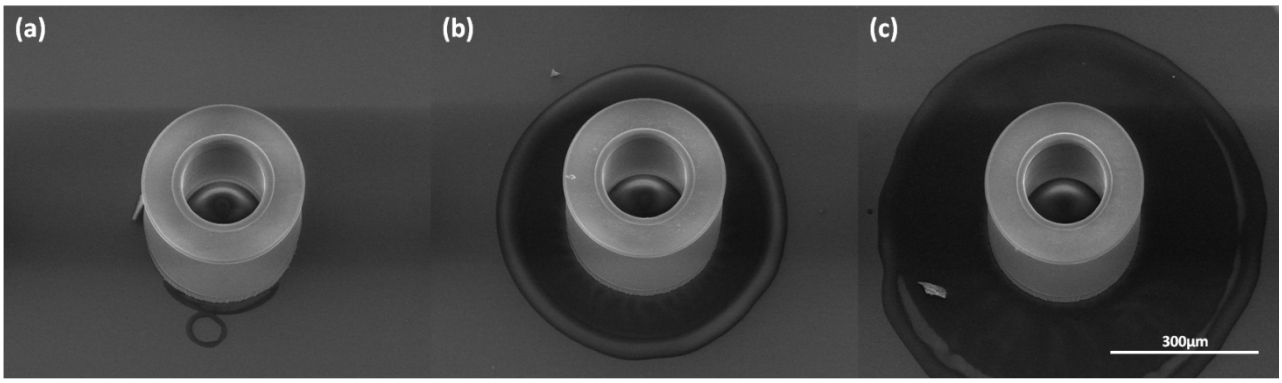

Figure 3.20: SEM pictures of microcontainers spotted with PVP in isopropanol solution (2% wt). The same solution volume was dispensed with a drop ejection frequency of 100 Hz (a), 200 Hz (b) and 500 Hz (c).

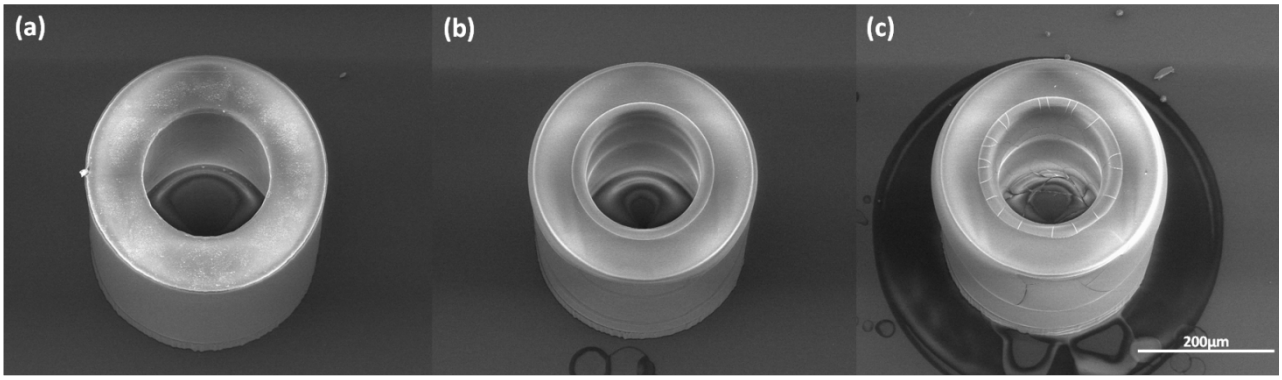

Figure 3.21: SEM images of microcontainers filled with an increasing number of droplets: 1000 (a), 2000 (b) and 6000 (c).

3.6.5 Effect of surface tension on deposition

The effect of surface tension of different solvents on the SU-8 surface is investigated by dispensing solutions of PVP in isopropanol. It was also believed that spotting of PVP in isopropanol could be compared with the results obtained with furosemide in DMSO and ethanol (described in section 3.4.2). For this purpose, solution of 2% wt PVP (M_w 10^6 Da) is dispensed into wells with a diameter of 200 µm. The substrate temperature is kept at 50˚C in order to shorten the solvent evaporation time. The droplet volume was 0.3 nL. Figure 3.20 shows SEM images of containers filled with 1000 droplets at different frequencies: 100 Hz (figure 3.20a), 200 Hz (figure 3.20b) and 500 Hz (figure 3.20c). For all three cases, the same volume of solution was dispensed, with equal droplet size (not depending on the jet frequency), but with different dispensing rates. In any case the solution did not fill the cavity, but tended to wet the surface of the container covering it with a uniform coating. However, at higher frequency, not only the container was coated but also an increasing part of the substrate in between the containers. In the SEM pictures in figure 3.21 the effect of droplet number on the coating is shown: 1000 (figure 3.21a), 2000 (figure 3.21b) and 6000 droplets (figure 3.21c) were dispensed at a constant frequency of 100 Hz. PVP layer thickness increases with the droplet number. 1000 droplets were dispensed without spillage. These results are explained by the low contact angle of isopropanol on SU-8. Before evaporation, the solvent wets the container distributing the polymer uniformly on its surface. The result is a conformal coating of the three dimensional structure. The effect of frequency could be explained by the different time it takes for the droplets of solution to dry once they land on the microcontainer bottom. The higher the spotting frequency, the longer was the time the solution remained wet. The droplets coalesced and formed a liquid volume that symmetrically flowed onto the surrounding available surface until the solvent dries.

3.7 Inkjet printing of lipid based formulations for insulin delivery

One of the formulations developed for microcontainers was a lipid based solutions and was composed of a mixture of oils and surfactants (see section 3.3.4), resulting in a viscous liquid. The shear viscosity of the solution was measured with a rotational rheometer, and was at room temperature approximately equal to 55 mPa·s. As a consequence, the liquid needed to be heated in order to be printed. A feasibility study performed by the equipment manufacturer revealed that the lipid formulation needed to be heated to 50°C in order to overcome the viscosity limit of the equipment.
The optimum set of parameters was a pulsing voltage of 100 V, a pulse width of 12 µs and a frequency of 50 Hz. The estimated droplets volume was 0.15 nL. SEM pictures of oil filled containers are shown in figures 3.22 and 3.23.
Spotting was successfully performed on microcontainers of different sizes, showing that it is possible to dose precisely picoliter amounts of SNEDDS formulation which potentially can incorporate bioactive ingredients.
However, the need to decrease viscosity with heat, represents a non negligible disadvantage for insulin. To study the effect of heat on the active ingredient, volumes of insulin-loaded formulation (with composition mentioned in section 3.3.4) were kept in an oven at different temperatures for a time period equal to the expected printing time (12-15 minutes). Thereafter, defined aliquots of the solution were analyzed with HPLC to measure if the concentration of insulin was equal to the one of the untreated insulin solution. At 50°C, the amount of active protein was measured to be between 70 and 80% (tests performed by our collaborators at KU Pharma).
The optimized SNEDDS formulation includes an insulin concentration of 2.5-10 mg/mg OIL.
An estimate of the total number of microdevices needed for an oral therapeutic dose of insulin can be calculated taking in account the following facts: i) the volume available for loading of a typical microdevice is 18 nL (300 µm containers), ii) the total daily average insulin dose for humans is 0.5-1 units per kg of body weight with injection for patients without a severe insulin resistance [38]. Assuming an absorption in the blood stream through the GIT of 10% of the one via injection, the dose needed daily becomes equal to 5-10 unit/kg that is, for a 70 kg human, 12.5-25 mg. The number of microcontainer needed for a therapeutic dose, considering the most favorable conditions (lowest dose, highest loading), is given by:

$$\#\text{microdevices} = \frac{\text{insuline dose}}{\text{insulin loaded per container}} = \frac{12.5\ (\text{mg})}{18 \cdot 10^{-6}(\text{ml}) * 0.95\left(\frac{\text{g OIL}}{\text{ml}}\right) * 10\left(\frac{\text{mg}}{\text{g OIL}}\right)} \cong 73100$$

assuming that the density of the formulation is equal to the one of its most abundant component (Miglyol 812). Such a number of microdevices, with the current microfabrication design, correspond approximately to 4 wafers. Furthermore, considering that one pipette takes approximately 12 minutes to fill 625 microdevices, with a printer like the one in use, equipped with 16 pipettes, the total printing time needed for one dose of insulin would be approximately 88 minutes. And considering the additional loss of activity of insulin due to the heating, the total time for one dose becomes 110 minutes.

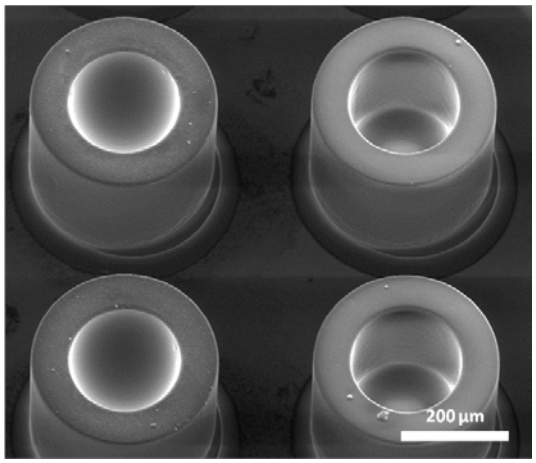

Figure 3.22: SEM image of containers filled with 100 droplets of lipid formulation (left) and empty containers (right).

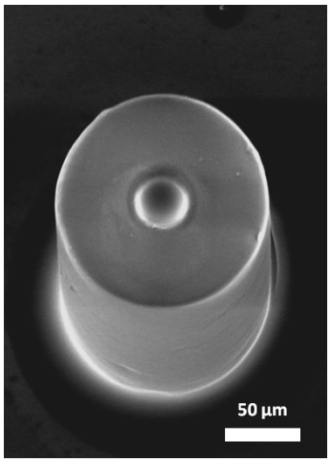

Figure 3.23: SEM image of 0.5 nL container willed with 4 droplets of lipid formulation.

3.8 Conclusion on inkjet printing

The use of DOD inkjet printing as a filling technique for furosemide demonstrated in general substantial limitations of the available equipment. The precipitation of the drug within the pipette was the main cause of irreproducible results. In certain cases, nozzle clogging compromised permanently the pipette operation. The need of dispensing diluted solutions limited the drug loading. The deposited amounts were too small to quantify drug loading or to be close to a therapeutic dose. A search in the literature confirmed that the same obstructions occurred in the printing experiments of felodipine solutions (another water unsoluble substance) with micropipettes of the same manufacturer [1]. Buffer solutions of furosemide exhibited a more stable jet formation, although pipette blocking could not be avoided. This fact suggested that water-based solutions can be suitable for printing. Controlled volumes of aqueous solutions of PVP were dispensed inside the microcontainers, with a good reproducibility in terms of alignment and dispensed volume. Polymer concentrations up to 20% (wt) were successfully dispensed. Water-based solutions completely fill the cavity volume and the polymer content is controlled by repeated spotting sessions. The deposition of both PVP in isopropanol and furosemide in DMSO-ethanol showed instead that organic solvents tend to wet SU-8 surface and that it is easier to coat containers rather than filling their cavities. However, the spotting of organic solvent based solutions on SU-8 could be an interesting method for the deposition of selective conformal coating on individual microstructures. The deposition of a hydrophilic polymer like PVP can be used to permanently change surface properties of SU-8. Viscous solutions like chemicals used for SNEDDS can be successfully printed, but in that case a heating dispensing system is required in order to decrease the viscosity to below 5 mPa·s.

Inkjet printing could be employed as a tool for filling microcontainers with drug formulations, as long as no water insoluble compounds precipitate within the pipette.

In conclusion, an innovative loading technique of microcontainers with poorly water soluble drugs could be divided into two steps: the DOD deposition of a polymer matrix (PVP, but potentially any water soluble filler), followed by an additional step fulfilling the drug loading. This second step will be discussed in the next chapter.

Bibliography

[1] N. Scoutaris, Home based formulation of personalised medicines by means of inkjet printing technique, in, University of Nottingham, 2011.
[2] P.O. Brown, T.D. Shalon, Methods for fabricating microarrays of biological samples, in, Google Patents, 1998.
[3] G. MacBeath, S.L. Schreiber, Printing Proteins as Microarrays for High-Throughput Function Determination, Science, 289 (2000) 1760-1763.
[4] T. Goldmann, J.S. Gonzalez, DNA-printing: utilization of a standard inkjet printer for the transfer of nucleic acids to solid supports, Journal of Biochemical and Biophysical Methods, 42 (2000) 105-110.
[5] E.A. Roth, T. Xu, M. Das, C. Gregory, J.J. Hickman, T. Boland, Inkjet printing for high-throughput cell patterning, Biomaterials, 25 (2004) 3707-3715.
[6] U. Gbureck, T. Hölzel, C.J. Doillon, F.A. Müller, J.E. Barralet, Direct Printing of Bioceramic Implants with Spatially Localized Angiogenic Factors, Advanced Materials, 19 (2007) 795-800.
[7] S. Goodall, N. Chew, K. Chan, D. Auriac, M.J. Waters, Aerosolization of protein solutions using thermal inkjet technology, Journal of aerosol medicine, 15 (2002) 351-357.
[8] P. Tarcha, D. Verlee, H. Hui, J. Setesak, B. Antohe, D. Radulescu, D. Wallace, The Application of Ink-Jet Technology for the Coating and Loading of Drug-Eluting Stents, Annals of Biomedical Engineering, 35 (2007) 1791-1799.
[9] S. Hauschild, U. Lipprandt, A. Rumplecker, U. Borchert, A. Rank, R. Schubert, S. Förster, Direct Preparation and Loading of Lipid and Polymer Vesicles Using Inkjets, Small, 1 (2005) 1177-1180.
[10] N. Genina, D. Fors, M. Palo, J. Peltonen, N. Sandler, Behavior of printable formulations of loperamide and caffeine on different substrates–effect of print density in inkjet printing, International Journal of Pharmaceutics, (2013).
[11] R. Kolakovic, T. Viitala, P. Ihalainen, N. Genina, J. Peltonen, N. Sandler, Printing technologies in fabrication of drug delivery systems, Expert Opinion on Drug Delivery, 10 (2013) 1711-1723.
[12] D. Raijada, N. Genina, D. Fors, E. Wisaeus, J. Peltonen, J. Rantanen, N. Sandler, A step toward development of printable dosage forms for poorly soluble drugs, Journal of Pharmaceutical Sciences, 102 (2013) 3694-3704.
[13] N. Genina, D. Fors, H. Vakili, P. Ihalainen, L. Pohjala, H. Ehlers, I. Kassamakov, E. Haeggström, P. Vuorela, J. Peltonen, N. Sandler, Tailoring controlled-release oral dosage forms by combining inkjet and flexographic printing techniques, European Journal of Pharmaceutical Sciences, 47 (2012) 615-623.
[14] N. Scoutaris, M.R. Alexander, P.R. Gellert, C.J. Roberts, Inkjet printing as a novel medicine formulation technique, Journal of Controlled Release, 156 (2011) 179-185.
[15] P.J. Marsac, H. Konno, L.S. Taylor, A comparison of the physical stability of amorphous felodipine and nifedipine systems, Pharmaceutical research, 23 (2006) 2306-2316.
[16] Y. Matsuda, E. Tatsumi, Physicochemical characterization of furosemide modifications, International Journal of Pharmaceutics, 60 (1990) 11-26.
[17] M. Lindenberg, S. Kopp, J.B. Dressman, Classification of orally administered drugs on the World Health Organization Model list of Essential Medicines according to the biopharmaceutics classification system, European Journal of Pharmaceutics and Biopharmaceutics, 58 (2004) 265-278.
[18] V. Iannuccelli, G. Coppi, E. Leo, F. Fontana, M.T. Bernabei, PVP solid dispersions for the controlled release of furosemide from a floating multiple-unit system, Drug Development and Industrial Pharmacy, 26 (2000) 595-603.
[19] F. Haaf, A. Sanner, F. Straub, Polymers of N-vinylpyrrolidone: synthesis, characterization and uses, Polymer Journal, 17 (1985) 143-152.
[20] M.L. Huggins, The viscosity of dilute solutions of long-chain molecules. IV. Dependence on concentration, Journal of the American Chemical Society, 64 (1942) 2716-2718.
[21] C. Leuner, J. Dressman, Improving drug solubility for oral delivery using solid dispersions, European Journal of Pharmaceutics and Biopharmaceutics, 50 (2000) 47-60.

[22] P. Caliceti, O. Schiavon, F.M. Veronese, Biopharmaceutical properties of uricase conjugated to neutral and amphiphilic polymers, Bioconjugate chemistry, 10 (1999) 638-646.
[23] V. Iyer, S. Katageri, R. Radhakrishnan, N.B. Gaddipati, Pharmaceutical formulation in a drug delivery system and process for preparing the same, in, Google Patents, 2002.
[24] V.P. Torchilin, T.S. Levchenko, K.R. Whiteman, A.A. Yaroslavov, A.M. Tsatsakis, A.K. Rizos, E.V. Michailova, M.I. Shtilman, Amphiphilic poly-N-vinylpyrrolidones:: synthesis, properties and liposome surface modification, Biomaterials, 22 (2001) 3035-3044.
[25] G.J.M. Fechine, J.A.G. Barros, L.H. Catalani, Poly (< i> N</i>-vinyl-2-pyrrolidone) hydrogel production by ultraviolet radiation: new methodologies to accelerate crosslinking, Polymer, 45 (2004) 4705-4709.
[26] L.C. Lopérgolo, A.B. Lugão, L.H. Catalani, Direct UV photocrosslinking of poly (< i> N</i>-vinyl-2-pyrrolidone)(PVP) to produce hydrogels, Polymer, 44 (2003) 6217-6222.
[27] E. Rudnic, J. Lausier, R. Chilamkurti, C. Rhodes, Studies of the Utility of Cross Linked Polyvinlpolypyrrolidine as a Tablet Disintegrant, Drug Development and Industrial Pharmacy, 6 (1980) 291-309.
[28] D. Perin, Biomaterials for biotechnological applications: synthesis and activity evaluations, (2010).
[29] C.W. Pouton, Lipid formulations for oral administration of drugs: non-emulsifying, self-emulsifying and 'self-microemulsifying'drug delivery systems, European Journal of Pharmaceutical Sciences, 11 (2000) S93-S98.
[30] P. Li, H.M. Nielsen, A. Müllertz, Oral delivery of peptides and proteins using lipid-based drug delivery systems, Expert Opinion on Drug Delivery, 9 (2012) 1289-1304.
[31] F.L. Mota, A.P. Carneiro, A.J. Queimada, S.P. Pinho, E.A. Macedo, Temperature and solvent effects in the solubility of some pharmaceutical compounds: Measurements and modeling, European Journal of Pharmaceutical Sciences, 37 (2009) 499-507.
[32] A. Jouyban, Handbook of Solubility Data for Pharmaceuticals, Taylor & Francis, 2010.
[33] Ullmann's Encyclopedia of Industrial Chemistry, John Wiley & Sons, 2003.
[34] F. Walther, T. Drobek, A.M. Gigler, M. Hennemeyer, M. Kaiser, H. Herberg, T. Shimitsu, G.E. Morfill, R.W. Stark, Surface hydrophilization of SU-8 by plasma and wet chemical processes, Surface and Interface Analysis, 42 (2010) 1735-1744.
[35] F. Walther, T. Drobek, A.M. Gigler, M. Hennemeyer, M. Kaiser, H. Herberg, T. Shimitsu, G.E. Morfill, R.W. Stark, Surface hydrophilization of SU8 by plasma and wet chemical processes, Surface and Interface Analysis, 42 (2010) 1735-1744.
[36] G. Turco, I. Donati, M. Grassi, G. Marchioli, R. Lapasin, S. Paoletti, Mechanical spectroscopy and relaxometry on alginate hydrogels: a comparative analysis for structural characterization and network mesh size determination, Biomacromolecules, 12 (2011) 1272-1282.
[37] R. Sadeghi, M. Taghi Zafarani-Moattar, Thermodynamics of aqueous solutions of polyvinylpyrrolidone, The Journal of Chemical Thermodynamics, 36 (2004) 665-670.
[38] J. Conget, E. Esmatjes, J. Ferrer, J. Vendrell, E. Moscoso, R. Gomis, Human insulin dosage and distribution at the onset of type 1 diabetes mellitus, Diabetes research and clinical practice, 9 (1990) 251-255.

4. Supercritical impregnation

The work presented in this chapter resulted in the scientific article “Polymer-filled microcontainers for oral delivery loaded using supercritical impregnation”, published in the Journal of Controlled Release (see Appendix 2). Some topics and results of this work were also shown in an oral presentation at the 7th Annual Symposium of the Pharmaceutical Solid State Research Cluster (PSSRC Lille, July 3-6, 2013) and in a podium presentation at the 40th Annual Meeting and Exhibition of Controlled Release Society (CRS Honolulu, July 21-24, 2013). The experiments were partially performed in the lab facilities of Chempilots A/S (Farum, Denmark). The study described in section 4.3.6 was conducted at the Univesity of Trieste (Italy), in a co-supervised master project.

4.1 Concepts of drug loading by polymer swelling

In chapter 3, the deposition of aqueous PVP solutions by inkjet printing was described. Once precise amounts of polymer were deposited inside the microcontainers, the loading of poorly soluble drugs could be performed on large arrays of devices by swelling the polymer matrix with a solution containing the drug, followed by a short washing step. The steps of drug loading by swelling are schematically depicted in figure 4.1.

In such a loading process the chemical nature of the swelling solvent plays a crucial role. The solvent must act as drug carrier. The solvent should dissolve the drug of interest but not the polymer matrix, which just has to be swelled and loaded with drug. At the same time, the affinity between polymer and API must prevail over the one between API and solvent in order to make the loading efficient. Furthermore, it is important that the solvent is easily removed from the polymer matrix once the loading has taken place with minimal unspecific deposition of API. In the optical case, the solvent evaporation would be fast to avoid drug recrystallization within the polymer matrix.

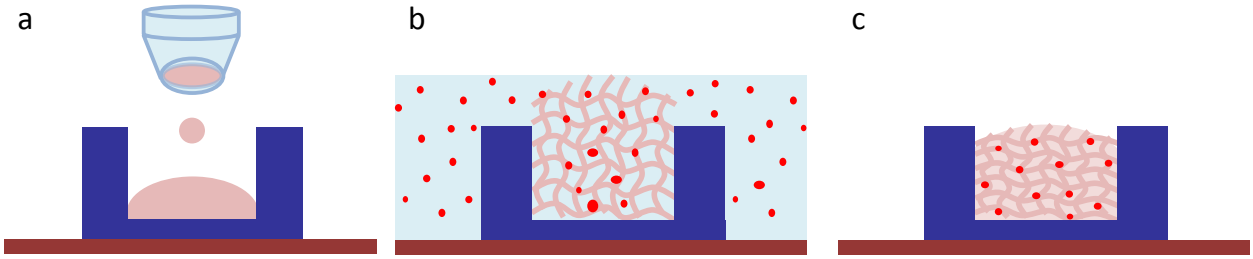

Figure 4.1: Drug loading via polymer swelling: (a) inkjet printing of polymer solution; (b) swelling with drug solution; (c) polymer deswelling by solvent removal.

As a preliminary experiment, swelling was performed on a chip with microcontainers filled with alginate prepared with the procedure described in section 3.5. The array was immersed in DI water for 30 minutes at room temperature to investigate the behaviour of confined volumes of alginate in a liquid solvent. Pictures of gel-laden microcontainers were collected with a scanning electron microscope (FEI Quanta 200 ESEM FEG) at room temperature and 2 mbar partial water vapor pressure with the gaseous secondary electron detector (acceleration voltage 15 eV). An array of polymer filled-containers are shown in figure 4.2 before (figure 4.2a) and after swelling (figure 4.2b). It can be observed that the solvent absorption in the polymer matrix is so pronounced that the swelling induces a "pop corn" effect. This is probably also enhanced by the hydrophobicity of SU-8 container surfaces, which might expell the polymer out of the containers.

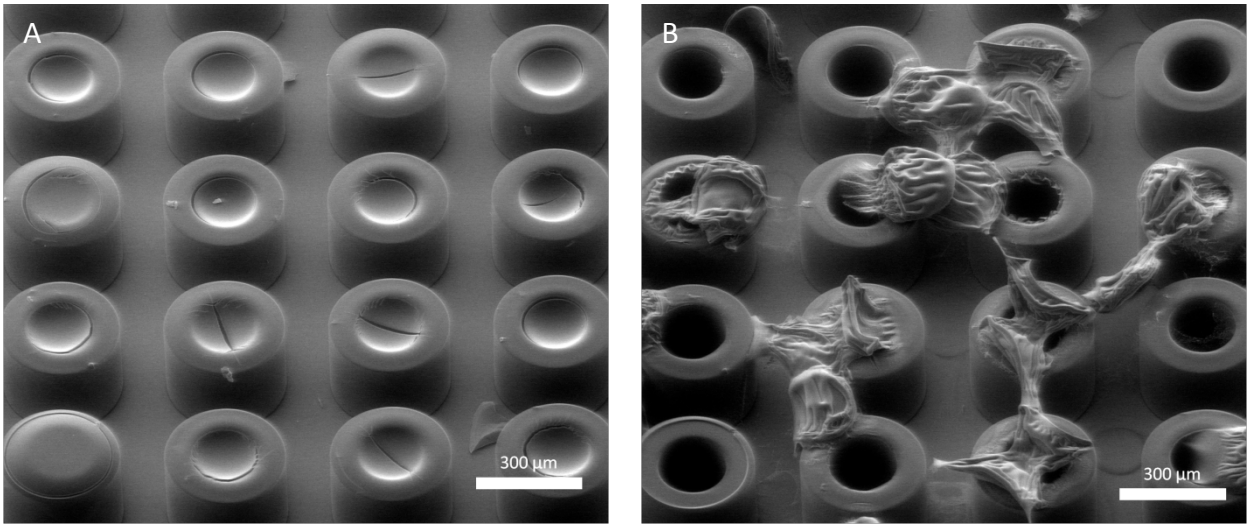

Figure 4.2: E-SEM pictures of arrays of alginate –filled microcontainers, (a) before swelling and (b) after swelling for 30 min in DI water (from R. Mateiu).

Although the extent of polymer swelling might be modulated by varying for instance solvent and time of immersion, it was believed that in general the loading by immersion in a liquid drug solution would have been difficult to control. Therefore, this strategy was not further explored for the loading of microcontainers with poorly soluble drugs.

An optimal solution for controlled swelling would be represented by a solvent, whose diffusivity and solvent power can be modulated during the different steps of the loading process. A high diffusivity, or more precisely a proper combination of viscosity and diffusion coefficient, enables the drug carrier to penetrate the polymer matrix more in depth, and to leave it more rapidly and with minimum residuals. A tunable solvent power would permit to dissolve a proper quantity of API, but at the same time to change its affinity in order to promote the API partition between solvent and polymer in favour of the latter.

The need of such properties is not new for the preparation of solid dispersions of pharmaceutical interest. The choice of volatile solvents is always preferred, but often implicates the use of synthetic organic compounds. The presence of traces of potentially toxic organic solvents in pharmaceutical products entails a substantial risk for safety as well as to the stability of the formulation [1].

In the last decade, research in pharmaceutical technology found in supercritical carbon dioxide ($scCO_2$) a valuable alternative to organic solvents. As discussed in section 2.3, CO_2 above its critical point acquires a density (i.e. solvent power) similar to a liquid, and a viscosity of a gas, which makes it particularly suitable for tuning impregnation of polymers. In this work, $scCO_2$ was used to load a poorly soluble drug into microcontainers previously filled with PVP by inkjet printing. To prove the feasibility of the supercritical technology with respect to microcontainers, the drug of choice was ketoprofen, a well known poorly soluble compound whose dissolution in $scCO_2$ already had been studied in several research works [2-4].

4.2 Materials and methods

4.2.1 Solubility of ketoprofen in supercritical CO_2

Ketoprofen is a non steroidal anti-inflammatory drug (NSAID) with analgesic and antipyretic properties, used to treat rheumatoid arthritis osteoarthritis, dysmenorrheal and in general prescribed as a pain-killer [6]. In figure 4.3a, the molecular structure ketoprofen is shown. The ketoprofen molecule has one asymmetric carbon atom which gives rise to two enantiomers, both showing biological activity [7]. In this thesis experiments were carried out with the racemic mixture. Ketoprofen is considered in different pharmacopeias as practically insoluble in water. Its solubility in pure water at ambient temperature (22-24°C) was reported to be 0.010 mg/mL [8]. As for many drugs, the preferred site of absorption in the oral route is the small intestine [9]. After oral administration, the dose fraction absorbed was reported to be 90%, and thus ketoprofen is considered as a "highly permeable" drug [6]. Thus, ketoprofen is classified as a class II in the BCS standard, mentioned in figure 1.1.

From a chemical perspective, ketoprofen is a weak acid with reported pK_a values of 4.39 at 25°C [10]. Ketoprofen side effects are similar to other anti-inflammatory agents. However, it is one of the most ulcerogenic [6]. The solubility of NSAIDs in supercritical $scCO_2$ has been extensively studied [2-4, 11, 12]. The solubility of ketoprofen follows a profile similar to the one shown in figure 4.4 [5]. In general solubility is a monotonic function of pressure, as a result of the increasing volatility and CO_2 density [13]. As discussed in section 2.3.2, the plots of solubility versus pressure at different temperatures (solubility isotherms) exhibit two crossover points, at defined values of pressure P_L^* (lower value) and P_U^* (upper value). The upper crossover pressure P_U^* of solubility isotherms was reported between 160 and 180 bar. Several authors confirmed this discovery [2, 3]. In light of its solubility issues in water, its suitability for the supercritical operation, as well as the existing need to reduce side effects, ketoprofen was considered an eligible model API for impregnation in microcontainers.

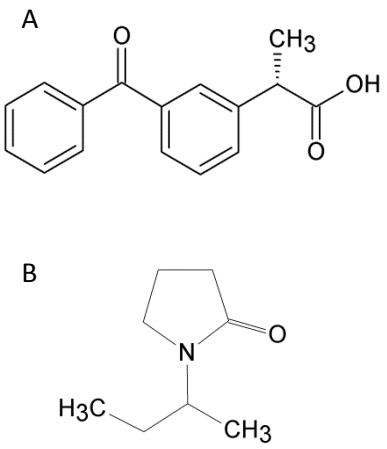

Figure 4.3: Chemical structure of (a) ketoprofen, (b) monomer of poly (vinyl pyrrolidone) (PVP).

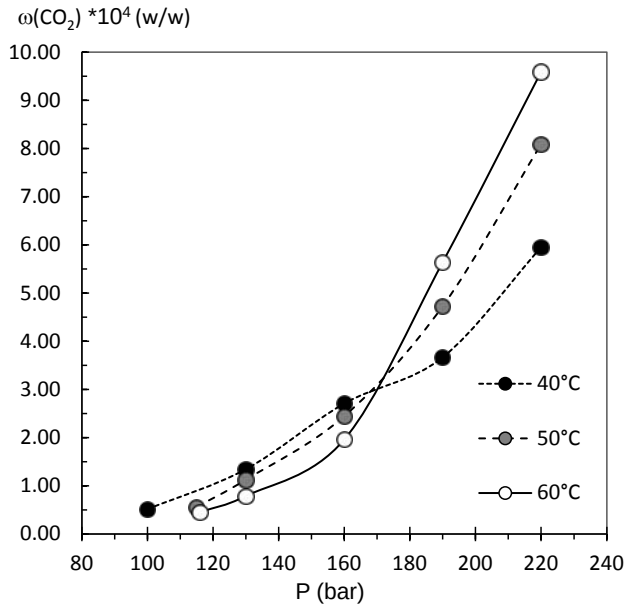

Figure 4.4: Solubility isotherms of ketoprofen in $scCO_2$ as a function of pressure at 40, 50 and 60 °C (adapted from [5]). The lines are guides for the eyes.

4.2.2 Swellability of PVP by supercritical CO_2

The chemical structure of poly(vinylpyrrolidone) (PVP) is depicted in figure 4.3b. PVP is a polymer with many functions as discussed in section 3.3.2. The effects of CO_2 on PVP was studied by Kikic and coworkers [14]. Gaseous CO_2 sorption in PVP matrices (K25 M_w $2.9 \cdot 10^4$ Da and K90 10^6 Da) generates a plasticization of the polymer, resulting in a decrease of the T_g. This fact caused the so called *retrograde vitrification* where at a constant pressure an increase of the temperature invokes a liquid to glass transition, opposite to the typical behavior. In the same research group, Alessi *et al*. [15] showed how the molecular weight influences the CO_2 sorption in PVP swelling ratio.

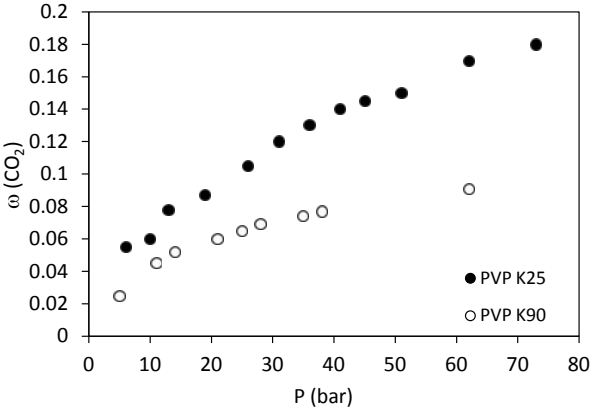

Figure 4.5: Absorbed CO_2 (weight fraction) in PVP at different fluid pressures for two molecular weights (adapted from [15]; courtesy of Alessi et al.).

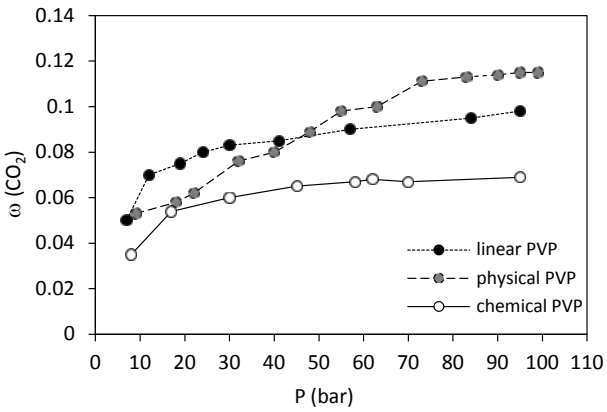

Figure 4.6: Absorbed CO_2 (weight fraction) in linear and chemically and physically crosslinked PVP as a function of pressure at 47°C (from [16]; courtesy of Kikic et al.).

In figure 4.5 the CO_2 sorption in PVP is shown as a function of the fluid pressure for polymer grades K90 (white dots) and K25 (black dots). Both curves follow a monotonic trend, and it appears that at a given pressure, the CO_2 uptake is higher for lower the polymer molecular weight. This difference in polymer penetration becomes more pronounced with increasing pressure because of the concomitant increase of fluid density. As a reasonable assumption, a K17 grade (M_w 10^4) of the polymer as it was used in this work is expected to have an even higher absorption than K25. Finally, Kikic *et al.* [16] compared the CO_2 sorption in linear PVP and in its crosslinked versions, observing that polymer permeability depends on the level and the strength of entanglement between polymer chains (see figure 4.6). At low pressures, the linear PVP is permeated more easily by CO_2 than the crosslinked versions. However, above a pressure of around 40 bar the chain stiffness and the entanglement due to the physical crosslinks is reduced by the CO_2 pressure and the swelling is enhanced [16]. The impregnation of PVP with ketoprofen has also previously been investigated. Manna *et al.* [17] prepared solid dispersions of ketoprofen and PVP K30 via supercritical carbon dioxide in a continuous operation. The drug was put in excess amounts (according to a previous solubility study) in a chamber (*dissolution vessel*) and dissolved in pressurized CO_2 under stirring together with glass beads. The API concentration was measured and when it reached saturation at the chosen conditions of P and T, the drug enriched $scCO_2$ was conveyed in a second vessel (*impregnation vessel*). There, the PVP powder had previously been mixed with glass beads and swollen with pure supercritical CO_2 for 1 hour in advance. This operation aimed to ensure complete polymer swelling prior to impregnation. The impregnation was carried out in dynamic conditions where the CO_2-ketoprofen flow is recycled to the dissolution vessel. With this procedure, the impregnation is carried out in saturation conditions during the whole operation. The drug partition equilibrium between CO_2 and polymer was attained by monitoring the drug concentration in the flow leaving the impregnation vessel. The experiment was stopped when the drug concentration in the flow returned to be equal to the solubility value. Certain experiments required long times to reach equilibrium (up to 5 days), attaining drug loading of 58% wt of ketoprofen in PVP.

4.2.3 Deposition of PVP solution in the microcontainers and preparation of PVP films

The microwells with diameter 200 µm were filled with PVP by means of an inkjet printer as described previously in section 3.6.3. PVP K17 was chosen for the feasibility for inkjet printing (discussed in section 3.6) and for the expected high degree of swelling in $scCO_2$ (as mentioned in section 4.2.2). The polymer was dissolved in DI water (10% wt) and the solution was stirred for 3 h. The chips were weighed before and after the polymer deposition and the polymer weight per chip was estimated. Characterization of polymer filled microcontainers was done with a Plu Neox 3D Optical Profiler (Sensofar) in the confocal mode. Polymer films were prepared with the same solution used for the inkjet printing (10% wt in DI water). These samples were intended for spectroscopic characterization studies. The films were cast in a cylindrical cavity of a teflon mold (diameter 5 mm, height 0.255 mm) with a volume equal to the sum of the cavity volumes of 625 microcontainers. A volume of 5 µl of solution was dispended in the mold and left on a hotplate at 50 °C for 1 h to remove the solvent.

4.2.4. High pressure equipment and experimental procedure

In this work the impregnations were performed in batch conditions: The chips with polymer filled containers and the solid drug were placed in the reactor chamber, which was sealed and filled with $scCO_2$.

The implant used in this research work is schematically represented by the flow diagram in figure 4.7. Weighed amounts of crystalline ketoprofen powder were poured on the bottom of a 100 mL high pressure reactor with sapphire windows (Thar SFC). Different weights of drug, 4.7 and 14.1 mg for 100 and 200 bar batched respectively, were dissolved in order to reach saturation conditions according to the data shown by Macnaughton *et al*. [2]. One chip with the microcontainers was placed on a steel grid fitting the chamber cross section.

Then, the valve V5 was closed, and desired temperature was set. The apparatus was pressurized through valves V2 (on/off valve) and V4 (needle valve) by the pump with a controlled ramp. The pressure was monitored through pressure gauge PI3: The CO_2 filled the chamber slowly to avoid fluid hammers of the pipes and to prevent the need of excessive mass of fluid to fill the chamber. The CO_2 inlet stream was generally colder than the operating T. If the feed flow was too high, the CO_2 cooled down the chamber and once the chamber was again heated up to correct set point T, the fluid pressure overshoots the desired value. It is therefore important that the filling step is performed at constant T and that the chamber is slowly filled with CO_2. The volumes of residual air in the chamber at 40°C at 100 and 200 bar were estimated to be 1 and 0.5 mL respectively which was considered negligible because this was lower than the available surplus chamber volume (4 mL). Once the set point pressure was reached, V4 was closed and impregnation started by activating the stirring. The experiments were carried out at constant T, P and stirring speed. At the end of the experiment, the reactor was depressurized at a controlled rate during 2 and 3 hours when the operating pressures were 100 and 200 bar respectively. For this purpose, the valve V5 (needle valve) was gradually opened and the fluid pressure was slowly released. The depressurization step was performed at a controlled rate of 1.1 bar/min. At V5 level, where the major CO_2 pressure drop occurs, higher rates caused pipe freezing and frequent occlusions due to fluid densification. The drug rich-CO_2 outlet stream was bubbled through ethanol (99.5 %) and ketoprofen concentration was measured with a UV spectrophotometer to cross check the drug mass balance of the operation.

The main differences compared to the previously mentioned work of Manna *et al.* [17], is that the polymer inside the microcontainers was grade K17 (i.e. lower molecular weight) in our case, which might be dissolved or excessively swollen by CO_2. No related data in the literature were found. Furthermore, polymer and drug might not be mixed because of the confinement in the microwells.

It was expected that the impregnation of microcontainers was controlled by the dissolution of the drug in the fluid, and by its diffusion in the polymer matrix. After depressurization, the chip with impregnated containers was weighed and stored in a desiccator until further study. The morphology of the impregnated microcontainers was examined using SEM. The investigations were carried out using a Nova600 NanoSEM from FEI (Eindhoven, the Netherlands).

Imaging was performed in low-vacuum-mode at a pressure of 0.6 mbar and an operation voltage of 5 kV. Prior to examination, the samples were mounted onto metal stubs and were tilted by 30 degrees.

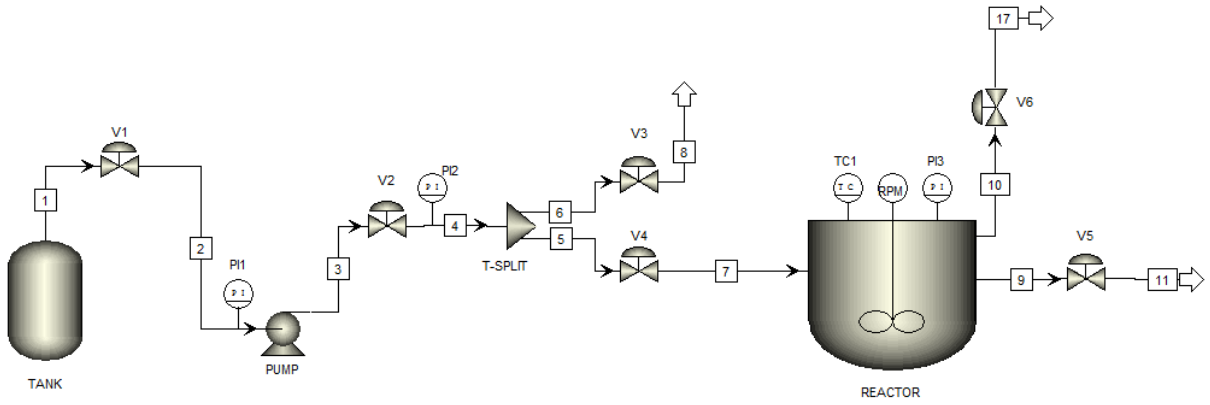

Figure 4.7: Process flow diagram of the supercritical implant utilized in the experiments. V3 and V6 are purge valves, used to empty the pipes after the experiments. V1, V4 and V5 are needle valves, V2, V3, V6 are on/off valves. TC is a temperature controller, PI1-3 are pressure gauges, RPM a magnetic stirring system.

4.2.5 Preparation of micro-tablets

For comparison with impregnated samples, microcontainers were filled with PVP-ketoprofen physical mixtures, and the drug dissolution curves were measured. Physical mixtures were prepared by gently mixing the two powders with a mortar (1:9 drug: polymer weight ratio). The dispersions were compacted into empty microcontainers following a procedure developed by our collaborators at KU Pharma [18], resulting in an array of *micro-tablets*. The residual material in between adjacent containers was removed using pressurized air. The chips were weighed before and after the filling. Micro-tablets with amorphous drug were obtained by heating containers filled with the physical mixture at 120 °C for 3 minutes on a hotplate and quenching in liquid nitrogen for 1 minute. This sequence was repeated thrice. In the preparation of micro-tablets a relevant amount of chemicals was wasted and the procedure was quite laborious and time consuming.

4.2.6 Spectroscopic characterization and X-ray diffraction

Raman and ATR–IR spectroscopy measurements were performed on microcontainers and films to investigate the drug–polymer interactions after supercritical treatment. Raman spectra from the impregnated microcontainers 24 h after the CO_2 treatment were collected with a DXR Raman microscope (Thermo Scientific, Germany) equipped with a frequency-stabilized single mode diode laser (780 nm). The laser power was set to 10 mW at the sample position (center of the container cavity) and the estimated resolution was 2.4–4.4 cm^{-1}. An exposure time of 1 s and the average/integration of 40 scans were used. Because of the strong auto-fluorescence of SU-8, a dedicated correction was applied to the spectra during the collection. A Spectrum 100 spectrometer (Perkin Elmer, Germany) with an MIR source and a TGS detector was used to measure the ATR–IR spectra of the impregnated PVP films 24 h after preparation. The resolution was set to 4 cm^{-1} and 16 accumulations with a scan speed of 0.2 were collected. The X-ray powder diffraction (XRPD) study was carried out to characterize the physical state of the drug in the impregnated microcontainers and micro-tablets. The basic principles of this technique were introduced in section 2.5.1. All XRPD analyses were performed using an X'Pert PRO X-ray diffractometer (PANalytical, λ = 1.541 Å; 45 kV; 40 mA). A starting angle of 5° (2θ) and an end angle of 45° (2θ) were employed for the scans. A scan speed of 0.6565° 2θ/min and a step size of 0.01313° (2θ) were employed. Data were collected using the X'Pert Data Collector software (PANalytical B.V.).

4.2.7 In vitro drug dissolution studies

Dissolution of PVP and ketoprofen from loaded microcontainers was measured in 10 mL DI sonicated water at 37 °C using a µDISS profiler (Pion) as described in section 2.4.2. Individual chips were glued with carbon pads on teflon-coated magnetic stirrers. For the detection of ketoprofen release, the UV probe wavelength was set at 259 nm. After dissolution, the microcontainers were analyzed with an optical microscope to confirm complete emptying. The amount of drug loaded per chip was estimated from the final concentration value in the dissolution profiles obtained after 16 h. Solubility of ketoprofen at 37 °C in aqueous solutions changes significantly with pH between 1 and 7 [6]. The dissolution tests were performed at pH 7 where ketoprofen solubility is >1.4 mg/mL. With ketoprofen being a weak acid (pKa = 4.5) the pH of the dissolution medium did not change sensitively during the dissolution tests. According to solubility data reported in [6], in can be assumed that dissolution tests were performed in sink conditions, meaning at conditions sufficiently far from saturation conditions where solubility is not limiting drug dissolution.

4.3 Result and discussion

4.3.1 Inkjet printing of PVP solutions into microcontainer

The number of droplets to dispense in each container is estimated dividing the cavity volume by the droplet volume. Three subsequent printing sessions have been performed on the same array and a waiting time between the sessions has been included in order to enable solvent evaporation and to avoid spillover. After drying, the level of container filling has been measured with an optical profilometer. The measured average thickness is 141 ± 9 µm. The weight of polymer dispensed onto one chip (625 microcontainers) is 1.6 ± 0.04 mg. The high accuracy of polymer deposition shows that inkjet printing can be used to dispense precise quantities of polymer with a quasi-no-waste performance. The precise control of the dispensed polymer mass is important to control the drug loaded in each microreservoir.

4.3.2 Loading of ketoprofen into polymer-filled microreservoirs

Figure 4.8 shows SEM images of microcontainers subjected to sc impregnation. The fluid pressure during the impregnation has a relevant influence on the volume of the polymer which increases with increasing CO_2 pressure, as appears clearly by the comparison of figures 4.8a and 4.8b. This is likely explained by an increase of CO_2 uptake in the PVP matrix with pressure, as shown by Kikic and Vecchione [19]. As $scCO_2$ acts as a plasticizer for polymers, the viscosity of the CO_2 saturated matrix decreases during the impregnation, causing in some cases spillages from the containers. This aspect is more pronounced for longer experiments (see figures 4.8c and 4.8d). Polymer softening and swelling play an essential role with respect to the desired quasi no-waste performance. For an optimal combination of inkjet printing and sc impregnation, the PVP must remain confined in the cylindrical cavity of the micro-well. During impregnations at 200 bar, several droplets were deposited in the space in between adjacent microcontainers (see figure 4.8d). This effect was observed when the depressurization rate at the CO_2 critical pressure was higher than 1.1 bar/min. Compared to that, there was a negligible polymer spillage with a slower pressure decay. The holes in the de-swelling matrix, also shown in figure 4.8d, are probably due to the formation of micropores during CO_2 release. All the SEM images show no effect of the supercritical fluid on SU-8 at the micro-scale.

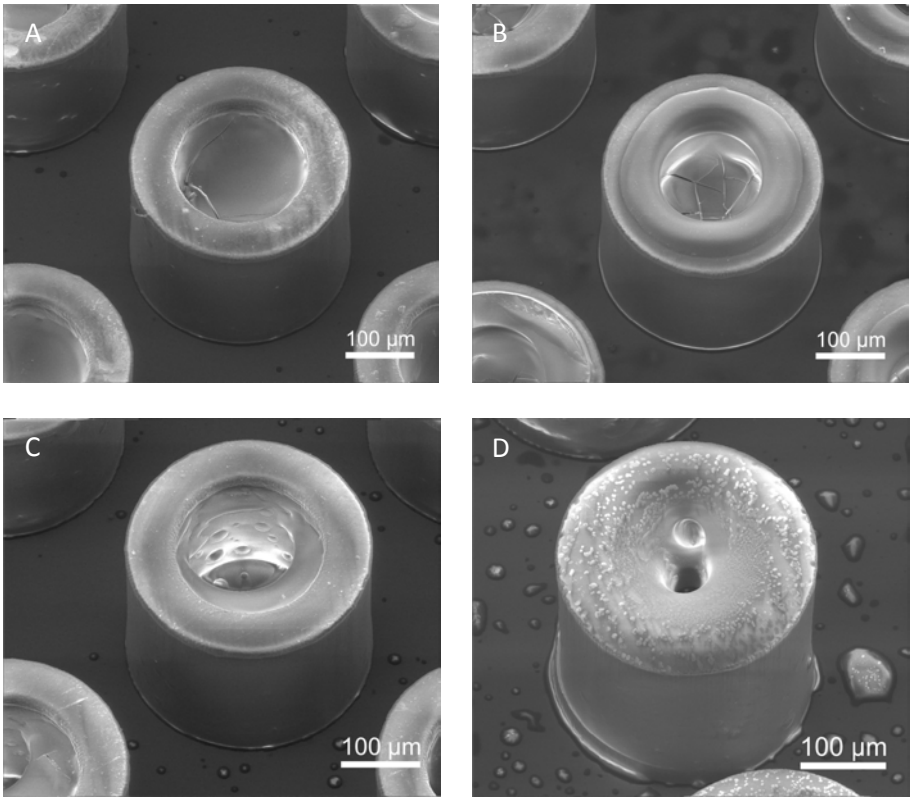

Figure 4.8: Scanning electron microscopy images of the polymer-filled microcontainers impregnated with ketoprofen using $scCO_2$ at different conditions: (a) 100 bar 1 hour; (b) 200 bar 1 hour; (c) 100 bar 4 hours; (d) 200 bar 4 hours.

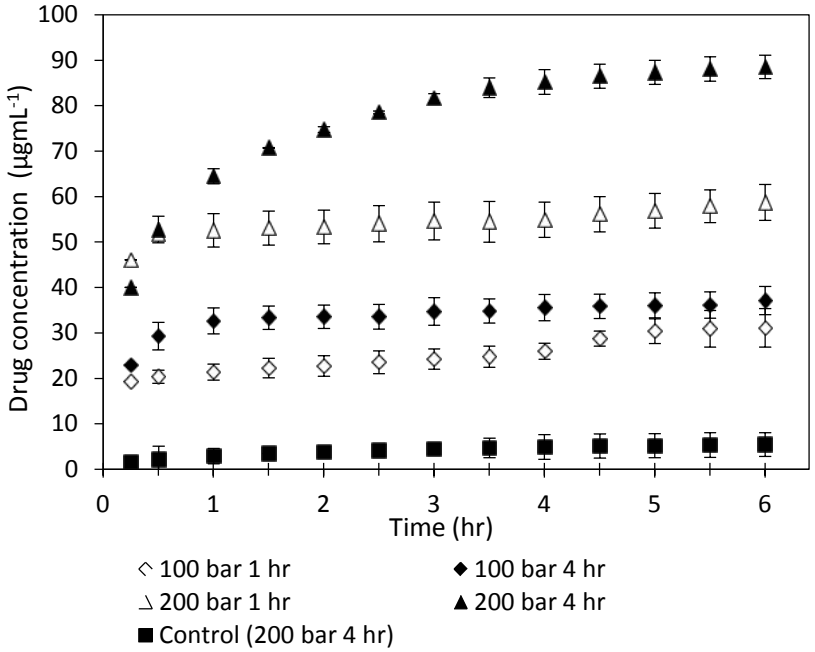

Figure 4.9: Controlled release of the model drug from polymer-filled microcontainers loaded at different pressures and times as compared to empty microcontainers (control; without polymer). Release test on individual chips with 625 microcontainers in 10 mL DI water (N=3).

4.3.3 Controlled in vitro drug release from impregnated microdevices and Raman characterization

To measure the ketoprofen release from the microcontainers, dissolution measurements were carried out with individual chips. Figure 4.9 shows the in vitro dissolution profiles of microcontainers loaded via $scCO_2$ impregnation at different conditions.

As a control experiment, microcontainers without PVP were submitted to ketoprofen impregnation at 200 bar 40 °C for 4 h. The different amounts of drug released show that both the sc fluid pressure and the impregnation time significantly influence the loading. As shown in the release profiles in figure 4.9, the drug uptake increases with an increase in the fluid pressure and with a larger duration of the impregnation. This suggests that the polymer swelling and the drug diffusion play a relevant role in the loading. In table 4.1 the weights of loaded drug per chip in terms of absolute value, drug/polymer weight ratio and weight fraction are shown. The effect of the pressure may be attributed to the fact that both the drug solubility and the CO_2 uptake in the polymer increase with the sc fluid pressure. At 200 bar a higher number of drug molecules can interact with the polymer chains, and this results in an enhanced loading. The effect of time can be explained supposing that the impregnation follows a diffusion-limited mechanism. A previous work shows that SU-8 microstructures treated with $scCO_2$ undergo only small mechanical changes [20], which is also confirmed by our SEM micrographs. Therefore it may reasonably be assumed that SU-8 containers undergo a negligible swelling by the CO_2 if compared with the one of PVP. As a consequence, we assume that container walls provide a spatial shielding to the loading and that the drug is mainly conveyed across the interface PVP/sc fluid.

Finally, the combination of these two effects can give an explanation of the different loading gains for impregnation time which can be obtained at the two considered pressures. At 100 bar the CO_2 moderately swells the polymer chains, the drug diffuses with difficulty and the gain over time is poor. At 200 bar the CO_2 uptake is higher and swollen polymer offers a larger interfacial area and a reduced resistance to drug diffusion, resulting in an enhanced loading gain from 1 to 4 hours. As shown in table 4.1, at the hardest conditions of 200 bar and 4 hours the drug deposited in the microcontainers without PVP is less than 8% of the drug loaded into polymer filled containers at the same conditions. The control experiment shows that a negligible amount of drug is observed in the SU-8 container and that the preliminary deposition of the PVP is required to achieve drug loading. From a technological perspective, the possibility of tuning the drug loading with a change in fluid pressure and time of impregnation represents a relevant advantage. The times of 90% of drug dissolution ($t_{90\%}$) are also shown in table 4.1. The samples impregnated at 100 bar show similar $t_{90\%}$ around 270 minutes, while the samples at 200 bar exhibit a markedly faster drug dissolution: For containers impregnated for 1 hour $t_{90\%}$ is equal to 60 minutes, for those impregnated for 4 hours $t_{90\%}$ is approximately 180 minutes. All dissolution profiles show a burst effect, which might be explained by the presence of a fast dissolving drug coating on the microcontainer surface after the treatment with the carbon dioxide. To clarify this aspect, a Raman mapping of containers was carried out just after the experiments. The Raman spectra are shown in figure 4.10: Pattern (a) and (b) are the spectral fingerprints of crystalline pure ketoprofen and PVP respectively. The vibrational patterns of all impregnated samples exhibit characteristic peaks of the drug where PVP does not show any signal. In particular the band at 1657 cm^{-1}, attributed to the stretching vibration of the ketoprofen carbonyl ν(C=O) and the band at 1198 cm^{-1}, regarding the ring CH in plane bending, seem to have an intensity which is proportional to the impregnation pressure and in particular for 200 bar increases with time. This fact seems to confirm the results of the dissolution tests. In [21] De Carvalho *et al.* attribute these two peaks to the amorphization of the drug in the presence of the excipient.

Table 4.1: Drug loading of impregnated samples and of physical mix-laden micro-tablets. The drug weight refers to total loaded mass on individual chips with 625 microcontainers and is normalized with respect to the polymer mass in the micro-wells (N=3).

Samples	Loaded drug per chip (mg)	Resulted drug/polymer weight ratio	Drug weight fraction after dissolution keto / (PVP+keto)	Time at 90% dissolution $t_{90\%}$ (hours)
100 bar 40°C 1 hour	0.33±0.03	0.22±0.04	0.16±0.03	4.46
100 bar 40°C 4 hour	0.41±0.02	0.28±0.02	0.22±0.02	4.63
200 bar 40°C 1 hour	0.61±0.05	0.37±0.05	0.27±0.03	1.0
200 bar 40°C 4 hour	0.82±0.02	0.52±0.03	0.32±0.01	3.3
Empty containers (200 bar 40°C 4 hour)	0.07±0.02	-	-	6.0
Physical mix laden micro-tablets (1:9 keto:PVP, 10%wt)	0.22±0.06	0.18±0.10	0.15±0.07	6.32

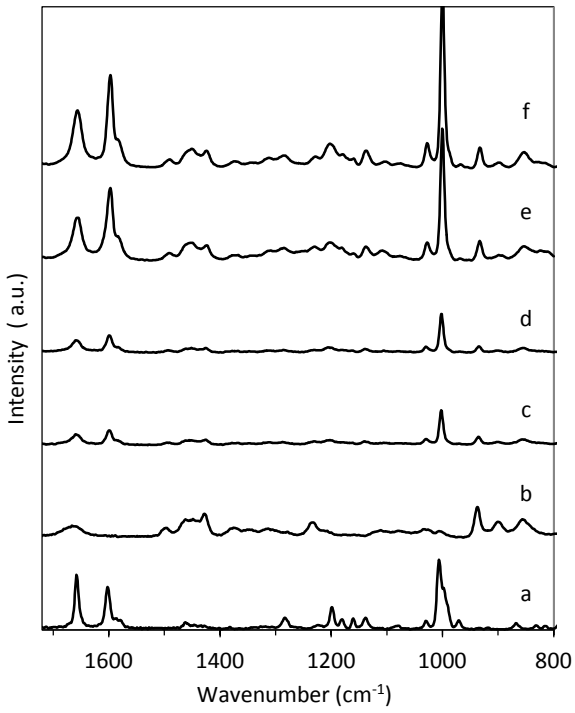

Figure 4.10: Raman spectra for (a) solid ketoprofen, (b) PVP and (c) polymer filled microcontainers impregnated at 100 bar 1 h, (d) 100 bar 4 h, (e) 200 bar 1 h, (f) 200 bar 4 h.

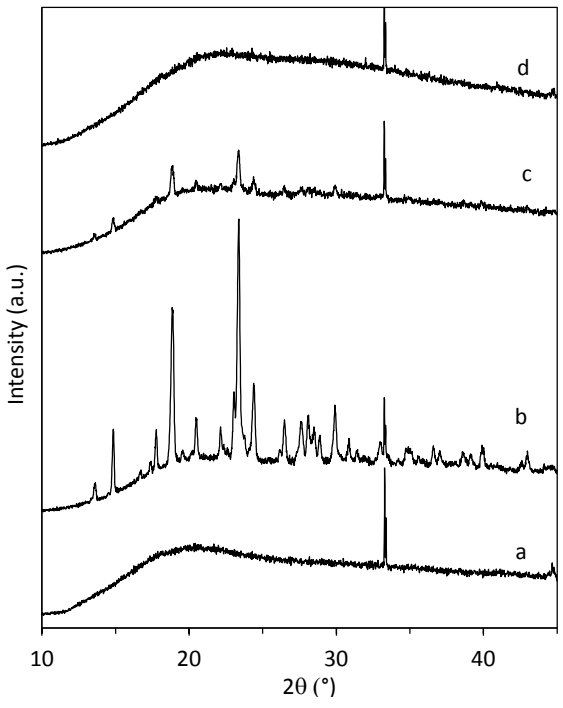

Figure 4.11: X-ray diffraction patterns of (a) empty microcontainers, containers filled with (b) crystalline ketoprofen, (c) 1:9 (wt) keto:PVP physical mixture with crystalline drug (crystalline micro-tablets), (d) 1:9 (wt) keto:PVP physical mixture with amorphous drug (amorphous micro-tablets).

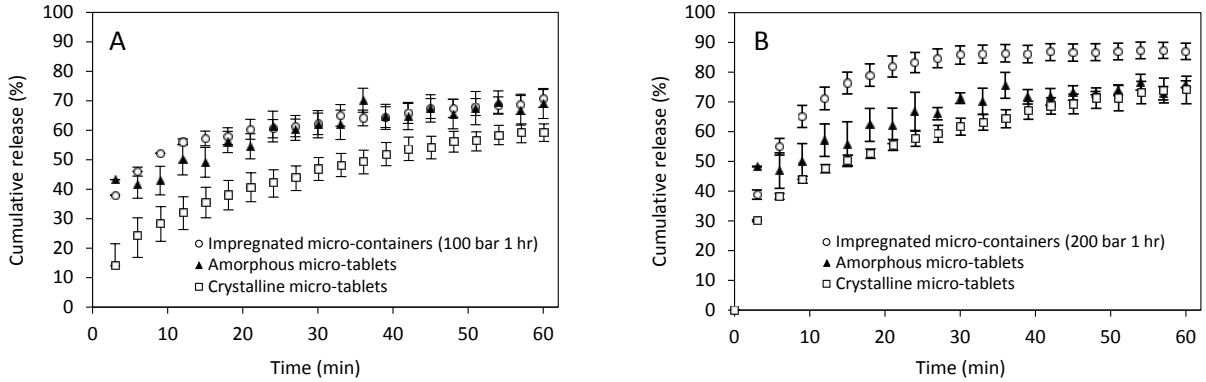

Figure 4.12: The enhanced dissolution kinetics of the model drug from impregnated microdevices (a) 100 bar 1 hr and (b) 200 bar 1 h as compared to drug-polymer physical mixtures laden micro-tablets with similar loaded drug masses. The concentration was normalized with respect to the total drug loaded in each chip (625 microcontainers) released in 10 mL DI water (N= 3).

4.3.4 Comparison with physical mixtures and XRPD characterization

After preparation, the samples called micro-tablets (see section 4.2.5) were examined with X-ray diffraction to check out the solid state of the drug.

The diffractograms of crystalline and amorphous micro-tablets, are shown in figure 4.11. The silicon chip with empty containers (Figure 4.11a) exhibits a broad scattered band meaning that the SU-8 is an amorphous material with one single peak at $2\theta = 33.3°$ belonging to the Silicon substrate. The chip filled with pure fresh crystalline ketoprofen (Figure 4.11b) shows defined peaks emerging from the scattered background signal of the containers. The containers filled with a physical mixture containing crystalline drug show a diffractogram with some peaks of the drug (Figure 4.11c) but with a lower intensity than for the pure crystalline ketoprofen. The samples submitted to melt and quench cooling (d) do not show distinguishable peaks of ketoprofen. The drug content and the drug/polymer weight ratios in these samples were cross-checked by dissolution tests afterwards. XRPD measurements were also performed on all impregnated microcontainers and all the samples showed scattered patterns. In table 4.1 the drug loading data in terms of drug/polymer weight ratio are shown. In micro-tablets the average relative drug content (15% wt) differs from the original physical mixture (1:9, i.e. 10% wt) which demonstrates that the drug and the polymer are demixed during the preparation. The large variation of 50% associated to the data shows that the micro-tablets filling method has a lower accuracy than the sc impregnation where variations are below 18%. Figure 4.12 shows the in vitro cumulative drug release from impregnated microcontainers and the crystalline and amorphous micro-tablets with a similar drug content. Due to the high standard deviation of micro-tablets (see in table 4.1), additional experiments were done and only those with the drug/polymer weight ratio numerically close to the one for impregnated containers were considered for the comparison. The dissolution curve of microcontainers treated at 100 bar (figure 4.12a) overlaps the amorphous micro-tablets profile. Samples loaded at 200 bar (figure 4.12b) show instead a slightly faster dissolution than both amorphous and crystalline micro-tablets.

The similarity factor f_2 of the cumulative dissolution profiles of impregnated microcontainers and micro-tablets was estimated. The results of the comparison are shown in the table 4.2. In all the comparisons the similarity factor is greater than 50 and the profiles is considered similar according to the FDA regulations. Di Martino and coworkers [22] showed that already in physical mixtures of crystalline ketoprofen and PVP K30 (1:1 wt), the drug undergoes a significant decrease of crystallinity just after preparation. That can explain why in general the profiles of amorphous and crystalline drug are quite similar. Nonetheless, impregnated containers show at both pressures faster dissolution compared to the corresponding crystalline and amorphous mixture laden containers. In the system loaded at 200 bar this enhancement is more pronounced and 87% of the drug is dissolved in the medium after only 30 minutes.

Table 4.2: Similarity factors f_2 of cumulative dissolution profiles shown in figure 4.12 of impregnated microcontainers and corresponding micro-tablets.

Impregnation conditions	Similarity factor f_2	
	Crystalline micro-tablets	Amorphous micro-tablets
100 bar 40˚C 1 hour	50.8	51
200 bar 40˚C 1 hour	50.7	50.8

A possible mathematical model for the dissolution kinetics of these systems would have to consider the Fick´s law, the drug-polymer interactions and the particular geometry of the microdevice. For what concerns the material aspects, for a similar impregnated system of PVP K30 and ketoprofen, Manna and coworkers [17] observed a behaviour based on two dissolution mechanisms: At low drug concentration the release rate is fast and is governed by the PVP dissolution, at higher concentrations a stagnant drug-rich layer is formed, and the drug dissolution rate is mainly constant. From a qualitative perspective this trend was also noticed in our experiments. The fast drug dissolution observed for the sample loaded at 200 bar might be explained by the presence of intimate interaction between drug and polymer in the $scCO_2$ aided-loading and the dissolution rate seems to be controlled by the polymer dissolution.

4.3.5 Spectroscopic characterization of impregnated PVP films

The impregnated PVP films were studied via ATR-IR spectroscopy in order to investigate the physical state of the drug in the formulation and eventual presence of interactions with the polymer. The spectra are reported in the ν (C=O) stretching regions in figure 4.13. Pure crystalline ketoprofen (figure 4.13a) is characterized by two well defined peaks at 1697 cm^{-1} and 1655 cm^{-1}, which represent the stretching vibration of the carbonyl group in the carboxylic and in the ketonic groups respectively. The former peak indicates the presence of a dimer of ketoprofen molecules as reported in [17]. In the impregnated films (figure 4.13c and d) this peak is shifted to a higher wavenumber (1723 cm^{-1}) which indicates, as suggested in [17], the breakage of ketoprofen-ketoprofen interactions. The intensity of this shifted peak is stronger for the 200 bar impregnated films (see figure 4.13d). This observation indicates that ketoprofen is molecularly dispersed in the polymer.

A closer analysis of the PVP ν(C=O) region shows that in the impregnated films the ν(C=O) band of PVP at 1625 cm^{-1} is shifted to lower wavenumbers compared to the ν(C=O) band of pure PVP (1652 cm^{-1}) (figure 4.13b). This fact is again more evident in the impregnation at 200 bar. This shift might be assigned to the formation of H-bonds between the carbonyl group of PVP and the hydroxilic group of ketoprofen as suggested for the supercritical impregnation of PVP films with ibuprofen in [23]. On the other hand, the peak of virgin PVP is still strong in the films, which suggests that a considerable portion of the C=O bonds in the polymer does not interact with the drug.

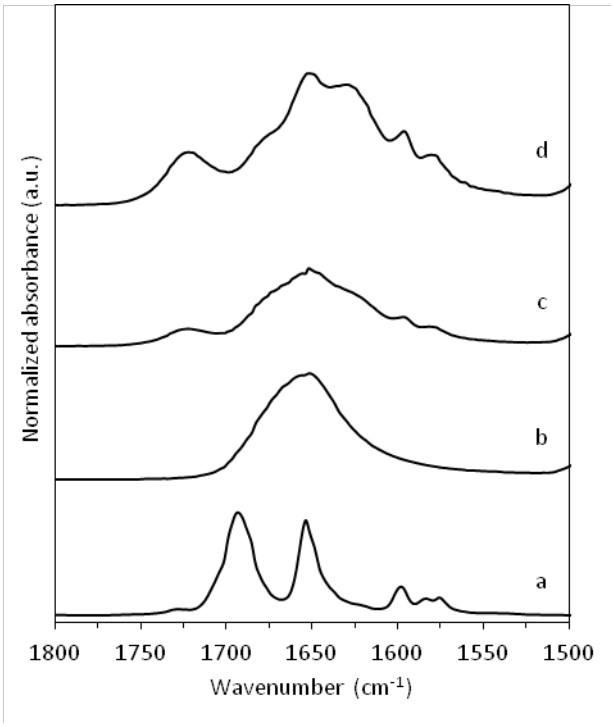

Figure 4.13: ATR-IR spectra in the ν(C=O) spectral region: (a) pure solid ketoprofen, (b) pure PVP film, (c) impregnated PVP film at 100 bar for 1 hour, (d) impregnated PVP film at 200 bar for 1 hour.

4.3.6 Effect of temperature on impregnation yield

An important parameter influencing supercritical impregnation is temperature. At constant pressure, an increase in T produces a decrease of density in the supercritical fluid. As discussed in section 2.3.2, the effect of T on the solvent power depends on the pressure value: Solubility of a drug in scCO_2 increases with T if the increase of solute volatility prevails over the decrease of the density of the sc phase. As shown by the solubility profiles in figure 4.4, this occurs for pressures above the upper crossover value of 170 bar in the case of ketoprofen. In the attempt of investigating the effect of temperature on the loading of microcontainers, further tests were conducted at different T (40, 50 and 60°C) and times (1 and 4 hours), at a fixed pressure of 200 bar and dissolving a drug amount corresponding to the saturation conditions at 40°C. In these tests, the only effect of T was investigated. These experiments were carried out in collaboration with the Department of Industrial Engineering at the University of Trieste in the MSc-project of Laura Pontoni. Microcontainers were filled with PVP powder following a procedure previously used in the preparation of micro-tablets (see section 4.2.5): The polymer powder was compacted in the microwells and the residual amount was blown away with a pressured air gun. The chip was weighed before and after the filling and the PVP weight was in average 1.78 mg per chip with 625 microcontainers. The filling was homogeneous and with minimal residues in between microwells, as representatively illustrated in figures 4.14a and b. A fixed weighed amount of drug (14.1 mg) and the chip were placed in two separate compartments of a sample carrier in the bottom of a 100 mL high pressure unit. The impregnation experiment was performed with the same procedure as described in section 4.2.4. After the CO_2 treatment the chips were left in a desiccator until submission to dissolution in 10 mL DI water at 37°C and a stirring rate of 100 rpm. Dissolution was monitored for approximately 17 hours and at the end all the concentration profiles were approaching a stable concentration. An observation at microscope confirmed that the material in the wells was completely dissolved. The drug loading was calculated by the concentration values at the end of the dissolution. The results of the impregnation are shown in figure 4.15. The drug loading is strongly influenced by T: After 1 hour, the drug loading increases from 0.55 mg to 0.75 mg passing form 40°C to 60°C, which corresponds to an increase by 39%. For longer impregnations of 4 hours, the gain is even more remarkable from 0.62 mg to 1.05 mg, corresponding to a 68% increase. This might be explained by the following considerations: At higher temperatures the density of CO_2 decreases, that is there is a lower mass of fluid per unit volume. The amount of drug dissolved was set constant for all the experiments. Therefore, the mass fraction of the drug in the supercritical solution is higher at higher T. In figure 4.16, the drug loading is represented as a function of CO_2 density (density data extracted from [24]). Moreover, the solution diffusivity also increases with T and, despite a weaker tendency for the drug to leave the supercritical phase due to a higher solubility, the final combination of these competing factors results in a higher drug loading. The higher increase in drug concentration for 4 h experiments compared to 1 h also supports the hypothesis that the increased loading at 60°C is related to a higher diffusivity which has a time-dependent effect.

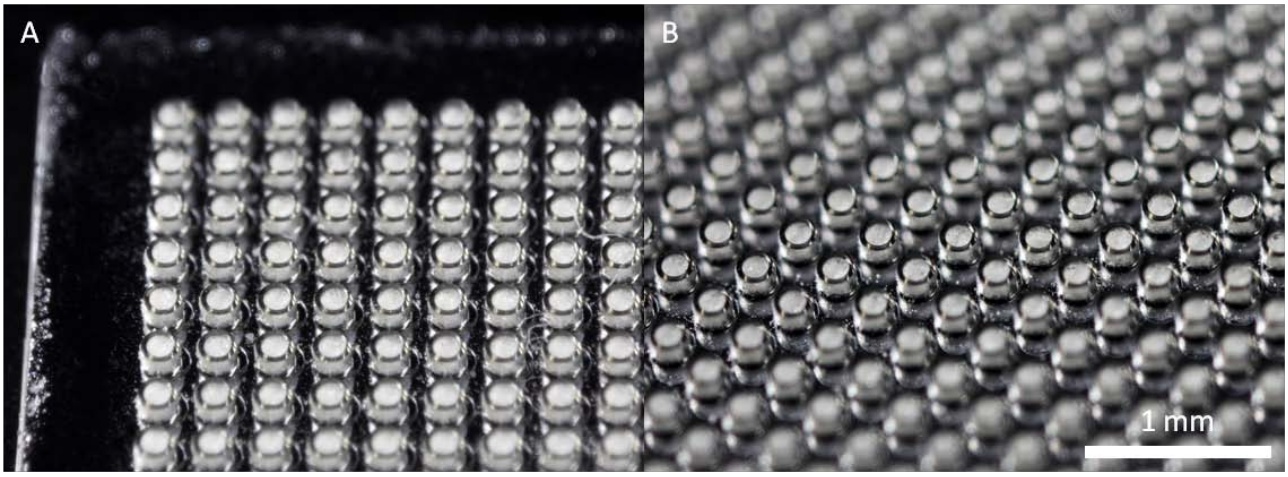

Figure 4.14: Containers filled with PVP powder by manual compaction: (a) detail of the chip corner, (b) arrays in the middle of the chip.

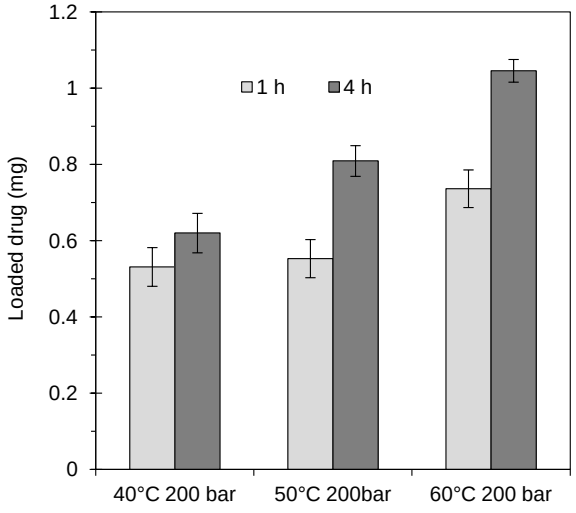

Figure 4.15: Impregnated drug per chip (625 microwells) at 200 bar for different T and times.(N=3).

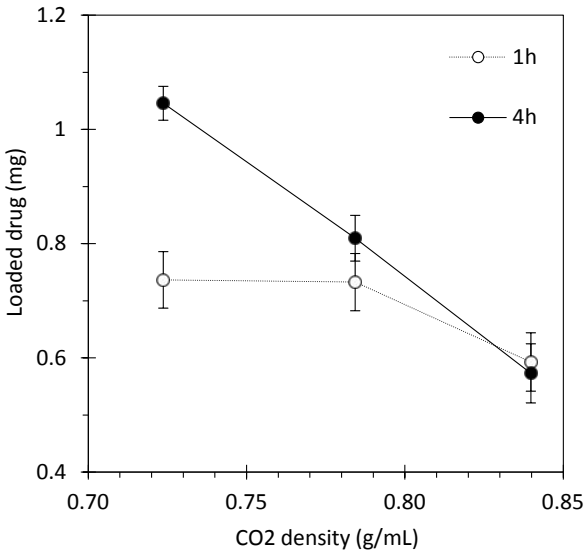

Figure 4.16: Loaded drug as a function of CO_2 density (in different impregnation conditions (N=3).

4.4 Conclusions

This chapter describes a technological solution for the drug loading of reservoir-based microdevice with a poorly soluble model drug. The microcontainers were filled with precisely controlled amounts of aqueous PVP solutions by means of inkjet printing. The sc CO_2 impregnation was shown to be a compatible loading method which allows to tune the drug loading by varying fluid pressure, temperature and impregnation time. At 200 bar 40°C 4 hours a ketoprofen concentration of 32 % wt was obtained, corresponding to a drug:polymer ratio of 1:2. Further experiments showed that temperature has also a significant effect on drug loading: a change in temperature of 20°C corresponded to an increase of drug content of 39% in 1 h and 68% in 4 h. Spectroscopic characterizations like Raman and ATR-IR were performed. Raman spectroscopy shows that there is amorphous drug-rich phase on the containers surface and a chemical interaction between the components. ATR-IR spectroscopy of PVP films confirms these evidences, showing also the presence of H bonds in samples treated at 200 bar. Impregnated containers exhibit an enhanced dissolution rate compared to reservoirs laden with solid dispersions of crystalline and amorphous drug. Up to 87% of the drug can be released within 30 minutes demonstrating that microcontainers can deliver the active ingredient in compatibility with average tablets transit time in the GI tract. The combination of inkjet printing and scCO_2 impregnation allows microcontainers to be filled with precise doses of drug. The combination of these two technologies enables to load CO_2-soluble hydrophobic drugs without the use of organic solvents and with a minimum waste of chemicals in a potentially up scalable process. The use of inkjet printing and sc impregnation shows significant improvements and promising perspective in the framework of the microfabricated devices for oral therapeutics.

Bibliography

[1] C. Witschi, E. Doelker, Residual solvents in pharmaceutical products: acceptable limits, influences on physicochemical properties, analytical methods and documented values, European Journal of Pharmaceutics and Biopharmaceutics, 43 (1997) 215-242.
[2] S.J. Macnaughton, I. Kikic, N.R. Foster, P. Alessi, A. Cortesi, I. Colombo, Solubility of anti-inflammatory drugs in supercritical carbon dioxide, Journal of Chemical & Engineering Data, 41 (1996) 1083-1086.
[3] A. Stassi, R. Bettini, A. Gazzaniga, F. Giordano, A. Schiraldi, Assessment of Solubility of Ketoprofen and Vanillic Acid in Supercritical CO2 under Dynamic Conditions, Journal of Chemical & Engineering Data, 45 (2000) 161-165.
[4] M.A. Sabegh, H. Rajaei, F. Esmaeilzadeh, M. Lashkarbolooki, Solubility of Ketoprofen in Supercritical Carbon Dioxide, The journal of Supercritical fluids, (2012).
[5] M. Banchero, L. Manna, A. Ferri, S. Sicardi, The ketoprofen partition between supercritical CO2 and poly-vinyl-pyrrolidone for drug delivery systems preparation, CHEMICAL ENGINEERING, 11 (2007).
[6] I.E. Shohin, J.I. Kulinich, G.V. Ramenskaya, B. Abrahamsson, S. Kopp, P. Langguth, J.E. Polli, V.P. Shah, D. Groot, D.M. Barends, Biowaiver monographs for immediate-release solid oral dosage forms: Ketoprofen, Journal of Pharmaceutical Sciences, 101 (2012) 3593-3603.
[7] J.C. Leffingwell, Chirality & bioactivity I.: pharmacology, Leffingwell Rep, 3 (2003) 1-27.
[8] T. Loftsson, D. Hreinsdôttir, Determination of aqueous solubility by heating and equilibration: A technical note, AAPS PharmSciTech, 7 (2006) E29-E32.
[9] J.J. Sheng, N.A. Kasim, R. Chandrasekharan, G.L. Amidon, Solubilization and dissolution of insoluble weak acid, ketoprofen: Effects of pH combined with surfactant, European Journal of Pharmaceutical Sciences, 29 (2006) 306-314.
[10] M. Tubic-Grozdanis, M.B. Bolger, P. Langguth, Application of gastrointestinal simulation for extensions for biowaivers of highly permeable compounds, AAPS J, 10 (2008) 213-226.
[11] C.-S. Su, Y.-P. Chen, Measurement and correlation for the solid solubility of non-steroidal anti-inflammatory drugs (NSAIDs) in supercritical carbon dioxide, The journal of Supercritical fluids, 43 (2008) 438-446.
[12] D. Suleiman, L.A. Estevez, J.C. Pulido, J.E. García, C. Mojica, Solubility of anti-inflammatory, anti-cancer, and anti-HIV drugs in supercritical carbon dioxide, Journal of Chemical & Engineering Data, 50 (2005) 1234-1241.
[13] P. York, U.B. Kompella, B.Y. Shekunov, Supercritical fluid technology for drug product development, CRC Press, 2004.
[14] I. Kikic, F. Vecchione, P. Alessi, A. Cortesi, F. Eva, N. Elvassore, Polymer plasticization using supercritical carbon dioxide: experiment and modeling, Industrial & engineering chemistry research, 42 (2003) 3022-3029.
[15] E. Reverchon, Proceedings of the 6th conference on supercritical fluids and their applications, September 9-12, 2001-07-03, Maiori (Salerno) - Italy, Cooperativa Universitaria Editrice Salerno CUES, 2001.
[16] I. Kikic, M. Lora, A. Cortesi, P. Sist, Sorption of CO2 in biocompatible polymers: experimental data and qualitative interpretation, Fluid Phase Equilibria, 158–160 (1999) 913-921.
[17] L. Manna, M. Banchero, D. Sola, A. Ferri, S. Ronchetti, S. Sicardi, Impregnation of PVP microparticles with ketoprofen in the presence of supercritical CO< sub> 2</sub>, The journal of Supercritical fluids, 42 (2007) 378-384.
[18] L.H. Nielsen, S.S. Keller, K.C. Gordon, A. Boisen, T. Rades, A. Müllertz, Spatial confinement can lead to increased stability of amorphous indomethacin, European Journal of Pharmaceutics and Biopharmaceutics, (2012).
[19] I. Kikic, F. Vecchione, Supercritical impregnation of polymers, Current Opinion in Solid State and Materials Science, 7 (2003) 399-405.
[20] C. Ishiyama, T.-F. Mark Chang, M. Sone, Effects of supercritical carbon dioxide treatment on bending properties of micro-sized SU-8 Specimens, Microelectronic Engineering, 88 (2011) 2272-2274.

[21] L. Carvalho, M.P.M. Marques, J. Tomkinson, Drug-excipient interactions in ketoprofen: A vibrational spectroscopy study, (2006).
[22] P. Di Martino, E. Joiris, R. Gobetto, A. Masic, G.F. Palmieri, S. Martelli, Ketoprofen-poly (vinylpyrrolidone) physical interaction, Journal of crystal growth, 265 (2004) 302-308.
[23] S. Kazarian, G. Martirosyan, Spectroscopy of polymer/drug formulations processed with supercritical fluids: in situ ATR–IR and Raman study of impregnation of ibuprofen into PVP, International Journal of Pharmaceutics, 232 (2002) 81-90.
[24] R. Span and W. Wagner, A new equation of state for carbon dioxide covering the fluid region from the triple-point temperature to 1100 K at pressures up to 800 MPa, Journal of physical and chemical reference data 25 (1996) 1509.

5. Photocrosslinking of PVP hydrogels

5.1 Hydrogels in drug delivery

5.1.1 Introduction

Hydrogels are hydrophilic three dimensional polymer networks, where molecular chains are entangled or connected along limited lengths or at punctual sites (*crosslinks*) of the polymer backbone by physical junctions or chemical bonds. Hydrogels can absorb and retain large amounts of aqueous media, swelling to up to dozens of times their dry volume. The high water content, together with a low cytotoxicity and biocompatible features place them among the most suitable materials to resemble natural living tissues [1, 2], as well as to serve as binders for several biomedical and pharmaceutical purposes [3, 4]. Polymeric hydrogels are a very important class of materials, which in recent years has attracted an increasing interest for a large number of applications in the biomedical and pharmaceutical research areas including transdermal drug delivery and wound dressing [5, 6], drug delivery systems [7-9], injectable formulations [10, 11], dental medications [12, 13], implants [14, 15], and ophthalmic systems [16, 17].

Since the discovery of crosslinked poly(2-hydroxyethyl methacrylate) (pHEMA) [18] by Wichterle and Lim in 1960, the synthesis and applications of hydrogels have been widely investigated.

Hydrogels can be prepared by crosslinking of both natural and fully synthetic hydrophilic polymers. The crosslinking reaction converts the solution, where polymer chains are free to diffuse in the solvent, in a semi-ordered three dimensional network, where the chains are connected to each other. From a rheological viewpoint, the transition from solution to gel (also called *sol-gel*) in most cases corresponds to a change from a purely viscous to a viscoelastic behaviour. Additionally, dramatic loss of solubility in water occurs.

A great variety of methods have been developed for hydrogel preparation. Hydrogels can be divided into the two main groups of physical and chemical hydrogels according to the nature of the crosslinks [19]. In the first group we find examples of crosslinking by ionic interactions (like alginate [20], whose application was discussed also in this thesis in section 3.5), by polymer freeze-thawing (like PVA [21]), by hydrogen bonding (like complexes of poly(acrylic acid) (PAA), poly(methacrylic acid) and poly(ethylene glycol) (PEG) [22]) or, in more recent discoveries, by protein interactions. Examples for the latter are genetically engineered proteins, which by coil-coil interactions serve as crosslinkers for synthetic polymers [23] and crosslinks by antigen-antiboby interactions, like in the case of an antigen-selective hydrogel for binding with antibodies [24]. Among the chemically crosslinked hydrogels, the main classification criterion is the chemical mechanism: There are hydrogels prepared by radical polymerization of low molecular weight monomers (like for instance the above cited pioneering work of Wichterle and Lim [18]), reaction of complementary groups (like NH_x- COOH) [25, 26], addition and condensation reactions [27], or enzymatic reactions (like for PEG functionalized with glutaminyl groups) [28]. Finally, also the exposure to high energy irradiation (gamma ray and electron beam) and UV light can induce crosslinking. This technique was investigated for polymers like poly(vinyl alcohol) (PVA) [29], PEG [30] and PAA [31]. The use of gamma radiation has been explored for PEG, PVP and agar based hydrogels [32] and for polymers such as biodegradable PCL [33] and polyurethanes (PCL-PEO)[34].

The crosslinking and polymerization upon exposure to UV radiation was investigated for several compounds of biomedical interest and in particular for oral drug delivery. Casadei *et al.* prepared photocrosslinked dextran methacrylate (DM) [35] and loaded it with lipid nanosuspension of ibuprofen resulting in a delayed release of the drug. In the same group, Pitarresi and coworkers [36] crosslinked modified DM by UV exposure in the presence of a polyaminoacid derivative, such as α,β-poly(N-2-hydroxyethyl)-DL-aspartamide methacrylate (PHM). The resulting hydrogel was specifically modified to survive degradation in the GI tract and reach the colon, where a medicine against inflammatory bowel diseases was delivered while the hydrogel was degraded by dextranase enzymes. A similar modification was previously performed for the natural polysaccharide inulin (INU) derivatized with methacrylic anhydride (MA) and succinic anhydride (SA) [37] which conferred a stronger resistance to gastric hydrolysis.
In case of hydrogels, the UV radiation induces crosslinking by radical polymerization [38]. Generally, the reaction is activated by a *photoinitiator*. Photoinitiators can be grouped into two main types [39].
Type I initiators are splitted into free radicals when exposed to UV light. These radicals attack the polymer backbone generating macroradicals [29], which themselves react with other chains. This reaction propagates, resulting in the formation of a polymer network. Examples of this type of photoinitiator are acetophenone derivatives and α-hydroxyalkyl phenones. Type II photoinitiators react with a compounds called *co-initiator* (generally a tertiary amine) prior to creating active radicals. The process continues with an electron and a hydrogen transfer resulting in the radical formation.
The chemical reactivity of the photoinitiator determines the reaction rate, the spectral sensitivity (wavelength of absorption), the light resistance and the stability of the materials under storage conditions [39]. Sometimes macroradicals can also be activated by homolytic scission of C–H bonds in the polymer backbone. In that case, the presence of a *photoinitiator* is not needed. Since the generated macroradicals can react with oxygen, radiation is normally performed in an inert atmosphere saturated by nitrogen or argon. Biocompatibility of photoinitiators used for crosslinking of biomaterials is a critical issue as many of them in fact are cytotoxic [40].
From a microfabrication perspective, UV photocrosslinkable hydrogels represent an extremely interesting class of materials for the design of drug delivery microdevices. These materials allow to use of photolithography for patterning, which is a key technique in the field of micro- and nanofabrication. This fact entails the possibility of using radiation to create a hydrogel-laden microdevice.

5.1.2 UV Photocrosslinking of PVP hydrogels

Photocrosslinking of poly(vinylpyrrolidone) (PVP) was investigated by several researchers. Rosiak and coworkers [41, 42] developed a successful methodology for the preparation of PVP hydrogel wound dressings based on the use of high energy irradiation (electron beam or gamma radiation). However, the use of energetic radiation usually entails the availability of expensive equipment. More important, the exposure to high energy radiation produced a non negligible degradation of the polymer chains which often turned out to be more prominent than the crosslinking reaction. More recently, the use of ultraviolet radiation (UV) was proposed by Lopérlogo *et al.* [43] for the crosslinking of aqueous solutions of PVP as an alternative to high energy radiation. In that study, no photoinitiator was used and the first radicals were generated by radiolysis of water molecules. A good degree of crosslinking was only achieved by long exposures, i.e. high radiation doses, which again entailed a consistent photodegradation of the polymer and a consequent low reticulation yield. As a solution to this drawback, the addition of hydrogen peroxide (H_2O_2) as photoinitiator was suggested [44]. In that case, the gelification yields were sensitively increased and a gel fraction of 90% could be obtained for reduced UV doses compared to without H_2O_2 as initiator. The chemical mechanism of PVP photocrosslinking reaction was also elucidated through spectroscopic techniques [45]. H_2O_2 is a type I photoinitiators, being splitted into radical which attack the polymer backbone. The structural and mechanical properties of crosslinked hydrogels were recently studied by D´Errico and coworkers [46].

5.1.3 Hydrogel matrices in microcontainers

In section 3.5.1, first attempts to immobilize polymer matrices inside microcontainerswere tried with alginate as polymer. Here, selective UV crosslinking of PVP was considered an interesting technique to define polymer matrices inside microcontainers as alternative to inkjet printing presented in section 3.6.2. A schematic of this approach is depicted in figure 5.1.

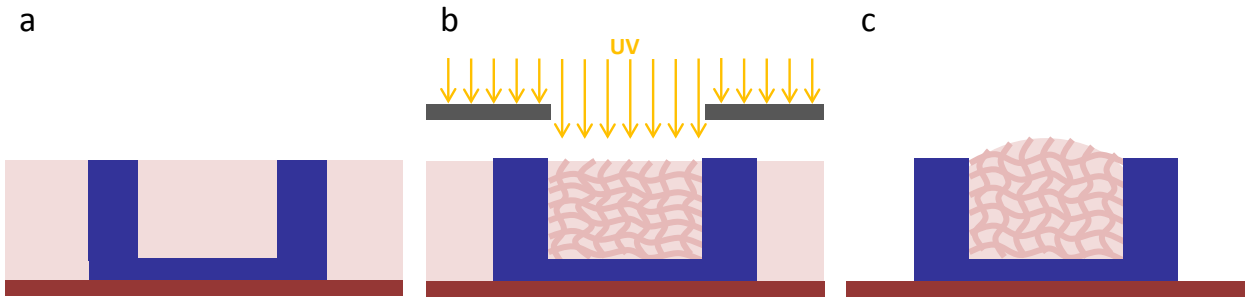

Figure 5.1: Schematic of selective crosslinking of a polymer film (negative photolithography): (a) spin coating of polymer solution on microcontainers, (b) selective exposure of polymer film through a photolithographic mask, (c) development in solvent.

PVP is used as a photoresist in a process of *negative photolithography* similar to the fabrication of microcontainers with SU-8 (see section 2.1.1). A PVP solution is spin coated onto the empty microstructures (Figure 5.1a). Then a mask is aligned on top of the microcontainers and only the cavities are exposed to UV light and crosslinked (Figure 5.1b). Finally, the uncrosslinked portions of the polymer are dissolved and removed in a solvent (Figure 5.1c). Subsequently, the defined polymer micro volumes could be loaded with the desired drug. The choice of PVP represents a valuable advantage, since it can be successfully loaded with hydrophobic drugs by supercritical impregnation, as described in chapter 4. Alternatively, the swelling properties of PVP hydrogels could also be exploited to load bioactive macromolecules of pharmaceutical interest.

5.1.4 Microgels

Previous attempts of loading SU-8 microcontainers with polymer solutions resulted in an uneven cavity filling because of air bubbles (as sketched in figure 3.12 in section 3.5.1). The definition of patterns by UV photolithography, permits to conceive a new fabrication concept of microcapsules for oral delivery that we will call *microgels*. In the microgel fabrication process the first step consists of the definition of a drug loaded matrix. As a second step, the container shell is deposited on top. This approach is represented in the schematic of figure 5.2: (a) a film is spin coated on a substrate and the pattern is defined by exposure to UV light without need of alignment, (b) the film is developed, and (c) the deposition of a shell is performed by spray coating through an aligned shadow mask. The focus of this thesis was to elucidate the properties of drug-loadable microfabricated structures. Therefore, the deposition of the shell by spray coating was not investigated and should be part of eventual future development of this concept.

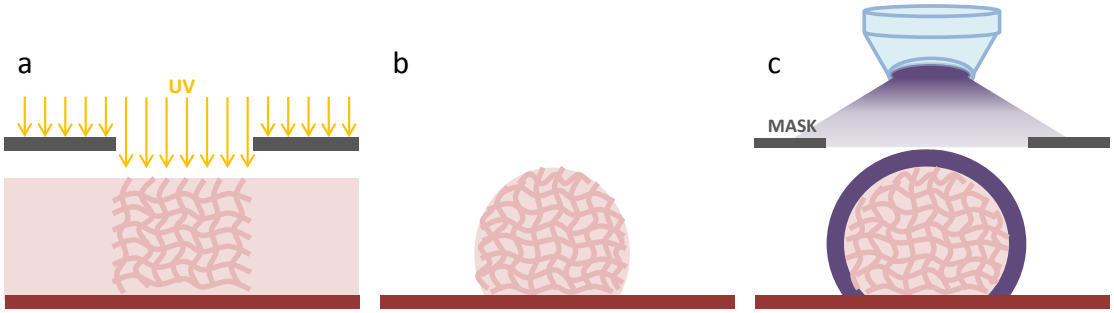

Figure 5.2: Schematic of microgel fabrication process: (a) spin coating of polymer film on a substrate and selective UV irradiation, (b) development of uncrosslinked portions, (c) deposition of a protective shell by spray coating through a shadow mask.

5.2 Fabrication of PVP microgels

5.2.1 Overview of the process

As discussed in the previous section, photocrosslinking of bulk PVP hydrogels has been demonstrated. However, the use of radiation to transfer patterns on PVP films was barely investigated. Burkert *et al.* [47] used electron-beam lithography to define structures in films of solutions of PVP in ethane, while no work was found regarding the definition of patterns in films of aqueous solutions. A first step consisted in the fabrication of masks used for the selective exposure to UV light. The fabrication process was previously explained in section 2.1.3. The masks consisted of glass wafers with a patterned metal coating (chromium or aluminum) on one side, representing the negative image of the pattern which is supposed to be transferred to the PVP film. The masks were fabricated with the same pattern design as the SU-8 microcontainer bottom, with circles of different diameters and center-to-center distances. The typical mask had arrays of transparent spots ranging from 100-500 µm in diameter with a centre-to-centre pitch of 450-600 µm. The glass masks were diced into squares (called *mask chips*) containing 625 spots aligned in a 25×25 matrix as previously shown in figure 2.4. For the study of the swelling properties of individual microgels (see section 5.3), additional mask chips were fabricated with a design including only 4 transparent spots of variable diameter of 100-500 µm and a centre-to centre pitch of 5 mm.

In an optimal pattern transfer, the crosslinking should be confined to the exposed areas. Furthermore, the reaction should propagate anisotropically through the whole thickness of the irradiated film. The most important parameter is the gap between the mask and the layer where the pattern is replicated. In general, if the gap is too wide, the irradiated areas are larger than the actual mask pattern, i.e. there is a loss of resolution in the pattern dimensions. This phenomenon is due to light diffraction effects, and is more pronounced if the radiation is not collimated as in the case of this study. Therefore, the polymer was spin coated directly onto the glass mask and the exposure to UV light was performed from the mask back side. In this way, the film was physically in contact with the mask and the gap between mask and polymer layer was reduced to zero. Moreover, to reduce light diffraction within the glass, the polymer was deposited on the metal coated-side of the mask, while the glass side faced the UV light.

In figure 5.3, the fabrication process of PVP microgels through backside exposure is schematized. A solution of PLLA is spin coated (Figure 5.3a). A layer of PVP solution is spin coated on PLLA (Figure 5.3b). The mask is flipped and exposed to UV light form the back side (Figure 5.3c). Finally, the chip is immersed in a solvent to dissolve the uncrosslinked polymer and the PVP microgels are developed (Figure 5.3d). The PLLA film serves as substrate layer for the microgels. PLLA is biodegradable and can be peeled off the mask chip after PVP development. Eventually, it could be rolled and put in a capsule ready for oral ingestion. Also, the hydrophobicity of PLLA facilitated the removal of uncrosslinked material. In the following sections the single operation steps schematized in figure 5.3 will be described in detail.

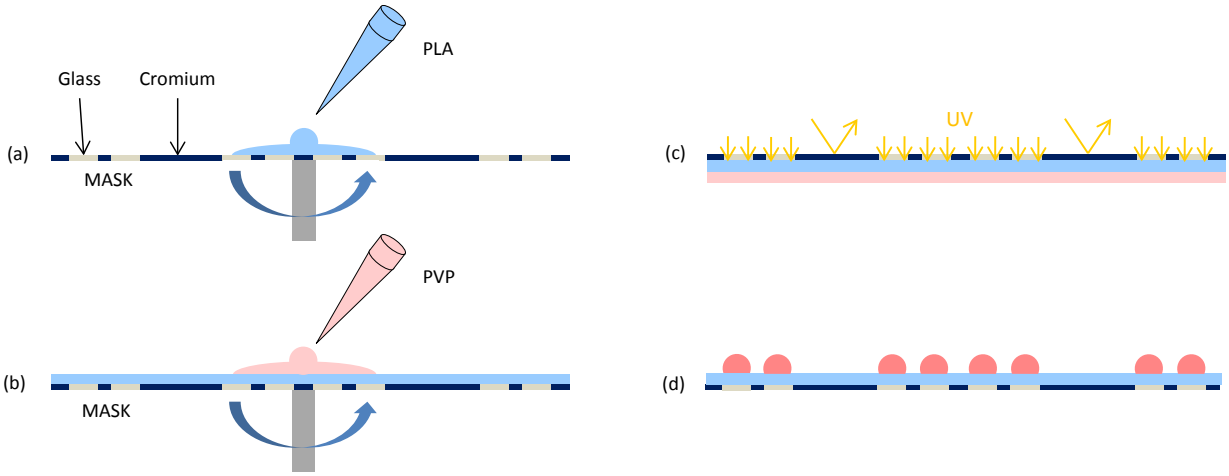

Figure 5.3: Fabrication steps of PVP microgels: (a) spin coating of PLLA substrate layer, (b) spin coating of PVP layer, (c) mask flipping and UV exposure form the back side, (d) development in water.

5.2.2 Materials and methods

Poly(L-lactic-acid) (PLLA) was purchased from Natureworks (M_w=126000 Da, determined by size exclusion chromatography measurements). Poly(vinylpyrrolidone) (PVP K90, M_w=360000 Da), hydrogen peroxide (H_2O_2) aqueous solution (30% wt) and dichloromethane (DCM) (anhydrous >99.8%) were supplied by Sigma Aldrich. PLLA pellets were dissolved in DCM (20% wt) under stirring at room temperature for 24 h. PVP solutions were prepared dissolving powder in mixtures of DI water (99.1% v/v) and H_2O_2 solution (0.9% v/v), with polymer concentration of 10, 20 and 30% wt under stirring (250 rpm) at 50°C for 36 h. PVP has a very high solubility in water [48]. Even at the highest concentration, PVP was perfectly dissolved, resulting in very viscous and transparent solutions. The polymer solutions were poured into syringes and stored overnight in vertical position for air bubbles removal. PLLA solution was kept in a fridge at 4°C. Spin coating steps were performed on single mask chips mounted on a custom made Teflon chip holder (WS-650Mz-23NPP Spin processor, Laurell, USA). The use of the holder was beneficial for uniform PVP deposition reducing film thickening at the edges (edge bead) due to surface tension effects. After spin coating, the mask chips were flipped over and mounted into squared slots milled in a Teflon rod, which was then transferred into the UV chamber. The slots had dimensions perfectly fitting the mask chips and included small pools previously filled with water-imbibed cotton which kept the film humid during irradiation. Irradiation was carried out in a UV chamber (BS-02, Dr. Gröbel UV Elektronik, Germany) equipped with 8 tubes: 4 lamps emitting in the UVC range (emission spectrum with a single peak at 253.4 nm) and 4 lamps emitting UVB range (broad band in the region 265-400 nm). The samples were placed at a distance of 15 cm from the light source, where the total radiant flux was measured with a radiometer ranging from 29-32 mW/cm^2. After exposure, the mask chips were immersed in DI water, rinsed with moderate stirring for 10 minutes and left drying overnight at room temperature. The thickness of dry films and microgels was measured with a contact profiler (KLA Tencor Alpha-Step IQ, stylus force 8.33 mg) with a scanning length of 4-6 mm, a scan speed of 100 µm/s and a data acquisition frequency of 50 Hz.

5.2.3 Spin coating

The spin coating of the PLLA was performed dispensing 0.5 mL of solution and spinning at 2400 rpm for 30 sec with an acceleration of 200 rpm/s. The layer was left drying for 3 min at room temperature. The PLLA film was transparent and absorbed a limited amount of UV radiation (lower than UV sensor resolution, 0.1 mW/cm^2). The spin coating of PVP was studied in more detail. An important aspect in the spin coating of films is the viscosity of the polymer solution. In figure 5.4 the viscosity of PVP solutions with different solid polymer concentrations are shown as a function of applied stress.

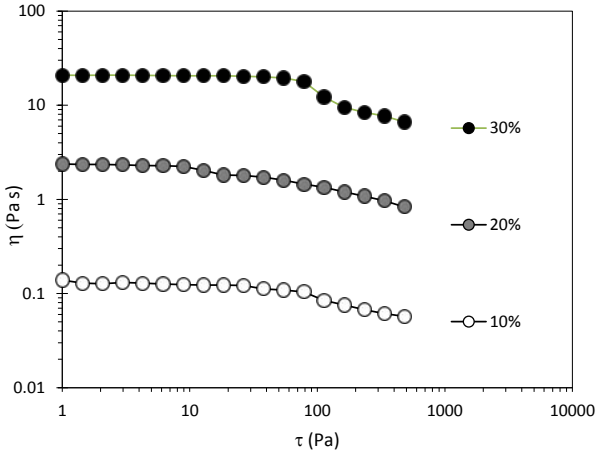

Figure 5.4: Viscosity curves of aqueous solutions of PVP K90 at different concentrations.

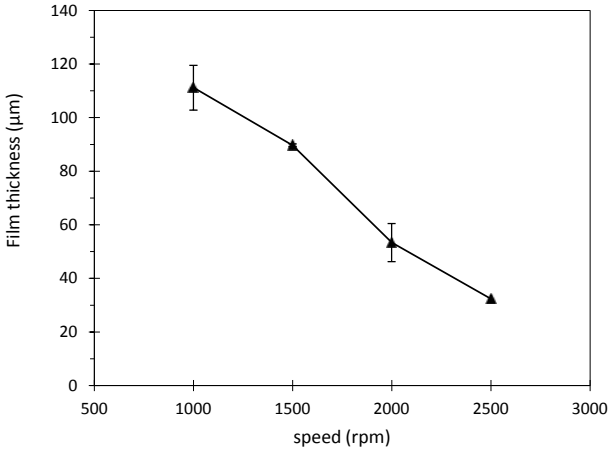

Figure 5.5: Thickness of dried uncrosslinked? PVP films prepared at different spinning rates with 30% wt solution (N=4).

The solutions exhibit a Newtonian behaviour with a weak shear thinning tendency within the range of 20-80 Pa. The viscosity plateau values increase by approximately one order of magnitude with an increase of the concentration by 10%.
Preliminary tests on spin coating of PVP solutions revealed that only the concentration of 30% PVP was giving uniform films, while more diluted solutions coated the chips only partially even at low spin rates. Therefore, it was decided to proceed only with 30% PVP solutions. Moreover the photoreticulation of 30% solutions gives a maximum gelification yield according to a previous work [46].
Fixed amounts of polymer solution (approx. 34 mg) were dispensed on mask chips with one of corners covered by tape. The chip was spinned for 60 sec with a ramp of 100 rpm/s at various spin speeds ranging from 1000-2500 rpm. The obtained films were left drying at room temperature overnight. For thickness measurements, a scratch was made with a scalpel in the film next to the corner covered by tape before the spin coating. By removing the tape with the layer on, a step was obtained in the film along the scratch. A stylus profile was recorded across the step. The results of the scanning are shown in figure 5.5. Each data point corresponds to 4 samples. As expected, the film thickness becomes lower for increasing spinning speed. For the fabrication of microgels, the procedure with a spin speed of 2500 rpm was preferred because it resulted in a more homogeneous film.
The thickness of the polymer film in the wet state (i.e. just after spin coating, before drying) could not be directly measured because of the softness of the material. However, an estimation can be made by knowing the polymer concentration and the weight of the films. For the spin coating at 2500 rpm, the mass of the polymer film on the chips was 16.5±0.7 mg. For a solution 30% wt having a density of 1.08 g/mL (value extrapolated from [48]), the film thickness after spin coating z is calculated as follows:

$$z = \frac{\text{film mass}}{\text{solution density} \cdot \text{chip surface area}} = \frac{16.5(\text{mg})}{1.08\left(\frac{\text{mg}}{\text{mm}^3}\right) \cdot 163.84(\text{mm}^2)} \cong 94\ \mu\text{m} \qquad (5.1)$$

5.2.4 UV exposure of PVP films

After the spin coating, PVP films were exposed to UV light for different irradiation times: 5.5, 11, 22, 33, 44 min. In table 5.1, the energy received by an individual microgel volume is reported as a function of dimension and irradiation time assuming a mean exposure density of 29 mW/cm^2 (UVB+UVC radiation).
After irradiation, samples were washed in DI water for 5 min under moderate stirring (100 rpm, higher rates caused delamination). The developed microgels were then left drying at room temperature in a desiccator overnight. Figures 5.6 and 5.7 show images of microgels after development and drying.
Thereafter, size and shape of dried microgels were analyzed by means of the contact profilometer with the same recipe as the one used for films. The profiles of microgels with different diameters and irradiation times are shown in figure 5.8. Each profile is the average of 15 measurements. For all the gel sizes, the thickness is proportional to the exposure time. Moreover, the height of gels irradiated for 22 min (32.1 µm) was similar to the film thickness after spin coating (32.4 µm), and exposures longer than 22 min resulted in microgels with the same height. Therefore it was concluded that there is a radiation dose, above which the whole thickness of the exposed polymer layer is crosslinked. The volume of the microgels can easily be modulated according to the design specifications of the drug delivery system.

Table 5.1: Irradiation energies for each exposed microgel.

Microgel diameter	Exposed area (10^{-3} µm^2)	Irradiation power (µW)	Irradiation energy at different exposure times (mJ)		
			22 min	33 min	44 min
100 µm	7.85	20.5	3	4.5	6
200 µm	31.41	9.1	12	18	24
300 µm	70.68	2.3	27	40.5	54

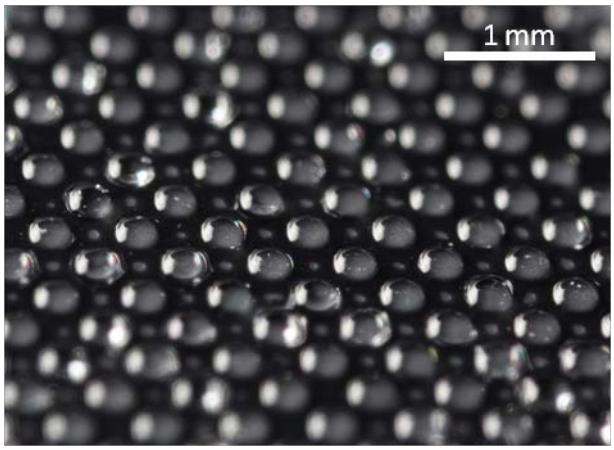

Figure 5.6: Arrays of PVP microgels (300 µm in diameter) on PLLA film.

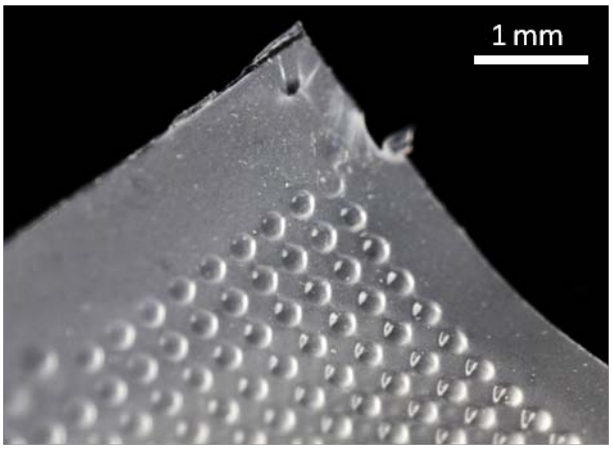

Figure 5.7: Film of PLLA with arrays of PVP microgels after being peeled off the mask chip.

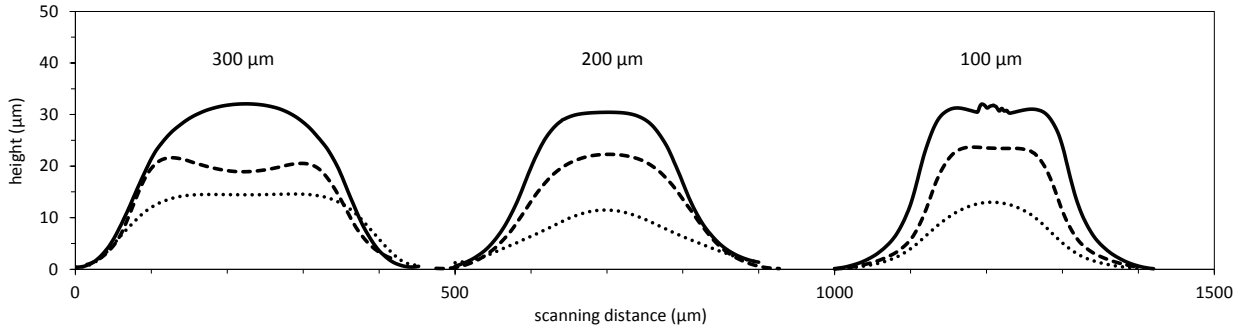

Figure 5.8: Microgel Profiles of microgels with different nominal diameters (300, 200, 100 µm), UV irradiated for 5.5 min (dotted line), 11 min (dashed line), 22 min (solid line). The axes have different scales.

If we approximate the microgels as spherical caps, we can calculate their volume with the following equation:

$$V = \frac{\pi h}{6}(3a^2 + h^2) \tag{5.2}$$

Where *a* is the radius of the base of the cap (microgel base), and *h* is the height of the cap (central height). According to equation (5.2), the volumes of microgels fabricated with different irradiation times can be computed from the values of *a* and *h* measured by contact profiling. The results are listed in table 5.2.

Table 5.2: Estimated microgel volume for different sizes and irradiation times.

Microgel diameter (µm)	Cap radius (a) (µm)	Cap height (h) (µm)			Volumes of microgels (nL)		
		Irradiation time (min)			Irradiation time (min)		
		5.5	11	22	5.5	11	22
100 µm	50	14.59	22.29	32.08	0.06	0.09	0.14
200 µm	100	10.52	21.62	30.45	0.27	0.34	0.49
300 µm	150	12.98	23.68	32.04	0.46	0.84	1.15

5.3 Loading of microgels

The loading of hydrogels was performed after the crosslinking step, in order to avoid the well known photolysis reactions induced by UV irradiation on both small active ingredient [49] and biomacromolecules [50]. Indeed, these reactions are often sensitively enhanced by the presence of H_2O_2 [51]. Loading of hydrogels can be performed by swelling with several solvents. Besides in water based solutions, photocrosslinked PVP also swells in ethanol and DMSO. As an example, PVP hydrogel swelled in ethanol (>99.5%) in 24 h, reaching up to 14 times its dry weight. As a consequence, a large number of hydrophobic APIs, dissolvable in ethanol or DMSO, could potentially be loaded into PVP hydrogels (or microgels).

5.3.1 Confocal microscopy

Confocal microscopy was used to investigate the swelling properties of the gels and the loading of model macromolecules. Confocal micrograph stacks were acquired with a Zeiss LSM 5 microscope (Carl Zeiss, Oberkochen, Germany). For the detection of Rhodamin, a 20x objective with 0,5 numerical aperture (NA) with excitation light at 543 nm (HeNe laser) and collecting emitted light at 560 nm was used.
For the detection of FITC-avidin imaging was performed with a 40x objectve, 1.2 NA, using excitation light at 488 nm (argon laser) and collecting emitted light from 505-530 nm. The recorded stacks were processed using the software ImageJ.

5.3.2 Loading of small molecules

To study the dimensions of swollen microgels, the uptake of fluorescent dye (Rhodamin B, Sigma Aldrich) was visualized by confocal microscopy. For this purpose, mask chips with only 4 well separated microgels were utilized. Individual microgels were wetted by manual pipetting with fixed aliquots of the aqueous fluorophore solution (8 µl, 20 µg/mL) and left swelling for defined times. Confocal images where acquired while microgels were in a swollen state (see figure 5.9a) and in a dry state after having whiped the excess solution surrounding the gel with cotton buds (figure 5.9b). Comparing the swollen and the dry states, a significant increase of volume can be noticed. By analyzing the white zone heights in figure 5.9a and b (where the luminescent dye reaches fluorescent saturation) the gel thickness increases from 28 to 128 µm during immersion for 8 min. From a qualitative viewpoint, the confocal images show that small molecules like Rhodamin can easily be incorporated into PVP microgels by a short immersion in a liquid solution.

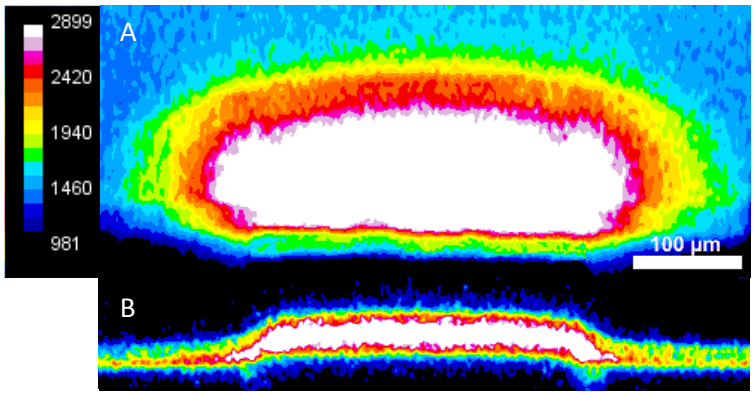

Figure 5.9: Fluorescent micrographs showing the XZ sections of a confocal scanning through a 300 µm wide microgel, swollen for 8 minutes with fluorescent dye. (a) Microgel in the swollen state (immersed in the Rhodamin solution) and (b) in the dry state. The color palette and the scale bar are referred to both (a) and (b) images. Colors are referred to fluorescent intensity.

To test the compatibility of this new polymer structures with the supercritical loading technique discussed in chapter 4, photocrosslinked PVP films were submitted to CO_2 impregnation with ketoprofen. To test the effect of crosslinking on impregnation, two polymer films were prepared as described previously (section 5.2.3). One film was crosslinked by UV radiation for 22 min, and the other one not. After solvent evaporation in a desiccator overnight, the dried films were weighed. The weight of the deposited polymer estimated by subtraction of the chip weight is shown in table 5.3. Both samples were impregnated in the same experiment with ketoprofen at a CO_2 pressure of 200 bar at 40°C for 1 hour. The drug amount dissolved in the batch corresponded to saturation condition, as indicated by Macnaughton *et al.* [52]). The dissolution was measured with a similar procedure as described in section 4.2.7. Impregnated films were immersed in 10 mL of sonicated DI water, at 37°C and a stirring rate of 100 rpm.
The loaded drug amounts were estimated from the final concentrations in the dissolution media and the loading yields from the ratio of drug to the polymer weight. In table 5.3 the results of impregnation are shown. The loading yields in the two films seem to be almost the same. The presence of crosslinking does not have an effect on the loading for such low film thicknesses. However, during the dissolution experiments the polymer films behaved quite differently: The uncrosslinked film gradually detached from the chip and dissolved in the medium and the drug dissolved together with the film. Compared to that, the gel film swelled in the dissolution medium and was still bonded to the substrate at the end of the test. In this case the drug diffused out of the swollen matrix. The dissolution curves are represented in figure 5.10. Although the drug release mechanisms from the two samples were different, unexpectedly the cumulative release profiles appear quite similar. This can be explained by the high diffusivity of the drug in the polymer network due to the low size of ketoprofen.

Table 5.3: Results of impregnation of PVP films with ketoprofen: Polymer and drug weight at the different fabrication steps.

Sample	PVP after spinning (mg)	PVP after (washing*) and drying (mg)	Loaded drug weight (mg)	Drug mass fraction
uncrosslinked	17.9	9.32	1.66	0.15
crosslinked	17.9	7.73	1.22	0.14

*only for the crosslinked films.

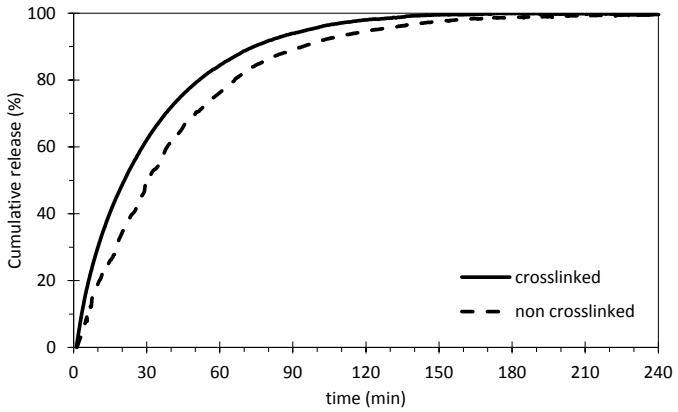

Figure 5.10: Cumulative release profiles of ketoprofen from PVP films with and without crosslinking

5.3.3 Loading of macromolecules

Microgels can be potentially used to deliver bioactive macromolecules like proteins and nucleic acid based-therapeutics in the GIT. To test the feasibility of the system to this purpose, the loading of a model macromolecule was performed. The microgels were swollen with solutions containing a labelled protein with a similar procedure as the one explained previously in section 5.3.1. A FITC Avidin stock solution (phosphate-buffered saline 2.5 mg/mL, 66 kDa, Invitrogen) was diluted to 20 µg/mL concentration. Aliquots of 4 µl of the solution were manually dispensed onto single microgels and thereafter a sequence of confocal microscope scannings of the gel volume were taken at defined times. In figure 5.11 the fluorescent micrograph of a gel incubated for 25 minutes is represented from different viewpoints: (a) shows the top view, with focus on the microgel upper surface. Here, precipitated particles of avidine can be recognized. Figures 5.11b and 5.11c show orthogonal cross sections of the gel. Apparently, a thin layer of tagged-protein has deposited on the surface whereas no protein has been incorporated within the gel volume. Other tests were performed increasing dispensed solution volumes (8 and 16 µl) and the immersion time (up to 1 h), but no significant protein uptake could be detected in the microgels. This fact suggested that most likely longer times were needed for the absorption of large molecules like proteins. To further elucidate the feasibility of protein encapsulation in microgels for, PLLA films with 625 PVP microgels irradiated for 33 min were incubated in a 0.5 mL droplet of buffer solution with higher concentrations of FITC avidin (0.1 mg/mL). The microgel film was placed on top of the droplet dispensed inside a parafilm-coated box which was then closed and protected from light. In this way, solvent evaporation was delayed and protein precipitation on top of microstructures was minimized. The incubation was carried out for 24 h and 48 h. After 24 h gels were still wet, and a confocal scan revealed that protein absorption was uniform but the fluorescence signal was still weak. After 48 h, the solution was completed sucked up by the gels, which looked yellowish and were completely dry. After solution drying, no traces of solute precipitation were found, which suggested that the whole 0.5 mL incubation volume had been absorbed by the microgels. A total of four incubated microgels, chosen from different points on the film, were visualized by confocal microscopy. A representative example of the microgel z scanning is shown in figure 5.12. These experiments quantitatively show that the loading of macromolecules into microgels is possible but that protein diffusion is significantly hindered in the polymer network.

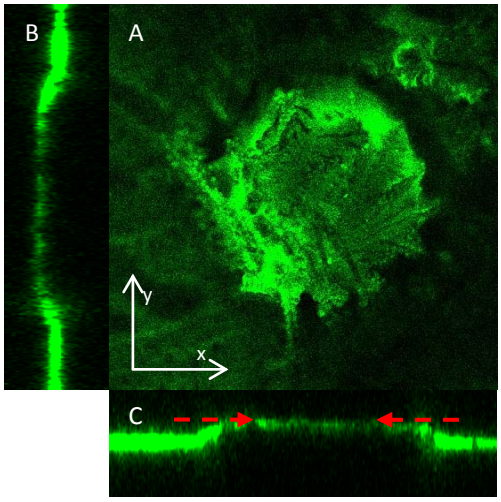

Figure 5.11: Fluorescence micrograph of a 300 µm wide microgel irradiated for 33 min after immersion in FITC Avidin solution for 25 min and drying. (a) Top view of the gel showing precipitated dye particles; (b) YZ section and (c) XZ section of confocal scan. The top view image is taken at height shown by the red arrows in (c).

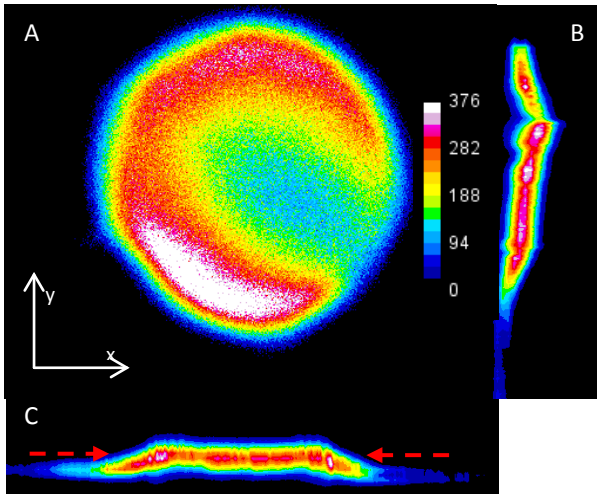

Figure 5.12: Fluorescence micrograph of a 300 µm wide microgel irradiated for 33 min after immersion in FITC Avidin solution for 48 h. (a) Top view of the gel; (b) YZ section and (c) XZ section of confocal scan. The protein seems to be encapsulated uniformly inside the microgel. The top view image is taken at height shown by the red arrows in (c).

5.4 Structural properties of PVP hydrogels

From the perspective of a drug delivery system, the control of the release is a crucial feature. The experiments on the loading of PVP hydrogels with avidin presented in the previous section, showed that a non negligible hindrance of the protein diffusion exists. It is reasonable to assume that a macromolecule encounters a similar hindrance when it diffuses out of the gel. Generally the slow diffusion can be explained either by protein-polymer interactions, or by steric hindrance. Considered that PVP is a neutral polymer and no evidence of PVP interactions with proteins was reported in the literature, this resistance to diffusion is most likely related to the mesh dimensions of the polymer network. The polymer mesh size might be comparable to the molecular dimensions of avidin (6×5.5×4 nm^3 [53]). In the attempts of elucidating this phenomenon, a more in-depth characterization of UV-crosslinked PVP hydrogels networks was carried out by means of rheological techniques and nuclear magnetic resonance spectroscopy.

5.4.1 Gel preparation

For the rheological and the NMR investigations, macroscopic specimens of the hydrogel were prepared. From a short sequence of preliminary crosslinking tests performed on solution layers of different thickness, it was concluded that samples thicker than 1 mm exhibit a macroscopically inhomogeneous structure with a softer texture in the bottom and a more rigid one on the top. On the other hand, membranes thinner than 1 mm were very fragile and unpractical to handle. As a consequence a fixed thickness of 1 mm was used.

PVP hydrogels were prepared as follows: Solutions of PVP K90 were prepared with various concentrations of polymer (10, 20, 30% wt) as described in section 5.2.2. To investigate the influence of the crosslinker concentration on the structural properties, additional 30% PVP solutions were prepared with double and triple amounts of H_2O_2 (later referred as 30%+2H and 30%+3H). The mixtures were cast into cylindrical moulds (1 mm in depth, 15 mm in diameter) composed of an Aluminum sheet with circular holes clamped to a parafilm-coated plastic disc. The solutions were poured into the cavities and leveled with a spatula. Finally, the same kind of glass wafer as the ones used for the mask fabrication was clamped onto the mold. The placement of glass on the samples was necessary to reproduce experimental conditions as close as possible to the ones during microgel fabrication. Most importantly, the glass prevented water evaporation during the exposure. It was measured that the glass absorbs a negligible amount of the radiation emitted by the UV lamps of approx. 5 mW/cm^2. Considering a power density of 29 mW/cm^2, each sample was exposed to 67 J, 100 J, 134 J corresponding to irradiations of 22, 33 and 44 min respectively. After photoreticulation and prior to any analysis, all the considered gels were separated from the moulds with a spatula and dipped in DI water for 24 h under stirring to extract eventually unreacted polymer and crosslinker. During this operation, gel disks underwent a macroscopic swelling. Figure 5.13 shows an example of gel before (left) and after 24 h of swelling (right).

After the swelling, gels were dried and weighed. The water/polymer weight ratios were calculated as follows:

$$\frac{m_{H2O}(t)}{m_{dry}} = \frac{m(t) - m_{dry}}{m_{dry}} \tag{5.3}$$

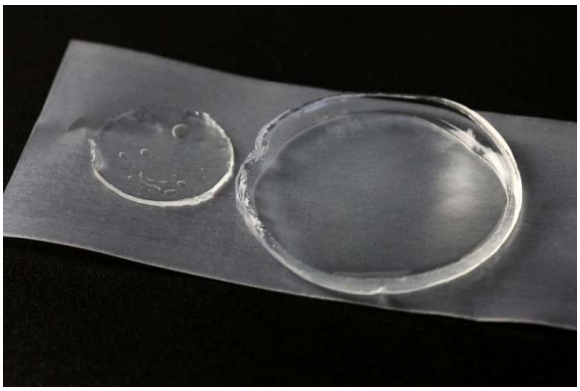

Figure 5.13: PVP hydrogel before (left) and after (right) the swelling.

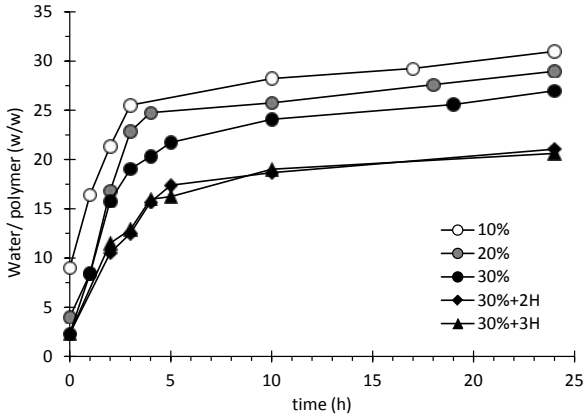

Figure 5.14: Plots of the water/polymer ratio in the gels as a function of time for different polymer and crosslinker concentrations.

In figure 5.14 the ratio is plotted as a function of swelling time for the considered concentrations. All the systems share a common trend described by a rapid swelling within the first 5 hours followed by a slower water uptake. From the slope of the curve at 24 h it seems that the systems have not yet reached equilibrium. However, a phenomenon of overswelling was observed for immersion for longer than 24 h characterized by the breakage of the membranes in smaller fragments. The values at the beginning of the experiment (t = 0) recorded before the swelling started, correspond to a water content very close to the water fraction in the solution. In fact, it was observed that the dry polymer weight was equal to the polymer concentration of the corresponding solution. Thus, it was deducted that most of the polymer was involved in the reticulation and a minimal portion of polymer is degraded or not bound to the gel lattice. This is reasonable, since polymer degradation is strictly connected to UV irradiation dose [54]. In these experiments a very limited UV dose was utilized, compared to other works where gels were submitted to energies in the range of kJ [43, 45] or prolonged irradiations of 2-6 h [46].

5.4.2 Rheological characterization of gels

Each gel was left swelling for 24 h and cut into a disc of 20 mm diameter fitting the rotating probe of the rheometer. The analyses were performed as previously explained in section 2.6.1.1. The results of the small oscillatory shear experiments (i.e. frequency sweep tests, FS, aimed at the determination of the mechanical spectrum), also called mechanical spectra, reveal different viscoelastic behaviours for the considered systems. The tests were performed on samples treated with UV light for 22, 33 and 44 minutes in three replica. To simplify the illustration only profiles 22 and 44 minutes are presented in the following, as those at 33 min were always placed in between (as can be seen in table 5.3). In figure 5.15 the mechanical spectra of samples at 10% are depicted. The sample irradiated for 22 min cannot strictly be defined as a gel, as the moduli G´ and G´´ almost are overlapping. The sample irradiated for 44 min exhibits a stronger elastic response and can be considered as an incipient gel as G’ and G” have a slight dependence on the shear frequency but G’ is close to G’’ (the viscous component is still important).

The mechanical spectra of 20% wt PVP systems are shown in figure 5.16. The sample with shorter irradiation is already a structured gel, with a stronger elastic component than for the 10% PVP films in figure 5.15. There is a residual dependency of the moduli on ω as it occurs in weak gels. The gel with 20% wt irradiated for 44 min is what is commonly called a strong gel, with an important elastic modulus, independent from oscillation frequency and dominant with respect to the viscous modulus (G’ > 10*G’’).

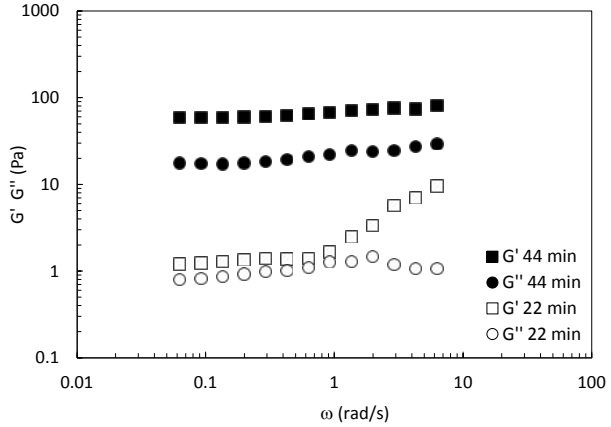

Figure 5.15: Mechanical spectra of hydrogels prepared from 10% wt solution at different irradiation times.

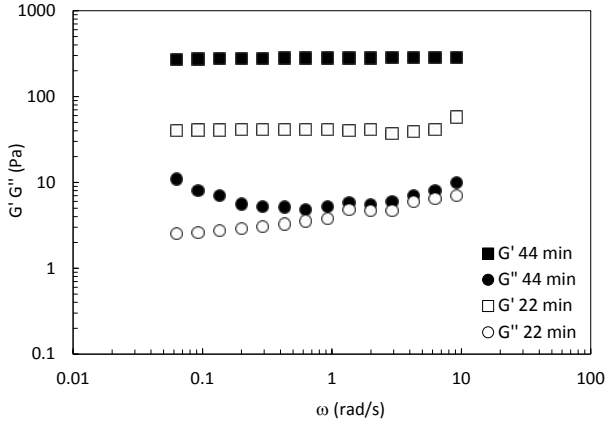

Figure 5.16: Mechanical spectra of hydrogels prepared from 20% wt solution at different irradiation times.

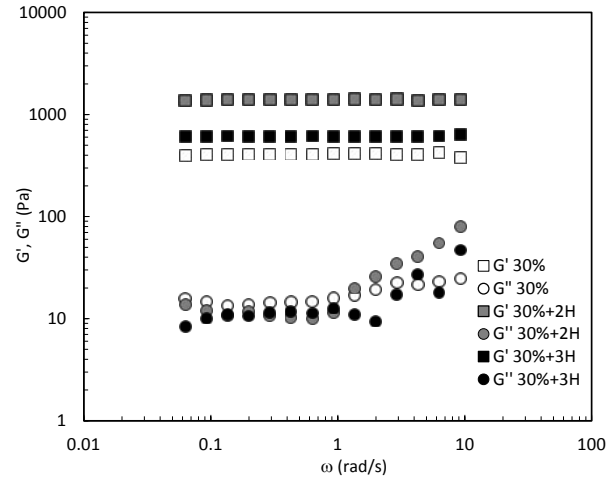

Figure 5.17: Mechanical spectra of hydrogels prepared from 30% wt solution (white), with double (grey) and triple (black) crosslinker concentrations, irradiated for 44 min.

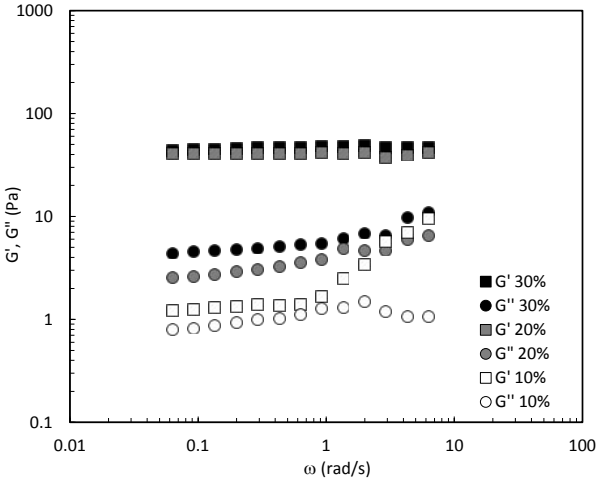

Figure 5.18: Comparison between elastic and viscous moduli for gels of different concentrations irradiated for 22 min.

In figure 5.17 the comparison of gels prepared with different crosslinker concentration in solutions with 30% PVP is shown. All the samples exhibit the typical features of strong gels. This is an evidence that UV radiation has induced the formation of chemical crosslinks between polymer chains. Elastic moduli differ from respective viscous moduli with more than one order of magnitude and in case of 2H even two. A double concentration of H_2O_2 in the solution has a clear effect on the value of G'(ω) which increases from around 400 Pa to 1400 Pa. In the sample 3H this effect seems to be smaller.

Finally, figure 5.18 shows the moduli of gels at a fixed UV dose (67 J) and for different initial polymer concentrations. With the increase of concentration there is a clear transition from solutions close to gel point (sample 10% wt) to more structured materials (20 and 30%). There is a significant increase of the elastic response from 10% to 20% and this is another typical feature of chemically crosslinked gels [55, 56]. The increase of G' plateau values is less pronounced from 20% to 30%. The influence of polymer content on viscoelastic properties is certainly less important than the one of the UV irradiation dose/time. The rheological characterization provides important informations about the structural properties of photocrosslinked films: The strong nature of the gels indicates that the polymer chains are connected by punctual crosslinks, most likely by chemical bonds. This fact permits the use of Flory´s model to calculate the average mesh size of the network.

5.4.3 Average mesh size estimations

5.4.3.1 Estimation according to the theory of Flory

The mechanical spectra of the systems were fitted with the generalized Maxwell model proposed in section 2.6.1.4:

$$G'(\omega) = \sum_{k=1}^{n} \frac{g_k(\lambda_k\omega)^2}{1+(\lambda_k\omega)^2} \qquad g_k(\omega) = \frac{\eta_k}{\lambda_k} \tag{5.4}$$

$$G''(\omega) = \sum_{k=1}^{n} \frac{g_k\lambda_k\omega}{1+(\lambda_k\omega)^2} \qquad g_k(\omega) = \frac{\eta_k}{\lambda_k} \tag{5.5}$$

where n is the number of considered Maxwell elements, g_k, η_k, λ_k represent the spring constant, the dashpot viscosity and the relaxation time of the i^{th} Maxwell element, respectively. The data fitting was performed assuming that the relaxation times are scaled by a factor of 10. Thus G_E, g_k and λ_1 are the n+2 fitting parameters. The number of Maxwell elements was selected according to the statistical criterion of the minimization of the product $\chi^2 N_p$, where χ^2 is given by the sum of the squared errors while N_p is the number of fitting parameters equal to n+1. The data fitting procedure was written in a Visual basic "user defined" program and executed by Microsoft Excel "Solver" function. With the fitted values of G_E and g_i, and λ_k, the crosslink density ρ_x and the mesh size ξ_a were estimated using the equations showed in section 2.6.1.5. In table 5.3 the results are summarized.

From table 5.3 it can be noticed that the mesh size ξ_a is strictly related to $\sum g_i+G_E$ that is the contribution of elastic elements to G'. Indeed, there is a direct correlation between these two parameters in the theory of Flory. The mesh sizes at different UV exposures are plotted in figure 5.19 comparing different PVP concentrations. All the profiles show a decrease of the crosslink-to-crosslink distance upon longer exposure to UV radiation.

Table 5.3: Results of the fitting of mechanical spectra with Maxwell´s generalized model.

Sample	UV time (min)	G' (Pa) (from FS)	$\sum g_i+G_E$ (Pa)	ρ_x (10^{-9} mol/cm^3)	ξ_a (Flory) (nm)
10%	22	5.74	4.61	1.54	127.3 ±6.10
	33	24.06	41.77	6.29	79.58±2.54
	44	75.76	134.96	20.8	53.39 ±2.24
20%	22	37.29	52.52	7.61	74.70 ±1.79
	33	170.00	113.05	28.8	47.94±1.82
	44	284.10	290.67	38.3	43.58 ±0.59
30%	22	47.03	71.04	11.9	64.39 ±2.22
	33	97.33	119.75	48.4	40.33 ±1.41
	44	426.2	457.98	62	37.11 ±1.03
30%+2H	22	10.12	15.05	1.74	122.15 ±6.26
	33	161.90	181.84	25.7	49.81 ±1.08
	44	1404.00	1435.10	194	25.36 ±0.08
30%+3H	22	4.75	4.19	0.98	147.80 ±3.69
	33	208.8	274.77	31.1	46.71 ±0.92
	44	620.70	742.65	0.96	32.06 ±0.53

In the sample with 10% PVP the radiation dose significantly influences the gel structure. The estimated mesh size is more than halved when passing from 22 to 44 min exposures, which can explain the transition from a solution to a gel behaviour shown in the mechanical spectra in figure 5.15. Networks generated by the photocrosslinking of 10% solutions exhibit meshes larger than the ones obtained from more concentrated solutions for all the tested exposures. Membranes prepared with 20% and 30% PVP show a very similar structure for all of the studied cases. This fact could also be predicted from the comparison of elastic moduli in figure 5.18. The density of crosslinks for these systems is less dependent on the UV dose than for 10% PVP. Passing from 10% to 20-30% there is in fact a reduced decrease in the mesh size with irradiation time. The plots depicted in figure 5.20 represent the mean mesh size for 30% PVP hydrogels crosslinked with different H_2O_2 amounts. These systems exhibit a more complex behaviour. At the lowest UV dose, higher concentrations of the photoinitiator seem to create larger meshes with dimension comparable to the system with 10% PVP irradiated for 22 min. This fact might be explained by a recombination of OH radicals back to H_2O_2 with a termination of the reaction. This might be more prominent for higher concentrations of crosslinker. For a longer irradiation there is a drastic thickening of the networks. For 30+3H at 33 min the estimated ξ_a value is reduced to one third, for 30+2H to one half of the value for 22 min. After 33 min of crosslinking, the structure of the gels seems to be very similar independent of the H_2O_2 concentration. For 44 min, there is a reduction in ξ_a for higher concentrations of photoinitiator, primarily due to a substantial increase of G' moduli (see table 5.3).
In conclusion, there is no clear advantage in having higher concentration of the photoinitiator, at least for the system at 30% and the irradiation times considered. The irradiation dose is more suitable parameters for tuning of the structural properties of the hydrogel. We can show that longer irradiations yield in general denser networks, but the values obtained by the theory of Flory cannot explain yet the hindrance encountered during the protein loading. The loading experiments would be explained by tighter networks.
However, it is not excluded that for longer or more energetic irradiation, the polymer network can be thickened (i.e. with smaller values of ξ_a) and designed for controlling the release of small molecules with dimensions comparable to the mesh size. Other works about photoreticulation of PVP hydrogels [43,44] reported smaller values for ξ_a , but in those cases the irradiation energies were significantly higher (300-4000 J) than those used in this study.

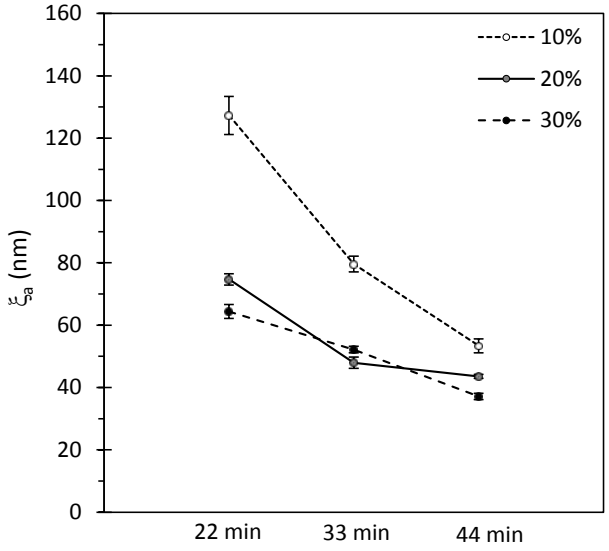

Figure 5.19: Average mesh size, according to the theory of Flory, as a function of UV exposure times for different PVP concentrations. The lines are guides for the eyes.

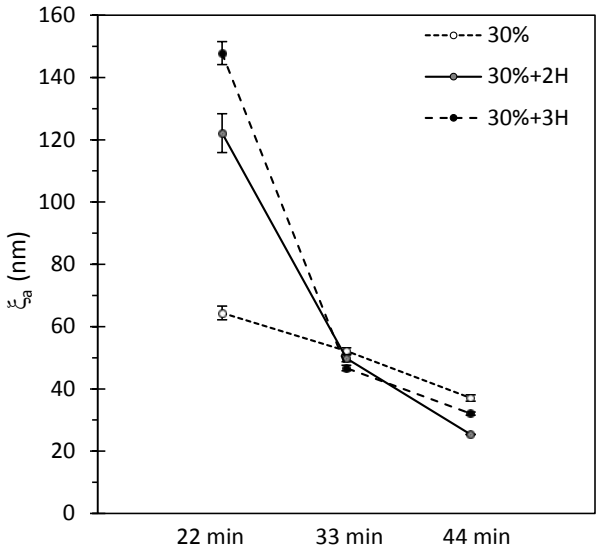

Figure 5.20: Average mesh size, according to the theory of Flory, as a function of UV exposure times for different H_2O_2 concentrations in 30% PVP gels. The lines are guides for the eyes.

5.4.3.2 Estimation according to the theory of Scherer and its approximation

An alternative method based on the theory of Scherer about polymer networks was used for the estimation of the mean mesh size, as described in section 2.6.1.6. The method provides an analytical solution of mean crosslink-to-crosslink distance that will be called ξ_a analytical [57] by assuming that the gel structure is a lattice divided into regular and identical domains. In addition, an approximated expression (called ξ_a approx, see equation 2.28) based on Scherer´s solution, was developed. As discussed in 2.6.1.6, this approximation has the advantage of establishing a direct (linear) relationship between ξ_a and hydraulic radius of polymer fiber R_f. The validity of the proposed approximation is clearly presented in the plots in figure 5.21, where analytical and approximated versions are compared for the range of interest of ν_p in this study. In table 5.4 the results are shown for the considered gel systems. The relative error between the analytical and the approximated values for the mesh size are in average below 6.5% which corresponds to a dimensional error lower than 0.8 nm. All the values of ξ_a provided by this method are significantly lower than those obtained with the theory of Flory. Furthermore, there is no clear trend for ξ_a: Scherer´s model does not provide any evidence of the presence of denser networks in the case of longer UV exposures or more concentrated solutions. All the mesh diameters seem to fall in a range between 8 and 20 nm.

A possible explanation for these results can be found looking at Scherer´s equation (2.28). ξ_a depends mainly on the polymer volume fraction in the swollen state (ν_p), or likewise on the swelling capability of the gel. It was experimentally observed by weight measurements that the quantity of water absorbed by the membranes in 24 h (to which ν_p is directly linked), only differs slightly with polymer and crosslinker concentration. This fact was also observed in figure 5.14, in terms of water/polymer ratios. Scherer´s approach gave reliable estimations of the mesh size for hydrogels formed by Alginate and Pluronics [57]. However, in the case of photocrosslinked PVP, this method cannot explain the structural difference between the considered systems, which instead are observed in the rheological study and coherently described by the theory of Flory.

Finally, to discuss the different results obtained by the rheology and the theory of Scherer, we can give the following interpretation: The photoreticulation leads to the formation of relatively few and sparse junction points in the PVP solutions. An elastically-active network is formed which can be detected by rheology and large values of ξ_a are obtained with the Flory model. Conversely, the theory of Scherer is based on purely geometrical assumptions and considers all the polymer chains involved in the network, both those that are elastically-active and non-active. The non-active portions of the network can be imaged as “loose” polymer chains topologically anchored to the elastic network. A similar situation was recently observed for a polysaccharide-based gel [58], where rheology and release test of a probe molecule gave different estimations of the network mesh size. In that case, it was supposed that the network was composed of a “mesoscopic” network responsible for the elastic response and polymer chains entangled in the network contributing only to the viscous response. Furthermore, the presence of a non homogeneous network in photocrosslinked PVP is consistent with results shown by D´Errico *et al.* [46]. In that work, the existence of polymer rich-portions surrounded by water rich-regions in the network was detected by means of Small angle neutron scattering (SANS). The average distance between polymer rich domains was reported to be 52 nm, a value very close to the mesh sizes estimated for most of the gel systems.

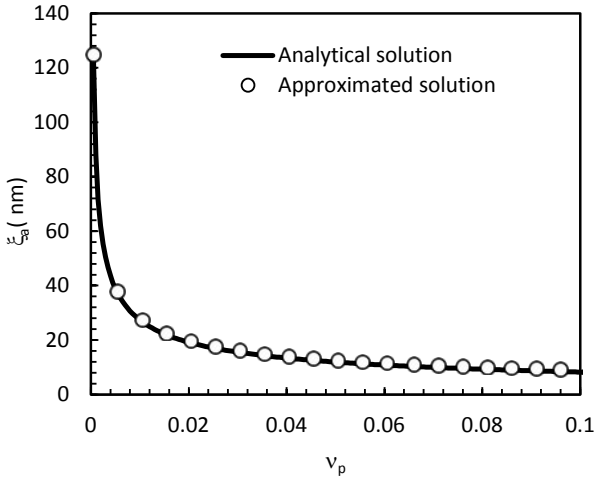

Figure 5.21: Comparison between the approximated average mesh size ξ_a (circles) and the Scherer´s analytical solution (solid line) as a function of the polymer volume fraction ν_p.

Table 5.4: Estimation of average mesh sizes in the considered hydrogels, according to Scherer´s method (ξ_a analytical) and the proposed approximation(ξ_a approx).

Sample	UV time (min)	Δw	ν_p	ξ_a analytical	ξ_a approx	% Relative error
10%	22	0.02	0.067	10.18	10.93	7.42
	33	20.07	0.020	18.98	19.63	3.45
	44	20.80	0.021	18.62	19.28	3.53
20%	22	0.03	0.038	13.63	14.33	5.13
	33	16.14	0.090	8.676	9.47	9.17
	44	16.89	0.033	14.68	15.37	4.69
30%	22	0.05	0.072	9.81	10.57	7.79
	33	13.83	0.079	9.32	10.10	8.33
	44	14.61	0.054	11.34	12.08	6.46
30%+ 2H	22	0.06	0.041	13.16	13.86	5.36
	33	12.27	0.056	11.14	11.87	6.61
	44	13.08	0.052	11.60	12.33	6.28
30%+ 3H	22	0.07	0.119	7.45	8.29	11.30
	33	11.08	0.041	13.27	13.98	5.31
	44	11.91	0.049	12.02	12.75	6.00

5.4.4 NMR spectroscopy of gels

As discussed in section 2.6.2, the purpose of the NMR analysis is to describe more properly the nanoscopic structure of polymer networks. In particular NMR is used to determine the distribution for the mesh sizes, whose values were in the previous sections calculated as an average, assuming that the gel lattices are composed of identical cells with spherical (Flory) or cubic (Scherer) geometry. The crosslink distribution is computed by measuring the relaxation times T_2 of the magnetic spins of protons in the water trapped in the hydrogel. The response of ^1H spins upon a magnetic excitation is strictly connected to their degree of interaction with the polymer chains, i.e. from the size of the nanoscopic domains where water molecules are confined. The T_2 measurement consists of a sequence of magnetic excitations and measurement intervals: First a 90° magnetic pulse, a time measurement interval τ, a series of 180° pulses applied at 2τ intervals are forwarded by the last 180° pulse after a τ interval. The sequence is repeated 8 times every 5 seconds. In table 5.5, the measured values of T_2 for the considered gel systems are listed. All the measured values are below the relaxation time of bulk water ($T_{2,\,H2O}$ = 3007 ms), but there is no significant change in T_2 with respect to the reticulation levels observed in the rheological tests. This fact confirms that polymer meshes are considerably larger than water molecules and that most of the water is not perturbated by the presence of the polymer macromolecules.

Table 5.5: Relaxation time values T_2 measured for the considered PVP hydrogel systems at 25°C, with an interval of τ=0.25 ms between excitations.

	Relaxation times T_2 (ms) for each irradiation energy		
Sample	22 min	33 min	44 min
10%	2104	2380	2291
20%	2447	2328	2393
30%	2631	2412	2489
30% + 2H	2329	2480	2692
30% + 3H	2209	2201	2228

The method used for the data analysis, discussed more in details in section 2.6.2.5, consists briefly in the fitting of the magnetization decay of hydrogen nuclei recorded in the NMR experiment with a multi-exponential function. An example of fitting for the gel with 20% PVP irradiated for 22 min is shown in figure 5.22. In all the systems under study, the decay of magnetization intensity $I_s(t)$ could be fitted satisfactorily by a single exponential function I(t). After this result, it was suspected that not only the relaxation of water but also the relaxation of ^1H of the polymer backbone were measured. This could cause distortions of the signal. To clarify this aspect, a gel was prepared irradiating a solution of PVP 30% in heavy water (D_2O, Deuterium oxide, 99.9% atoms purity, Sigma Aldrich) for 44 min.

The crosslinked sample was then left for swelling in a large volume of D_2O overnight. The viscoelastic properties where measured by rotational rheometry and were very close to the corresponding gels in normal water previously tested. In these samples, only the presence of polymer of protons could have been, in principle, detected, as D_2O is not affected by the magnetic field. Since the NMR measurements on D_2O-gels did not show any signal, we could conclude that polymer protons relaxation was too fast to be detected by our equipment. This proved that the NMR relaxation spectra of the hydrogel in water were not affected by PVP protons relaxation.

This fact proved that the relaxation spectra of the hydrogel in water were not affected by any distortion due to polymer hydrogens. From the fitting of $I_s(t)$, the distribution $a(T_2)$ (also shown in figure 5.22) is calculated. All the gel studied a relaxation spectrum $a(T_2)$ similar to the one in figure 5.22.
The parameters obtained from the fitting of the T_2 relaxation decays were used in a second fitting step leading to a continuous distribution of T_2.
Finally, from the average value of T_2 (T_{2a}) and the mesh dimension ξ_a (Flory or Scherer values), the parameter k is calculated with the following relation:

$$\frac{1}{T_{2,a}} = \frac{1}{T_{2,H_2O}} + \frac{2\mathcal{M}}{R_h} \tag{5.6}$$

By knowing $\mathcal{M}$, a direct relationship between T_2 and ξ is established, and the T_2 distribution can be translated in a distribution of ξ.
In figure 5.23, an example of mesh size distributions in the gel network is shown. In the plot mesh distributions computed from T_2 curves fitted by one exponential function (grey profile) and by a continuous weighted T_2 function (black profile) are compared in the plot. The two distributions are overlapping, which confirms that one single exponential function is sufficient to describe the hydrogel nanostructure. For all the gels studied, ξ distributions were characterized by one single peak, broadening towards larger values of mesh size. The peak is centered in the value of ξ_a provided either by the rheological studies or by the theory of Scherer. In figure 5.23 we chose to show a distribution based on a value provided by Scherer´s model, from which in general estimations were smaller than the ones provided by the theory of Flory. This was to demonstrate that, for any gel considered, mesh distributions do not cover sizes which can interfere with the spatial arrangement of water molecules and proton spin orientation, and this fact is also confirmed by the values of T_2 comparable to the bulk water (see table 5.5).
Comparing the relaxation spectrum obtained for all the PVP gels (representatively characterized by figure 5.22) with a typical relaxation spectrum $a(T_2)$ of a hydrogel (depicted in figure 2.21 in section 2.6.2.5), there is a remarkable difference. In general hydrogels are characterized by several peaks, meaning that water molecules are confined in meshes of quite different sizes. Instead, all the considered PVP hydrogels are characterized by one single peak, meaning that the network is quite regular.

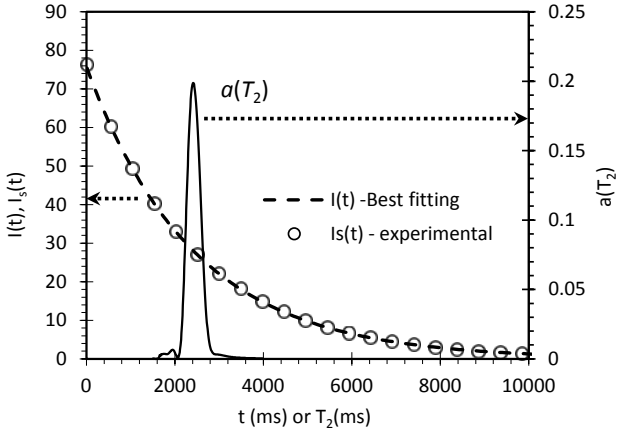

Figure 5.22: Fitting curve I(t) of the magnetization decay curve $I_s(t)$ of water inside the gel meshes (sample 20%, 22 min). The distribution $a(T_2)$ results from the fitting operation.

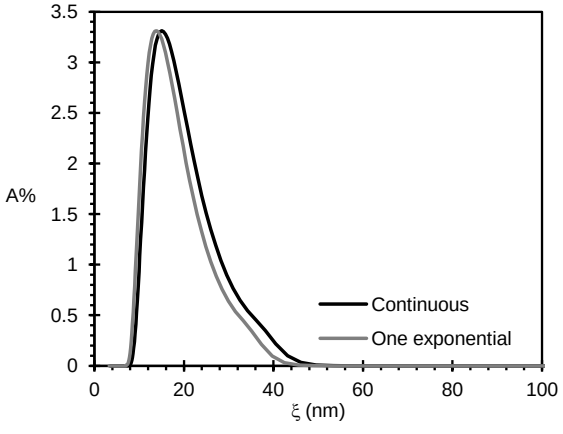

Figure 5.23: Mesh size distribution for the system 20% 22 min irradiation assuming an average value ξ_a of 14.33 nm (sample 20%, 22 min, Scherer´s estimation).

5.5 Integration in microcontainers

The patterning of hydrogels can also be integrated with embossed microcontainers, in a scheme previously mentioned in figure 5.1 (section 5.1.2). As a proof of concept, a preliminary experiment was carried out on PLLA containers: 0.5 mL of aqueous solution of PVP K90 30% wt were spin coated on the microwells. In figure 5.24a an optical micrograph of the result is shown. The limited depth of the microcontainers (65 µm) allowed a uniform coating with a limited number of air bubbles. Thereafter, a mask chip with a single circular opening was manually aligned on top of a selected container by means of a microscope and the sample was subsequently exposed to UV light. Only one container cavity was exposed to UV radiation, to test the feasibility of crosslinking and to have an immediate comparison with unexposed areas. Finally the whole chip was dipped in water solution, under stirring for 5 min. In figure 5.24b the halo of an exposed and crosslinked microgel can be recognized on the container (upper center). This experiments shows that the photocrosslinking technique can easily be transferred to the prototype of microcontainers fabricated with biodegradable polymers.

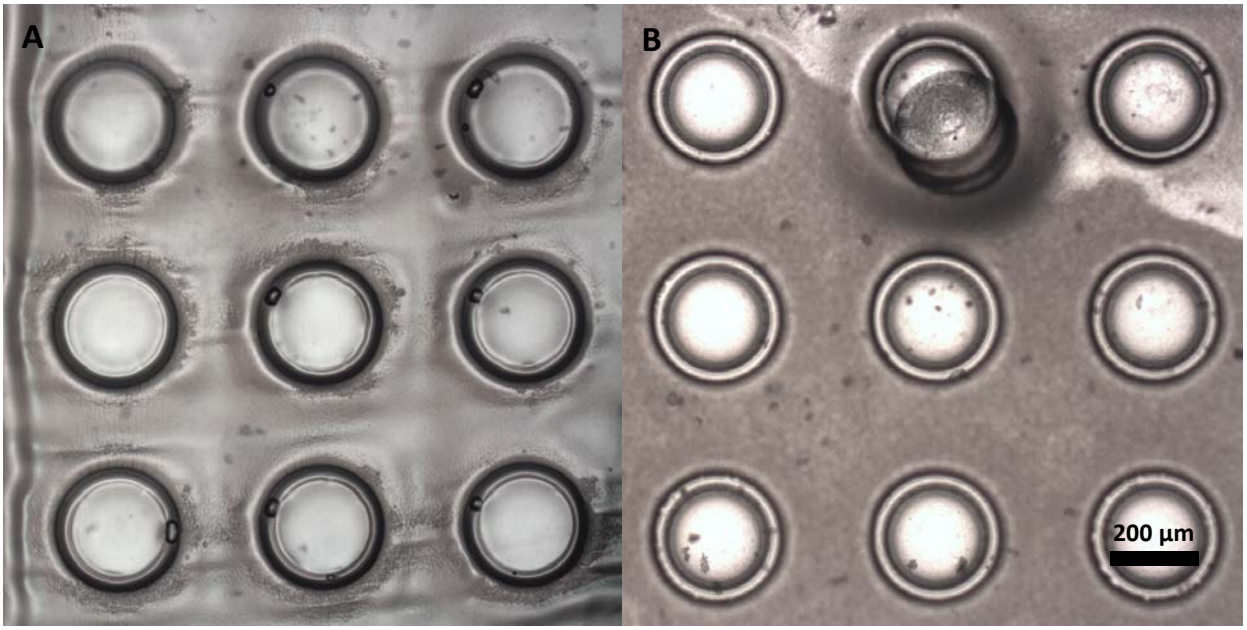

Figure 5.24: (a) PLLA microcontainers filled with aqueous solution of PVP K90 30% wt by spin coating (air bubbles are small spots in the upper left edge of containers). (b) Containers after selective crosslinking. The halo on the upper centred container is the microgel almost centered in the container cavity.

5.6 Conclusions

The use of selective photocrosslinking proved a successful technique to fabricate large arrays of polymer microgels. This method represents a valuable replacement of inkjet printing for the loading of microcontainers. The developed process is very simple and cost effective, compared to a drop-on-demand deposition. Although photocrosslinking entails an unavoidable loss of material, it offers a faster polymer deposition and an improved reproducibility. The characterization studies on PVP hydrogels revealed that both the dimensional and the structural properties of microgels can be modulated changing the UV exposure according to the specific needs of the drug delivery device. The combination of rheological and NMR analysis showed the existence of a three dimensional network. The diffusive properties will be particularly interesting for controlled delivery of macromolecules of pharmaceutical interest. The study of the mesh size requires still a deeper understanding, maybe supported by the estimation of the diffusion coefficient upon the release of a model macromolecule. The amphiphilic properties of PVP, make microgels a versatile carrier to encapsulate both small hydrophobic APIs, and bioactive macromolecules. Photocrosslinked microgels can be successfully loaded by supercritical impregnation. The combination of these two methods is at the moment the loading technique for microfabricated drug delivery devices which represents the smallest waste of active ingredient while preserving the therapeutic activity of the drug. Finally, all the different techniques explored can be potentially integrated with the biopolymer microcontainers concept.

References

[1] M.J. Mahoney, K.S. Anseth, Three-dimensional growth and function of neural tissue in degradable polyethylene glycol hydrogels, Biomaterials, 27 (2006) 2265-2274.
[2] K.T. Nguyen, J.L. West, Photopolymerizable hydrogels for tissue engineering applications, Biomaterials, 23 (2002) 4307-4314.
[3] A.S. Hoffman, Hydrogels for biomedical applications, Advanced Drug Delivery Reviews, (2012).
[4] N. Peppas, P. Bures, W. Leobandung, H. Ichikawa, Hydrogels in pharmaceutical formulations, European Journal of Pharmaceutics and Biopharmaceutics, 50 (2000) 27-46.
[5] M. Ishihara, K. Nakanishi, K. Ono, M. Sato, M. Kikuchi, Y. Saito, H. Yura, T. Matsui, H. Hattori, M. Uenoyama, Photocrosslinkable chitosan as a dressing for wound occlusion and accelerator in healing process, Biomaterials, 23 (2002) 833-840.
[6] K.R. Kirker, Y. Luo, J.H. Nielson, J. Shelby, G.D. Prestwich, Glycosaminoglycan hydrogel films as bio-interactive dressings for wound healing, Biomaterials, 23 (2002) 3661-3671.
[7] P. Gupta, K. Vermani, S. Garg, Hydrogels: from controlled release to pH-responsive drug delivery, Drug Discovery Today, 7 (2002) 569-579.
[8] T.R. Hoare, D.S. Kohane, Hydrogels in drug delivery: Progress and challenges, Polymer, 49 (2008) 1993-2007.
[9] Y. Qiu, K. Park, Environment-sensitive hydrogels for drug delivery, Advanced Drug Delivery Reviews, (2012).
[10] B. Jeong, Y.H. Bae, S.W. Kim, Drug release from biodegradable injectable thermosensitive hydrogel of PEG–PLGA–PEG triblock copolymers, Journal of Controlled Release, 63 (2000) 155-163.
[11] L. Yu, J. Ding, Injectable hydrogels as unique biomedical materials, Chemical Society Reviews, 37 (2008) 1473-1481.
[12] K.M. Galler, J.D. Hartgerink, A.C. Cavender, G. Schmalz, R.N. D'Souza, A customized self-assembling peptide hydrogel for dental pulp tissue engineering, Tissue Engineering Part A, 18 (2011) 176-184.
[13] B. Mizrahi, A.J. Domb, Mucoadhesive Polymers for Delivery of Drugs to the Oral Cavity, Recent Patents on Drug Delivery & Formulation, 2 (2008) 108-119.
[14] J. Elisseeff, K. Anseth, D. Sims, W. McIntosh, M. Randolph, R. Langer, Transdermal photopolymerization for minimally invasive implantation, Proceedings of the National Academy of Sciences, 96 (1999) 3104-3107.
[15] D.B. Pike, S. Cai, K.R. Pomraning, M.A. Firpo, R.J. Fisher, X.Z. Shu, G.D. Prestwich, R.A. Peattie, Heparin-regulated release of growth factors in vitro and angiogenic response in vivo to implanted hyaluronan hydrogels containing VEGF and bFGF, Biomaterials, 27 (2006) 5242-5251.
[16] L. Xinming, C. Yingde, A.W. Lloyd, S.V. Mikhalovsky, S.R. Sandeman, C.A. Howel, L. Liewen, Polymeric hydrogels for novel contact lens-based ophthalmic drug delivery systems: A review, Contact Lens and Anterior Eye, 31 (2008) 57-64.
[17] F. Stapleton, S. Stretton, E. Papas, C. Skotnitsky, D.F. Sweeney, Silicone hydrogel contact lenses and the ocular surface, The ocular surface, 4 (2006) 24-43.
[18] O. Wichterle, D. Lim, Hydrophilic gels for biological use, (1960).
[19] W. Hennink, C. Van Nostrum, Novel crosslinking methods to design hydrogels, Advanced Drug Delivery Reviews, (2012).
[20] G. Turco, I. Donati, M. Grassi, G. Marchioli, R. Lapasin, S. Paoletti, Mechanical spectroscopy and relaxometry on alginate hydrogels: a comparative analysis for structural characterization and network mesh size determination, Biomacromolecules, 12 (2011) 1272-1282.
[21] F. Yokoyama, I. Masada, K. Shimamura, T. Ikawa, K. Monobe, Morphology and structure of highly elastic poly(vinyl alcohol) hydrogel prepared by repeated freezing-and-melting, Colloid & Polymer Sci, 264 (1986) 595-601.
[22] D. Eagland, N.J. Crowther, C.J. Butler, Complexation between polyoxyethylene and polymethacrylic acid—the importance of the molar mass of polyoxyethylene, European Polymer Journal, 30 (1994) 767-773.

[23] A. Tang, C. Wang, R.J. Stewart, J. Kopeček, The coiled coils in the design of protein-based constructs: hybrid hydrogels and epitope displays, Journal of Controlled Release, 72 (2001) 57-70.
[24] T. Miyata, N. Asami, T. Uragami, Preparation of an Antigen-Sensitive Hydrogel Using Antigen−Antibody Bindings, Macromolecules, 32 (1999) 2082-2084.
[25] W.S. Dai, T.A. Barbari, Hydrogel membranes with mesh size asymmetry based on the gradient crosslinking of poly(vinyl alcohol), Journal of Membrane Science, 156 (1999) 67-79.
[26] N.A. Peppas, R.E. Benner Jr, Proposed method of intracordal injection and gelation of poly (vinyl alcohol) solution in vocal cords: Polymer considerations, Biomaterials, 1 (1980) 158-162.
[27] A.J. Kuijpers, P.B. Van Wachem, M.J.A. Van Luyn, G.H.M. Engbers, J. Krijgsveld, S.A.J. Zaat, J. Dankert, J. Feijen, In vivo and in vitro release of lysozyme from cross-linked gelatin hydrogels: A model system for the delivery of antibacterial proteins from prosthetic heart valves, Journal of Controlled Release, 67 (2000) 323-336.
[28] J.J. Sperinde, L.G. Griffith, Synthesis and characterization of enzymatically-cross-linked poly(ethylene glycol) hydrogels, Macromolecules, 30 (1997) 5255-5264.
[29] N.A. Peppas, A.G. Mikos, Preparation methods and structure of hydrogels, Hydrogels in medicine and pharmacy, 1 (1986) 1-27.
[30] P. Kofinas, V. Athanassiou, E.W. Merrill, Hydrogels prepared by electron irradiation of poly(ethylene oxide) in water solution: Unexpected dependence of cross-link density and protein diffusion coefficients on initial PEO molecular weight, Biomaterials, 17 (1996) 1547-1550.
[31] E. Jabbari, S. Nozari, Swelling behavior of acrylic acid hydrogels prepared by γ-radiation crosslinking of polyacrylic acid in aqueous solution, European Polymer Journal, 36 (2000) 2685-2692.
[32] Z. Ajji, I. Othman, J. Rosiak, Production of hydrogel wound dressings using gamma radiation, Nuclear Instruments and Methods in Physics Research Section B: Beam Interactions with Materials and Atoms, 229 (2005) 375-380.
[33] F. Yoshii, D. Darwis, H. Mitomo, K. Makuuchi, Crosslinking of poly (< i> ε</i>-caprolactone) by radiation technique and its biodegradability, Radiation Physics and Chemistry, 57 (2000) 417-420.
[34] K. Gorna, S. Gogolewski, The effect of gamma radiation on molecular stability and mechanical properties of biodegradable polyurethanes for medical applications, Polymer Degradation and Stability, 79 (2003) 465-474.
[35] M.A. Casadei, F. Cerreto, S. Cesa, M. Giannuzzo, M. Feeney, C. Marianecci, P. Paolicelli, Solid lipid nanoparticles incorporated in dextran hydrogels: A new drug delivery system for oral formulations, International Journal of Pharmaceutics, 325 (2006) 140-146.
[36] G. Pitarresi, M.A. Casadei, D. Mandracchia, P. Paolicelli, F.S. Palumbo, G. Giammona, Photocrosslinking of dextran and polyaspartamide derivatives: A combination suitable for colon-specific drug delivery, Journal of Controlled Release, 119 (2007) 328-338.
[37] G. Tripodo, G. Pitarresi, F.S. Palumbo, E.F. Craparo, G. Giammona, UV-Photocrosslinking of Inulin Derivatives to Produce Hydrogels for Drug Delivery Application, Macromolecular Bioscience, 5 (2005) 1074-1084.
[38] C. Decker, Kinetic study and new applications of UV radiation curing, Macromolecular Rapid Communications, 23 (2002) 1067-1093.
[39] P. Ferreira, J. Coelho, J. Almeida, M. Gil, Photocrosslinkable Polymers for Biomedical Applications, (2011).
[40] C.G. Williams, A.N. Malik, T.K. Kim, P.N. Manson, J.H. Elisseeff, Variable cytocompatibility of six cell lines with photoinitiators used for polymerizing hydrogels and cell encapsulation, Biomaterials, 26 (2005) 1211-1218.
[41] J. Rosiak, J. Olejniczak, W. Pęka, Fast reaction of irradiated polymers—I. Crosslinking and degradation of polyvinylpyrrolidone, International Journal of Radiation Applications and Instrumentation. Part C. Radiation Physics and Chemistry, 36 (1990) 747-755.

[42] J. Rosiak, A. Rucinska-Rybus, W. Pekala, Method of manufacturing hydrogel dressings, in, Google Patents, 1989.
[43] L.C. Lopérgolo, A.B. Lugão, L.H. Catalani, Direct UV photocrosslinking of poly(N-vinyl-2-pyrrolidone) (PVP) to produce hydrogels, Polymer, 44 (2003) 6217-6222.
[44] G.J.M. Fechine, J.A.G. Barros, L.H. Catalani, Poly (< i> N</i>-vinyl-2-pyrrolidone) hydrogel production by ultraviolet radiation: new methodologies to accelerate crosslinking, Polymer, 45 (2004) 4705-4709.
[45] X. Zhu, P. Lu, W. Chen, J. Dong, Studies of UV crosslinked poly (< i> N</i>-vinylpyrrolidone) hydrogels by FTIR, Raman and solid-state NMR spectroscopies, Polymer, 51 (2010) 3054-3063.
[46] G. D'Errico, M. De Lellis, G. Mangiapia, A. Tedeschi, O. Ortona, S. Fusco, A. Borzacchiello, L. Ambrosio, Structural and mechanical properties of UV-photo-cross-linked poly (N-vinyl-2-pyrrolidone) hydrogels, Biomacromolecules, 9 (2007) 231-240.
[47] S. Burkert, T. Schmidt, U. Gohs, I. Mönch, K.F. Arndt, Patterning of thin poly (N-vinyl pyrrolidone) films on silicon substrates by electron beam lithography, Journal of Applied Polymer Science, 106 (2007) 534-539.
[48] J. Goldfarb, S. Rodriguez, Aqueous solutions of polyvinylpyrrolidone, Die Makromolekulare Chemie, 116 (1968) 96-106.
[49] A. Zanocco, Kinetics and Mechanism of the Photosensitized Oxidation of Furosemide*, Photochemistry and photobiology, 68 (1998) 487-493.
[50] G. Friso, R. Barbato, G. Giacometti, J. Barber, Degradation of D2 protein due to UV-B irradiation of the reaction centre of photosystem II, FEBS letters, 339 (1994) 217-221.
[51] V.J. Pereira, H.S. Weinberg, K.G. Linden, P.C. Singer, UV degradation kinetics and modeling of pharmaceutical compounds in laboratory grade and surface water via direct and indirect photolysis at 254 nm, Environmental science & technology, 41 (2007) 1682-1688.
[52] S.J. Macnaughton, I. Kikic, N.R. Foster, P. Alessi, A. Cortesi, I. Colombo, Solubility of anti-inflammatory drugs in supercritical carbon dioxide, Journal of Chemical & Engineering Data, 41 (1996) 1083-1086.
[53] N. Green, M. Joynson, A preliminary crystallographic investigation of avidin, Biochemical Journal, 118 (1970) 71.
[54] L.C. Lopérgolo, A.B. Lugão, L.H. Catalani, Direct UV photocrosslinking of poly (< i> N</i>-vinyl-2-pyrrolidone)(PVP) to produce hydrogels, Polymer, 44 (2003) 6217-6222.
[55] M. Grassi, G. Grassi, R. Lapasin, I. Colombo, Understanding drug release and absorption mechanisms: a physical and mathematical approach, CRC, 2006.
[56] R. Lapasin, S. Pricl, Rheology of industrial polysaccharides: theory and applications, Blackie Academic & Professional London, 1995.
[57] M. Abrami, I. D'Agostino, G. Milcovich, S. Fiorentino, R. Farra, F. Asaro, R. Lapasin, G. Grassi, M. Grassi, Physical characterization of alginate–Pluronic F127 gel for endoluminal NABDs delivery, Soft Matter, 10 (2014) 729-737.
[58] T. Coviello, P. Matricardi, F. Alhaique, R. Farra, G. Tesei, S. Fiorentino, F. Asaro, G. Milcovich, M. Grassi, Guar gum/borax hydrogel: Rheological, low field NMR and release characterizations, Express Polymer Letters, 7 (2013).

6. Conclusions and perspectives

The goal of this project has been to develop techniques for the loading of poorly soluble drugs and fragile biological macromolecules into microcontainers for oral drug delivery. The research study was focused on simple and cost effective methods, using technologies compatible with the operation limits imposed by the materials in use. Techniques were developed both for the largest group of APIs with poor oral bioavailability and for oral formulations already existing. Moreover, attention was paid to the perspective of industrial applications. Therefore, the research was directed towards the use of automated equipments and to solutions allowing control of the design and performance of the device.
At the beginning of the project, the state of the art in the loading of reservoir based-microdevices entailed a large waste of API and worked only for flat microcontainers with low capacity volumes.

6.1 Conclusions

The use of direct DOD inkjet printing of furosemide solutions with the available equipment demonstrated in general substantial limitations. The spotting of solutions based on organic solvent showed low reproducibility and drug precipitation caused frequent nozzle clogging. The spotting of SNEDDS formulations for insulin was instead performed with success by means of heating the dispensing system to 50°C with an efficiency of 80%.
Inkjet printing was successfully employed for the deposition of controlled volumes of aqueous solutions of PVP. Polymer concentrations up to 20% wt were successfully dispensed into microcontainers with a quasi-no-waste performance and with high reproducibility in terms of alignment and dispensed volume. The method allowed a high control of the level of filling by means of repeated spotting sessions.

The achievement in the spotting of polymer solutions allowed to develop a loading technique divided into two steps: The DOD deposition of PVP aqueous solutions, followed by a step of drug loading, which was performed by supercritical impregnation.

Supercritical impregnation of ketoprofen was shown to be an effective method, allowing the simultaneous loading of large arrays of microcontainers in a single batch. The impregnation of confined nanoliter volumes of polymer defined by microfabrication represents an important achievement for the loading of microdevices, which no one has shown before. The control of drug loading was demonstrated by tuning fluid pressure, temperature and time of impregnation. At 200 bar, 40°C and 4 hours a drug concentration of 32 % wt was obtained. The effect of temperature on impregnation was also elucidated. The increase from 40°C to 60°C resulted in a substantial increase of drug content. For longer impregnation times, at 200 bar the increase in temperature corresponded to an increase from 0.6 to 1 mg of drug per chip. Raman spectroscopy analyses of impregnated containers demonstrated the presence of amorphous drug and ATR-IR spectroscopy showed strong chemical interactions between the PVP and the drug. *In vitro* drug release tests showed an enhanced dissolution rate for impregnated containers compared to solid dispersion laden microdevices. Here, 87% of the total drug was released within 30 minutes.

The combination of inkjet printing and $scCO_2$ impregnation demonstrated good reproducibility and accuracy of the final drug dose. Furthermore, the loading was performed without the use of organic solvents and with a minimum waste of chemicals, which makes the process potentially suitable for up scaling.

The use of selective photocrosslinking was investigated to fabricate large arrays of PVP microgels. UV crosslinking allowed to define micropatterns of the polymer with diameter in the range of 100-300 µm, and height within 10-30 µm. The volume of microgel ranges from 0.06-1.15 nL and can be controlled with high accuracy and reproducibility by modifying the exposure dose during UV radiation. This method was proved to be a successful technique which can be used as alternative of inkjet printing for the definition of PVP volumes inside the microcontainers. The swelling properties of microgels were studied by means of confocal fluorescence microscopy. Microgels can swell significantly in both aqueous and organic solvent based solutions. After few minutes of swelling in water, microgel height increased from 28 to 128 µm.

The hydrogel obtained by photocrosslinking was loaded with ketoprofen by supercritical impregnation. *In vitro* dissolution studies showed that crosslinked and uncrosslinked films release the drug very similarly. Furthermore, the loading of microgels with protein was accomplished. The loading of gels was carried out by swelling with defined volumes of protein solution. Confocal microscopy showed that the loading of macromolecules required longer times compared to small molecules.

The nanoscopic structure of photocrosslinked hydrogels was investigated by means of rheological techniques and NMR spectroscopy. Theoretical models based on Flory´s and Scherer´s theories were developed to analyze experimental data and to calculate the average mesh size of the hydrogel network as well as the mesh size distribution. The study confirmed the existence of regular three dimensional networks. The application of the theory of Flory showed the presence of relatively large mesh dimensions between 25-150 nm. The application of this model for the analysis of rheological measurements showed that the degree of reticulation depends both on the initial polymer concentration and on the irradiation energy. Compared to that, the influence of the crosslinker concentration on the mesh dimensions is smaller for the investigated range. Instead, the mesh size estimations derived from the theory of Scherer resulted in much smaller mesh dimensions of 8-19 nm. However, this theory could not explain the influence of concentration and UV exposure observed in the experiments. The NMR data analysis confirmed the presence of large meshes, showing that the polymer chains do not interfere with the magnetic relaxation of water hydrogens. In the swollen gels water molecules behave like in bulk liquid phase.
From gel structure characterization studies it emerges that PVP hydrogels are suitable systems for the controlled release of bioactive macromolecules of pharmaceutical interest.

In conclusion, the loading techniques developed in this thesis represent a novelty in the field of microfabricated drug delivery devices. Compared to the other techniques used in this field, the combination of inkjet printing and supercritical impregnation allows to minimize the waste of possibly expensive active ingredients, preserving the drug therapeutic activity. Also, the use of UV light to micropattern polymer films offers a valuable alternative to inkjet deposition of polymer solutions. The methods utilized in this research work can potentially be integrated in the fabrication process of biopolymer microcontainers developed in NAMEC.

6.2 Outlook

The loading techniques discussed in this thesis present substantial progress towards the goals described in section 1.6. However, further improvements are possible by combining the different techniques and by optimizing the methods to improve understanding and yields. Developments can be directed towards new applications (new drugs and polymers) and to an integration with the overall NAMEC vision, i.e. the loading of biopolymer containers, the application of lids, and all the activities mentioned in section 1.4.

With respect to the optimization of fabrication processes, improvements are possible in each technique.
Inkjet printing of concentrated PVP solutions can be accomplished and microcontainers can be filled by polymer by multiple spotting sessions. However, the process could be speeded up by increasing the polymer concentration and thereby reducing the spotting time. At present, the high viscosity of concentrated solutions is a substantial limit. A way to overcome this limitation is to use heatable pipettes or special nozzles designed for highly viscous liquids. Both these kinds of nozzles are currently available for the equipment used in the project. The selective exposure to UV light requires a setup for mask alignment. Several UV-aligners are available in DTU Nanotech, but none of them were suitable to the purpose because of the low light power and the clamping system.
From the structural characterization of PVP hydrogels it emerged that mesh size estimations strongly depend on the model chosen for the data treatment. An experimental validation of this aspect is therefore necessary. Several techniques can be used for this purpose. Small Angle Neutron Scattering (SANS) [1] and Transmission Electron Microscopy (TEM) [2] can be useful techniques to obtain a direct measurement of mesh size. The mesh size of polymer networks was also estimated by Pescosolido and coworkers by means of cryoporometry [3]. From the loading aspect of the study, it would be interesting to elucidate the biological activity of macromolecules after the loading in the gel.

The methods developed can find further applications with other challenging drugs and polymers. The supercritical impregnation process developed for ketoprofen potentially works for all CO_2 soluble drugs. Unfortunately, the majority of class II and IV drugs do not dissolve in supercritical CO_2. As mentioned in section 2.3.2, a possible solution would be to add surfactants or co-solvent to the supercritical phase, and increase the solubility of the drug in the fluid phase.
Microgels fabricated on mask chips by backside exposure to UV (see section 5.2.1) could be coated with a biodegradable container shell by spray coating through a shadow mask.

Regarding the possibility of integration in NAMEC, further developments are possible in several directions. With the perspective of transferring the developed loading methods to biodegradable microcontainers, the effect of supercritical impregnation on PCL and PLLA should be tested. Similar to PVP, these polymers also absorb CO_2 in supercritical conditions. Therefore, their T_g might also decrease with the uptake of CO_2 and potentially induce deformation of the microstructure shaped in the hot embossing process. In that case, the use of biopolymers with higher molecular weight could avoid deformation. Alternatively, impregnations could be performed at lower pressure and temperature and eventually conducted for longer times.
Some possible improvements concern fabrication aspects: UV micropatterning can be used to define microgels inside PLLA microcontainers. A preliminary result was already shown in section 5.5 (figure 5.24). The spin coating of PVP layers on PLLA microcontainers was already successfully accomplished. Further developments are linked to the design of a custom made alignment system for UV exposure.
Subsequently, the hydrogel laden-microcontainers could be impregnated with $scCO_2$.

From a more general viewpoint, the microdevices must be able to compete with established drug delivery systems like tablets and pills. To advance the concept of microdevices for oral drug delivery, the *in vitro* tests must be followed by *in vivo* tests in animals where the efficacy of the different features (drug protection, mucoadhesion, unidirectional release) must be verified. Finally, the research on microdevices should be focused on the treatment of a specific disease, and all the steps (device fabrication, drug loading, coating applications, etc) should be optimized for the development of a prototype designed for that purpose.

Bibliography

[1] G. D'Errico, M. De Lellis, G. Mangiapia, A. Tedeschi, O. Ortona, S. Fusco, A. Borzacchiello, L. Ambrosio, Structural and mechanical properties of UV-photo-cross-linked poly (N-vinyl-2-pyrrolidone) hydrogels, Biomacromolecules, 9 (2007) 231-240.
[2] M. Abrami, I. D'Agostino, G. Milcovich, S. Fiorentino, R. Farra, F. Asaro, R. Lapasin, G. Grassi, M. Grassi, Physical characterization of alginate–Pluronic F127 gel for endoluminal NABDs delivery, Soft Matter, 10 (2014) 729-737.
[3] L. Pescosolido, L. Feruglio, R. Farra, S. Fiorentino, I. Colombo, T. Coviello, P. Matricardi, W.E. Hennink, T. Vermonden, M. Grassi, Mesh size distribution determination of interpenetrating polymer network hydrogels, Soft Matter, 8 (2012) 7708-7715.

Appendix 1

Microelectronic Engineering 111 (2013) 391–395

Contents lists available at SciVerse ScienceDirect

Microelectronic Engineering

journal homepage: www.elsevier.com/locate/mee

Inkjet printing as a technique for filling of micro-wells with biocompatible polymers

Paolo Marizza *, Stephan Sylvest Keller, Anja Boisen

Department of Micro- and Nanotechnology, Technical University of Denmark, DTU Nanotech, Building 345E, DK 2800 Kongens Lyngby, Denmark

ARTICLE INFO

Article history:
Received 8 October 2012
Received in revised form 20 March 2013
Accepted 26 March 2013
Available online 9 April 2013

Keywords:
Inkjet printing
Micro-wells
PVP
Drug delivery

ABSTRACT

We present an innovative technique to dispense precise amounts of polymer solutions into large arrays of microscopic wells. An inkjet printer (NP 2.1 GeSim, Germany) is used to fill micro-wells with poly (vinyl pyrrolidone) (PVP K10). The micro-wells are fabricated with cavity diameters of 300 μm down to 50 μm with SU-8 with two steps of negative photolithography. Inkjet printing is shown to be a suitable technique to dispense defined volumes of solution (down to 0.3 nL) in a highly reproducible way. The filling with polymer can be controlled varying the concentration of the solution and the number of dispensed droplets. Solutions of up to 20 wt.% PVP in water are successfully spotted.

1. Introduction

Inkjet printing is a familiar technology which has been originally conceived to transfer electronic data onto flexible substrates like paper and overhead transparencies. Recently, a variety of new applications of this technology have been investigated. Versatile tools have been developed to dispense minute amounts of a broad range of materials for various industrial manufacturing processes. Inkjet has been employed for high precision dispensing of polymer into MEMS switches [1], metallic solders in micro-electronic soldering [2], and UV curable epoxy resins for micro-optical applications [3], representing a valuable mold-free manufacturing technique to fabricate large arrays of 3D micro-objects [4]. In more recent years inkjet printing has been introduced in the fields of biotechnology and nanomedicine for large-scale screening of genomic material [5], for cell culturing [6,7], for functionalization of Bio MEMS [8] and for drug delivery applications [9,10]. This technique in so-called drop-on-demand mode (DOD) allows dispensing precise volumes of liquid solutions with a quasi-no-waste performance. For this reason it has received increasing attention in the biotechnological and pharmaceutical fields since it enables performing complex analysis on small amounts of material, which are often expensive or in limited supply. A frequent issue in dispensing biological solutions onto flat substrates deals with control of size, shape and relative distance of dots as well as alignment and regularity of realized micro-arrays which occurs when spots are formed with a large number of droplets [11]. As a solution, preliminary micro-patterning of the substrate has been proposed [12]. As alternative approach for spatial confinement of liquid volumes in nano and pico-liter scale we here present microfabricated SU-8 wells.

SU-8 is a commonly used negative photoresist, well suited for low-cost prototyping of high aspect ratio structures by standard photolithography. Furthermore SU-8 has been shown to exhibit biocompatible properties [13] which makes it a suitable support for cells and biomolecules [14].

Previously, filling of microfabricated wells with discontinuous de-wetting has been demonstrated [15]. The use of inkjet printing for filling of micro-wells having cavity diameter from 50 to 300 μm allows to confine liquid volumes of pico up to nanoliter range on precisely arranged positions, preserving the circular shape and the size of dots. To accomplish that we use a commercial system designed to spot on glass slides which prints large arrays of dots with high speed. We dispense micro-arrays of various solutions of PVP. Poly(vinyl pyrrolidone) (PVP) is a biocompatible polymer [16] widely used as excipient for drugs for oral dosage forms [17] as well as promoter of cell growth and differentiation. PVP exhibits high solubility in water and many organic solvents [18], giving low viscous polymer solutions [19].

Additionally, the effect of surface tension on the process of filling the micro-wells is studied by dispensing PVP solutions with different solvents (isopropanol and water). This has shown very different results revealing that the surface tension of the solvent plays a key role in the filling process of three dimensional micro-structures.

2. Materials and methods

2.1. Fabrication of micro-wells

The fabrication of the micro-wells is a process divided into two main steps. (I) Anisotropic etching is used to define trenches in a

* Corresponding author. Tel.: +45 45255759.
E-mail address: paom@nanotech.dtu.dk (P. Marizza).

0167-9317/$ - see front matter © 2013 Elsevier B.V. All rights reserved.
http://dx.doi.org/10.1016/j.mee.2013.03.168

silicon substrate in order to obtain easy-breakable rectangular substrates fitting into the slots of the inkjet printer tray, (II) negative photolithography is used for the definition of the micro-wells. In Fig. 1 the fabrication steps of the overall process are presented. On a silicon wafer an oxide layer (2 μm) is deposited by LPCVD (Fig. 1a). A positive photoresist (AZ 5214e) is spin coated on the front side and patterned by photolithography (Fig. 1b). Afterwards, the same resist is spin coated on the back side. In this way the resist pattern on the front side and the back side layer act as protective mask for the etching of the silicon oxide layer (BHF for 30 min) (Fig. 1c). The resist is then stripped and an anisotropic etching in KOH (4 h, 80 °C) defines the trenches for the aligned cleavage of the wafer after micro-well fabrication (Fig. 1d). The remaining oxide layer is then removed in BHF (4 min) to improve SU-8 adhesion in the next fabrication step. For the well fabrication, a first layer of SU-8 2075 (thickness 35 μm) is spin coated and selectively exposed to define the bottom of the micro-wells (Fig. 1e). A second layer (255 μm) of the same resist is spin coated and patterned (Fig. 1f). Finally, the uncrosslinked resist is developed in propylene glycol methyl ether acetate (PGMEA) (Fig. 1g). Fig. 2a shows a wafer after microfabrication. The silicon chips are cleaved (Fig. 1h) along the trenches (red lines shown in Fig. 2a) defining a rectangle which fits into the slide slots of the inkjet printer tray (Fig. 2b). Each slide contains ten squares (outlined in green in Fig. 2(a) which contains 625 micro-wells each. The micro-wells are aligned into a 25 × 25 matrix. Micro-wells are fabricated with cavity diameters of 50 μm, 100 μm, 200 μm, 300 μm corresponding to volumes going from 0.5 to 18 nL. The width of the well walls is 50 μm and the center-to-center spacing is 450 μm for all wells.

2.2. Inkjet printing of PVP solutions

Solution of poly (vinyl pyrrolidone) PVP K10 (Mw 10^5 Da) is dissolved in deionized water and isopropanol in different concentrations (5, 10 and 20% wt). For the more concentrated solutions, viscosity measurements are performed to ensure that the liquid exhibits a Newtonian behavior and a viscosity value below 5 mPa s. This is the minimum viscosity value for dispensable liquids according to the specifications of the equipment used. All the chemicals are purchased from Sigma–Aldrich.

The inkjet printer used in this work is schematically represented in Fig. 3. It is mainly composed of a XYZ movable inkjet head (Nanoplotter NP 2.1 GeSim, Germany) equipped with a piezo driven dispenser with 70 μm orifice (GeSim nanotip) and a slide tray where the substrate is mounted. The solution is aspired by the pipette from a well in a titer plate where the sample is stored at the desired temperature. The inkjet head is monitored by a control unit connected to a computer. A top microscope camera is integrated into the pipette head and allows the alignment of the pipette. The system is supplied with a stroboscope camera (side view camera) to visualize and tune the jet direction and stability, as well as shape and diameter of the generated droplets. The intensity, duration, and frequency of the voltage applied to the piezoelectric actuator of the dispenser are tuned for optimized micro-well filling. The optimum set of parameters is a pulsing voltage of 90 V, a pulse width of 90 μs and a frequency of 175 Hz for all the solutions. The diameter of the droplets is measured with the stroboscope imaging, and is 47 μm for 20 wt.% PVP and 53 μm for 5 and 10 wt.% PVP.

2.3. Micro-well filling

PVP solutions are dispensed by DOD inkjet printing into wells of different sizes. The number of droplets to dispense in each well is estimated dividing the cavity volume by the droplet volume. An overview of the spotting plan is shown in Table 1. The typical time needed for spotting an array of 625 wells is around 12 min. To increase the polymer content inside the micro-wells, the spotting process is repeated up to three times on the same arrays in subsequent printing sessions, where during each session a solution volume equal to the cavity volume is dispensed into each micro-well. Between the sessions, a waiting time for solvent evaporation is introduced in order to avoid spillover. The evaporation of the drops is observed with the top view camera and the time is measured. The typical drying times for isopropanol and water based-solutions are 1 and 2 min respectively. The polymer concentration dose not

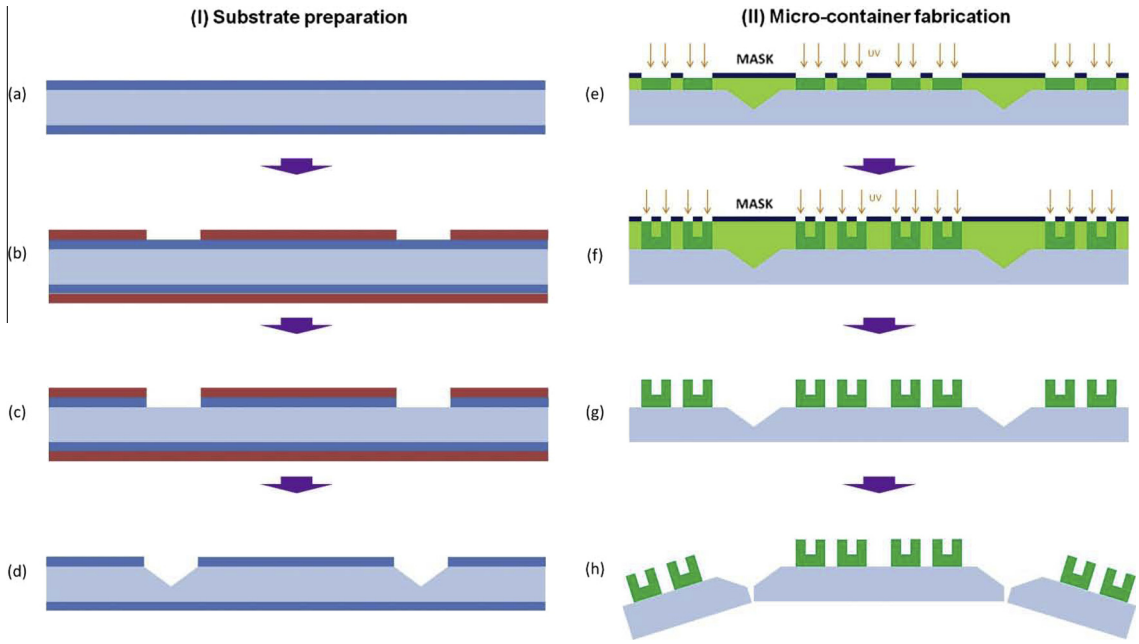

Fig. 1. Process flow for the fabrication of micro-well on Si microscope slides: (a) LPCVD (2 μm) on silicon wafer; (b) photolithography with positive resist on the front side (2.2 μm), spin coating of the resist (2.2 μm) on the back side; (c) wet etching of oxide in BHF; (d) resist stripping and wet etching in KOH of Si; (e) SU-8 spin coating (34 μm) and selective UV exposure; (f) spin coating of second layer of SU-8 (255 μm) and masked exposure; (g) SU-8 development; (h) Chips are cleaved in microscope slides.

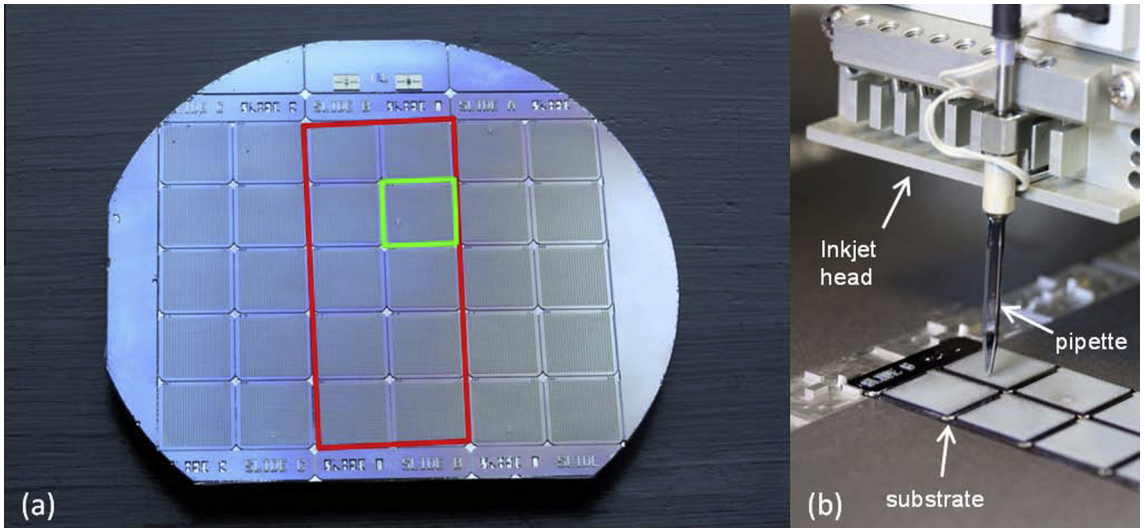

Fig. 2. Wafer after the fabrication process: (a) red rectangle outlines the Si microscope slide composed by 10 square chips (green). Each square contains a 25 × 25 matrix of micro-wells. (b) Si slide placed on the nano-plotter tray. (For interpretation of the references to colour in this figure legend, the reader is referred to the web version of this article.)

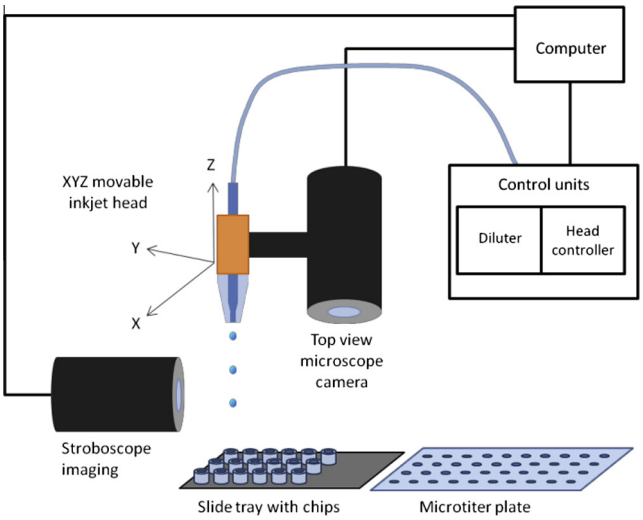

Fig. 3. Scheme of the inkjet printer setup. The micro-pipette is mounted on a XYZ movable head. It aspires the liquid sample to be dispensed from a microtiter plate. The aspiration is driven by a dilutor pump. A functional pipette check takes place in the stroboscope, and if it is successful, the spotting on the substrate begins. During spotting the pressure of the diluter pump is kept constant by system liquid (water).

Table 1
Dispensed volumes of polymer solution for different well sizes for one inkjet session.

Cavity diameter (μm)	Cavity volume (nL)	Dispensed volume for one inkjet session			
		5%, 10% wt PVP	Number of droplets	20% wt PVP	Number of droplets
300	18	18	60	18	75
200	8	7.5	25	7.7	32
100	2	1.8	6	1.9	8
50	0.5	0.3	1	0.5	2

sensitively affect the evaporation time of dispensed solutions. To measure the filling level of the micro-wells, the chips are coated with an Aluminum layer (15 nm, Alcatel SCM 600). The PVP thickness is then measured by means of an optical profiler (PLu Neox Optical Profiler, Sensofar), equipped with 50× objective to measure cavity diameter (300 and 200 μm) and 20× (100 and 50 μm). The profiler is set in confocal mode, with a monochromatic blue light (460 nm). Each micro-well is scanned along a cross section passing through the well center within a scanning range of 400 μm with a resolution of 1 μm.

3. Results and discussion

3.1. Level of micro-well filling

Arrays of wells with cavity diameter of 50, 100, 200 and 300 μm are filled with aqueous solutions of PVP at different concentrations. In Fig. 4a a microscope picture of three arrays of filled wells is shown. In Fig. 4b a SEM picture of an empty well (bottom right) and a filled one (top left) is shown. SEM pictures of micro-wells after filling reveal that large arrays of micro-wells can be filled with high precision and a quasi-no-waste deposition (see Fig. 4c) can be achieved when subsequent printing steps are performed on the same wells and a waiting time for solvent evaporation is included. According to the viscosity limit of the dispensing system, a concentration of polymer up to 20 wt.% is successfully spotted. It is observed that water solutions can be spotted with a higher volume than the micro-well cavity, because the high surface tension of water on SU-8 confines the solution in a cap on the top of the micro-structures (see Fig. 5). Upon drying of the liquid, the liquid cap shrinks, and the polymer is deposited in the cavity. After water evaporation the micro-wells are analyzed with scanning electron microscopy and the polymer deposition looks similar to Fig. 4c. The change of jet frequency is also investigated but it did not affect the coating performance. Thus the content of polymer in each micro-well can be controlled by varying its original concentration in the solution and repeating several printing sessions. The level of polymer filling is measured with an optical profiler. An array of 25 micro-wells is scanned for each micro-well dimension, for the three different level of filling (i.e. inkjet sessions), along their cross section passing through the center. In Table 2 the thickness of the polymer layer in the center of the micro-wells is shown. The reported values are given by the difference of the height of the polymer layer and the well bottom thickness (35 μm). By comparing

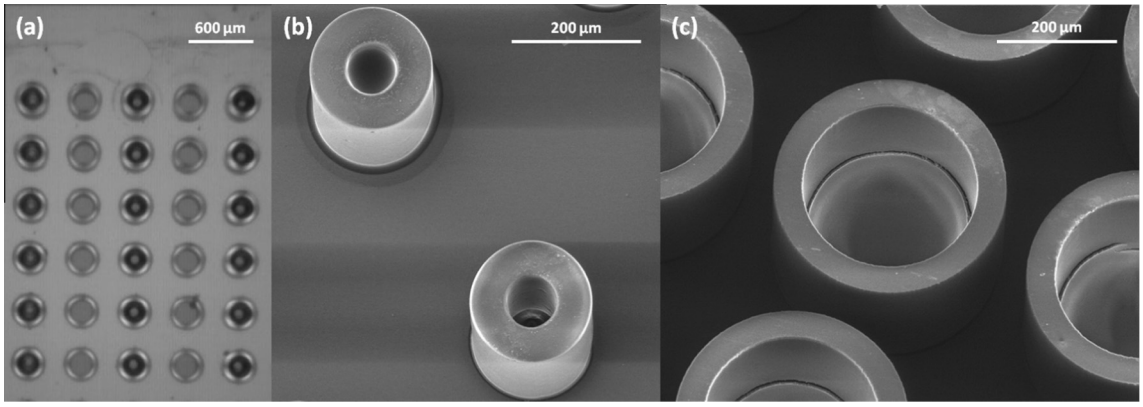

Fig. 4. (a) Microscope image of three arrays of micro-wells filled with 10 wt.% PVP. SEM images of (b) an empty (bottom right) and a filled well with diameter 50 µm (top left), (c) 300 µm inner diameter wells filled with 5 wt.% PVP.

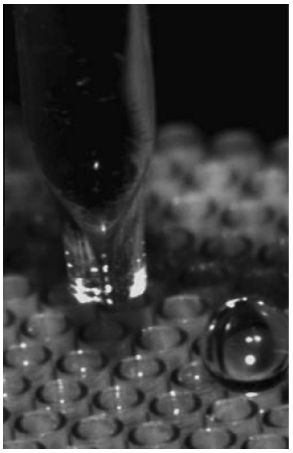

Fig. 5. Microscope picture from the side of one micro-well spotted with 4000 droplets of PVP in deionized water (2 wt%) with a drop ejection frequency of 100 Hz.

the filling level with the corresponding number of droplets it can be noticed that the increase is non-linear. This is due to the fact that the polymer tends to be distributed also on the walls of the wells, and this coating layer gets gradually thicker with the level of filling. The roughness of the surface due to cracks induced by the polymer shrinking does not allow a more accurate computation of the polymer volume by numerical integration.

3.2. Effect of surface tension on deposition

The effect of surface tension is investigated by dispensing solutions of PVP in isopropanol. This is motivated by the intention of testing a selective conformal coating of three dimensional microstructures. The deposition of a hydrophilic polymer like PVP can be used to permanently change surface properties of SU-8. For this purpose, solution of 2 wt.% PVP K10 is dispensed into wells with cavity diameter of 200 µm. The substrate temperature is kept at 50 °C in order to shorten the solvent evaporation time. The droplet volume is 0.3 nL. Fig. 6 shows SEM images of wells filled with 1000 droplets at different frequencies: 100 Hz (Fig. 6a), 200 Hz (Fig. 6b)

Table 2
Filling level of polymer for different well sizes after one, two and three inkjet sessions with solutions of PVP 20wt% in water. Each value is the average of 25 micro-wells.

Cavity diameter (µm)	Polymer thickness after subsequent inkjet sessions					
	Number of droplets	Polymer height (µm)	Number of droplets	Polymer height (µm)	Number of droplets	Polymer height (µm)
300	75	8 ± 2	150	20 ± 1	225	24 ± 1
200	32	88 ± 7	64	132 ± 9	96	155 ± 2
100	8	102 ± 3	16	223 ± 7	24	246 ± 5
50	2	125 ± 5	4	182 ± 4	6	282 ± 8

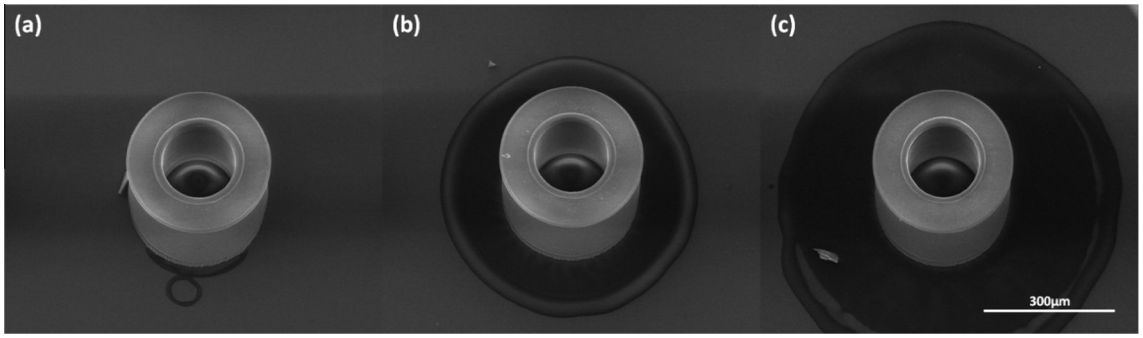

Fig. 6. SEM pictures of micro-wells spotted with PVP in isopropanol solution (2 wt.%). The same solution volume is dispensed with a drop ejection frequency of 100 Hz (a), 200 Hz (b) and 500 Hz (c).

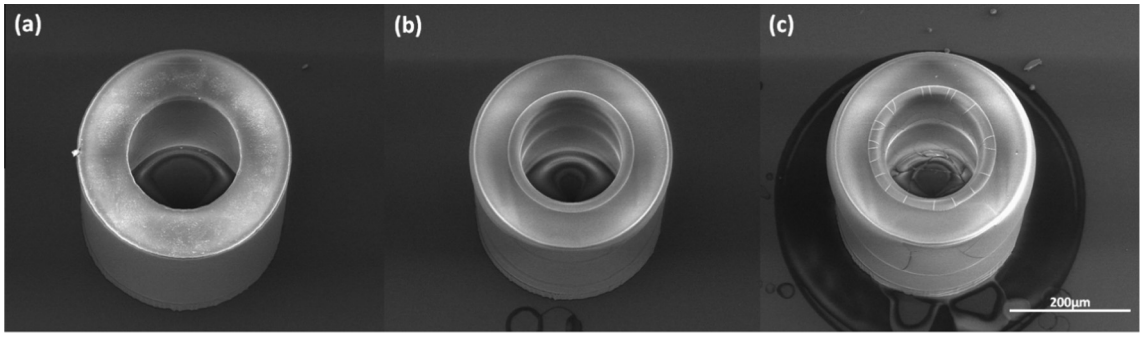

Fig. 7. SEM images of micro-wells filled with an increasing number of droplets: 1000 (a), 2000 (b) and 6000 (c).

and 500 Hz (Fig. 6c). For all three cases, the same volume of solution is dispensed, with equal droplet size (not depending on the jet frequency), but with different dispensing rates. In any case the solution does not fill the cavity, but tends to wet the surface of the well and covers it with a homogeneous coating. However, at higher frequency, not only the well is coated but also an increasing part of the substrate in between the wells.

In the SEM pictures in Fig. 7 the effect of droplet number on the coating is shown: 1000 (7a), 2000 (7b) and 6000 droplets (7c) are dispensed at a constant frequency of 100 Hz. PVP layer thickness increases with the droplet number. 1000 droplets are dispensed without spillage. These results are explained by the low contact angle of isopropanol on SU-8. Before evaporation, the solvent wets the well distributing the polymer uniformly on its surface. The result is a conformal coating of the three dimensional structure. The effect of frequency can be explained by the different time it takes for the droplets of solution, to dry once they land on the micro-well bottom. The higher the spotting frequency, the longer is the time the solution remains wet. The droplets coalesce and form a liquid mass that symmetrically flows onto the surrounding available surface until the solvent dries.

4. Conclusions

In this work we show the fabrication of polymer-filled micro-wells using DOD inkjet printing technology. By means of wet etching, silicon microscope slides are obtained. On top of them SU-8 micro-wells with cavity volumes down to 0.5 nL are fabricated with a two step photolithography process. Controlled volumes of PVP in aqueous solutions are dispensed inside the micro-wells, with a good reproducibility in terms of alignment and dispensed volume. Polymer concentrations up to 20% (wt) are successfully dispensed. Water-based solutions completely fill the cavity volume and the polymer content is controlled by repeated spotting sessions.

Other deposition types are investigated by changing the solvent of the PVP solution. Inkjet printing of isopropanol solutions results in a conformal coating as an effect of the lower contact angle on SU-8. Thus, according to the purpose of the deposition, it is possible to obtain either a conformal coating of the exposed surface or a filling with the same polymer just by changing the solvent of the dispensed solution. The conformal coating with PVP can allow to selectively modify the surface tension of three dimensional micro-structures. This potentially avoids the limitations of other methods, like plasma activation and wet chemical functionalization, which usually change surface properties on wafer scale. In conclusion, we demonstrate a very versatile filling technique for three dimensional micro-structures that can be tuned for several purposes, including promising applications in the field of micro-devices for drug delivery and biomedical research.

Acknowledgements

The authors acknowledge the Villum Kann Rasmussen Foundation for financial support.

References

[1] S. Nakano, T. Sekitani, T. Yokota, T. Someya, Appl. Phys. Lett. 92 (2008) 053302.
[2] Q. Liu, M. Orme, J. Mater. Process. Technol. 115 (2001) 271–283.
[3] V.J. Cadarso, J. Perera-Núñez, L. Jacot-Descombes, K. Pfeiffer, U. Ostrzinski, A. Voigt, A. Llobera, G. Grützer, J. Brugger, Opt. Express 19 (2011) 18665–18670.
[4] L. Jacot-Descombes, M.R. Gullo, V.J. Cadarso, J. Brugger, J. Micromech. Microeng. 22 (2012) 074012.
[5] T. Goldmann, J.S. Gonzalez, J. Biochem. Biophys. Methods 42 (2000) 105–110.
[6] T. Xu, J. Jin, C. Gregory, J.J. Hickman, T. Boland, Biomaterials 26 (2005) 93–99.
[7] E.A. Roth, T. Xu, M. Das, C. Gregory, J.J. Hickman, T. Boland, Biomaterials 25 (2004) 3707–3715.
[8] P. Cooley, D. Wallace, B. Antohe, J. Assoc. Lab. Autom. 7 (2002) 33–39.
[9] S. Hauschild, U. Lipprandt, A. Rumplecker, U. Borchert, A. Rank, R. Schubert, S. Förster, Small 1 (2005) 1177–1180.
[10] N. Scoutaris, M.R. Alexander, P.R. Gellert, C.J. Roberts, J. Controlled Release 156 (2011) 179–185.
[11] H. Kang, D. Soltman, V. Subramanian, Langmuir 26 (2010) 11568–11573.
[12] J.L. Tan, W. Liu, C.M. Nelson, S. Raghavan, C.S. Chen, Tissue Eng. 10 (2004) 865–872.
[13] C. Sung-Hoon, L. Hong Meng, L. Cauller, M.I. Romero-Ortega, L. Jeong-Bong, G.A. Hughes, Sens. J. IEEE 8 (2008) 1830–1836.
[14] G. Voskerician, M.S. Shive, R.S. Shawgo, Biomaterials 24 (2003) 1959–1967.
[15] R.J. Jackman, D.C. Duffy, E. Ostuni, N.D. Willmore, G.M. Whitesides, Anal. Chem. 70 (1998) 2280–2287.
[16] O.Z. Higa, S.O. Rogero, L.D.B. Machado, M.B. Mathor, A.B. Lugão, Radiat. Phys. Chem. 55 (1999) 705–707.
[17] C. Leuner, J. Dressman, Eur. J. Pharm. Biopharm. 50 (2000) 47–60.
[18] V.P. Torchilin, T.S. Levchenko, K.R. Whiteman, A.A. Yaroslavov, A.M. Tsatsakis, A.K. Rizos, E.V. Michailova, M.I. Shtilman, Biomaterials 22 (2001) 3035–3044.
[19] R. Sadeghi, M. Taghi Zafarani-Moattar, J. Chem. Thermodyn. 36 (2004) 665–670.

Appendix 2

Journal of Controlled Release 173 (2014) 1–9

Contents lists available at ScienceDirect

Journal of Controlled Release

journal homepage: www.elsevier.com/locate/jconrel

Polymer-filled microcontainers for oral delivery loaded using supercritical impregnation

Paolo Marizza [a,*], Stephan S. Keller [a], Anette Müllertz [b], Anja Boisen [a]

[a] Department of Micro- and Nanotechnology, Technical University of Denmark, Kongens Lyngby 2800, Denmark
[b] Department of Pharmacy, University of Copenhagen, Copenhagen 2100, Denmark

ARTICLE INFO

Article history:
Received 30 May 2013
Accepted 23 September 2013
Available online 2 October 2013

Keywords:
Microcontainer
Supercritical fluids
Drug delivery
Ketoprofen
PVP
Poorly soluble drugs

ABSTRACT

In the last years a large variety of drug delivery systems have been developed to improve bioavailability of therapeutics in oral administration. An increasing interest has arisen in reservoir-based microdevices designed for active ingredients like water insoluble compounds and fragile biomolecules. Such microdevices are designed to protect the active ingredient against degradation and deactivation, and to allow cytoadhesion and unidirectional drug release. There are few works which optimize the drug loading step and often therapeutics are dosed in the microdevices through laborious and time consuming procedures. This work proposes an effective loading technique for a poorly soluble model drug in microcontainers, by combining inkjet printing and supercritical fluid impregnation. Well defined quantities of poly(vinyl pyrrolidone) (PVP) solutions are dispensed into microcontainers by inkjet printing with a quasi-no-waste performance. Then ketoprofen is impregnated in the polymer matrix by using supercritical carbon dioxide ($scCO_2$) as loading medium. The amount of polymer is controlled by the volume and the number of droplets of dispensed polymer and drug loading is tuned by varying the impregnation parameters. Compared to solid dispersions of the same drug and polymer, $scCO_2$-impregnated microcontainers exhibit a more reproducible drug loading and a faster dissolution rate of the active compound which allows drug release to be modulated. The combination of these loading techniques potentially allows the high throughput fabrication of microdevices for oral drug delivery with a safe and solvent-free solution.

1. Introduction

In these last years one of the most challenging tasks in the pharmaceutical research is finding effective and safe solutions to administrate active principles through the oral delivery that still represents the preferred administration route, being less invasive, simple and usually requiring no assistance. However between the oral ingestion and the therapeutic effect there is a sequence of barriers which limits the bioavailability of a molecule in the oral delivery [1]. Traditional pharmaceutical dosage forms deliver the active ingredient in an omni-directional release, through a limited interfacial area in the physiological fluids. As a consequence, frequent administrations are needed in order to maintain an efficient therapeutic action. Therefore high drug doses are swallowed, which is the cause of serious side effects for the GI tract of patients [2]. Furthermore such an ineffective delivery mechanism results to be unpractical and economically prohibitive for expensive drugs. One option is given by the downscaling of drug delivery systems to dimensions, which at the same time can allow a more intimate contact with the irregular surface of the mucosa and avoid unspecific endocytosis. In recent years microtechnology has substantially contributed with innovative drug delivery systems at the micro- and nanoscales [3–5]. In particular there has been an increasing interest in reservoir-based microdevices [6–9] for carriers of water insoluble compounds and fragile biomolecules. These microdevices are designed to provide protection against drug degradation, cytoadhesion, and unidirectional drug release. There are few works in this field which focus on optimizing the drug loading step. Indeed the fabrication processes investigated so far require the use of relatively high temperature [10], or exposure to energetic UV radiation [7,8], which can cause degradation of the active ingredient [11], and may give unknown and possibly harmful products. The active ingredients are loaded by means of techniques which either require laborious and time-consuming procedures, or include large waste of chemicals [12]. Moreover, when the drug being loaded is poorly soluble in water, potentially toxic organic solvents are used largely.

In this work we present the reproducible drug loading of microcontainers for oral delivery of a poorly water soluble compound. A prototype of these devices is made with epoxy resin (SU-8) through a double step photolithography process. The microcontainers are designed with a circular base, cylindrical walls, and an open top side with a cylindrical cavity of 50 to 300 μm in diameter. Dimensions can

* Corresponding author at: Department of Micro- and Nanotechnology, Technical University of Denmark, Ørsteds Plads 345Ø, Kongens Lyngby 2800, Denmark. Tel.: +45 45255759.
E-mail address: paom@nanotech.dtu.dk (P. Marizza).

0168-3659/$ – see front matter © 2013 Published by Elsevier B.V.
http://dx.doi.org/10.1016/j.jconrel.2013.09.022

easily be modified by changing process parameters. For the drug loading we sequentially combine inkjet printing and supercritical fluid (sc) impregnation. These two different technologies allow the minimization of the waste of therapeutic compound used in the loading process and the provision, at the same time, of a safe, solvent-free and ecologically friendly solution.

The use of inkjet printing is already established in the fields of biotechnology and nanomedicine, mostly for large scale screening of genomic material [13], for cell culturing [14,15], and surface functionalization of Bio MEMS [16]. The reason of such a wide use is mainly due to the so called drop-on-demand (DOD) mode which allows precise volumes of liquid to be dispensed with a quasi-no-waste performance. More recently it was also applied in drug delivery, for example in the production of nanoliter doses of felodipine in ethanol and DMSO mixtures [17]. In a previous work we demonstrated that the deposition of aqueous solutions of poly(vinyl pyrrolidone) (PVP) by inkjet printing resulted in well defined filling of microcontainer cavities, while dispensing of organic solvent-based polymer solutions gave a pronounced spilling out of the microwells [18]. Moreover, our investigation of inkjet printing of several solutions containing water insoluble drugs showed a low reproducibility of the spotting performance, as well as low drug loading capacity. Therefore aqueous solutions are the most suitable for the purpose of drug loading of microcontainers. This implicates that the poorly soluble drug of interest cannot be directly spotted in the microwells and another drug loading step is needed.

In this work inkjet printing is used to dispense water-based solutions of poly(vinyl pyrrolidone) (PVP) in water with precise volumes in the pico up to nanoliter range into microcontainers. PVP is a non-toxic polymer [19,20], which is widely used as excipient for oral dosage forms [19], and as solubility enhancer for water insoluble pharmaceuticals [21].

As a second step, the poorly soluble model drug ketoprofen, is loaded by means of sc fluid impregnation into the PVP filled containers. The sc fluid is a high pressure phase characterized by a liquid-like density, and a gas-like viscosity and in recent times its use in the impregnation of polymers has been studied extensively [22–25]. Carbon dioxide has a critical point of 73.8 bar and 31.1 °C and is a non-polar, safe, non-flammable and ecologically friendly chemical, which makes it a versatile solvent for temperature sensitive hydrophobic drugs [26,27]. In this process the crystalline drug dissolves in the supercritical carbon dioxide ($scCO_2$) and the drug-enriched fluid swells the polymer matrix acting as a plasticizer for the polymer chains; in this way the fluid acts both as a dissolution medium for the drug and as a mixing agent for drug and polymer, where the solute is physically conveyed into the PVP matrix by convection and diffusion. As the pressure of CO_2 is reduced, it flows out of the polymer matrix due to its high mobility, leaving the drug molecules entrapped between the polymer chains. By proper choice of pressure and temperature, it is possible to keep the polymer confined in the micro-wells while the swelling occurs, and at the same time dissolve and load the drug in the matrix in controlled amounts. A remarkable aspect of this process is the easy modularity of the loading: a simple change in pressure and time allows different and controllable moieties of therapeutic ingredients to be impregnated into large arrays of containers, allowing potential upscaling of the process for production.

Drug absorption can be enhanced by improving the dissolution rate with respect to the retention time of the microdevice across the GI tract. The use of $scCO_2$ as formulation medium, allows accelerated drug release from polymer–drug solid dispersions [26]. Several studies [27–29] have showed that impregnated polymers release active ingredients faster than comparable conventional tablets. Herein, we demonstrate that microcontainers loaded using $scCO_2$ release ketoprofen quicker than microcontainers filled with solid dispersions conventionally used in tablet preparation.

2. Materials and methods

2.1. Fabrication of SU-8 microdevices

2.1.1. Materials for microfabrication

Ketoprofen (>98%, racemate) and polyvinylpyrrolidone (PVP, Mw 10,000) were supplied by Sigma Aldrich. Carbon dioxide was supplied by BOC (Guildford, UK).

Silicon wafers (4-inch <100> n-type) were supplied by Okmetic (Vantaa, Finland). SU-8 2075 and SU-8 developer were purchased from Microresist Technology GmbH (Berlin, Germany). The chromium mask was designed using L-Edit from Tanner EDA (Monrovia, CA, USA) and supplied by DeltaMask B.V. (GJ Enschede, The Netherlands).

2.1.2. Microfabrication process

The cylindrical microcontainers were fabricated with a similar procedure as outlined earlier [18]. Two steps of negative photolithography with the epoxy-based photoresist SU-8 were performed to define the bottom and the walls of the containers, respectively. Fig. 1 shows the sequence of steps involved in the overall microfabrication process. Several baking steps on a hotplate, with a ramping rate of 2 °C min^{-1} leading to the final bake temperature of 50 °C were involved in the microwell fabrication procedure. For the definition of the bottom of the microcontainers, SU-8 2075 was dispensed onto 4 inch silicon wafers by a Liquid Dispenser 1500-XL (Nordson EFD, Bougival, France). The SU-8 was spin coated using a RC8 spin-coater (Karl Süss, Lyon, France) with an

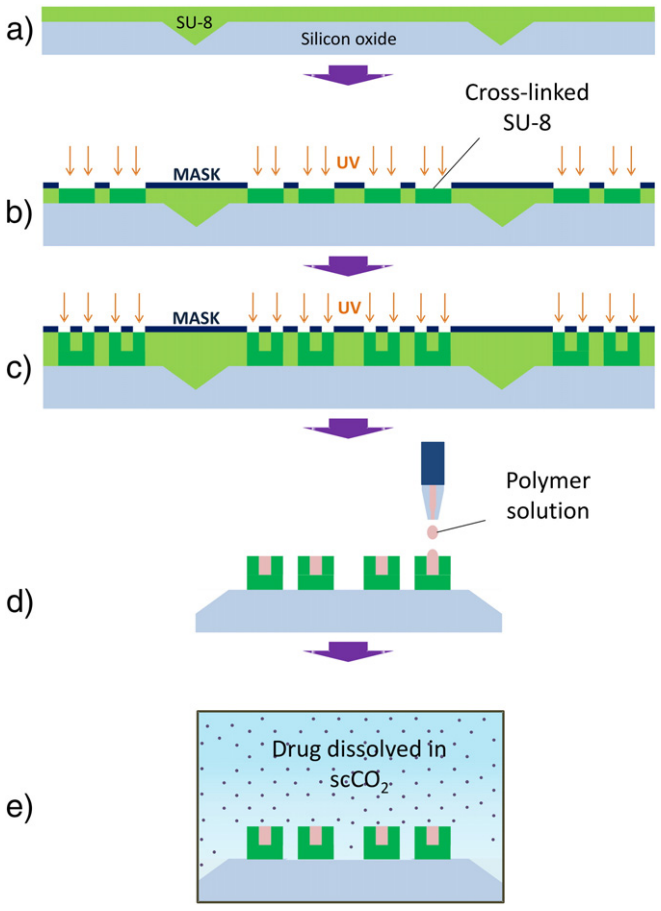

Fig. 1. Schematic representation of the fabrication process of SU-8 microcontainers: (a) resist spin coating on etched Si wafer, (b) mask alignment, UV exposure and development, (c) spin coating, mask alignment, exposure of second resist layer and development, (d) inkjet printing of polymer solution, and (e) $scCO_2$ impregnation of the drug (for more details see Section 2.1.2).

installed GYRSET rotating cover plate (Fig. 1a). Spin coating was carried out in two steps, the first one with an acceleration of 200 rpm s^{-1} to a speed of 1000 rpm maintained for 30 s, followed by an acceleration of 400 rpm s^{-1} to a speed of 3000 rpm maintained for 120 s. The resulting SU-8 film thickness was 33.5 ± 0.9 μm. The solvent was then removed during a soft-bake for 2 h. The SU-8 was then selectively exposed to a dose of 2 × 250 mJ cm^{-2} of UV light through a chromium mask in soft-contact mode (Fig. 1b) with a break of 30 s between the intervals in a MA6/BA6 mask aligner (Karl Süss, Garching, Germany) equipped with an I-line filter (365 nm, 20 nm FWHM). To achieve polymerization of the exposed areas, a post-exposure bake (PEB) for 6 h followed the exposure. For the definition of the container walls, a second step of UV lithography with SU-8 was included. Spin coating was performed with an acceleration of 100 rpm s^{-1} to a speed of 300 rpm maintained for 30 s, followed by an acceleration of 100 rpm s^{-1} to a speed of 600 rpm maintained for 60 s (Fig. 1c). The thickness of the second layer of SU-8 as a result of this process was 255 ± 10 μm. Both soft bake and PEB had a duration of 10 h. UV exposure was performed with a dose of 3 × 250 mJ cm^{-2} using a second chromium mask in proximity mode. Finally, the non-polymerized SU-8 was developed by immersion in propylene glycol methyl ether acetate (PGMEA) for 40 min, followed by rinsing in isopropyl alcohol for 30 s and drying in air. The resulting microcontainers had inner diameters of 200 ± 3 μm and volumes of 8 ± 0.5 nl, respectively. The silicon wafers supporting the fabricated microcontainers were finally parted into squares of 12.8 × 12.8 mm^2 by simple manual cleavage each containing 625 containers. The is enabled by a preliminary wet etching step in KOH defining trenches, as described in a previous work [18]. SU-8 is not approved by FDA as a material for medical use, because it has not shown acceptable non-toxic properties. In this work it has been used for the fabrication of a prototype microdevice, because of its simple and relatively fast preparation and to validate the loading technique presented.

2.2. Deposition of PVP solution in the microcontainers and preparation of PVP films

The microwells were filled with PVP by means of an inkjet printer (Fig. 1d) as described previously [18]. PVP was dissolved in DI water (10 wt.%) and the solution was stirred for 3 h. The viscosity of the solution (data not shown) was checked with a controlled stress rotational rheometer (Haake RheoStress 300) equipped with a cone-plate rotor device, in order to confirm the Newtonian behavior and measure the viscosity of the liquid which must be below the technical limit of 5 mPa·s of the inkjet printer.

The inkjet printer is composed of a XYZ movable inkjet head (Nanoplotter NP 2.1 GeSim, Germany) equipped with a piezo-driven dispenser with a 70 μm orifice (GeSiM nanotip). The silicon substrate is placed on the slide tray. The solution is aspired by the pipette from a well in a titer plate where the liquid is stored at the desired temperature. The printer works in a semi-automatic mode, since the inkjet head is monitored by a control unit connected to a computer. The jet direction, its stability and the droplet size are visualized by means of a stroboscope camera (side view). The intensity, duration, and frequency of the voltage applied to the piezoelectric actuator of the dispenser were tuned for optimized microcontainer filling [18]. The optimum set of parameters is a pulsing voltage of 90 V, a pulse width of 90 μs and a frequency of 175 Hz for all the solutions and the corresponding droplet volume is 0.3 nl. After the polymer deposition the chips were left on a hotplate at 50 °C for 1 h to remove the solvent. The chips were weighted before and after the polymer deposition and the polymer weight per chip was estimated. Characterization of polymer filled microcontainers was done with a Plu Neox 3D Optical Profiler (Sensofar) in the confocal mode.

Polymer films were prepared with the same solution used for the inkjet printing (10 wt.% in DI water). These samples were intended for spectroscopic characterization studies. The films were cast in a cylindrical cavity of a teflon mold (diameter 5 mm, height 0.255 mm) with the volume equal to the sum of 625 microcontainers. A volume of 5 μl of solution was dispended in the mold and left on a hotplate at 50 °C for 1 h to remove the solvent.

2.3. Drug loading of microdevices

2.3.1. Supercritical fluid impregnation

The drug was loaded into polymer-filled microdevices by means of supercritical carbon dioxide impregnation (Fig. 1e). The operation was performed in a 100 ml high pressure reactor with sapphire windows (Thar SFC) in batch conditions, with steady state values of CO_2 pressure, temperature and stirring velocity. Impregnation experiments on microcontainers were performed at 40 °C, 100 and 200 bar, 1 and 4 h. Different weights of active ingredient were placed on the bottom of the high pressure chamber, according to the quantities tested by Macnaughton et al. [30] to achieve saturation condition at defined pressures of supercritical carbon dioxide. The chip with microcontainers was placed on a steel grid fitting the chamber's cross section. The reactor was sealed and filled with liquid carbon dioxide by means of a high pressure pump with a controlled pressure ramp. With the increase of the pressure, the drug dissolved in the supercritical fluid. Once the fluid achieved the desired pressure and temperature, the mixing was activated. PVP films in the Teflon holder were submitted with the same procedure to supercritical impregnation at 100 and 200 bar for 1 h. At the end of the experiment the reactor was depressurized at a controlled rate in 2 and 3 h when the operating pressures were 100 and 200 bar respectively. The CO_2 with the excess of active principle was bubbled through an ethanol solution (99.5%), where the drug is solubilized and collected. The ketoprofen concentration in the ethanol solution was measured with a UV spectrophotometer (data not shown) to cross check the drug mass balance of the operation. The morphology of the impregnated microcontainers was examined using SEM. The investigations were carried out using a Nova600 NanoSEM from FEI (Eindhoven, the Netherlands). Imaging was performed in low-vacuum-mode at a pressure of 0.6 mbar and an operation voltage of 5 kV. Prior to examination, the samples were mounted onto metal stubs and were tilted by 30°.

2.3.2. Preparation of micro-tablets

PVP–ketoprofen physical mixtures were prepared by gently mixing the two powders with a mortar (1:9 and drug:polymer weight ratio). The physical mixtures were filled into empty microcontainers resulting in an array of micro-tablets. The residual material in between adjacent containers was removed using pressurized air. The chips were weighted before and after the filling. The amorphous drug micro-tablets were obtained by heating containers filled with the mixture at 120 °C for 3 min on a hotplate and quenching in liquid nitrogen for 1 min. This sequence was repeated thrice.

2.4. Spectroscopic characterization and X-ray diffraction

Raman and ATR–IR spectroscopy measurements were performed on microcontainers and films to investigate the drug–polymer interactions after supercritical treatment.

Raman spectra were collected from the impregnated microcontainers 24 h after the CO_2 treatment with a DXR Raman microscope (Thermo Scientific, Germany) equipped with a frequency-stabilized single mode diode laser (780 nm). The laser power was set to 10 mW at the sample position (center of the container cavity) and the estimated resolution was 2.4–4.4 cm^{-1}. An exposure time of 1 s and 40 scans were used. Because of the strong auto-fluorescence of SU-8, a dedicated correction was applied to the spectra during the collection.

A Spectrum 100 spectrometer (Perkin Elmer, Germany) with an MIR source and a TGS detector was used to measure the ATR–IR spectra from the impregnated PVP films 24 h after preparation. The resolution was

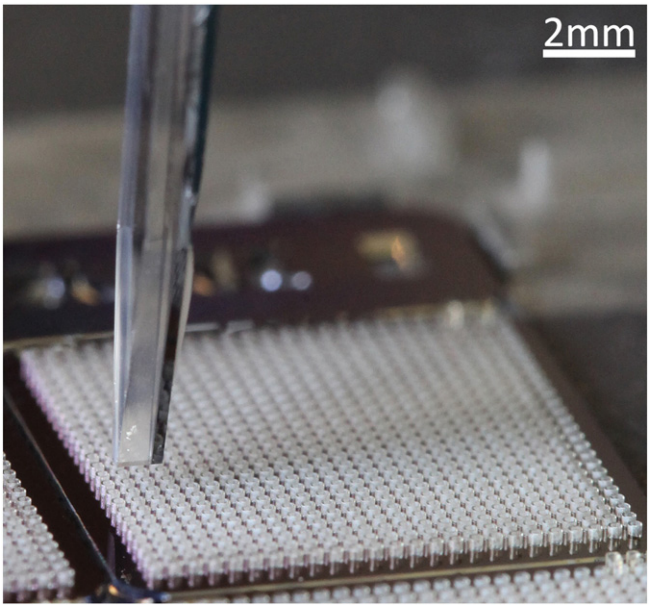

Fig. 2. Picture image of an inkjet tip on a chip containing a 25 × 25 container matrix.

set to 4 cm^{-1} and 16 accumulations with a scan speed of 0.2 were collected.

The X-ray powder diffraction (XRPD) study was carried out to characterize the physical state of the drug in the impregnated microcontainers and micro-tablets. All XRPD analyses were performed using an X'Pert PRO X-ray diffractometer (PANalytical, Almelo, The Netherlands; MPD PW3040/60 XRD; Cu KR anode; λ = 1.541 Å; 45 kV; 40 mA). A starting angle of 5° 2θ and an end angle of 45° 2θ were employed for the scans. A scan speed of 0.6565° 2θ/min and a step size of 0.01313° 2θ were employed. Data were collected using the X'Pert Data Collector software (PANalytical B.V.).

2.5. In vitro drug dissolution studies

Dissolution of PVP and ketoprofen from loaded microcontainers was measured in 10 ml DI water at 37 °C using a μDISS profiler (Pion). Individual chips were glued with carbon pads on teflon-coated magnetic stirrers. For the detection of ketoprofen release, the UV probe wavelength was set at 259 nm. After dissolution, the microcontainers were checked with an optical microscope to confirm complete emptying. The amount of drug loaded per chip was estimated by the final concentration value in the dissolution profiles obtained after 16 h. Solubility of ketoprofen at 37 °C in aqueous solutions changes significantly with pH between 1 and 7 [31]. The dissolution tests were performed at pH 7 where ketoprofen solubility is >1.4 mg/ml. With ketoprofen being a weak acid (pK_a = 4.5) the pH of the dissolution medium did not change sensitively during the dissolution tests. Therefore dissolution tests were performed in sink conditions.

3. Result and discussion

3.1. Fabrication of microcontainers

Cylindrical microcontainers have been fabricated on silicon wafers as previously described [18]. At first, the silicon wafer undergoes a wet etching step to define trenches along which it can be cleaved manually after completed processing. The fabrication process is composed of two steps of photolithography with the negative photoresist SU-8 which is used for the definition of the micro-wells. In Fig. 1 the fabrication steps of the overall process are presented. The silicon wafer is then cleaved into three rectangular slides fitting on the inkjet printer tray. Each slide holds ten squared chips containing 625 microcontainers arranged in a 25 × 25 matrix (see Fig. 2). Subsequently the rectangular slides are manually broken into individual chips for sc impregnation with the drug. The prototype device has a cavity of approximately 200 μm in diameter and 255 μm in depth. Cavity volume is approximately 8 nl. The dimension can be changed by varying the spin-coating procedure of photoresist layers.

3.2. Inkjet printing of PVP solutions into microcontainer

The microcontainers were filled with PVP 10 wt.% in deionized water solution with an inkjet printer as described in a previous work [18]. The printer works in a drop-on-demand mode and the droplet diameter can be tuned in the range of 50–80 μm. The printer works in a semi-automatic mode: once the alignment is set, the inkjet head dispenses controllable volumes of liquid in pre-defined patterns. The number of droplets to dispense in each container is estimated dividing the cavity volume by the droplet volume. Three subsequent printing sessions have been performed on the same array and waiting time between the sessions has been included in order to enable solvent evaporation and to avoid spillover. The level of container filling has been measured

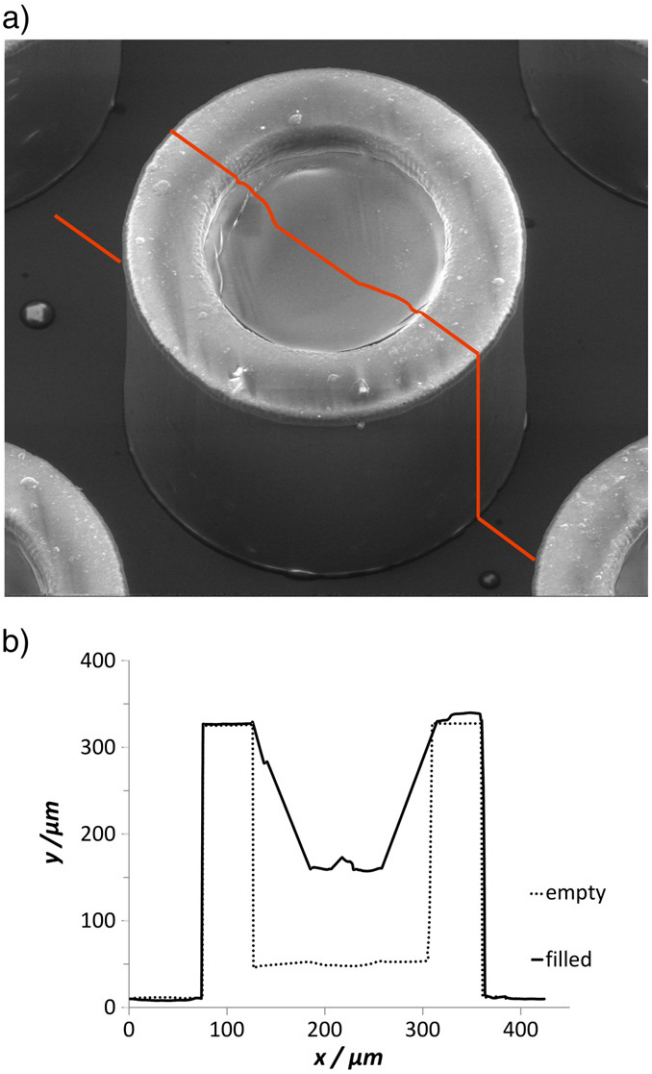

Fig. 3. (a) SEM picture of a polymer filled microcontainer with outlined cross section, (b) 2D profiles of an empty (dotted line) and filled microcontainer (solid line) with 64 droplets of PVP 10 wt.% in water scanned with the optical profiler.

with an optical profilometer. Fig. 3 shows the two dimensional profile of a polymer-filled container. The measured average thickness is 141 ± 9 μm. The weight of polymer dispensed onto one chip (625 micro-wells) corresponds to 1.6 ± 0.04 mg. The high accuracy of polymer deposition shows that inkjet printing can be used to dispense precise quantities of polymer with a quasi-no-waste performance. The precise control of the dispensed polymer mass is important to control the amount of drug loaded in each microreservoir.

3.3. Loading of ketoprofen into polymer-filled microreservoirs

After the polymer deposition, silicon slides have been cleaved into chips. The drug loading is performed on individual chips. The weighted ketoprofen amounts have been dissolved in $scCO_2$ in saturation conditions, according to the results found by Macnaughton and co-workers [30]. As shown in several works [30,32] the solubility of ketoprofen in sc CO_2 monotonically increases with the fluid density, hence with fluid pressure in isothermal conditions [33]. The impregnations were performed at 100 and 200 bar at 40 °C and for 1 and 4 h in order to investigate the role of the operating conditions on the drug loading. Fig. 4 shows scanning electron microscopy (SEM) images of microcontainers subjected to sc impregnation. The fluid pressure during the impregnation has a relevant influence on the volume of the polymer which increases with rising CO_2 pressure, as appears clearly by the comparison of Fig. 4a and b. This is likely explained by an increase of CO_2 uptake in the PVP matrix with pressure, as shown by Kikic and Vecchione [34]. As $scCO_2$ acts as a plasticizer for polymers, the viscosity of the CO_2 saturated matrix decreases during the impregnation, causing in some cases spillages from the containers. This aspect is more pronounced for longer experiments (see Fig. 4c and d). Polymer softening and swelling play an essential role with respect to the desired quasi-no-waste performance. For an optimal combination of inkjet printing and sc impregnation, the PVP must remain confined in the cylindrical cavity of the micro-well. During impregnations at 200 bar, several droplets were deposited in the space in between adjacent microcontainers (see Fig. 4d). This effect was observed when the depressurization rate at the CO_2 critical pressure was higher than 1.1 bar min. Compared to that, there was a negligible polymer spillage with a constant pressure decay over time. The holes in the de-swelling matrix, also shown in Fig. 4d, are probably due to the formation of micropores during CO_2 release. All the SEM images show no effect of the supercritical fluid on SU-8 in the micro-scale.

3.4. Controlled in vitro drug release from impregnated microdevices and Raman characterization

To measure the ketoprofen release from the microcontainers, dissolution measurements were carried out on individual chips.

Fig. 5 shows the *in vitro* dissolution profiles of microcontainers loaded via $scCO_2$ impregnation at different conditions. As a control experiment, microcontainers without PVP were submitted to ketoprofen impregnation (at 200 bar 40 °C 4 h). The different amounts of drug released show that both the sc fluid pressure and the impregnation time significantly influence the loading. As shown in the release profiles in Fig. 5, the drug uptake increases with an increase in the fluid pressure and with a larger duration of the impregnation. This suggests that the polymer swelling and the drug diffusion play a relevant role in the loading. In Table 1 the weights of loaded drug per chip in terms of absolute value, drug/polymer weight ratio and weight fraction are shown. The effect of the pressure may be attributed to the fact that both the drug solubility and the CO_2 uptake in the polymer increase with the sc fluid pressure. At 200 bar a higher number of drug molecules can interact with the polymer chains, and this results in an enhanced loading. The effect of time can be explained supposing that the impregnation follows a diffusion-limited mechanism. A previous work shows that SU-8 microstructures treated with $scCO_2$ undergo only small mechanical changes [35], which is also confirmed by our SEM micrographs. Therefore it may reasonably be assumed that SU-8 containers undergo a

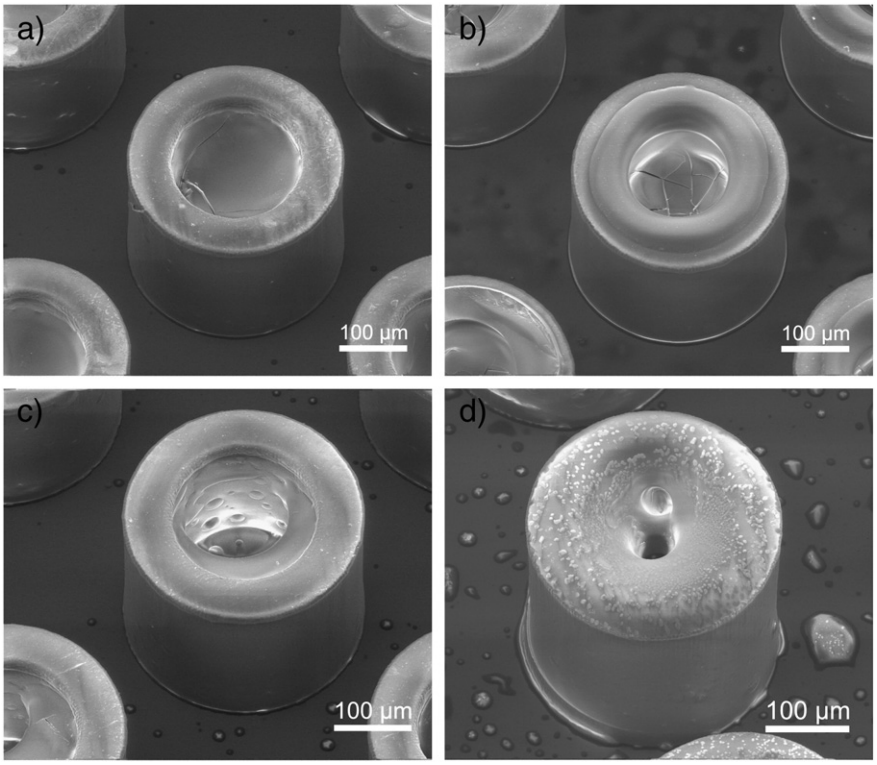

Fig. 4. Scanning electron microscopic images of the polymer-filled microcontainers impregnated with ketoprofen using $scCO_2$ at different conditions: (a) 100 bar 1 h; (b) 200 bar 1 h; (c) 100 bar 4 h; and (d) 200 bar 4 h.

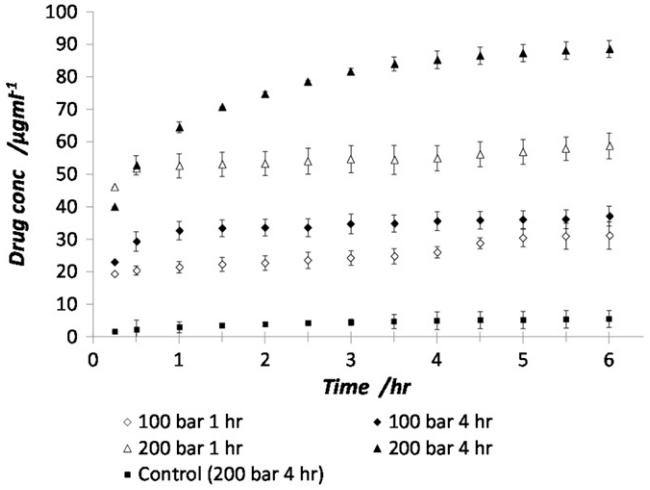

Fig. 5. Controlled release of the model drug from polymer-filled microcontainers loaded at different pressures and times compared to empty microcontainers (control; without polymer). Release test on individual chips (625 micro-containers) in 10 ml DI water (N = 3).

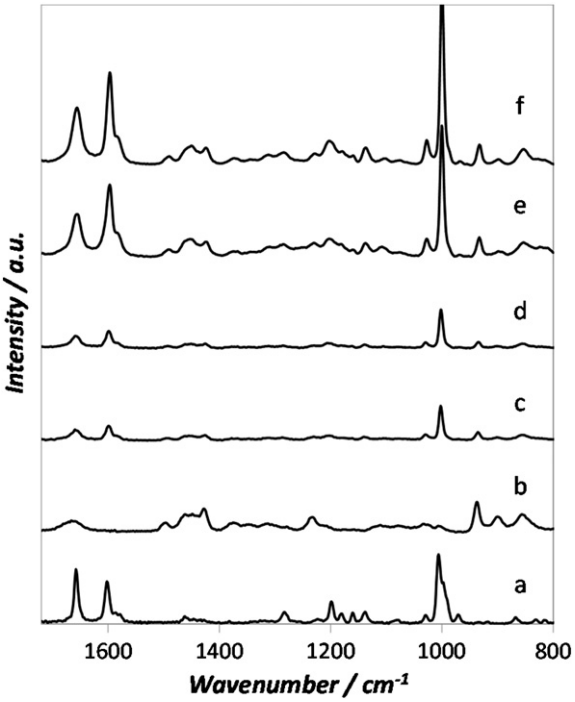

Fig. 6. Raman spectra for (a) solid ketoprofen, (b) PVP and (c) polymer filled microcontainers impregnated at 100 bar 1 h, (d) 100 bar 4 h, (e) 200 bar 1 h, and (f) 200 bar 4 h.

negligible swelling by the CO_2 compared with that of PVP. As a consequence, we assume that container walls provide a spatial shielding to the loading and that the drug is mainly conveyed across the interface PVP/sc fluid. Finally, the combination of these two effects can give an explanation of the different loading gains for impregnation time which can be obtained at the two considered pressures. At 100 bar the CO_2 moderately swells the polymer chains, the drug diffuses with difficulty and the gain over time is poor. At 200 bar the CO_2 uptake is higher and swollen polymer offers a larger interfacial area and a reduced resistance to drug diffusion, resulting in an enhanced loading gain from 1 to 4 h. As shown in Table 1, at the hardest conditions (200 bar and 4 h) the drug deposited in the microcontainers without PVP, is less than 8% of the drug loaded into polymer filled containers at the same conditions. The control experiment shows that a negligible amount of drug is absorbed in the SU-8 container and that the preliminary deposition of the PVP is required to achieve drug loading. From a technological perspective, the possibility of tuning the drug loading with a change in fluid pressure and time of impregnation represents a relevant advantage. The times of 90% of drug dissolution ($t_{90\%}$) are also shown in Table 1. The samples impregnated at 100 bar show similar $t_{90\%}$ of around 270 min, while the samples at 200 bar exhibit a markedly faster drug dissolution: for containers impregnated for 1 h $t_{90\%}$ is equal to 60 min, for those impregnated for 4 h $t_{90\%}$ is approximately 180 min. All dissolution profiles show a burst effect, which might be explained by the presence of amorphous drug coating in the microcontainers after the treatment with the carbon dioxide. A Raman mapping of containers was carried out just after the experiments. The Raman spectra are shown in Fig. 6: patterns (a) and (b) are the spectral fingerprints of crystalline pure ketoprofen and PVP respectively. The vibrational patterns of all impregnated samples exhibit characteristic peaks of the drug where untreated PVP does not show any signal. In particular the band at 1657 cm^{-1}, attributed to the stretching vibration of the ketoprofen carbonyl ν (C═O) and the band at 1198 cm^{-1}, regarding the ring CH in plane bending, seem to have an intensity which is proportional to the impregnation pressure and, more markedly at 200 bar, with time. This fact seems to confirm the results of the dissolution tests. In [36] De Carvalho et al. attribute these two peaks to the amorphization of the drug in the presence of the excipient.

3.5. Comparison with physical mixtures and XRPD characterization

An important aspect of poorly soluble drugs is their dissolution in the physiological media, which is slower than the typical retention times in the intestine. This is primarily due to the presence of drug crystals which have low solubility and slow dissolution rate in water. Typically, an amorphous drug dissolves faster in water than the crystalline phase [37]. The amorphous form is an unstable state and the drug tends to recover to its more stable crystalline form. In pharmacy, a typical way to improve the release rate of these drugs is to prepare solid dispersions with a water-soluble polymer and to induce amorphization of the drug. The polymer stabilizes the amorphous form and slows down the growth of drug crystals [38], improving the drug solubility and dissolution rate. In several works $scCO_2$ impregnation is shown to be suitable to prepare such stabilized drug–polymer dispersions [28–30]. To investigate whether the impregnation of microcontainers

Table 1
Drug loading of impregnated samples and of physical mix-laden micro-tablets. The drug weight refers to total loaded mass on individual chips (625 microcontainers) and is normalized with respect to the polymer mass into the micro-wells (N = 3).

Samples	Loaded drug per chip (mg)	Resulted drug/polymer weight ratio	Drug weight fraction after dissolution keto/(PVP + keto)	Time at 90% dissolution $t_{90\%}$ (hours)
100 bar 40 °C 1 h	0.33 ± 0.03	0.22 ± 0.04	0.16 ± 0.03	4.46
100 bar 40 °C 4 h	0.41 ± 0.02	0.28 ± 0.02	0.22 ± 0.02	4.63
200 bar 40 °C 1 h	0.61 ± 0.05	0.37 ± 0.05	0.27 ± 0.03	1.0
200 bar 40 °C 4 h	0.82 ± 0.02	0.52 ± 0.03	0.32 ± 0.01	3.3
Empty containers (200 bar 40 °C 4 h)	0.07 ± 0.02	–	–	6.0
Physical mix laden micro-tablets (1:9 keto:PVP, 10wt.%)	0.22 ± 0.06	0.18 ± 0.10	0.15 ± 0.07	6.32

produces similar results, an alternative fabrication method based on the conventional tablet preparation was carried out. Microcontainers were filled with a solid dispersion of crystalline ketoprofen and PVP, following a procedure shown by Nielsen and co-workers [39]. Solid powders of polymer and drug were gently mixed in a mortar, distributed and compressed into microcontainers. Containers filled with this method will be called crystalline micro-tablets. In the preparation of micro-tablets a relevant amount of chemicals was wasted and the procedure was quite laborious and time-consuming. To get the amorphous form of the drug a group of physical mixture laden chips underwent an additional treatment, consisting of a sequence of heating and quench cooling with liquid nitrogen repeated thrice. This group of samples, containing amorphous ketoprofen, will be called amorphous micro-tablets. The solid state of the drug in the physical mixture loaded container was characterized by mean of XRPD. The diffractograms are shown in Fig. 7. The silicon chip with empty containers (a) exhibits a broad scattered band (meaning that the SU-8 is an amorphous material) with one single peak at $\theta = 33.3°$ belonging to the silicon substrate. The chip filled with pure fresh crystalline ketoprofen (b) shows defined peaks emerging from the scattered halo of the containers. The containers filled with a physical mixture containing crystalline drug show a diffractogram with some peaks of the drug with a lower intensity (c). The samples submitted to melt and quench cooling (d) do not show distinguishable peaks of ketoprofen. The drug content and the drug/polymer weight ratios in these samples were cross-checked by dissolution tests. XRPD measurements were also performed on all impregnated microcontainers (data not shown) and all the samples showed a scattered pattern similar to 7(d). In Table 1 the drug loading data in terms of drug/polymer weight ratio are shown. In micro-tablets the average relative drug content (15 wt.%) differs from the original physical mixture (1:9, i.e. 10 wt.%) which demonstrates that the drug and the polymer are demixed during the preparation. The large deviation of the 50% variation associated to the data shows that the micro-tablet filling method has a lower accuracy than the sc impregnation where variations are below 18%. Fig. 8 shows the *in vitro* cumulative drug release from impregnated microcontainers and the crystalline and amorphous micro-tablets with a comparable drug content. Due to the high standard deviation of micro-tablets (see in Table 1), further tests were done and only those with the drug/polymer weight ratio numerically close to the one for impregnated containers, were considered for the comparison. The dissolution curve of microcontainers treated at 100 bar (Fig. 8a) overlaps the amorphous micro-tablet profile. Samples loaded at 200 bar (Fig. 8b) show instead a slightly faster dissolution than both amorphous and crystalline micro-tablets.

The similarity factor f_2 of the cumulative dissolution profiles of impregnated microcontainers and microtablets was estimated. The results of the comparison are shown in Table 2.

In all the comparisons the similarity factor is greater than 50 and the profiles can be considered similar according to the FDA regulations.

Di Martino and coworkers [40] showed that already in physical mixtures of crystalline ketoprofen and PVP K30 (1:1 wt), the drug undergoes a significant decrease of crystallinity just after preparation. That can explain why in general the profiles of amorphous and crystalline drugs are quite close. Nonetheless impregnated containers show at both pressures faster dissolution, compared to the correspondent crystalline and amorphous mixture laden containers. In the system loaded at 200 bar this enhancement is more pronounced and 87% of the drug is dissolved in the medium after only 30 min. This fast drug dissolution can be explained by the presence of an intimate interaction between drug and polymer in the $scCO_2$ aided-loading and the dissolution rate seems to be controlled by the polymer dissolution. A possible mathematical model for the dissolution kinetics of these systems would have to consider Fick's law, the drug–polymer interactions and the particular geometry of the microdevice. For what concerns the material aspects, for a similar impregnated system PVP K30-ketoprofen, Manna and coworkers [29] observed a behavior comprehending two dissolution mechanisms: at low concentrations the drug release rate is fast and is governed by the PVP dissolution, at higher concentrations a stagnant drug-rich layer is formed, and the drug dissolution rate is mainly

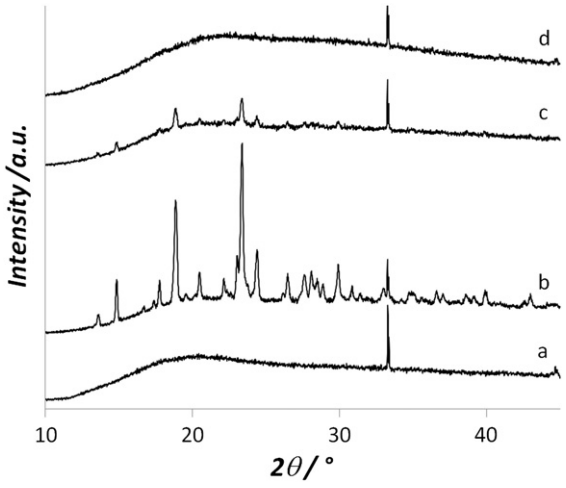

Fig. 7. The X-ray diffraction patterns of (a) empty microcontainers, containers filled with (b) crystalline ketoprofen, (c) 1:9 (wt) keto:PVP physical mixture with crystalline drug (crystalline micro-tablets), (d) 1:9 (wt) keto:PVP physical mixture with amorphous drug (amorphous micro-tablets).

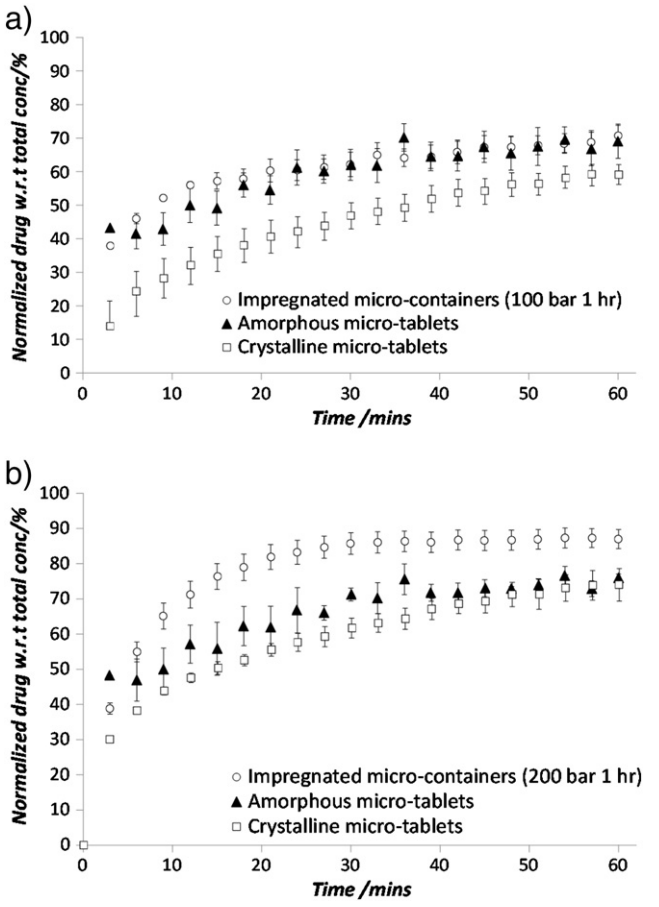

Fig. 8. The enhanced dissolution kinetics of the model drug from impregnated microdevices (a) 100 bar 1 h and (b) 200 bar 1 h as compared to drug–polymer physical mixtures laden micro-tablets with similar loaded drug masses. The concentration was normalized with respect to the total drug loaded in each chip (625 microcontainers) released in 10 ml DI water (N = 3).

Table 2
Similarity factors f_2 of cumulative dissolution profiles shown in Fig. 7 of impregnated microcontainers and correspondent micro-tablets.

Impregnation conditions	Similarity factor f_2	
	Crystalline micro-tablets	Amorphous micro-tablets
100 bar 40 °C 1 h	50.8	51
200 bar 40 °C 1 h	50.7	50.8

constant. From a qualitative perspective this trend was also noticed in our experiments.

3.6. Spectroscopic characterization of impregnated PVP films

The impregnated PVP films were studied via ATR–IR spectroscopy in order to investigate the physical state of the drug in the formulation and eventual presence of interactions with the polymer. The spectra are reported in the ν (C═O) stretching regions in Fig. 9. Pure crystalline ketoprofen (a) is characterized by two well defined peaks at 1697 cm^{-1} and 1655 cm^{-1}, which represent the stretching vibration of the carbonyl group in the carboxylic and ketonic groups respectively. The first peak indicates the presence of a dimer of ketoprofen molecules as reported in [29]. In the impregnated films (c and d) this peak is shifted to a higher wavenumber (1723 cm^{-1}) which indicates, as suggested in [29], the breakage of ketoprofen–ketoprofen interactions. The intensity of this shifted peak is stronger for the 200 bar impregnated films (see pattern d). This observation indicates that ketoprofen is molecularly dispersed in the polymer.

A closer analysis of the PVP ν (C═O) region shows that in the impregnated films the appearance of the ν (C═O) band of PVP at 1625 cm^{-1} is shifted to lower wavenumbers compared to the ν (C═O) of pure PVP (1652 cm^{-1}). This fact is again more evident in the impregnation at 200 bar. This shift might be assigned to the formation of H-bond between the carbonyl group of PVP and the hydroxilic group of ketoprofen as suggested for the supercritical impregnation of PVP films with ibuprofen in [41]. On the other hand, the peak of virgin PVP is still strong in the films, which suggests that still a portion of the C═O bonds in the polymer does not interact with the drug.

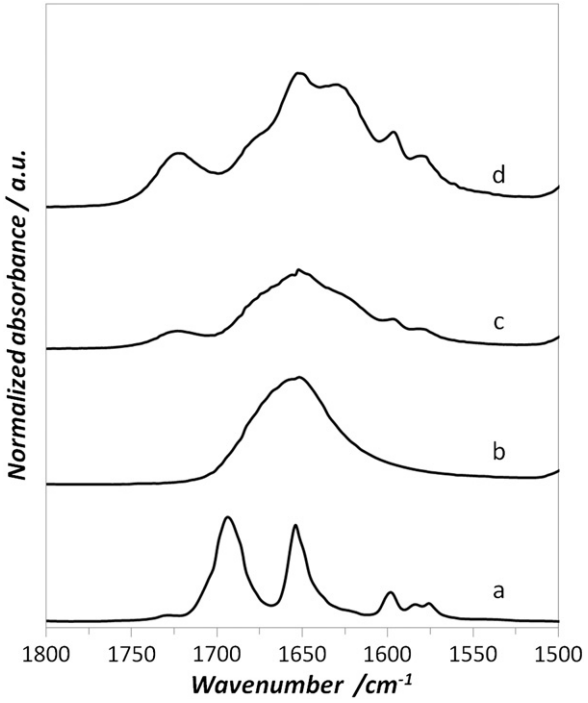

Fig. 9. ATR-IR spectra in the ν (C═O) spectral region: (a) pure solid ketoprofen, (b) pure PVP film, (c) impregnated PVP film at 100 bar for 1 h, and (d) impregnated PVP film at 200 bar for 1 h.

4. Conclusions

Micro-particle based therapeutics frequently exhibit a large size distribution, non uniform drug loading and omni-directional release, entailing a significant loss of drug in the lumen. Microfabricated devices are designed to solve these issues. Nevertheless the current state of the art of such microdevices still lacks of cost-effective solutions for the drug loading. This study shows a technological solution for the drug loading of a reservoir-based microdevice with a poorly soluble model drug. SU-8 microcontainers with various dimensions are fabricated with a two step photolithography process. The microwells are filled with precisely controlled amounts of aqueous PVP solutions by means of inkjet printing. The model drug ketoprofen is then loaded through $scCO_2$ impregnation. The drug impregnation is enhanced by increasing either fluid pressure or time. At 200 bar and 4 h a ketoprofen concentration of 32 wt.% is obtained, corresponding to a drug:polymer ratio of 1:2. Raman mapping reveals that there is an amorphous drug-rich phase in the container surface and a chemical interaction between the components. ATR–IR spectroscopy of PVP films confirms these evidences, showing also the presence of H bondings. Impregnated containers exhibit an enhanced dissolution rate compared to solid dispersion laden reservoirs, both with crystalline and amorphous drugs. Up to 87% of the drug can be released within 30 min showing that microdevices can deliver the active ingredient compatibly with the transit time in the GI tract. The combination of inkjet printing and $scCO_2$ impregnation allows micro containers to be filled with precise doses of drug with an accuracy of a microgram. The combination of these two technologies enables loading of hydrophobic drugs without the use of organic solvents and with a minimum waste of chemicals in a potentially scalable process. The use of inkjet printing and sc impregnation shows significant improvements and promising perspectives in the framework of the microfabricated devices for oral therapeutics and seems particularly suitable for the loading of CO_2 soluble-compounds which are expensive or available only in small amounts.

Acknowledgments

This project is part of NAMEC centre of excellence funded by the Villum Kann Rasmussen Foundation. The authors thank Robert Lessèl and ChemPilots A/S (Farum, Denmark) for the availability of the high pressure equipment. The authors would like to thank Thomas Rades and Line Hagner Nielsen for their comments and their valuable inputs to the research work.

References

[1] C.G. Wilson, B. O'Mahony, B. Lindsay, Physiological Factors Affecting Oral Drug Delivery, in: Marcel Dekker, J. Swarbrick (Eds.), Encyclopedia of Pharmaceutical Technology Third ed., 2013, pp. 2866–2874.
[2] K.D. Rainsford, An analysis of the gastro-intestinal side-effects of non-steroidal anti-inflammatory drugs, with particular reference to comparative studies in man and laboratory species, Rheumatol. Int. 2 (1) (1982) 1–10.
[3] M. Caldorera-Moore, N.A. Peppas, Micro- and nanotechnologies for intelligent and responsive biomaterial-based medical systems, Adv. Drug Deliv. Rev. 61 (15) (2009) 1391–1401.
[4] K.M. Ainslie, R.D. Lowe, T.T. Beaudette, L. Petty, E.M. Bachelder, T.A. Desai, Microfabricated devices for enhanced bioadhesive drug delivery: attachment to and small-molecule release through a cell monolayer under flow, Small 5 (24) (2009) 2857–2863.
[5] K.M. Ainslie, T.A. Desai, Microfabricated implants for applications in therapeutic delivery, tissue engineering, and biosensing, Lab Chip 8 (11) (2008) 1864–1878.
[6] C.L. Randall, T.G. Leong, N. Bassik, D.H. Gracias, 3D lithographically fabricated nanoliter containers for drug delivery, Adv. Drug Deliv. Rev. 59 (15) (2007) 1547–1561.
[7] K.M. Ainslie, C.M. Kraning, T.A. Desai, Microfabrication of an asymmetric, multi-layered microdevice for controlled release of orally delivered therapeutics, Lab Chip 8 (7) (2008) 1042–1047.

[8] T.G. Leong, C.L. Randall, B.R. Benson, A.M. Zarafshar, D.H. Gracias, Self-loading lithographically structured microcontainers: 3D patterned, mobile microwells, Lab Chip 8 (10) (2008) 1621–1624.
[9] H.D. Chirra, T.A. Desai, Multi-reservoir bioadhesive microdevices for independent rate-controlled delivery of multiple drugs, Small 8 (24) (2012) 3839–3846.
[10] S. Eiamtrakarn, Y. Itoh, J. Kishimoto, Y. Yoshikawa, N. Shibata, M. Murakami, K. Takada, Retention and transit of intestinal mucoadhesive films in rat small intestine, Biomaterials 23 (1) (2002) 145–152.
[11] B.A. Kerwin, R.L. Remmele, Protect from light: photodegradation and protein biologics, J. Pharm. Sci. 96 (6) (2007) 1468–1479.
[12] K. Whitehead, Z. Shen, S. Mitragotri, Oral delivery of macromolecules using intestinal patches: applications for insulin delivery, J. Control. Release 98 (1) (2004) 37–45.
[13] T. Goldmann, J.S. Gonzalez, DNA-printing: utilization of a standard inkjet printer for the transfer of nucleic acids to solid supports, DNA-printing: utilization of a standard inkjet printer for the transfer of nucleic acids to solid supports, J. Biochem. Biophys. Methods 42 (3) (2000) 105–110.
[14] T. Xu, J. Jin, C. Gregory, J.J. Hickman, T. Boland, Inkjet printing of viable mammalian cells, Biomaterials 26 (1) (2005) 93–99.
[15] E.A. Roth, T. Xu, M. Das, C. Gregory, J.J. Hickman, T. Boland, Application of inkjet printing to tissue engineering, Biomaterials 25 (17) (2004) 3707–3715.
[16] P. Cooley, D. Wallace, B. Antohe, Applications of ink-jet printing technology to BioMEMS and microfluidic systems, JALA 7 (5) (2002) 33–39.
[17] N. Scoutaris, M.R. Alexander, P.R. Gellert, C.J. Roberts, Inkjet printing as a novel medicine formulation technique, J. Control. Release 156 (2) (2011) 179–185.
[18] P. Marizza, S.S. Keller, A. Boisen, Inkjet printing as a technique for filling of micro-wells with biocompatible polymers, Microelectron. Eng. 111 (79) (2013) 391–395.
[19] C. Leuner, J. Dressman, Improving drug solubility for oral delivery using solid dispersions, Eur. J. Pharm. Biopharm. 50 (1) (2000) 47–60.
[20] P. Caliceti, O. Schiavon, F.M. Veronese, Biopharmaceutical properties of uricase conjugated to neutral and amphiphilic polymers, Bioconjug. Chem. 10 (4) (1999) 638–646.
[21] V. Iyer, S. Katageri, R. Radhakrishnan, N.B. Gaddipati, U.S. Patent 10/222 (2002) 046.
[22] A.R.C. Duarte, C. Martins, P. Coimbra, M.H.M. Gil, H.C. de Sousa, C.M.M. Duarte, Sorption and diffusion of dense carbon dioxide in a biocompatible polymer, J. Supercrit. Fluids 38 (3) (2006) 392–398.
[23] Y. Sato, T. Takikawa, S. Takishima, H. Masuoka, Solubilities and diffusion coefficients of carbon dioxide in poly(vinyl acetate) and polystyrene, J. Supercrit. Fluids 19 (2) (2001) 187–198.
[24] M.D. Elkovitch, L.J. Lee, D.L. Tomasko, Effect of supercritical carbon dioxide on PMMA/rubber and polystyrene/rubber blending: viscosity ratio and phase inversion, Polym. Eng. Sci. 41 (12) (2001) 2108–2125.
[25] I. Kikic, F. Vecchione, P. Alessi, A. Cortesi, F. Eva, N. Elvassore, Polymer plasticization using supercritical carbon dioxide: experiment and modeling, Ind. Eng. Chem. Res. 42 (13) (2003) 3022–3029.
[26] M. Charoenchaitrakool, F. Dehghani, N.R. Foster, H.K. Chan, Micronization by rapid expansion of supercritical solutions to enhance the dissolution rates of poorly water-soluble pharmaceuticals, Ind. Eng. Chem. Res. 39 (12) (2000) 4794–4802.
[27] B. Subramaniam, A.R. Roger, S. Kirk, Pharmaceutical processing with supercritical carbon dioxide, J. Pharm. Sci. 86 (8) (1997) 885–890.
[28] M. Banchero, L. Manna, S. Ronchetti, P. Campanelli, A. Ferri, Supercritical solvent impregnation of piroxicam on PVP at various polymer molecular weights, J. Supercrit. Fluids 49 (2) (2009) 271–278.
[29] L. Manna, M. Banchero, D. Sola, A. Ferri, S. Ronchetti, S. Sicardi, Impregnation of PVP microparticles with ketoprofen in the presence of supercritical CO_2, J. Supercrit. Fluids 42 (3) (2007) 378–384.
[30] S.J. Macnaughton, I. Kikic, N.R. Foster, P. Alessi, A. Cortesi, I. Colombo, Solubility of anti-inflammatory drugs in supercritical carbon dioxide, J. Chem. Eng. Data 41 (5) (1996) 1083–1086.
[31] I.E. Shohin, J.I. Kulinich, G.V. Ramenskaya, B. Abrahamsson, S. Kopp, P. Langguth, J.E. Polli, P.S. Vinod, D.W. Groot, D.M. Barends, J.B. Dressman, Biowaiver monographs for mediate-release solid oral dosage forms: ketoprofen, J. Pharm. Sci. 101 (10) (2012) 3593–3603.
[32] M.A. Sabegh, H. Rajaei, F. Esmaeilzadeh, M. Lashkarbolooki, Solubility of ketoprofen in supercritical carbon dioxide, J. Supercrit. Fluids 72 (2012) 192–197.
[33] N.R. Foster, G.S. Gurdial, J.S. Yun, K.K. Liong, K.D. Tilly, S.S. Ting, H. Singh, J.H. Lee, Significance of the crossover pressure in solid-supercritical fluid phase equilibria, Ind. Eng. Chem. Res. 30 (8) (1991) 1955–1964.
[34] I. Kikic, F. Vecchione, Supercritical impregnation of polymers, Curr. Opin. Solid State Mater. Sci. 7 (4) (2003) 399–405.
[35] C. Ishiyama, T.-F. Mark Chang, M. Sone, Effects of supercritical carbon dioxide treatment on bending properties of micro-sized SU-8 specimens, Microelectron. Eng. 88 (8) (2011) 2272–2274.
[36] L.A.E. De Carvalho, M.P.M. Marques, J. Tomkinson, Drug-excipient interactions in ketoprofen: A vibrational spectroscopy study, Biopolymers 82 (2006) 420–424.
[37] B.C. Hancock, M. Parks, What is the true solubility advantage for amorphous pharmaceuticals? Pharm. Res. 17 (4) (2000) 397–404.
[38] H. Konno, L.S. Taylor, Influence of different polymers on the crystallization tendency of molecularly dispersed amorphous felodipine, J. Pharm. Sci. 95 (12) (2006) 2692–2705.
[39] L.H. Nielsen, S.S. Keller, K.C. Gordon, A. Boisen, T. Rades, A. Müllertz, Spatial confinement can lead to increased stability of amorphous indomethacin, Eur. J. Pharm. Biopharm. 81 (2) (2012) 418–425.
[40] P. Di Martino, E. Joiris, R. Gobetto, A. Masic, G.F. Palmieri, S. Martelli, Ketoprofen–poly(vinylpyrrolidone) physical interaction, J. Cryst. Growth 265 (1) (2004) 302–308.
[41] S.G. Kazarian, G.G. Martirosyan, Spectroscopy of polymer/drug formulations processed with supercritical fluids: *in situ* ATR–IR and Raman study of impregnation of ibuprofen into PVP, Int. J. Pharm. 232 (1) (2002) 81–90.